UNIVERSITÀ
DEGLI STUDI
DI PADOVA

Sede Amministrativa: Università degli Studi di Padova

Dipartimento di Biologia

SCUOLA DI DOTTORATO DI RICERCA IN: BIOSCIENZE E BIOTECNOLOGIE

INDIRIZZO: BIOTECNOLOGIE

CICLO: 27°

STUDIES OF Ca^{2+} DYNAMICS IN INTRACELLULAR COMPARTMENTS IN PLANTS: ADVANCED MOLECULAR TOOLS FOR *IN VIVO* IMAGING

Direttore della Scuola: Ch.mo Prof. Giuseppe Zanotti

Coordinatore d'indirizzo: Ch.ma Prof.ssa Fiorella Lo Schiavo

Supervisore: Ch.ma Prof.ssa Michela Zottini

Co-Supervisore: Ch.mo Prof. Alex Costa

Dottoranda: Giovanna Loro

Index

Riassunto pag 1

Abstract pag 7

Aim of the project pag 11

Chapter 1: Main introduction pag 13

1.1 The origin of Ca^{2+} as second messenger pag 15

1.2 Ca^{2+}-signature in plants pag 15

1.3 Formation of Ca^{2+}-signature pag 19

1.4 Ca^{2+}-dynamics in subcellular compartments pag 29

1.5 Intracellular Ca^{2+} measurement pag 32

Chapter 2: Mitochondrial Ca^{2+}-dynamics pag 35

2.1 Introduction on mitochondrial Ca^{2+}-dynamics pag 37

2.2 Targeting of Cameleons to various subcellular compartments reveals a strict cytoplasmic/ mitochondrial Ca^{2+} handling relationship in plant cell pag 41

2.3 The D3cpv Cameleon reports Ca^{2+} dynamics in plant mitochondria with similar kinetics of the YC3.6 Cameleon, but with a lower sensitivity pag 43

Chapter 3: Endoplasmic reticulum Ca^{2+}-dynamics pag 45

3.1 Introduction on ER Ca^{2+}-dynamics pag 47

3.2 Analyses of Ca^{2+} accumulation and dynamics in the endoplasmic reticulum of Arabidopsis root cells using a genetically encoded Cameleon sensor pag 49

Chapter 4: Chloroplast Ca^{2+}-dynamics pag 51

4.1 Introduction on chloroplast Ca^{2+} dynamics pag 53

4.2 Results and Discussion pag 58

4.3 Conclusions pag 83

4.4 Materials and Methods pag 87

Chapter 5: Main conclusions pag 93

Chapter 6: Appendix pag 99

Acknowledgments pag 101

References pag 103

Riassunto

Le piante reagiscono a diversi stimoli ambientali attivando vie di trasduzione del segnale in cui il calcio (Ca^{2+}) svolge un ruolo centrale come componente del signalling intracellulare. Una grande varietà di stimoli biotici, abiotici o di sviluppo causano specifici transienti di Ca^{2+}, i quali sono successivamente tradotti in risposte trascrizionali e metaboliche. La maggior parte delle ricerche sul Ca^{2+} come secondo messaggero è focalizzata sullo studio delle proteine coinvolte nella codifica di questo segnale e sui meccanismi di trasporto di questo ione attraverso le membrane (Kudla et al. 2010,Dodd et al. 2010). Recenti scoperte riportano che differenti organelli sono coinvolti nelle vie di segnale controllate dal Ca^{2+} ed, inoltre, sottolineano il loro ruolo nella percezione degli stress ambientali (Stael et al. 2012,Nomura and Shiina. 2014,Xiao et al. 2013).

Questo progetto di dottorato ha lo scopo di studiare il coinvolgimento dei diversi compartimenti sub-cellulari (quali mitocondri, reticolo endoplasmatico e plastidi/cloroplasti) nella formazione del transiente di Ca^{2+} generato dalle cellule vegetali in risposta a differenti stimoli. Per raggiungere questo obiettivo è stata sviluppata una serie di strumenti molecolari che permettano l'analisi *in vivo* a livello sub-cellulare del Ca^{2+} in tessuti vegetali complessi (come la radice) e a livello di singola cellula (come la cellula di guardia). Questi strumenti, combinati con approcci genetici e farmacologici, saranno indispensabili per capire in modo più approfondito il ruolo dei diversi organelli nella regolazione dell'omeostasi del Ca^{2+}. Oggigiorno, sono disponibili diverse sonde geneticamente codificate basate sul fenomeno della FRET (trasferimento di energia di Föster), chiamate Cameleon, che

presentano diverse affinità per lo ione Ca^{2+} e permettono di monitorare *in vivo* le sue dinamiche (Miyawaki et al. 1999,Palmer and Tsien. 2006).
In questo studio si riporta lo sviluppo di una nuova serie di costrutti in cui le sonde Cameleon sono state indirizzate a differenti compartimenti intracellulari (mitocondri, reticolo endoplasmatico e plastidi/cloroplasti) ed i costrutti generati sono stati introdotti stabilmente nella pianta modello *Arabidopsis thaliana*. Nello specifico, le sonde Cameleon localizzate nei mitocondri e nel reticolo endoplasmatico (ER) sono state efficientemente espresse in piante selvatiche (wild type), mentre l'espressione costitutiva della sonda localizzata nei cloroplasti/plastidi è stata inficiata da un fenomeno di silenziamento genico post trascrizionale. Per ovviare ciò, la sonda è stata introdotta nella linea mutante *rdr6* di *A. thaliana* (Peragine et al. 2004) la quale, presentando una soppressione del processo di silenziamento, ha permesso la costitutiva espressione della sonda Cameleon indirizzata ai plastidi/cloroplasti.
Nella prima parte di questo dottorato sono stati condotti una serie di esperimenti volti allo studio delle dinamiche del Ca^{2+} nella matrice mitocondriale, utilizzando le sonde Cameleon D3cpV e YC3.6 (K_d 600nM e K_d 250nM rispettivamente). Gli esperimenti condotti, hanno rivelato che entrambe le sonde (4mt-YC3.6 e 4mt-D3cpv) permettono di monitorare le dinamiche del Ca^{2+} in questi organelli. Il confronto sulla funzionalità delle due sonde ha però evidenziato che la sonda YC3.6 è in grado di offrire una migliore sensibilità, come dimostrato da un intervallo dinamico più ampio, ovvero a parità di variazioni di Ca^{2+} questa sonda mostra una maggiore variazione nell'efficienza di FRET. Inoltre, il confronto delle dinamiche del Ca^{2+} misurate con le due sonde suggerisce che le misure ottenute con la sonda YC3.6 non siano inficiate da una eventuale interazione con la CaM mitocondriale endogena. Le analisi condotte con la linea 4mt-YC3.6 mostrano che sottoponendo le piante a stress osmotico (nelle cellule di guardia) o trattandole con ATP extracellulare (eATP; nell'apice radicale) si induce un transiente di Ca^{2+} a livello del citosol che viene percepito dai mitocondri che a loro volta accumulano Ca^{2+} con dinamiche strettamente dipendenti da quelle citosoliche.

Successivamente, sono state condotte numerose analisi atte allo studio delle dinamiche del Ca^{2+} nel lume dell'ER. In questo compartimento sono state indirizzate le sonde Cameleon D1 (K_{d1} 0.8 e K_{d2} 60μM) e D4 (K_d 195μM). Nonostante la sonda D1 fosse stata precedentemente usata in cellule animali per monitorare le dinamiche del Ca^{2+} nell'ER (Palmer et al. 2004), le analisi condotte con la linea di *A. thaliana* esprimente la sonda CRT-D1ER hanno evidenziato che quest'ultima non mostrava nessuna variazione di FRET in risposta ad una serie di stimoli noti indurre transienti di Ca^{2+} citosolici. Al contrario la linea di *A. thaliana* esprimente la sonda CRT-D4ER si è rivelata essere in grado di monitorare lo stato e le dinamiche del Ca^{2+} in questo compartimento. Con l'uso di questa linea transgenica abbiamo valutato, attraverso un approccio farmacologico, il contributo di due classi di Ca^{2+}-ATPasi (ECA e ACA) nel mantenimento dell'omeostasi del Ca^{2+} luminale. I risultati hanno rivelato che le pompe ECA hanno un ruolo fondamentale nell'accumulo del Ca^{2+} nell'ER, dato che la loro inibizione comporta una sensibile diminuzione della concentrazione di Ca^{2+} nel lume. Inoltre sono state analizzate le dinamiche del Ca^{2+} in risposta a diversi stimoli come il glutammato, eATP, NaCl e l'alternata imposizione di un tampone per la de-polarizzazione e iper-polarizzazione della membrana plasmatica. Era noto che gli stimoli analizzati provocassero transienti di Ca^{2+} nel citosol e le analisi condotte nel lume dell'ER hanno mostrato che, anche questo compartimento, percepisce gli stimoli somministrati accumulando Ca^{2+}. Questi risultati suggeriscono che l'ER in pianta abbia un ruolo diverso rispetto a quello che ha nelle cellule animali. Infatti, i risultati dimostrano che l'ER in pianta è in grado di accumulare Ca^{2+} sequestrandolo dal citosol e rilasciarlo lentamente, mentre in cellule animali l'ER è anche un'importante sorgente di Ca^{2+}, che interviene nella formazione del transiente citosolico, comportamento non osservato nelle condizioni da noi analizzate.

Nell'ultima parte del mio triennio di dottorato sono state analizzate le dinamiche del Ca^{2+} nei plastidi e nei cloroplasti, in particolare, sono state saggiate la funzionalità di due sonde Cameleon, sia per espandere l'intervallo delle concentrazioni di Ca^{2+} analizzabili in questi organelli sia per

verificare quale sonda rappresentasse la miglior opzione. La prima sonda scelta è stata la YC3.6 (2Bam4-YC3.6) in quanto in letteratura è riportata una concentrazione basale di Ca^{2+} nei cloroplasti nell'ordine delle centinaia di nano-moli/L, simile alla concentrazione del citosol (Nomura et al. 2012). La seconda sonda indirizzata ai cloroplasti/plastidi è stata la YC4.6 (2Bam4-YC4.6), che presentando *in vitro* una curva di affinità bifasica per il Ca^{2+} (K_d 56nM and 14μM) può essere potenzialmente utilizzata per analizzare variazioni di Ca^{2+} in un intervallo di concentrazioni più ampio. Al fine di valutare se i plastidi siano in grado di accumulare Ca^{2+} in risposta ad uno stimolo capace di indurre un transiente citosolico, sono state analizzate, utilizzando le due linee transgeniche (2Bam4-YC3.6 e 2Bam4-YC4.6), le dinamiche del Ca^{2+} nell'apice radicale in risposta a diverse concentrazioni di eATP. Dall'analisi di questi dati si è rilevata una dose-dipendenza nella risposta in termini di Ca^{2+}, misurata con entrambe le linee. Tale dose-dipendenza è stata registrata anche nel citosol suggerendo una stretta correlazione tra le dinamiche dei due compartimenti, l'accumulo plastidiale potrebbe, infatti, essere dovuto al transiente di Ca^{2+} citosolico.

Successivamente è stato studiato il signaling del Ca^{2+} indotto nei cloroplasti delle cellule di guardia in seguito alla transizione luce-buio. La transizione luce-buio ha indotto un transiente di Ca^{2+} cloroplastico sostenuto nel tempo e già descritto in precedenza (Nomura et al. 2012,Sai and Johnson. 2002) in cui però è stata osservata una componente oscillatoria, sovrapposta a quella sostenuta, caratterizzata da transienti rapidi e successivi distinguibili come singoli picchi. I risultati ottenuti suggeriscono che le due componenti siano generate da sorgenti di Ca^{2+} diverse: il transiente sostenuto sembra collegato ad una riserva interna al cloroplasto, probabilmente il lume tilacoidale, mentre le oscillazioni sono generate da una riserva intracellulare, che potrebbe essere il citosol.

Le dinamiche del Ca^{2+} nel cloroplasto sono stata analizzate anche a livello di intera foglia, su questo sistema sono state condotte analisi preliminari sulla risposta allo stress da ferita. Il danneggiamento del tessuto fogliare, ha comportato, nelle cellule circostanti alla zona danneggiata, l'induzione di un

transiente di Ca^{2+} nel citosol e contemporaneamente un transiente di Ca^{2+} nei cloroplasti.

Riassumendo, in questo lavoro sono state caratterizzate le dinamiche del Ca^{2+} in diversi compartimenti intracellulari. È stata analizzata la risposta all'eATP in un tessuto complesso come l'apice radicale, i risultati hanno evidenziato come plastidi, mitocondri e ER siano coinvolti nel sequestro di Ca^{2+} dal citosol mostrando un accumulo di Ca^{2+} in risposta allo stimolo. Le linee generate in questo progetto di dottorato hanno permesso di valutare nello specifico le diverse e caratteristiche dinamiche di ciascun compartimento. I risultati, inoltre, suggeriscono che la fonte intracellulare di Ca^{2+} coinvolta nella formazione del transiente citosolico in risposta all'eATP potrebbe essere rappresentata dal vacuolo.

Sono state caratterizzate inoltre le dinamiche del Ca^{2+} nei mitocondri e nei cloroplasti a livello di singola cellula, studiando il sistema modello cellula di guardia durante la transizione luce-buio. I risultati hanno mostrato che solo i cloroplasti sono sensibili a questo stimolo, infatti, i mitocondri non mostrano transienti di Ca^{2+}.

In conclusione, nel presente lavoro si riporta lo sviluppo di una serie di nuovi strumenti molecolari per le analisi delle dinamiche del Ca^{2+} in diversi compartimenti intracellulari nelle cellule vegetali. Le linee transgeniche generate in questo progetto di dottorato saranno quindi utili per identificare il ruolo degli organelli nelle vie di trasduzione del segnale Ca^{2+} attivate in risposta a stress ambientali e/o a segnali di sviluppo.

Abstract

Plants react to environmental challenges through immediate signal-transduction pathways. Free calcium ions (Ca^{2+}) are one integral component of many transduction pathways, in both plant and animal cells. A wide variety of signals including biotic, abiotic, and developmental stimuli evokes specific spatio-temporal Ca^{2+}-transients, which are further transduced by Ca^{2+} sensor proteins into transcriptional and metabolic responses. Most of the research on Ca^{2+} signalling in plants has been focused on transport mechanisms of Ca^{2+} into and out of the cytoplasm as well as on the components involved in decoding cytoplasmic Ca^{2+} signals, which have been extensively reviewed (Kudla et al. 2010,Dodd et al. 2010). Recent advances report that the different organelles are involved in Ca^{2+} signaling and their role in stress perception has been highlighted (Stael et al. 2012,Nomura and Shiina. 2014,Xiao et al. 2013).

The aim of this PhD project was to elucidate the involvement of subcellular compartments (e.g. mitochondria, endoplasmic reticulum (ER) and chloroplasts/plastids) in shaping the Ca^{2+} signature triggered in plant cells by different stimuli. To pursue our aims, we developed a series of molecular tools that enabled subcellular Ca^{2+} analyses, thus we analyzed Ca^{2+}-dynamics in complex plant tissues (e.g. roots) as well as in single cells. These tools, together with both genetic and pharmacological approaches, will be instrumental to understand the role of organelles in Ca^{2+} homeostasis.

Several FRET-based genetically-encoded probes with different Ca^{2+} affinities, called Cameleons, have been developed and allow to measure Ca^{2+} dynamics *in vivo* (Miyawaki et al. 1999,Palmer and Tsien. 2006).

In the present study, we first developed a series of constructs for targeting Cameleon probes to different plant cell organelles (mitochondria, ER and chloroplast/plastids). Then, the constructs were introduced in *Arabidopsis thaliana* plants for the generation of stable transgenic lines. Whereas the mitochondrial and the ER Cameleon probes were efficiently expressed in wild type *A. thaliana* plants, the constitutive expression of the plastidial probe was affected by post transcriptional gene silencing. We bypassed this issue by introducing the chloroplastic/plastidial probe in the *A. thaliana rdr6* silenced suppressed mutant (Peragine et al. 2004), obtaining the constitutive expression of the probe.

First, we analyzed mitochondrial Ca^{2+} dynamics using the D3cpV and the YC3.6 Cameleon probes (K_d 600nM and K_d 250nM respectively) targeted to the mitochondrial matrix. The analyses performed using these two mitochondrial lines (4mt-YC3.6 and 4mt-D3cpv) revealed that although both probes are able to measure Ca^{2+}-dynamics in this organelle, the YC3.6 Cameleon offers a better sensitivity, showing a higher dynamic range. Moreover, the comparison of Ca^{2+}-dynamics monitored with the two probes suggests that measurements performed with the YC3.6 probe are unaffected by endogenous mitochondrial CaMs as well as D-family probes. The analyses performed with the 4mt-YC3.6 line showed that mitochondria are able to respond, in terms of Ca^{2+}-transient, to several stimuli that cause Ca^{2+}-transient in the cytosol, like osmotic stress in the guard cells and eATP in the root. Our results suggest that mitochondrial Ca^{2+}-accumulation is strictly dependent on cytosolic [Ca^{2+}] increase.

Then, we focused our analysis on the ER, targeting the D1 (K_{d1} 0.8 and K_{d2} 60μM) and the D4 (K_d 195μM) Cameleon probes to the ER lumen. Although, D1 was previously used to study ER Ca^{2+}-dynamics in mammalian cells (Palmer et al. 2004), in our analyses performed with on CRT-D1ER seedlings roots, this probe was not able to report any [Ca^{2+}] changes. On the contrary, the D4 (CRT-D4ER) probe proved to be suitable for monitoring ER Ca^{2+}-dynamics and the ER Ca^{2+}-status ($[Ca^{2+}]_{ER}$). By means of this transgenic line, we evaluated by a pharmacological approach the contribution of two Ca^{2+}-ATPase classes (ECA and ACA) in the maintenance of ER Ca^{2+}

homeostasis. Our results revealed that ECA pumps have a fundamental role in Ca^{2+}-accumulation in the ER, since their inhibition lead to a decrease in the $[Ca^{2+}]_{ER}$. Furthermore, we analyzed Ca^{2+}-dynamics in the ER under several stimuli known to induce cytosolic Ca^{2+}-transients, such as glutamate, eATP, NaCl, and the alternate imposition of depolarizing and hyperpolarizing buffers. Our experiments showed that plant ER responds to all these stimuli showing Ca^{2+}-accumulation, suggesting a different role for the ER in plants than in mammalian cells. In fact, in our experiments the ER behaves as a capacitor of cytosolic Ca^{2+} instead of as a primary source of Ca^{2+} in the generation of the cytosolic Ca^{2+}-transients.

At the end, we moved our attention to chloroplastic and plastidial Ca^{2+}-dynamics using two probes, to extend the range of measurable stromal Ca^{2+} concentrations ($[Ca^{2+}]_{str}$). We chose the YC3.6 probe (2Bam4-YC3.6) since the reported $[Ca^{2+}]_{str}$ is approximately hundreds of nano molar, similar to the cytosol (Nomura et al. 2012), and the probe YC4.6 (2Bam4-YC4.6), which has an *in vitro* biphasic Ca^{2+}-dependency (K_d 56nM and 14μM) and that should enable to image both subtle and large changes in $[Ca^{2+}]_{str}$.

Then, we analyzed plastidial Ca^{2+}-dynamics in response to several concentrations of eATP in the root tip. We observed that different concentrations evoked dose-dependent Ca^{2+} responses in plastids (both in 2Bam4-YC3.6 and in 2Bam4-YC4.6 lines) and in the cytosol, suggesting a correlation between Ca^{2+}-dynamics in these two compartments. Furthermore, we analyzed Ca^{2+}-dynamics in chloroplasts of the guard cell, during the light to dark transition. We identified two distinct components of the Ca^{2+}-uptake triggered by this stimulus: a previously described sustained Ca^{2+}-transient (Nomura et al. 2012,Sai and Johnson. 2002) and autonomous Ca^{2+}-oscillations. Moreover, our analyses suggest that the two events have different Ca^{2+}-sources, the sustained Ca^{2+}-transient is dependent on an intra-chloroplast Ca^{2+}-store, that might be the thylakoids lumen, while the oscillations are generated by an intracellular source, likely the cytosol. At the end, we performed experiments on entire leaf during wounding stress, by monitoring both cytosolic and chloroplastic Ca^{2+}-dynamics. In the cells surrounding the damaged area, wounding induced a

strong cytosolic Ca^{2+}-transient and concomitantly a rapid stromal Ca^{2+}-transient, suggesting that chloroplastic Ca^{2+} would contribute to the wounding-induced cellular response.

Summarizing we characterized the Ca^{2+}-dynamics in intracellular compartments in complex tissue like the root tip during the eATP treatment. Our analysis revealed that mitochondria, ER and plastids are able to accumulate Ca^{2+} in response to this stimulus and participate in the Ca^{2+} sequestration from the cytosol. These data suggest that, in response to eATP, the vacuole might represent the intracellular Ca^{2+}-store involved in the generation of the cytosolic Ca^{2+} transient. We also characterized Ca^{2+}-dynamics of mitochondria and chloroplasts at single cell level, studying the model system guard cell during the light to dark transition. Our experiments revealed that only chloroplasts are sensible to this stimulus, mitochondria, in fact, showed no Ca^{2+}-transients.

In conclusion, we report the development of a series of new molecular tools for the analyses of Ca^{2+}-dynamics in different plant organelles that will be useful for future researches aimed at identifying the role of organellar Ca^{2+} in the response to environmental and developmental stimuli.

Aim of the project

Plants react to changing environmental conditions through immediate signal transduction pathways. One integral component of many transduction pathways is the second messenger Ca^{2+}. A plethora of stimuli, including development and abiotic/biotic stresses, have been observed to evoke specific spatiotemporal Ca^{2+} transients, which are further transduced by Ca^{2+} sensor proteins into transcriptional and/or metabolic responses.

In the last years, the role of intracellular compartments in stress perception and Ca^{2+} signalling became more and more evident. Thus, the development of tools that allow the analysis of this important second messenger at sub-cellular level is mandatory to deepen the comprehension of its action mechanism.

The aim of this PhD project was to evaluate the Ca^{2+} dynamics triggered in mitochondria, ER and chloroplasts by external stimuli in order to depict a general framework of organelle involvement in Ca^{2+} signaling in *Arabidopsis thaliana* cells.

First, we generated the appropriate tools allowing high-resolution *in vivo* Ca^{2+}-imaging for each of these compartments. Cameleons were chosen as Ca^{2+} sensors since they allow analysis both at single cell level and in entire organs like the root. Once the tools were obtained, we measured specific Ca^{2+} dynamics in organelles in response to several stimuli and we investigated the relationship between cytosol and the different sub-cellular compartment Ca^{2+}-dynamics and their role in the modulation of the cytosolic Ca^{2+} signature.

Chapter 1:

Main introduction

1.1 The origin of Ca^{2+} as second messenger

Calcium is the chemical element with atomic number 20, it belongs to the metals family and it is the fifth most abundant element on Earth. The calcium ion (Ca^{2+}) can form insoluble products with orthophosphate (Pi) which is fundamental for cellular metabolism, in particular, for reactions associated with the transduction of free energy. The low solubility of Ca^{2+}-phosphate compounds required the early evolution of mechanisms for the maintenance of cytosolic Ca^{2+} concentration ($[Ca^{2+}]_{cyt}$) in the nano-molar range. These homeostatic mechanisms would have been ideal for the subsequent evolution of Ca^{2+}-based signalling pathways, in fact, elevation in Ca^{2+} concentration can occur more rapidly than for ions or solutes that are maintained at millimolar levels (Sanders et al. 1999). Moreover, the chemistry of Ca^{2+} provides further favorable features for signalling transduction, in fact, the ion can coordinate a considerable number of uncharged atoms (commonly six to eight) and Ca^{2+}-binding can induce conformational changes in proteins to elicit downstream events in signalling pathways (McPhalen et al. 1991,Sanders et al. 1999). For several reasons Ca^{2+} was adopted as a second messenger and now represent one of the most versatile signaling ion in all eukaryotic organisms.

1.2 Ca^{2+}-signature in plants

Ca^{2+} is an essential nutrient for plants, absorbed by root hairs and transported through the vascular system, using the driving force generated by evapotranspiration. The divalent cation (Ca^{2+}) plays structural roles in the cell wall and membranes, as a counter-ion for inorganic and organic anions in the vacuole, and as intracellular messenger in the cytosol (White and Broadley. 2003).

An increase in $[Ca^{2+}]_{cyt}$ have been observed in response to a wide range of environmental and developmental stimuli. This transient can occur in the entire organism or in specific tissues or cell types (White and Broadley.

2003), its spatial and temporal characteristic is called "Ca^{2+} signature" (McAinsh and Pittman. 2009) that is formed by tightly regulated activities of channels and transporters located on the different membranes in the cell (Batistic and Kudla. 2012).

How this omnipresent signal can be translated into stimulus-specific responses has been a long-standing question (McAinsh and Hetherington. 1998,Sanders et al. 1999,Scrase-Field and Knight. 2003). One hypothesis is that Ca^{2+} simply acts as a switch that activate Ca^{2+}-sensitive signal-transduction components, in this hypothesis, Ca^{2+} mediates an appropriate response only in conjunction with other signaling molecules. On the contrary, at least in guard cell, there are strong evidences that prove that Ca^{2+}-signature is sufficient for the specific end-response (McAinsh and Hetherington. 1998,Evans et al. 2001,Scrase-Field and Knight. 2003).

Guard cells surround stomatal pores in the epidermis of plant leaves and stems; this cell type has become a popular system for the study of protein function and signalling cascade, at different levels. In the wall between the guard cells and the neighboring there are not plasmodesmata connections and this peculiarity allows the study of different mechanisms at single-cell level. Guard cells, in fact, are able to respond autonomously to different stimuli in which second messengers are involved (Schroeder et al. 2001). $[Ca^{2+}]_{cyt}$-oscillations during stomata movement is a well-studied topic; in these cells Ca^{2+}-transients are involved in the control of cell turgor, thus in stomatal closure (Blatt. 2000). External treatments with Ca^{2+} ($[Ca^{2+}]_{ext}$), abscissic acid (ABA) or hydrogen peroxide (H_2O_2) induce $[Ca^{2+}]_{cyt}$ transients (McAinsh et al. 1995,Pei et al. 2000). The different stimuli use specific pathways for the formation of the Ca^{2+} transient: in ABA treatment the molecule inositol 1,4,5-triphosphate is involved, since the inhibition of phospholipase C interfered with Ca^{2+} transient generation; while the Ca^{2+}-signature induced by $[Ca^{2+}]_{ext}$ is not affected by the same inhibitor (Evans et al. 2001,Scrase-Field and Knight. 2003).

In the de-etiolated *(det3)* mutant of *Arabidopsis thaliana* defective for *VACUOLAR ATP SYNTHASE SUBUNIT C* gene, $[Ca^{2+}]_{cyt}$ transients induced by H_2O_2 and by $[Ca^{2+}]_{ext}$ are abnormal and the subsequent stomatal closure is

compromised. When Ca^{2+}-signature is imposed artificially the stomatal closure is restored (Allen et al. 2000,Allen et al. 2000). This result suggests that Ca^{2+}-signature itself contains information that specifically directs stomatal closure (Fig 1.1) (Scrase-Field and Knight. 2003) . Supporting this hypothesis, it was also demonstrated that stomata steady-state aperture is programmed by the frequency, number and amplitude of $[Ca^{2+}]_{cyt}$ oscillation (Allen et al. 2001). In fact, in guard cells of the ABA-insensitive *A. thaliana GROWTH CONTROLLED BY ABSCISSIC ACID 2 (gca2)* mutant, the treatment with ABA induces considerably different $[Ca^{2+}]_{cyt}$ oscillations compared to wild-type. Again, the artificially imposition of $[Ca^{2+}]_{cyt}$ oscillation, that lead in wild type to a steady-state stomatal closure, also in the mutant cause the same response (Allen et al. 2001).

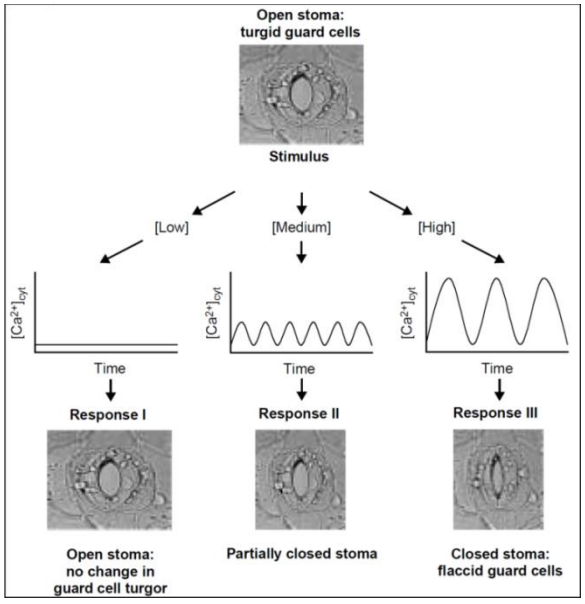

Figure 1.1: Schematic representation of specific responses to different Ca^{2+}-signatures. Guard cells are able to decode the Ca^{2+} signature and activate specific responses. Different signatures lead to a different stomatal status. Figure adapted from Evans et al.2001.

The correlation between Ca^{2+}-signature and specific responses is appreciable also in the symbiotic signalling. Oscillations in plant $[Ca^{2+}]_{cyt}$ during the

symbiotic process, defined Ca^{2+}-spiking, are one of the earliest measurable plant responses elicited by Rhizobial Bacteria and Mycorrhizal Fungi, and these microorganisms evoke specific Ca^{2+}-signatures in plant root hairs (Fig1.2) that occurred principally in the nucleus (Oldroyd and Downie. 2006).

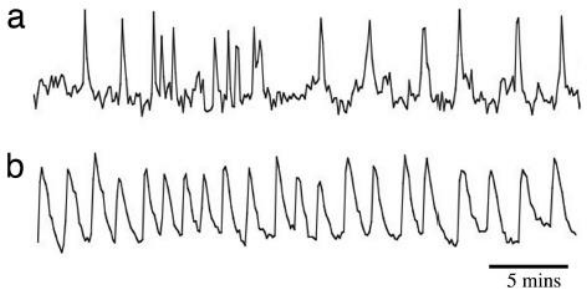

Figure 1.2: Ca^{2+}-spike in root hair during symbiosis initial step.

a) Ca^{2+}-spike induced by Mycorrhizal Fungi. b) Ca^{2+}-spike induced by Rhizobial Bacteria. Image adapted from Kosuta et al. 2008.

Studies on the nodulation-defective mutants, *DOESN'T MAKE INFECTIONS 1* (*dmi1*) and 2 (*dmi2*) of *Medicago truncatula,* revealed that both failed to exhibit Ca^{2+}-oscillations associated to nodulation (nod) event and to the mycorrhizal infection (Sun et al. 2007). This suggests that nodulation and mycorrhizal infection share components of the symbiotic signalling pathway to generate Ca^{2+} oscillations. Furthermore, the peptide mastoparan, an agonist of heteromeric G protein, causes Ca^{2+} oscillations with a similar kinetic to the one observed in the nod-factor response and it is able to induces the *EARLY NUDULIN11* (*ENOD11*) gene, in *M. truncatula*. Interestingly, this peptide has the same effects on the *dmi1* and *dmi2* mutants further suggesting that artificially imposed Ca^{2+} oscillations can rescue early nodulation responses in these mutants (Sun et al. 2007).

The activation of a specific pathway in response to a precise Ca^{2+}-signature seems not to be a prerogative of specific cells, as guard cells and root hairs, but a more general method for the activation of the correct response in plants (Whalley and Knight. 2013). In fact, microarray analysis performed on entire seedlings shown that imposing different Ca^{2+}-signatures activate specific gene responses. In this experiment, three different Ca^{2+}-signatures were imposed and the subsequent analysis of the promoters of the up-regulated genes, revealed that the most common motives were specific for each of the signatures. This result suggested that these regulative elements are specifically sensitive to different types of $[Ca^{2+}]_{cyt}$ oscillations (Whalley and Knight. 2013).

Many are the players involved in Ca^{2+} signalling: Ca^{2+}-channels and pumps shape the $[Ca^{2+}]_{cyt}$, while a complicated network of Ca^{2+}-binding proteins decodes the signature and activates a specific response.

1.3 Formation of the Ca^{2+}-signature

The initial step of Ca^{2+}-signalling is the formation of the transient through the activation of Ca^{2+}-permeable channels, which allow the influx of Ca^{2+}-into the cytosol, and Ca^{2+}-pumps, which provide the removal of the ions. The specific activation of a set of these channels and pumps lead to the formation of a transient with a specific signature.

Ca^{2+}-influx

Ion channels represent integral membrane proteins that allow diffusion of ions, otherwise impermeable to membranes, along their electrochemical gradient.

Three different Ca^{2+}-channel types were described by biophysical studies, hyperpolarization-activated channels (HACCs), depolarization-activated channels (DACCs) and voltage-independent Ca^{2+}-channels (VICCs) (Fig1.3) (Swarbreck et al. 2013).

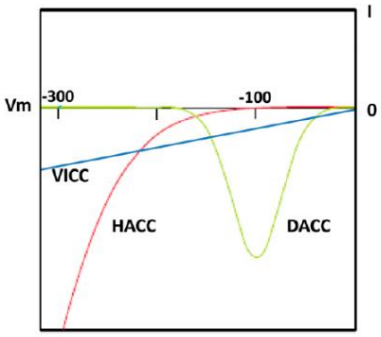

Figure 1.3: Schematic illustration of the effect of plasma membrane voltage (Vm) on the net Ca^{2+} current. The measure was done by "whole cell" patch clamp configuration. Negative current is generated by Ca^{2+} entry in the cytosol.(Swarbreck et al. 2013)

In plants, mechanosensitive Ca^{2+} channels (MCs), belonging to the VICC group, are pivotal in events associated to changes in turgor and to mechanical perturbation (Demidchik and Maathuis. 2007). The external stimuli are converted in electrical Ca^{2+} signals through the activation of this kind of channels. Although these channels are not selective for Ca^{2+}, but studies on mechanical stimulation of chloroplast-avoidance response in ferns, showed that chloroplast movement, following mechanical pressure on protonemal cells, occurs only in presence of Ca^{2+}. Moreover, the inhibition of MCs by Gd^{3+} also lead to the loss of the chloroplastic response (Demidchik and Maathuis. 2007,Sato et al. 2001). These results suggest that, despite the absence of selectivity, these channels seems to be involved in the formation of Ca^{2+}-signalling and they are therefore good candidates for the transduction of a mechanical stimulus into Ca^{2+} transients.

10 MC-like genes were described in *A. thaliana*, based on the homology with bacterial MCs, but very few data exist about their specific functions (McAinsh and Pittman. 2009,Swarbreck et al. 2013).

Although DACCs channels are present in many plant species, including *Maize* and *Arabidopsis*, and expressed in different tissues, this type of channels has received very scant experimental attention. In fact, there are

no direct experimental evidences that correlates DACCs activity to $[Ca^{2+}]_{cyt}$ elevation (Swarbreck et al. 2013).

On the other hand, HACCs are well characterized and several experiments prove their involvement in shaping Ca^{2+} signalling in response to ABA and reactive oxygen species (ROS) in guard cells (Pei et al. 2000). Furthermore, these channels are likely regulated by ROS and phosphorylation: in guard cells of *A. thaliana* NADPH double mutant *RESPIRATORY BURST OXIDASE HOMOLOGUE D* (*atrbohD*) and *F* (*atrbohF*), HACCs activity is impaired, thus linking their activity with the oxidative status of the cell (Kwak et al. 2003). ROS are not the only regulators of these channels, HACCs are responsive to different stimuli like cyclic nucleotides (cAMP and cGMP), status of actin filaments, activity of heterotrimeric G proteins and $[Ca^{2+}]_{cyt}$ itself (Swarbreck et al. 2013,Demidchik and Maathuis. 2007).

The cyclic nucleotide-gated channels (CNGCs) and the Glutamate receptor-like (GLR) (Demidchik and Maathuis. 2007) are channel regulated by the binding with specific ligands, but their activity is often additionally modulated by membrane-voltage.

Cyclic nucleotide gated channel

The first CNCG was identified in Barley (Schuurink et al. 1998), and initial indications of the involvement of CNGC in Ca^{2+}-signalling were produced in carrot cultured cells where cAMP is able to induce Ca^{2+}-influxes (Kurosaki et al. 1994). The putative structure of CNGC consists of four subunits, each of which forms six transmembrane domains in the last predicted alpha helix a calmodulin-binding domain is located (CaMBD) close to the cyclic nucleotide binding domains (CNBD) (Fig 1.4 A) (Dietrich et al. 2010).

20 full-length CNCG genes are present in the *A. thaliana* genome (Maser et al. 2001) and analyses in CNGC mutants revealed implication of these channels in immunity, senescence, salt and heavy metals stress response and in polar growth (Dietrich et al. 2010).

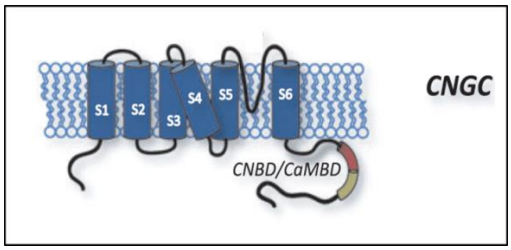

Figure 1.4: putative CNGC structure.

Putative CNGC structure shows six transmembrane domain (S1-S6) and both the N' and C'-terminus in the cytosol. At the C'-terminus there are the cyclic nucleotide mono phosphate (cNMP) binding domain (CNBD in red) and a calmodulin binding domain (CaMBD in yellow). Figure adapted from Dietrich et al. 2010.

The knowledge about function and regulation of the CNGC derived from the study made on two of them (AtCNGC2 AtCNGC10) in heterologous system. Experiments on CNGC2, expressed in HEK cells, revealed that, in presence of high [Ca^{2+}], the CaMBD causes the closure of the channel (Hua et al. 2003). This result was confirmed expressing CNGC10 in the K^+-deficient LB650 *Escherichia coli* strain. The transformed strain was able to grow in the growth medium supplemented with 2mM K^+, lethal for the control. Moreover, experimental evidences demonstrated that a Calmodulin protein (CaM) can regulate the closure of the channel AtCNGC10, in fact, the co-expression of AtCNGC10 and CaM in the bacteria, lead a decrease in cell growth rate upon addition of 1mM of Ca^{2+}, rescued by the addition of 1mM EGTA (Fig1.5) (Li et al. 2005).

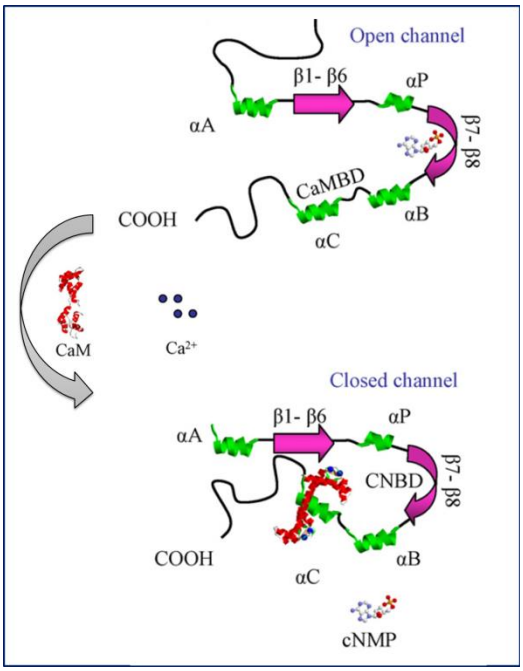

Figure 1.5: working model of plant CNCGs.
When cNMP (ball and stick structure) binds to the CNBD of a CNGC it causes the opening of the channel. Upon elevation of [Ca^{2+}] in the cytosol, the ions binds to the CaM, and Ca^{2+}/CaM binds the CNGC at the CaMBD closing the channel. Figure adapted from Kaplan et al. 2007.

Glutamate receptor-like

Glutamate is a central molecule in cellular metabolism of plants, is involved in nitrogen metabolism and it is a precursor of chlorophyll and γ-amino butyric acid (GABA) biosynthesis (Dietrich et al. 2010).

20 genes encoding for putative GLRs are present in *A. thaliana* genome, which show similarities to the animal ionotropic glutamate receptors (iGLRs) (Lacombe et al. 2001). These channels likely form tetrameric structures and the monomers in prokaryotes show two transmembrane domain and two glutamate-binding site, while the eukaryotic GLRs show a further transmembrane domain, that have a putative regulatory role, and two further extracellular regions that form the agonist binding site (Fig 1.6) (Dietrich et al. 2010,Chiu et al. 2002).

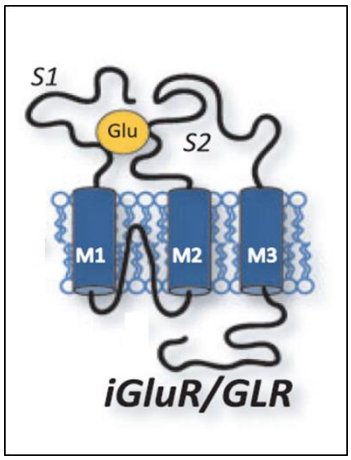

Figure 1.6: The eukaryotic GLR structure
Eukaryotic GLRs show three transmembrane domain (M1,M2 and M3), and 2 cytosolic domain (S1 and S2), where the binding with glutamate (Glu) occurs. Figure adapted from Dietrich et al. 2010.

Glutamate is involved in Ca^{2+}-dependent processes such as root elongation and root branching (Sivaguru et al. 2003). In the root of the *GLR3.1* mutant in rice, processes like cell division, differentiation and programmed cells death are impaired (McAinsh and Pittman. 2009,Sivaguru et al. 2003,Li et al. 2006). Furthermore, the over expression of a radish GLR in *A. thaliana* caused an increase in the Ca^{2+} transient in response to glutamate and enhanced resistance to pathogens (Kang et al. 2006). Moreover, the *A. thaliana glr3.3* mutant showed no Ca^{2+}-transient in response to glutamate (Qi et al. 2006). All together, these results support the involvement of GLRs in shaping Ca^{2+}-transient.

Ca^{2+}-efflux

Since high concentrations of Ca^{2+} are toxic, mechanisms for the extrusion of Ca^{2+} from the cell evolved developed early in the evolution. Two are the principal components involved in Ca^{2+} efflux: high affinity Ca^{2+}-ATPase pumps and high capacity Ca^{2+}-exchangers. The coordination of these two systems allows an extremely fine regulation of $[Ca^{2+}]_{cyt.}$

P-type ATPase

P-type ATPase are a large family of cation and lipid pumps, regulated by a transient phosphorylation of a conserved Aspartate, during the catalysis (Palmgren and Nissen. 2011) .

These pumps show five different structural and functional domains (Fig 1.7): three cytosolic and two transmembrane domain. Two of the cytosolic domains have kinase and phosphatase activity and act on the Aspartate residue present in the third cytosolic domain. The two membrane-embedded domains are involved in the transport of the ligand (Fig 1.7) (Palmgren and Nissen. 2011).

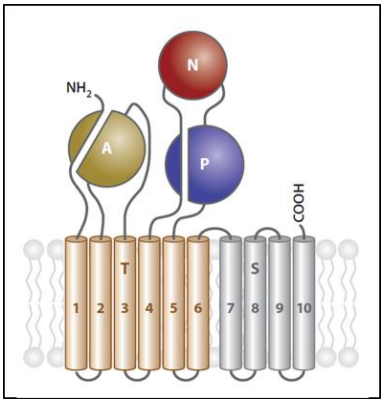

Figure 1.7: schematic representation of the structure of P-type ATPase.

The different domain are marked with capital letters. A: cytosolic kinase domain responsible for the phosphorylation of the P domain. N: cytosolic phosphatase domain that dephosphorylate the P domain. N: cytosolic domain that contain the Asp amino acid residue that is phosphorylated and dephosphorylated by respectively the A and N domains. T and S are the domain involved in the translocation of the specific ligand. Image adapted from Palmgren and Nissen. 2011.

The P-type ATPase family is divided in five subgroups (P_1-P_5) based on the transported ligand (Palmgren and Nissen. 2011).

The P_2-ATPases group that encompass Ca^{2+} pumps, is further divided in P_{2A}-ATPases and P_{2B}-ATPases. The P_{2A} group includes the animal

sarcoplasmic/endoplasmic reticulum Ca^{2+}-ATPase (SERCA) and the plant ER-type Ca^{2+}-ATPase (ECA) in; these pumps have two Ca^{2+} binding sites in their membrane domain both of which have to be occupied before ATP hydrolysis can occur (Moller et al. 2010). The P_{2B} group includes the CaM-regulated plasma membrane Ca^{2+}-ATPase (PMCA) and the autoinhibited Ca^{2+}-ATPase (ACA) (Palmgren and Nissen. 2011), differently from P_{2A}, they have only a single binding site for Ca^{2+} in the membrane domain and, furthermore in these pumps a Ca^{2+} sensor domain is present that allows the pump to change its activation state depending on $[Ca^{2+}]_{cyt}$ (Brini and Carafoli. 2009). Ca^{2+}-ATPases are high-affinity pumps activated by sub-micro molar concentrations of Ca^{2+}. Conversely to animal systems, Ca^{2+}-pump in plant cells are not restricted to one particular organelle or membrane (Fig1.8) (Bonza et al. 2000,Lee et al. 2007,Bonza and De Michelis. 2011).

ECAs

Four different homologues of ECAs are present in the genome of *A. thaliana* that show more than 50% identity to animal SERCA. ECA and SERCA show high affinity for Ca^{2+} (ECA1 $K_{0.5}$ is lower than 30nM), selectivity for ATP as substrate, and sensitivity to the inhibitor cyclopiazonic acid (CPA) (Brini and Carafoli. 2009,Bonza and De Michelis. 2011). Differently plant pumps are insensitive to thapsigargin and are able to transport other divalent cations such as Mn^{2+} and Zn^{2+} (Pittman et al. 2011). ECA isoforms are ubiquitously expressed in *A. thaliana*: ECA1 and ECA3 are the most characterized isoforms. The isoform 1 is localized on the ER, while ECA3 is associated to Golgi compartment and vesicles (Pittman et al. 2011,Mills et al. 2008)

ACAs

The P_{2B}-ATPases have unique regulatory proprieties due to the presence of an auto-inhibitory domain, deactivated by the interaction with calmodulin. In plant ACAs, the auto-inhibitory domain extends

from the N-terminus, while in animal PMCA this domain is located at the C-terminus preceding the first transmembrane domain (Bonza and De Michelis. 2011,Pittman et al. 2011).

ACAs show a lower affinity for Ca^{2+} compare to ECAs, their $K_{0.5}$ is estimated in the range of micro-molar, moreover this class of pumps can use alternative triphosphate nucleotide (ITP or GTP) to catalyze Ca^{2+} transport (Pittman et al. 2011).

The high redundancy of ACA pumps in *A. thaliana* genome (ten ACA homologues) makes difficult to observe specific phenotypes in knockout mutants (Baxter et al. 2003).

A definite phenotype has been described only for ACA9 that is located on the plasma membrane and mainly expressed in pollen. The *aca9* knockout mutant shows a reduced growth of pollen tube and a decreased fertility (Schiott et al. 2004). Ca^{2+}-oscillations in the apical zone of the pollen tube are fundamental indeed in polar growth, and ACA9 likely prevents long-lasting Ca^{2+} overloads in this region, allowing the formation of the correct Ca^{2+}-signature (Pittman et al. 2011,Bose et al. 2011).

Ca^{2+} exchangers

Ca^{2+} exchangers (CAX) are low affinity and high capacity Ca^{2+}-transporters that quickly remove Ca^{2+} from the cytosol in exchange with Na^+, in animal cells, or H^+, in plant cells (Shigaki and Hirschi. 2006). Six isoforms of CAXs are present in *A. thaliana,* and some of them are located to the tonoplast, in fact, compartmentalization in the vacuole is the major route removing Ca^{2+} from the cytosol. CAX activity has also been detected at the level of plasma membrane (Kasai and Muto. 1990) and thylakoid membrane (Fig1.8) (Ettinger et al. 1999), despite this evidences the molecular identity of non-tonoplast CAXs is not been identified so far (Pittman et al. 2011). CAXs are composed by eleven transmembrane domains, a negative-charged cytosolic loop with unknown function, and an N-terminal domain in the cytosol, with regulatory functions. The N-terminal domain has auto-inhibitory functions but, conversely to ACAs, it does not bind CaM (Shigaki and Hirschi. 2006).

In the case of CAX1 regulation likely involves phosphorylation events (Pittman et al. 2002) and interaction with CAX-interacting proteins (CXIP) (Cheng et al. 2004). Moreover, it has been demonstrated, in heterologous system, that CAX1 interacting with CAX3 forms an heteromeric protein complex that induce Ca^{2+} transport (Pittman et al. 2011,Zhao et al. 2009a). Studies on CAX knockout mutants in *A. thaliana* demonstrated these antiporters are involved in stress tolerance and homeostasis (Pittman et al. 2011). In particular, *cax1* and *cax3* mutants show an increase in sensitivity to ABA (Zhao et al. 2009b). Furthermore, *cax1* mutants show increased tolerance to freezing after cold acclimation, supporting a role for CAX1 as negative regulator in cold-acclimation response (Catala et al. 2003), while *cax3* mutants show increased sensitivity to salt stress (Zhao et al. 2009b).

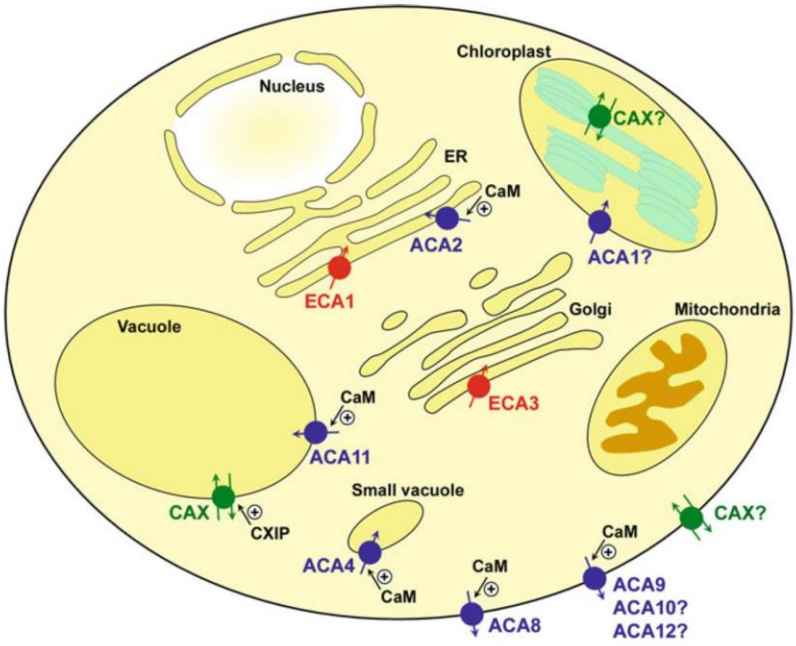

Figure 1.8: Sub-cellular localization of ACA and ECA pumps in the cell of *A. thaliana*.
The P_{2B}-ATPases (ACAs) are shown in blue, the P_{2A}-ATPases (ECAs) are shown in red and the Ca^{2+} exchangers (CAX) are shown in green. Ca^{2+} transport positive regulators of these pumps as calmodulin (CaM) and CAX-interacting proteins (CXIP) are reported in the figure. Putative Ca^{2+} pumps are marked with a question mark (?). Figure adapted from Pittman et al. 2011.

1.4 Ca^{2+}-dynamics in subcellular compartments

The major part of the research on Ca^{2+}-signature and signalling, in plants, focused on cytosolic Ca^{2+}-transient, which has been extensively reviewed (Kudla et al. 2010,Dodd et al. 2010), although Ca^{2+} transients occurs in subcellular compartment and organelles as well (Stael et al. 2012). Vacuole, ER, mitochondria and chloroplasts play a chief role in Ca^{2+}-signature formation. The study of Ca^{2+} signalling of intracellular compartments is still at its infancy, because the tools for a deep comprehension of Ca^{2+}-dynamics in these compartments are available only since few years.

Nuclear Ca^{2+}-dynamics

Ca^{2+} in the nucleus controls major nuclear functions such as transcription and cell division. Three are the principle protein families present in the nucleus of plant cells, that show EF-hand domains: CaMs, the Ca^{2+}-dependent Protein Kinases (CPKs) and the calcineurin-B-like (CBLs) (Mazars et al. 2011).

The existence of an autonomous nuclear Ca^{2+} signalling is a very debated field: the nucleus is physically separated from the cytosol by the Nuclear Envelope (NE), but this barrier contain pores, with a diameter of about 9 nm, that allow the diffusion of ions and molecules up to 60 KDalton (Mazars et al. 2011,Gerace and Burke. 1988). Although Ca^{2+} ions can freely diffuse through the NE, experimental evidences suggest that nuclear Ca^{2+} signalling could be independent from the cytosol (Mazars et al. 2011).

Experiments conducted on BY-2 tobacco cells line expressing the genetically encoded probe aequorin in the cytosol and in the nucleus separately demonstrated that(Pauly et al. 2001) change in osmolarity of the suspension media causes different Ca^{2+} transient in the two compartments (Pauly et al. 2001). On the contrary, in *A. thaliana* guard cells it was demonstrated that hyper and hypo-osmotic stress evoke similar Ca^{2+}-transients in the cytosol and in the nucleus, by the mean of Cameleon probes (Loro et al. 2012).

Further proofs supporting a nuclear specific Ca^{2+} signalling were produced in the previous tobacco cells line, treated with a biological-active derivate of jasmonic acid (jasmonate-isoleucine). This stimulus evoked a Ca^{2+} transient in the nucleus while no transient occurred in the cytosol (Mazars et al. 2011,Walter et al. 2007). Moreover experiments on isolated nuclei in tobacco, revealed their ability to generate autonomous Ca^{2+}-transient in response to several stimuli (Xiong et al. 2004,Xiong et al. 2008,Mazars et al. 2011).

Nuclear envelope likely act as Ca^{2+}-store (Mazars et al. 2011) and several Ca^{2+}-channels and transporters are present on this membrane. Two of them, named Castor and Pollux, are directly involved in Ca^{2+} spiking during symbiosis in roots in *Lotus japonicus* (Chen et al. 2009,Stael et al. 2012).

Peroxisome Ca^{2+}-dynamics

Peroxisomes are involved in several fundamental cellular processes, such as β-oxidation of fatty acid, production of phytohormones and signalling molecules, cellular detoxification and, together with mitochondria and chloroplasts, peroxisomes are involved in photorespiration (Costa et al. 2013).

The first evidence that Ca^{2+} can regulate peroxisomal enzyme activity was obtained, *in vitro,* by studying *A. thaliana* Catalase 3 (AtCAT3) (Yang and Poovaiah. 2002). In presence of Ca^{2+}, CaM binds to and activates AtCAT3 demonstrating, at least *in vitro*, that Ca^{2+}/CaM can down-regulate H_2O_2 levels in plant cells, by stimulating the catalytic activity of the catalase (Yang and Poovaiah. 2002). Ten years later was demonstrated that the Calmodulin-like protein AtCML30 is targeted, through an N-terminal non-cleavable transit peptide, specifically to the peroxisome (Chigri et al. 2012) .

Targeting of the Cameleon probe to the peroxisome lumen allowed quantitative analyses of Ca^{2+} kinetics in this organelle ($[Ca^{2+}]_p$) finding no active accumulation and evidencing that Ca^{2+} passively diffuses in peroxisomes (Costa et al. 2010). This study reported changes in the

$[Ca^{2+}]_p$ *in vivo*, supporting Ca^{2+}-regulation of AtCAT3 in intact cells (Costa et al. 2010). Moreover, an acceleration in the catabolism of H_2O_2 associated to the increase of $[Ca^{2+}]_p$ was observed (Costa et al. 2010). Degradation of H_2O_2 in response to the increase of $[Ca^{2+}]_p$ was correlated to the developmental phase of the plants: in old leaves H_2O_2 scavenging was faster than in young leaves in accordance with the expression of the AtCAT3 gene, suggesting its involvement in this event (Costa et al. 2010).

Vacuolar Ca^{2+}-dynamics

The vacuole is the main storage compartment of Ca^{2+} in plants, in fact, vacuolar Ca^{2+} concentration ($[Ca^{2+}]_{vac}$) is three order of magnitude higher than $[Ca^{2+}]_{cyt}$. The majority of vacuolar-Ca^{2+} is bound to chelating agents like malate, citrate and isocitrate, but free $[Ca^{2+}]_{vac}$ is still very high (0.2 - 5mM) (Conn and Gilliham. 2010). Since the high concentration, it is reasonable to assume that the vacuole contributes to shape cytosolic Ca^{2+}-transient. Supporting this hypothesis, the vacuolar voltage dependent channel TPC1 is regulated by $[Ca^{2+}]_{vac}$ (Dadacz-Narloch et al. 2011), and changes in $[Ca^{2+}]_{vac}$ may have physiological effects (Schönknecht. 2013). Moreover, the *A. thaliana tpc1* mutant show a delay in the long distance Ca^{2+}-transmission along the root, in salt stress response (Choi et al. 2014).

Mitochondrial Ca^{2+}-dynamics

See chapter 2

Endoplasmic reticulum Ca^{2+}-dynamics

See chapter 3

Chloroplastic Ca^{2+}-dynamics

See chapter 4

1.5 Intracellular Ca^{2+} measurement

The spatial and temporal study of intracellular Ca^{2+} is pivotal for studying Ca^{2+}-signature. Fluorescent Ca^{2+}-sensing molecules were widely used for intracellular Ca^{2+}-measurement. These molecules usually have a fast-response kinetic and are particularly indicated when timing is a critical factor (Kao. 1994). On the other hand, this kind of Ca^{2+}-sensors cannot be targeted to specific subcellular compartment and have to be loaded in the cell.

The development of genetically encoded Ca^{2+}-sensors (GECIs) lead to a great improvement in the *in vivo* measurements of this ion. These probes allow monitoring Ca^{2+} dynamics in specific intracellular compartments and they are directly produced by cells. It is possible distinguish two different type of GECIs, the ones based on chemiluminescence (aequorin) and the ones based on the Föster resonance energy transfer (FRET) (McCombs and Palmer. 2008).

Aequorin is a 22 kDa protein that reacts with Ca^{2+} via oxidation of the coelenterazine prosthetic group, this interaction results in emission of light (Bonora et al. 2013). Ca^{2+}-measurement using aequorin is well established in plant, and substantially contributed to the knowledge on Ca^{2+}- signalling. Although an entire toolset of aequorin reporter lines, targeted to different subcellular compartment, is available (Mehlmer et al. 2012). Even though the utility of aequorin system, the main inconvenient of this technique is the low light emission, which involves limits in terms of spatiotemporal resolution. Higher resolution is the major advantage of the FRET based probe.

Genetically encoded probe FRET-based Cameleons

Cameleon probes are the most used FRET-based GECIs in the study of Ca^{2+} dynamics. Two fluorescent proteins are present in these probes: the donor (blue or cyan emitting mutant of the green fluorescent protein) and the acceptor (an enhanced green or yellow emitting GFP). The emission spectrum of the donor and the absorption spectrum of the acceptor overlaps, thus, if the two fluorescent proteins are close enough (1-10nm) and correctly orientated, the fluorescence emitted from the donor is partially absorbed from the acceptor (FRET) that emits itself (Miyawaki et al. 1997).
The two fluorophores, in Cameleon probes, are linked by a Ca^{2+} responsive element (CaM) and by the calmodulin-binding peptide M13. When the $[Ca^{2+}]$ is low, the probe remains in an "open" conformation, where the two fluorophores are distant and the FRET cannot occurs. In this case, the excitation of the donor (e.g 440nm for the CFP) causes an emission at its specific emission wavelength (e.g. 480nm for the CFP) (Fig1.9). Upon Ca^{2+} binding, the probe undergoes a conformational change and the two fluorophores get closer. In this "close" conformation the FRET efficiency increases and the excitation of the donor causes only a partially emission at its specific wavelength, the most of the energy is absorbed by the acceptor fluorophore that in turn emits at its own wavelength (e.g. 535nm for YFP) (Miyawaki et al. 1997) (Fig 1.9). The ratio between acceptor and donor emission upon donor excitation is proportional to $[Ca^{2+}]$. The ratio-metric nature of these probes unties $[Ca^{2+}]$ measurements from focus changes and from the concentration of the probe. The Yellow Cameleon (YC) is the most used FRET GECI, where the FRET pair is composed by yellow (YFP) and cyan (CFP) fluorescents proteins (Miyawaki et al. 1999).

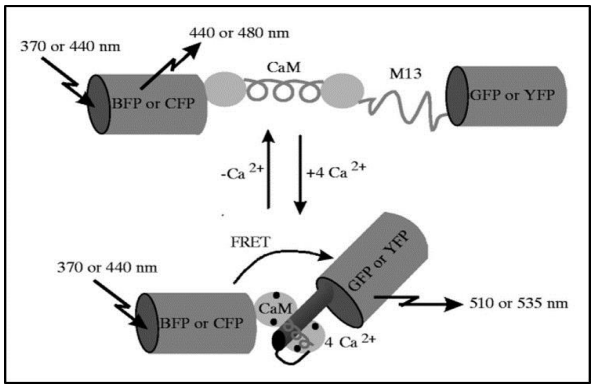

Figure 1.9: Schematic structure of Cameleon probe and its functioning.
The upper part of the picture represent the conformation of the probe at low [Ca^{2+}]. The probe is in the "open" conformation and excitation of the donor (BFP or CFP) causes an emission at its typical wavelength. The lower part of the picture represent the conformation of the probe at higher [Ca^{2+}]. When Ca^{2+} binds to CaM, the M13 domain wraps around the CaM and induces a conformational change. The "close" conformation of the probe enhances FRET between donor and acceptor (GFP or YFP). This increases acceptor emission and lowers donor emission that is adsorbed by the acceptor. The ratio of these two values is proportional to [Ca^{2+}]. Adapted from Miyawaki et al., 1997.

The first family of Cameleon probes suffered problems in the measure of intracellular Ca^{2+} due to the sensitivity of the EYFP to low pH. In order to overcome the pH-sensitivity, EYFP was replaced by normal or circularly permutated citrine or Venus as acceptor (Miyawaki et al. 1999). Moreover, the M13 peptide showed interactions with endogenous CaM. To solve this problem, a new generation of Cameleon was developed, inserting mutations in the M13 peptide to inhibit the binding with endogenous CaM. The resulting sensors belong to the "D-family" (Palmer and Tsien. 2006).
Modifications of the CaM domain lead to a full set of "YC" and "D" Cameleon probes, showing diverse affinity for $Ca^{2+,}$ (Palmer and Tsien. 2006).

Chapter 2:

Mitochondrial Ca^{2+}-dynamics

2.1 Introduction on mitochondrial Ca^{2+}-dynamics

The first evidence of a regulatory role of Ca^{2+} in several mitochondrial metabolic processes was reported more than 20 years ago, when the activity of the pyruvate dehydrogenase was found to be inhibited by calmodulin inhibitors (Miernyk et al. 1987). Only 30 years later a Calmodulin-Like protein (CML30) was observed in mitochondria (Chigri et al. 2012) supporting a Ca^{2+}/Calmodulin dependent signalling in this organelle (Nomura and Shiina. 2014).

Ca^{2+} regulates the activity of several key enzymes located in mitochondrial such as the NADH and NADPH dehydrogenase (NAD(P)H DHs). These enzymes are divided in two family: type I constitute by NADH: quinone oxidoreductase which is a multi-subunit proton pumping and the type II which are non-proton pumping respiratory enzymes. The type II are widely distributed among plants, fungi, many bacteria, and Archaea but not found in animals (Kerscher. 2000,Rasmusson et al. 2004).

In plants, are present several homologues that show different subcellular localization, are expressed in different tissues, and differently expressed upon several kind of stress (Michalecka et al. 2003,Clifton et al. 2005, Elhafez et al. 2006,Carrie et al. 2008,Smith et al. 2011). In particular two of the different homologs of the type II (NDB1 and NBD2), present in the intermembrane space, are positively activated by Ca^{2+} (Geisler et al. 2007).

In *A. thaliana* the members of the Mitochondrial Carrier Family (MCF): APC1, APC2 and APC3 are exclusively located to the mitochondrial membrane, and show an N-terminal EF-hand domain in the intermembrane space (Stael et al. 2011). In yeast and mammalian cells the homologs of these proteins are involved in the Ca^{2+}-dependent import of ATP in the mitochondrial matrix, in plants might have the same role, in fact, plant mitochondrial, release Ca^{2+} under anoxia, and take up Ca^{2+} after the re-oxygenation (Subbaiah et al. 1998). The Ca^{2+} dependent uptake of ATP thought MCF may play a crucial role in maintaining mitochondrial functions under anoxic conditions (Nomura and Shiina. 2014). Mitochondrial Ca^{2+} dynamics and Ca^{2+} influx and efflux from this organelle are object of

intensive studies in the animal field. Animal mitochondria have a role as Ca^{2+} store and in shaping cytosolic Ca^{2+} oscillations. Moreover, small increases of [Ca^{2+}] in the mitochondrial matrix ($[Ca^{2+}]_{mit}$) have a positive effect on ATP production, while a massive increase of $[Ca^{2+}]_{mit}$ is linked to the induction of apoptosis, by aperture of the permeability transition pore (PTP) and the consequent release of apoptotic markers such as cytochrome *c* (Mattson and Chan. 2003,Szabadkai and Duchen. 2008). These events have been observed also in plant cells, although mitochondrial Ca^{2+}-dynamics and transporters are largely unknown (Arpagaus et al. 2002,Tiwari et al. 2002).

Measurements performed in plants expressing mitochondrial GECI probes, observed a resting $[Ca^{2+}]_{mit}$ of approximately 200nM (Logan and Knight. 2003), and that $[Ca^{2+}]_{mit}$ is modified by several stimuli such as cold, osmotic, touch and extracellular ATP. Although mitochondrial Ca^{2+} response seems to be linked to the intensity of the cytosolic Ca^{2+}-transient, they showed peculiar Ca^{2+}-signature(Logan and Knight. 2003,Loro et al. 2012). Thus, Ca^{2+} dynamics in mitochondria are likely modulated in an autonomous way. Ca^{2+} transporters of this organelle are poorly described and the molecular identity of the Ca^{2+}-uniporter (MCU) was discovered, in mammalian mitochondria, only recently (De Stefani et al. 2011). *A. thaliana* genome contains six homologs of this 40KDalton MCU protein, five of them are highly predicted to localize to the mitochondria and their expression profile analyzed by GENEVESTIGATOR suggests a differential tissue expression (Stael et al. 2012). The MCU is a low affinity Ca^{2+} channel and its function is regulated by an EF-protein called MICU1 (Perocchi et al. 2010), for this regulatory protein *A. thaliana* presents only one homolog in its genome (Stael et al. 2012). In mammalian mitochondria the presence of an high affinity Ca^{2+} transporter, the Ca^{2+}/H^{+} antiporter LETM1 (Leucine zipper-EF hand-containing Transmembrane), is also reported (Jiang et al. 2009). LETM1-like proteins were observed in *A. thaliana* mitochondria (AtLETM1 and AtLETM2), and resulted lethal if simultaneously inactivated (Zhang et al. 2012), but, a direct demonstration of their Ca^{2+} antiport activity is still lacking.

In *A. thaliana*, the presence of homologues of all the animal proteins involved in mitochondrial Ca^{2+} dynamics, raises the interesting possibility of translating findings produced in mammalian directly into plants (Stael et al. 2012), but further studies are needed to confirm this hypothesis.

The development of a tool allowing high-resolution *in vivo* imaging of Ca^{2+} in plant mitochondria is the starting point to clarify the mechanisms of Ca^{2+} transport in this organelle. In the papers reported in this chapter, the generation of *A. thaliana* lines harboring Cameleon probes in the mitochondrial matrix is presented. The probes YC3.6 and D3cpVenus were compared on the basis of their efficiency in monitoring Ca^{2+} dynamics in the mitochondrial matrix. The YC3.6 resulted the best choice for this kind of analysis, and Ca^{2+} transients were analyzed at single cell and entire organ level, revealing a unique mitochondrial Ca^{2+} dynamic in response to cytosolic Ca^{2+} increase.

2.2 Targeting of Cameleons to various subcellular compartments reveals a strict cytoplasmic/ mitochondrial Ca^{2+} handling relationship in plant cells

the plant journal

SEB Society for Experimental Biology

The Plant Journal (2012) doi: 10.1111/j.1365-313X.2012.04968.x

TECHNICAL ADVANCE

Targeting of Cameleons to various subcellular compartments reveals a strict cytoplasmic/mitochondrial Ca^{2+} handling relationship in plant cells

Giovanna Loro[1], Ilaria Drago[2], Tullio Pozzan[2,3], Fiorella Lo Schiavo[1], Michela Zottini[1,*] and Alex Costa[1,*,†]

[1]*Dipartimento di Biologia, Università degli Studi di Padova, Via U. Bassi 58/B, 35131 Padova, Italy,*

[2]*Dipartimento di Scienze Biomediche e Istituto di Neuroscienze CNR, Università degli Studi di Padova, Viale G. Colombo 3, 35121 Padova, Italy, and*

[3]*Istituto Veneto di Medicina Molecolare, Via Orus 2, 35129 Padova, Italy*

Received 22 July 2011; revised 11 February 2012; accepted 21 February 2012.

*For correspondence (e-mails alex.costa@unimi.it or michela.zottini@unipd.it).

†Present address: Dipartimento di Biologia, Università degli Studi di Milano, Via G. Celoria 26, 20133 Milano, Italy.

SUMMARY

Here we describe use of a mitochondrial targeted Cameleon to produce stably transformed Arabidopsis plants that enable analyses of mitochondrial Ca^{2+} dynamics *in planta* and allow monitoring of the intra-mitochondrial Ca^{2+} concentration in response to physiological or environmental stimuli. Transgenic plants co-expressing nuclear and mitochondrial targeted Cameleons were also generated and analyzed. Here we show that mitochondrial Ca^{2+} accumulation is strictly related to the intensity of the cytoplasmic Ca^{2+} increase, demonstrating a tight association between mitochondrial and cytoplasmic Ca^{2+} dynamics. However, under all experimental conditions, mitochondrial Ca^{2+} dynamics were substantially different from those monitored in the cytoplasm, demonstrating that mitochondria do not passively sense cytosolic Ca^{2+}, but actively modulate the intra-mitochondrial level of the cation. In particular, our analyses show that the kinetics of Ca^{2+} release from mitochondria are much slower than in the cytoplasm and nucleus. The mechanisms and functional implications of these differences are discussed.

Keywords: plant mitochondria, Cameleon, Ca^{2+}, imaging analyses, guard cells, root tip, *Arabidopsis thaliana*, technical advance.

INTRODUCTION

Mitochondria are key organelles that are involved in many aspects of cell functions from plants to humans, ranging from cell metabolism to stress responses and programmed cell death regulation (McAinsh and Pittman, 2009; Contreras *et al.*, 2010).

Despite the pronounced metabolic connection between mitochondria and other cellular compartments in plants, little is known regarding the signals that mediate these inter-communications or coordination of the activities by signaling molecules. Many factors have been suggested to be involved in retrograde signaling control, including reactive oxygen species, cellular carbohydrate status, mitochondrial electron transfer chain reduction state (Yoshida *et al.*, 2010) and calcium (Ca^{2+}) (Subbaiah *et al.*, 1998).

As far as Ca^{2+} is concerned, it is one of the most versatile second messengers in all eukaryotic organisms. In plants, Ca^{2+} is involved in nearly all aspects of development and participates in many regulatory processes (Dodd *et al.*, 2010; Kudla *et al.*, 2010). Ca^{2+} signals take the form of transient increases in the cytosolic free Ca^{2+} concentration ($[Ca^{2+}]_c$) arising in the cytosol as a result of fluxes from the external medium and subcellular compartments (Hetherington and Brownlee, 2004; Dodd *et al.*, 2010). Cytoplasmic Ca^{2+} signal specificity is guaranteed by a decoding mechanism based on the amplitude and/or frequency of the Ca^{2+} transients: series of repetitive Ca^{2+} oscillations are commonly referred to as 'Ca^{2+} signatures' (McAinsh and Pittman, 2009).

In plants, *in vivo* analysis of the intra-mitochondrial Ca^{2+} concentration, $[Ca^{2+}]_m$, is still in its infancy (Logan and Knight, 2003), mainly due to technical difficulties in measuring changes in the mitochondrial free Ca^{2+} concentration. For a long time, it was only possible to measure $[Ca^{2+}]_m$ in isolated mitochondria loaded with Ca^{2+}-specific indicators (Zottini and Zannoni, 1993). The introduction of genetically encoded Ca^{2+} indicators (e.g. aequorin and GFP-based Ca^{2+} probes), and their detection either by photon emission measurements or by fluorescence microscopy, have revolutionized the detection and visualization of intracellular Ca^{2+} dynamics in living plants. The first tools developed for *in vivo* intracellular analyses of Ca^{2+} dynamics in plants were based on use of aequorin targeted to the cytoplasm (Knight *et al.*, 1991), nucleus (van Der Luit *et al.*, 1999), chloroplasts (Johnson *et al.*, 1995), tonoplast (Knight *et al.*, 1996) and mitochondria (Logan and Knight, 2003). In particular, *in vivo* analyses of mitochondrial Ca^{2+} dynamics showed that several stress stimuli, including osmotic stress, induced $[Ca^{2+}]_m$ increases with dynamics that were different from those in the cytoplasm (Logan and Knight, 2003). Experiments performed using aequorin produce very reliable data, but reflect the response of a population of cells or plants, and intercellular heterogeneity could not be investigated.

In order to improve cellular and subcellular resolution, use of other Ca^{2+} sensors has been pursued in recent years, and, among the genetically encoded Ca^{2+} indicators, the most frequently used in plants are Cameleons. Cameleons are fluorescence resonance energy transfer (FRET)-based indicators in which two GFP variants, CFP and YFP (or circularly permuted variants of YFP) are linked together by the Ca^{2+}-binding protein calmodulin and the calmodulin-binding peptide M13. Binding of Ca^{2+} to the Ca^{2+}-responsive elements alters the efficiency of FRET, allowing a quantitative measurement of Ca^{2+} dynamics. In recent years, Cameleon variants have been developed (Palmer and Tsien, 2006; Palmer *et al.*, 2011) with improved fluorescence, greater changes in FRET upon Ca^{2+} binding, and a broad range of Ca^{2+} affinities. Cameleons have been widely used to monitor $[Ca^{2+}]$ in the cytoplasm of plant cells (Allen *et al.*, 1999; Swanson *et al.*, 2011). They have also been targeted to the cytoplasm/nucleus (Allen *et al.*, 1999; Monshausen *et al.*, 2008; Yang *et al.*, 2008; Krebs *et al.*, 2012), nucleus (Sieberer *et al.*, 2009; Krebs *et al.*, 2012), endoplasmic reticulum (Iwano *et al.*, 2009), plasma membrane (Krebs *et al.*, 2012) and peroxisomes (Costa *et al.*, 2010).

Here we report data on *in vivo* analyses of Arabidopsis transgenic plants harboring the genetically encoded Ca^{2+} probe Cameleon YC3.6 specifically targeted to the mitochondrial matrix. By use of external stimuli, it was possible to monitor mitochondrial Ca^{2+} dynamics in guard and root tip cells. Moreover, by crossing plants expressing Cameleons targeted to the nucleus or mitochondria, we were able to monitor Ca^{2+} dynamics simultaneously in these two subcellular compartments *in vivo*.

RESULTS AND DISCUSSION

Construction of the YC3.6 Cameleon targeted to mitochondria

In order to analyze Ca^{2+} dynamics in mitochondria, two main issues must be addressed: (i) choice of the most appropriate Ca^{2+} sensor, and (ii) precise targeting of the sensor to the mitochondrial matrix.

Plant mitochondria are highly dynamic organelles that display very fast movements, morphological changes (Zottini *et al.*, 2006) and frequent fusion/fission events (Logan, 2010). Thus use of a ratiometric Ca^{2+} probe/sensor, such as Cameleon, is mandatory (Palmer and Tsien, 2006; Palmer *et al.*, 2006; Iwano *et al.*, 2009; Costa *et al.*, 2010; Krebs *et al.*, 2012). After testing a few alternative Cameleons, we eventually concentrated on the YC3.6 variant (Nagai *et al.*, 2004). YC3.6 has been already used in plant cells for Ca^{2+} monitoring in the cytoplasm, nucleus and plasma membrane (Monshausen *et al.*, 2008; Yang *et al.*, 2008; Costa *et al.*, 2010; Rincón-Zachary *et al.*, 2010; Swanson *et al.*, 2011; Krebs *et al.*, 2012). YC3.6 appeared to be particularly suitable for monitoring mitochondrial Ca^{2+} in plant cells *in vivo*, because of its very large changes in fluorescence upon Ca^{2+} binding, pH stability and an *in vitro* K_d for Ca^{2+} (0.25 μM) (Nagai *et al.*, 2004; Palmer and Tsien, 2006) that is close to the expected $[Ca^{2+}]_m$ in non-stimulated cells (Zottini and Zannoni, 1993; Logan and Knight, 2003).

In order to target YC3.6 to plant mitochondria matrix, we fused the mitochondrial targeting sequence from subunit VIII of human cytochrome *c* oxidase to the N-terminal end of the probe. This sequence has been shown to be highly efficient in targeting other Cameleons to mammalian

Figure 1. The 4mt-YC3.6 Cameleon probe is ubiquitously expressed in Arabidopsis seedlings.
(a–f) CLSM analyses of leaf cells expressing the 4mt-YC3.6 probe. cpVenus signal was detected in punctuate structures in epidermal (EC), stomata (GC) and mesophyll cells (MC).
(a, d) Chlorophyll fluorescence.
(b, e) cpVenus Cameleon fluorescence.
(c, f) Overlaid images of chlorophyll, cpVenus and transmitted light.
(g–i) cpVenus signal was detected in hypocotyl cells in all cell layers. (g) Chlorophyll fluorescence. (h) cpVenus Cameleon fluorescence. (i) Overlaid images of chlorophyll, cpVenus and transmitted light.
(j–m) In root cells, 4mt-YC3.6 probe was present in all cell types of the root mature zone (j, k), including root epidermal cells (REC) and root hair cells (RH). In the tip region (l, m) the probe was present in the meristematic (MZ), transition (TZ) and elongation zones (EZ). (j, l) cpVenus Cameleon fluorescence. (k, m) Overlaid images of cpVenus and transmitted light.

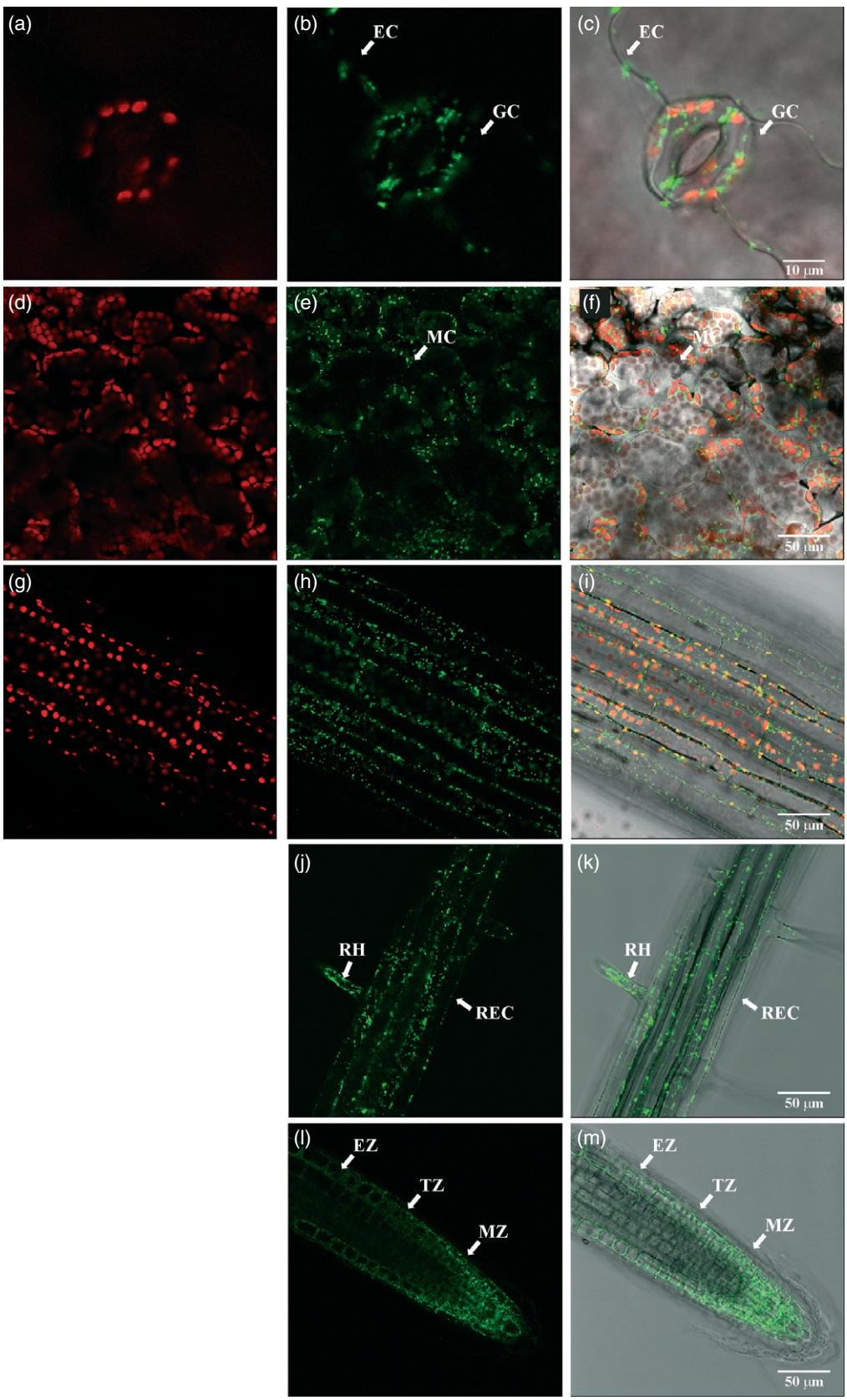

mitochondria, especially when repeated four times (4mt) (Filippin *et al.*, 2005; Palmer *et al.*, 2006). To ensure ubiquitous expression of the probe, YC3.6 was placed under the control of a single CaMV 35S promoter (Figure S1), and the entire cassette was inserted into the pGreen 0179 binary vector. This vector confers hygromycin resistance to transgenic plants, but the Cameleon cassette can be easily transferred to other pGreen backbones (e.g. pGreen 0029 or pGreen 0229) (Hellens *et al.*, 2000) by a one-step subcloning procedure (see Experimental Procedures and Figure S2) in order to change the antibiotic used for the plant selection. The construct generated was renamed 4mt-YC3.6 (Figure S1).

Generation of Arabidopsis transgenic plants expressing mitochondria-targeted YC3.6

The construct 4mt-YC3.6 was introduced into Arabidopsis plants (Columbia ecotype) by the floral-dip method (Clough and Bent, 1998), and eight independent transgenic lines were obtained. In order to verify ubiquitous expression of the probe, we performed confocal laser scanning microscopy (CLSM) analyses in 7-day-old Arabidopsis seedlings (Figure 1). Figure 1(a–f) shows expression of the 4mt-YC3.6 probe in leaves, where fluorescence was clearly detected in epidermal, stomata (Figure 1a–c) and mesophyll cells (Figure 1d–f). The signal was also present in cells of the hypocotyl (Figure 1g–i), mature root cells (Figure 1j,k), including root hairs and in all the cell types present in the root tip region: meristematic cells, transition and elongation zones (Figure 1 l-m)). We did not observed silencing effects when using this construct.

In order to confirm the correct mitochondrial localization of 4mt-YC3.6, we performed co-localization experiments by staining 4mt-YC3.6-expressing root tissues (Figure 2a) with the tetramethylrhodamine methyl ester dye (TMRM), a potentiometric cationic probe (Figure 2b) (Zottini *et al.*, 2006). Fluorescence of 4mt-YC3.6 perfectly merged with the TMRM signal of stained cells (Figure 2c). In order to determine whether the presence of YC3.6 in the mitochondria could have undesirable effects on them, we analyzed independently, by means of CLSM, mitochondria of transgenic plants (Figure 2d,e) and mitochondria of wild-type plants stained with TMRM (Figure 2f,g). Mitochondria morphology and distribution appeared comparable in the analyzed tissues of the two lines. Moreover, time-lapse analyses, performed in leaf epidermal cells of 4mt-YC3.6 transgenic (Movie S1) and wild-type (Movie S2) lines, showed typical plant mitochondria motility (Logan, 2010).

Osmotic stress induces Ca^{2+} transients in the cytoplasm, nucleus and mitochondria of Arabidopsis leaf cells

In order to evaluate the functionality of 4mt-YC3.6 localized to mitochondria, we performed a series of experiments in guard cells, which are often used as model system for single-cell analyses of Ca^{2+} dynamics (Allen *et al.*, 1999; Hetherington and Brownlee, 2004; Costa *et al.*, 2010; Kim

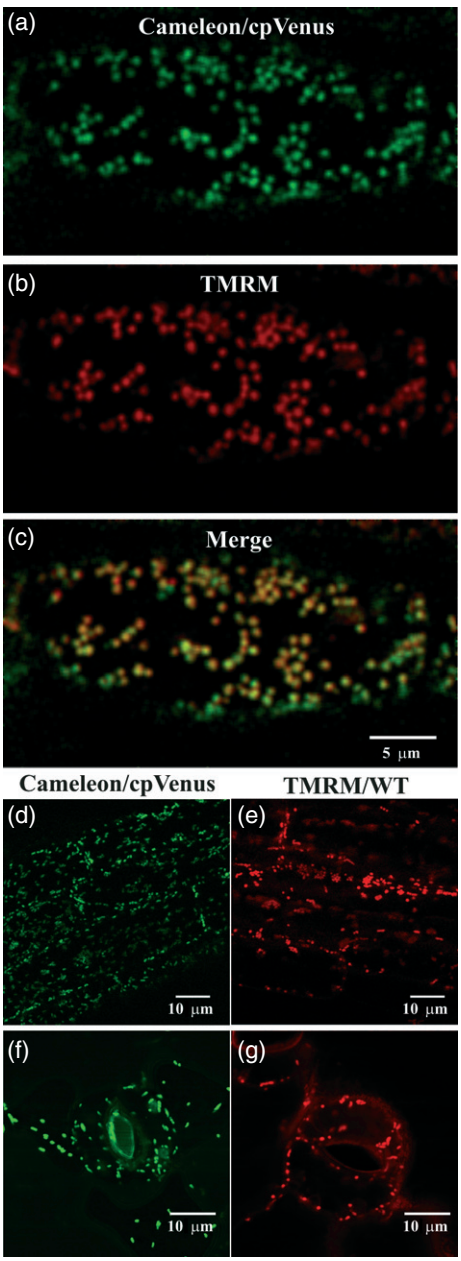

Figure 2. The 4mt-YC3.6 probe localizes to mitochondria.
Sequential CLSM acquisitions indicate co-localization of the cpVenus and TMRM fluorescences in root cells. The correspondence of the TMRM emitted signal with the Cameleon cpVenus signal demonstrates correct mitochondrial localization of the probe.
(a–c) Root cell expressing 4mt-YC3.6 stained with TMRM potentiometric probe. (a) cpVenus Cameleon fluorescence. (b) TMRM fluorescence. (c) Merged image of (a) and (b).
(d–g) Comparison of mitochondria from plants expressing the YC3.6 Cameleon and wild-type plants stained with TMRM. (d) cpVenus Cameleon fluorescence in mature root cells. (e) TMRM fluorescence in mature root cells. (f) cpVenus Cameleon fluorescence in guard cells. (g) TMRM fluorescence in guard cells.

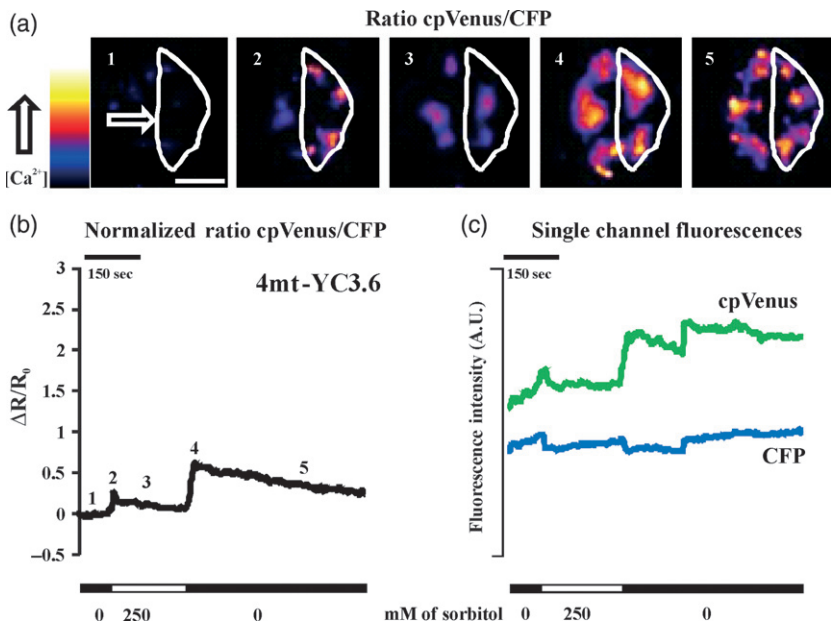

Figure 3. Osmotic stress induces mitochondrial Ca^{2+} accumulation in guard cells.
Cells were bathed in 5 mM KCl, 10 mM MES, 50 μM Ca^{2+}, pH 6.15, and perfused with 250 mM sorbitol at the indicated time. When the osmoticum was removed, there was a clear increase in the volume of guard cells. Mitochondrial Ca^{2+} uptake followed both addition and removal of the osmoticum, with a subsequent slow $[Ca^{2+}]$ decrease. Scale bar = 10 μm.
(a) Ratiometric images from one stomatal pair expressing the 4mt-YC3.6 probe and challenged by osmotic stress.
(b) Normalized cpVenus/CFP ratios, reported as $\Delta R/R_0$, corresponding to the guard cells marked with an arrow. The ratio trace represents the response of all mitochondria present in the outlined guard cell.
(c) Single wavelength emissions (540 and 480 nm) used for the ratio measurements shown in (b).

et al., 2010). We specifically assayed guard cells undergoing osmotic stress, a condition known to induce substantial and reproducible cytoplasmic Ca^{2+} transients in plant cells (Knight *et al.*, 1998; Logan and Knight, 2003). In parallel, we monitored Ca^{2+} dynamics in the cytoplasm and nucleus. For this second group of experiments, we used Arabidopsis transgenic plants expressing YC3.6 targeted to the cytoplasm (NES-YC3.6) or the nucleus (NLS-YC3.6) (Krebs *et al.*, 2012).

First we tested the effect of 250 mM sorbitol (as osmoticum) on pre-opened stomata (see Data S1) in leaf epidermal strips (Costa *et al.*, 2010) of 4–5-week-old 4mt-YC3.6 Arabidopsis plants (Figure 3) using a simple protocol. Guard cells bathed in standard solution (see Data S1) were first challenged with 250 mM sorbitol and then returned to the standard normo-osmotic medium. Both addition of sorbitol (hyper-osmotic stress) and removal of sorbitol (hypo-osmotic stress) caused an increase in the 540/480 nm fluorescence emission ratio $\Delta R/R_0$ Δ(R/R$_0$. ratio at time ''t_n''-ratio at time ''t_0''/ratio at time ''t_0''), which is proportional to the $[Ca^{2+}]$. Pseudocolor ratio images of a typical cell (taken at the times indicated in Figure 3b) are shown in Figure 3(a). The kinetics of the $\Delta R/R_0$ changes for the same cell are shown in Figure 3(b). A rapid $[Ca^{2+}]_m$ increase was induced by hyper-osmotic stress, followed by a slow $[Ca^{2+}]_m$ decrease toward the initial basal level. Similar behavior was observed after sorbitol removal (hypo-osmotic stress) (Figure 3a,b), but the mitochondria Ca^{2+} peak was larger (see also Table 1). The $\Delta R/R_0$ for the second peak was 0.48 ± 0.16, a value that falls in the probe linear range response in mitochondria ($\Delta R_{max}/R_0$ 0.73 ± 0.14), as determined in experiments performed in permeabilized leaf epidermal cells (see Experimental Procedures). Figure 3(c) shows that, after application of hypo- and hyper-osmotic stresses, the fluorescence emissions at 540 nm (cpVenus) and 480 nm (CFP) mostly showed anti-parallel behavior (Figure 3c). In some cases (e.g. Figure 3c), a movement artifact occurred, resulting in a parallel change in the fluorescence intensity at both wavelengths. However, this artifact is corrected by the ratiometric values, which show no change. Other possible artifacts, for example due to focus changes associated with stomata morphological modification after release of the osmotic stress (Figure 3a), are similarly corrected by the ratiometric calculation (Rudolf *et al.*, 2004, and data not shown).

Table 1 Values of $\Delta R/R_0$ (means ± SD) corresponding to the first and second Ca^{2+} peaks measured in the nucleus, cytoplasm and mitochondria after addition and removal of 250 mM of sorbitol

	First peak		Second peak	
	$\Delta R_{max}/R_0$	$T/2$ (sec)	$\Delta R_{max}/R_0$	$T/2$ (sec)
NLS-YC3.6	2.73 ± 0.82	8.64 ± 2.34	2.74 ± 0.55	13.5 ± 4.74
NES-YC3.6	1.86 ± 0.28	5.91 ± 3.02	2.05 ± 0.29	14.5 ± 4.97
4mt-YC3.6	0.2 ± 0.1	31.08 ± 10.84	0.48 ± 0.16	199.22 ± 34.74

$T/2$ corresponds to the time at which $[Ca^{2+}]$ was halved in the various compartments.

The same osmotic stress assayed in 4mt-YC3.6 plants was then repeated using Arabidopsis plants expressing the YC3.6 probe in the cytoplasm and nucleus (Figure 4a,d). Both $[Ca^{2+}]_c$ and the nuclear Ca^{2+} concentration ($[Ca^{2+}]_n$) showed qualitatively a very similar behavior (Figure 4b,e): a steep $[Ca^{2+}]$ increase was evoked by addition of sorbitol, followed by a fast decrease with complete recovery of the basal $[Ca^{2+}]$ in <20 sec (Table 1). In the cytoplasm, the first peak observed after hyper-osmotic stress was less intense

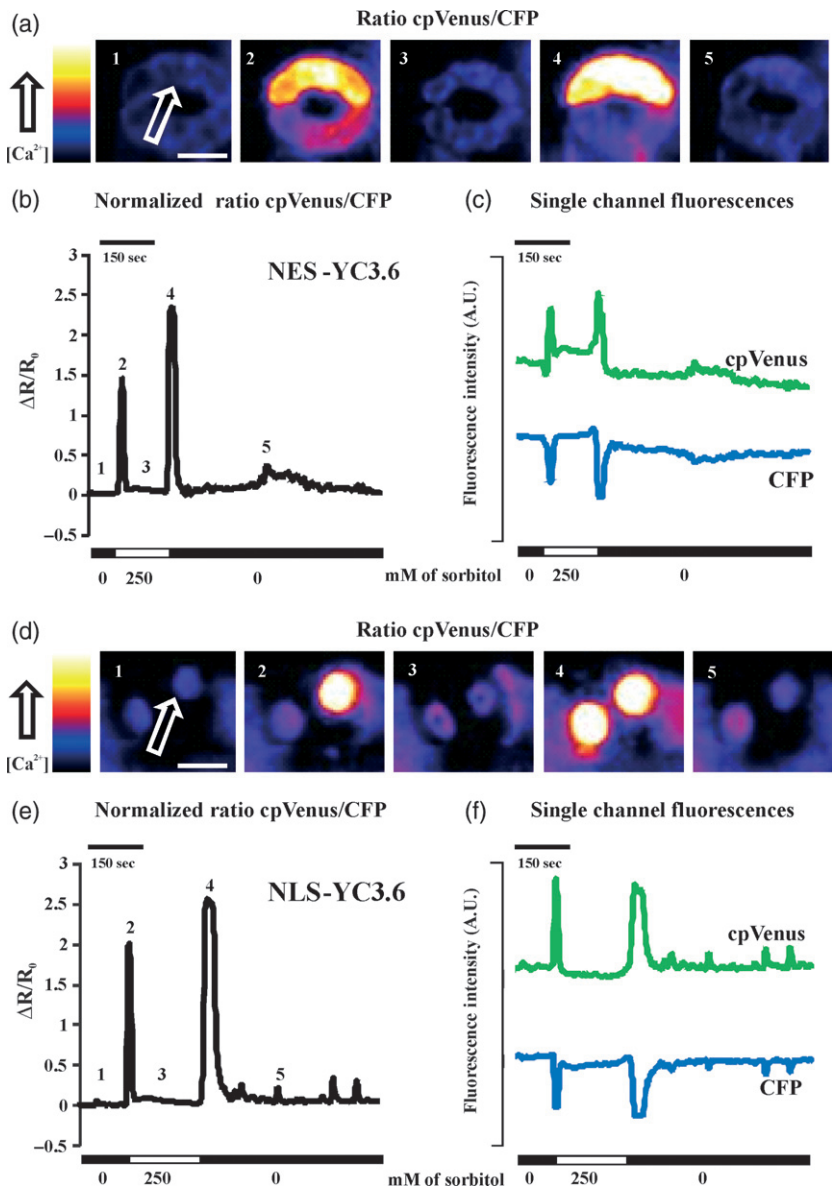

Figure 4. Osmotic stress induces cytoplasmic and nuclear Ca^{2+} transients in guard cells.
Cells were treated as described in Figure 3. The cytoplasmic and nuclear Ca^{2+} uptake induced by addition and removal of osmoticum was followed by fast $[Ca^{2+}]$ recovery. Scale bar = 10 μm.
(a) Ratiometric images from one stomatal pair expressing the NES-YC3.6 probe and challenged by osmotic stress.
(b) Normalized cpVenus/CFP ratio, reported as $\Delta R/R_0$, corresponding to the guard cell indicated by an arrow.
(c) Single wavelength emissions (540 and 480 nm) used for the ratio measurements shown in (b).
(d) Ratiometric images from one stomatal pair expressing the NLS-YC3.6 probe and challenged by osmotic stress.
(e) Normalized cpVenus/CFP ratio, reported as $\Delta R/R_0$, corresponding to the guard cell indicated by an arrow.
(f) Single wavelength emissions (540 and 480 nm) used for the ratio measurements shown in (e).

than that induced by the hypo-osmotic one (as in mitochondria), but the amplitudes of the two peaks were not statistically different in the nucleus (Table 1). The absolute amplitude of the peak in the cytosol was smaller than that in the nucleus. However, the kinetics of the $[Ca^{2+}]$ decreases were not significantly different in the two compartments. Thus, in guard cells subjected to osmotic stress, the responses in terms of the $\Delta R/R_0$ for cytoplasm and nuclear dynamics are similar, but not identical. The reasons for the larger peaks in the nucleus compared to the cytoplasm are presently unknown, and may depend either on a real difference in the $[Ca^{2+}]$ of the two compartments or different behavior of the probe in the two environments. In kinetic terms, however, it can be concluded that, at least for the osmotic stress stimuli investigated here, the nuclear Ca^{2+} dynamics mirror the cytosolic dynamics. This result is consistent with what is now generally agreed for various mammalian cell types (Rizzuto and Pozzan, 2006; Giacomello *et al.*, 2010), but is partially in contrast with previous data in plants (Mazars *et al.*, 2011, and references therein). The osmotic stress-induced Ca^{2+} increases measured here depend on Ca^{2+} influx from the extracellular environment, as the presence of 500 μM EGTA in the bath solution prevented any change in $[Ca^{2+}]$ in the various compartments (data not shown).

Two major differences were noted between the increases in $\Delta R/R_0$ in mitochondria and those in the cytoplasm and nucleoplasm: (i) the amplitude of the $\Delta R/R_0$ in the mitochondria is much smaller, and (ii) while accumulation of Ca^{2+} in the mitochondria is similar to that in the other two compartments, the return to basal level is much slower in

mitochondria (Figures 3 and 4, and Table 1). With regard to the difference in amplitudes, it should be stressed that the dynamic range of the YC3.6 within mitochondria ($\Delta R_{max}/R_0$ 0.73 $\pm$ 0.14) is much smaller than that in the nucleus ($\Delta R_{max}/R_0$ 3.31 $\pm$ 0.46), as assessed in permeabilized leaf epidermal cells (see Experimental Procedures). With regard to the prolonged Ca^{2+} retention in mitochondria, the simplest explanation is that the Ca^{2+} efflux mechanism of the organelles in plants is intrinsically slow, and the Ca^{2+} released from mitochondria is either rapidly sequestered by other compartments such as the endoplasmic reticulum and/or extruded into the external medium without leading to a detectable cytoplasmic Ca^{2+} increase.

Finally, we observed that only half of the cells responded to the addition of sorbitol by a Ca^{2+} increase in all compartments, but a Ca^{2+} increase was observed in all cells analyzed after removal of sorbitol. One explanation could be that the turgor reached by guard cells during stomata pre-opening differed between cells, and the most turgid ones did not respond to hyper-osmotic stress. However, removal of sorbitol was always perceived, probably through activation of channels, such as stretch-activated channels, that mediate Ca^{2+} entrance after being specifically stimulated by hypotonic conditions, as reported for *Vicia faba* (Zhang *et al.*, 2007).

The experiments here reported were performed in guard cells, but a similar behavior was observed in epidermal cells in response to osmotic treatment (particularly sorbitol removal), with an increase in Ca^{2+} concentration in the cytoplasm, nucleoplasm and mitochondria. In all cells of the imaged leaf (Movie S3), epidermal cells expressing NES-YC3.6 responded with a series of cytoplasmic Ca^{2+} oscillations. In epidermal cells, the dynamics of $[Ca^{2+}]_m$ were very similar to what was observed in guard cells, with two rapid Ca^{2+} increases after addition and removal of sorbitol, followed by a slow decrease in $[Ca^{2+}]_m$ (Movie S4). However, no significant Ca^{2+} oscillations were observed in mitochondria.

Plant cells co-expressing nuclear and mitochondrial targeted Cameleons allow simultaneous analyses of Ca^{2+} dynamics in two compartments of guard cells

The measurements reported in Figure 3 and 4 were performed in parallel in cells from different transgenic plants, thus preventing direct comparison between the kinetics of mitochondrial and cytoplasmic Ca^{2+} signals in the same cell. Crossing plants expressing a cytosolic Cameleon and a mitochondrial Cameleon cannot resolve this issue, as the two signals cannot be spatially resolved. However, experiments performed in guard cells exposed to osmotic stresses demonstrate that the Ca^{2+} transients in nucleoplasm and cytoplasm are kinetically similar, suggesting that the nuclear Ca^{2+} signature mirrors what occurs in the cytoplasm. The mitochondrial and nuclear signals are spatially segregated and can be independently monitored in the same cell (Giacomello *et al.*, 2010). We thus crossed Arabidopsis plants expressing the Cameleon in the nucleus (NLS-YC3.6) with plants expressing the Cameleon in mitochondria (4mt-YC3.6). In order to determine whether the two probes were simultaneously expressed in different tissues/organs, we performed CLSM analyses in 7-day-old Arabidopsis seedlings (Figure S3). As observed with parental plants, the expression of YC3.6 present in both, nuclei and mitochondria, was observed in epidermal cells, stomata (Figure S3a–c) and mesophyll cells (Figure S3d–f) of young leaves. The two probes were also co-expressed in other tissues/organs, such as hypocotyl (Figure S3g–i), root and the root tip (Figure S3j–m).

To monitor the Ca^{2+} dynamics in the two compartments, we subjected leaf epidermal strips of plants, expressing Cameleons in both compartments, to the osmotic stress protocol described in Figures 3 and 4. Pre-opened stomata were perfused with 250 mM of sorbitol, and then the osmoticum was removed (Figure 5a,b). The osmotic stress induced both nuclear and mitochondria Ca^{2+} transients, whose dynamics mimicked those observed in the respective single transgenic lines (Figures 3b and 4e). Only half of the analyzed cells showed Ca^{2+} transients in response to hyper-osmotic stress, whereas all cells responded to hypo-osmotic stress. Moreover, a mitochondrial Ca^{2+} transient was observed only if there was a corresponding Ca^{2+} transient at the level of the nucleoplasm/cytoplasm: in no cells did mitochondria accumulate Ca^{2+} in the absence of a Ca^{2+} increase in the nucleoplasm/cytoplasm (Figure 5b, after hyper-osmotic stress). Application of osmotic stress in the presence of the Ca^{2+} chelator EGTA (500 μM) in the bath solution completely abolished both nucleoplasm/cytoplasm and mitochondrial Ca^{2+} transients (data not shown).

Mitochondria Ca^{2+} transient analyses in Arabidopsis root tips evoked by eATP

In order to study mitochondrial Ca^{2+} handling in a more physiological context, we analyzed the response in the root tip, an organ that integrates various environmental stimuli, often mediated by Ca^{2+}, to direct root growth (Fasano *et al.*, 2002). Extracellular ATP (eATP) has recently been recognized as a key signaling molecule in plant roots (Roux and Steinebrunner, 2007; Tanaka *et al.*, 2010a) that is able to inhibit growth and cause root curling in Arabidopsis seedlings (Tang *et al.*, 2003). In particular, Tanaka *et al.* (2010b) showed that Arabidopsis root cells responded to eATP with a large and rapid cytoplasmic Ca^{2+} increase. Recent data strongly suggest that the eATP response is mediated by ATP receptors located in the plasma membrane of root cells (Demidchik *et al.*, 2009), although their molecular identity is still unknown.

We studied the reciprocal interaction in terms of Ca^{2+} handling between the cytoplasm, nucleus and mitochondria in response to eATP, performing the experiments in parallel using independent plants expressing YC3.6 targeted to the

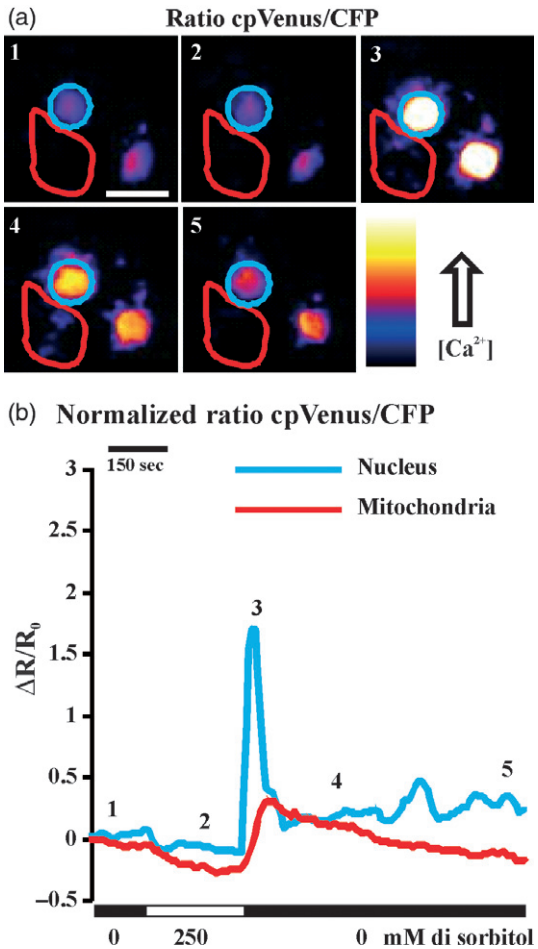

Figure 5. Analyses of Ca^{2+} dynamics in mitochondria and nucleus in guard cells challenged by osmotic stress.

Guard cells expressing both Cameleons were bathed in 5 mM KCl, 10 mM MES, 50 μM Ca^{2+}, pH 6.15, and perfused with 250 mM sorbitol at the indicated time. Nuclear and mitochondrial Ca^{2+} uptake was detected only when osmoticum was removed. The recovery of $[Ca^{2+}]_n$ and $[Ca^{2+}]_m$ was comparable to that obtained with independent Cameleon transgenic lines (NLS-YC3.6 and 4mt-YC3.6). Scale bar = 10 μm.

(a) Ratiometric images from one stomatal pair co-expressing NLS-YC3.6 and 4mt-YC3.6 probes and challenged by osmotic stress. The ratiometric fluorescence signals for the nucleus and mitochondria are different due to adjustment of the minimum and maximum displayed values. To avoid signal saturation for the nucleus, the maximum value was decreased, leading to a darker signal for mitochondria.

(b) Normalized cpVenus/CFP ratios reported as $\Delta R/R_0$. The ratio traces represent the average response of all mitochondria present in the area outlined in red, and for the single nucleus outlined in blue in (a). We did not include signal from the regions close to the nucleus in the mitochondrial analysis.

various compartments. We then monitored the dynamics of $[Ca^{2+}]$ in Arabidopsis roots in various regions of the root tip (from the meristematic cells to the cells of the elongation zone) (Figure 6, blue, red and green traces). Administration of eATP led to a rapid $[Ca^{2+}]$ increase in both cytoplasm and nucleoplasm (Figure 6a,c), with the external cells being the first to respond to the stimulus (Figure 6b,d). Seedlings expressing YC3.6 in the cytoplasm and nucleus showed Ca^{2+} transients that spread throughout the entire tip region (Figure 6b,d and Movies S5 and S6), reaching a maximum $\Delta R/R_0$ after 31.25 ± 4.78 and 38 ± 8.3 sec, respectively. Analysis of the various tip regions (meristematic and transition/elongation zones in Figure 6) showed that the Ca^{2+} transients differed in terms of magnitude, but not shape, within the cytoplasm and nucleoplasm (Figure 6a,c). The typical Ca^{2+} signature comprised a first Ca^{2+} peak followed by a series of smaller peaks, with complete recovery of the basal $[Ca^{2+}]$ in <5 min (Figure 6a,c). Notably, the Ca^{2+} signals were indistinguishable between nucleus and cytoplasm in the various root regions in terms of both amplitude and kinetics. The lack of clear recognition of second and third Ca^{2+} peaks (and higher orders) in the very tip region (blue in Figure 6) is due to the resolution power of the epifluorescence microscope. We then performed the same analyses in the root tip of Arabidopsis 4mt-YC3.6 plants (Figure 6e,f). The first cells that responded to eATP were those in the meristematic region (blue), and then a Ca^{2+} wave propagated to the entire tip region (Figure 6f and Movie S7). However, the dynamics of mitochondrial Ca^{2+} accumulation were quite different from those of the other two compartments: mitochondria showed only one main peak with no significant oscillations, occurring in the meristematic/transition zone 128.3 ± 8.2 sec after eATP treatment (Figure 6e, blue and red traces), and in the upper part of the tip 234.75 ± 64 sec after eATP treatment (Figure 6e, green trace). After reaching a maximum, $[Ca^{2+}]_m$ started to decrease, approaching the basal level after 20 min; in the meristematic region, $[Ca^{2+}]_m$ remained high for longer durations. These experiments indicate that mitochondrial Ca^{2+} accumulation in roots in response to eATP shows different dynamics in different regions that, appear to depend on the magnitudes of cytoplasmic/nuclear Ca^{2+} increase (Figure 6a,c). The fastest mitochondrial Ca^{2+} accumulation was observed in the meristematic zone (Figure 6e, blue trace), i.e. the same region that showed the highest cytoplasmic/nuclear Ca^{2+} increase. To confirm this observation, we performed an eATP dose–response analysis. We subjected Arabidopsis root tip seedlings to three eATP concentrations (2, 0.5 and 0.01 mM), and analyzed the response, in terms of FRET changes, of cytoplasm and mitochondria in the tip region (Figure 7). An increase in eATP concentration led to a clear dose-dependent response in terms of the maximum $[Ca^{2+}]_c$ (Figure 7a,c) and $[Ca^{2+}]_m$ (Figure 7b,c) reached by the cells. The experiments demonstrate that the larger the cytoplasm $[Ca^{2+}]_c$ response, the larger the mitochondrial response, an observation that is consistent with the presence of a low-affinity, highly regulated, Ca^{2+} transport system in the membrane of plant mitochondria. The mechanism responsible for mitochondrial Ca^{2+} uptake in plants could be the so-called 'Ca^{2+} uniporter', a low-affinity Ca^{2+} channel recently identified at

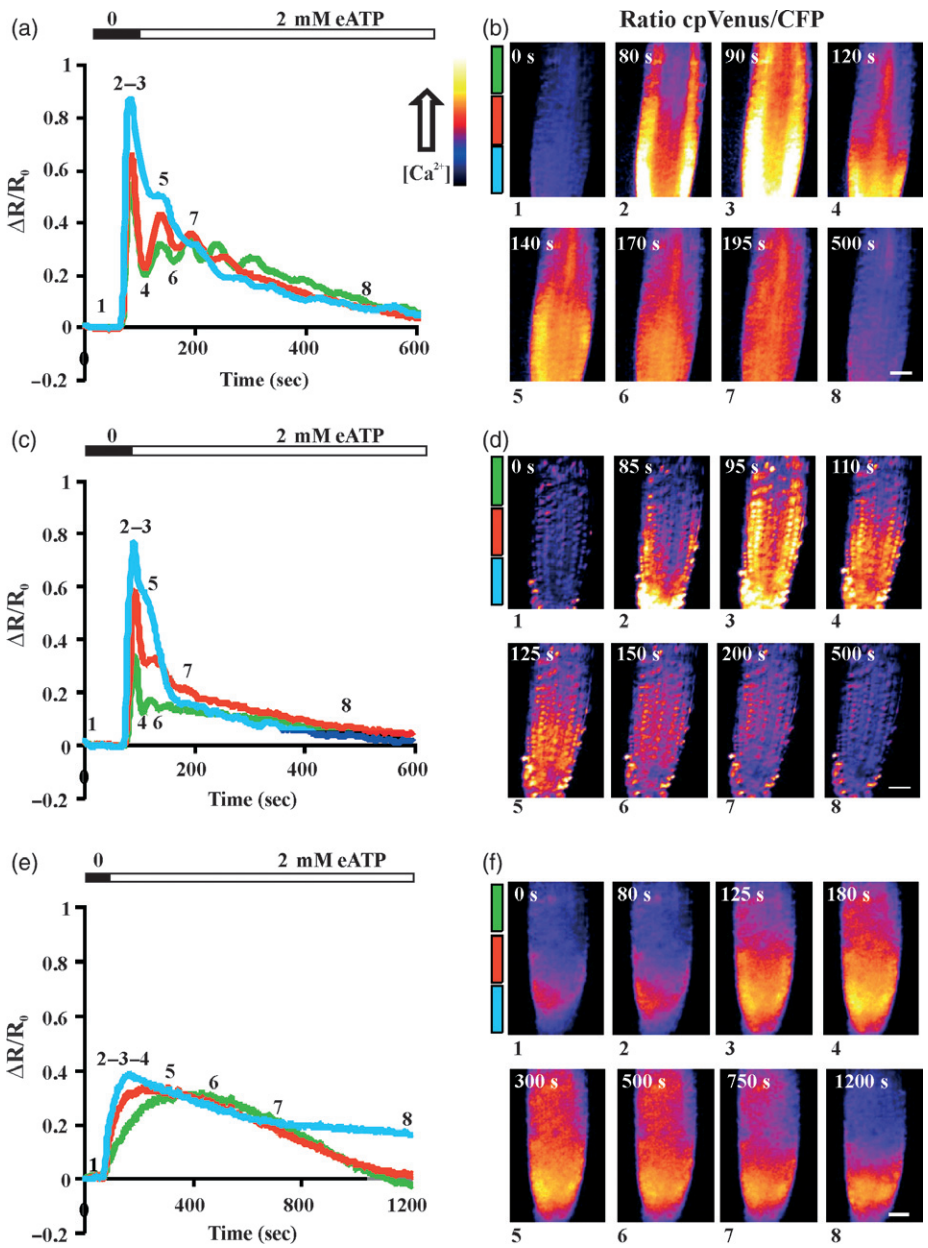

Figure 6. eATP induces cytoplasmic, nuclear and mitochondrial Ca^{2+} transients, with various amplitudes and dynamics in the meristematic and transition/elongation zones of the root tip.

Root tips of 12-day-old seedlings of NES-YC3.6, NLS-YC3.6 and 4mt-YC3.6 lines were bathed in 5 mM KCl, 10 mM MES, 10 mM Ca^{2+}, pH 5.8, and 2 mM of ATP were added to the chamber at the indicated time. The root tips of NES-YC3.6 and NLS-YC3.6 plants challenged with ATP showed a Ca^{2+} transient that propagated as a wave from external regions to the entire tip, with two clear main peaks followed by smaller Ca^{2+} peaks, and complete recovery to the basal Ca^{2+} level. The highest response occurred in the very tip region, corresponding to the cells that first responded to eATP. Scale bar = 25 μm.

(a) Normalized cpVenus/CFP ratio, reported as $\Delta R/R_0$, measured in response to eATP. The colored traces correspond to regions indicated in (b).

(b) Ratiometric images from a root tip expressing NES-YC3.6 and challenged with eATP.

(c) Normalized cpVenus/CFP ratio, reported as $\Delta R/R_0$, measured in response to eATP. The colored traces correspond to regions indicated in (d).

(d) Ratiometric images from a root tip expressing NLS-YC3.6 and challenged with eATP.

(e) Normalized cpVenus/CFP ratio, reported as $\Delta R/R_0$, measured in response to eATP. The colored traces correspond to regions indicated in (f).

(f) Ratiometric images from a root tip expressing 4mt-YC3.6 and challenged with eATP.

the molecular level in mammalian cells (Baughman *et al.*, 2011; De Stefani *et al.*, 2011), for which six predicted isoforms are present in Arabidopsis (Stael *et al.*, 2011).

Using aequorin, Logan and Knight (2003) showed that the maximum Ca^{2+} concentration in the cytoplasm and mitochondria was reached almost simultaneously for all

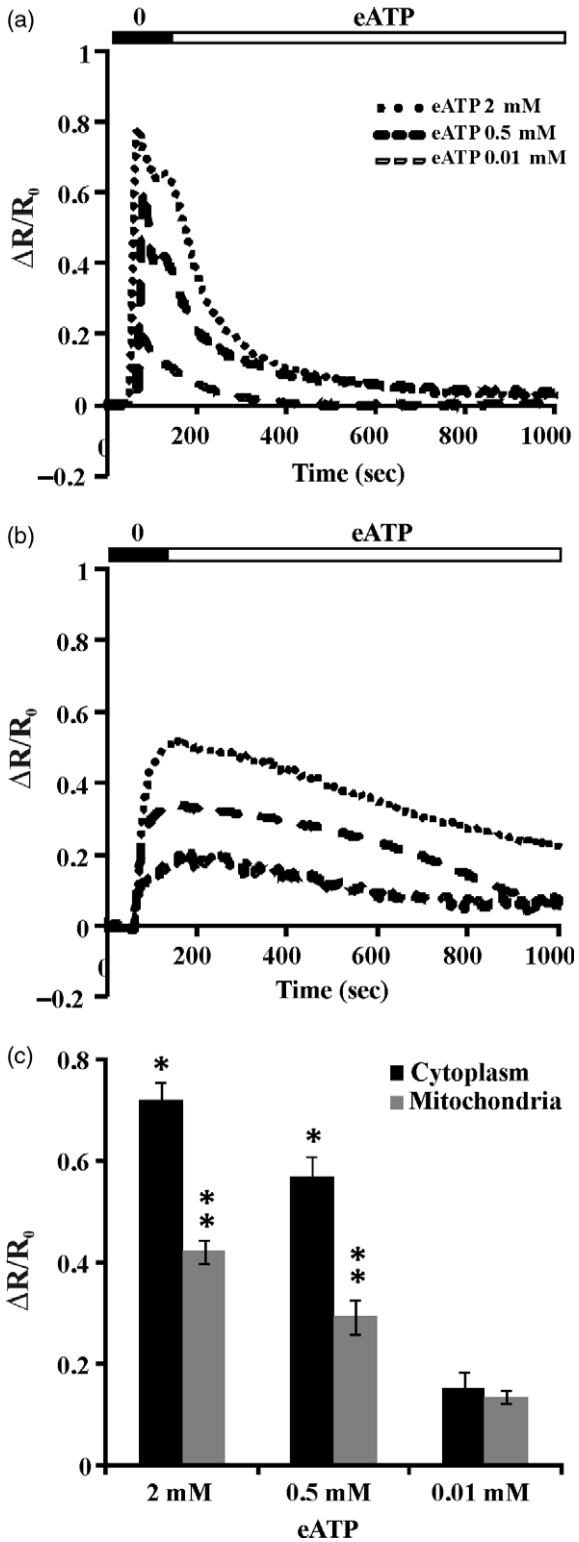

Figure 7. eATP induces a Ca^{2+} increase in both cytoplasm and mitochondria in a dose-dependent fashion.
Root tips of 12-day-old seedlings expressing NES-YC3.6 and 4mt-YC3.6 were bathed in 5 mM KCl, 10 mM MES, 10 mM Ca^{2+}, pH 5.8, and 2, 0.5 or 0.01 mM of eATP was added to the chamber at the indicated time. The analyses were performed by considering the entire imaged root, and the response, in terms of maximum Ca^{2+} rise after the stimulus, was clearly dose-dependent in both the cytoplasm and mitochondria.
(a) Normalized cpVenus/CFP ratio, reported as $\Delta R/R_0$, measured in response to eATP in seedlings expressing the NES-YC3.6 probe (cytoplasm).
(b) Normalized cpVenus/CFP ratio, reported as $\Delta R/R_0$, measured in response to eATP in seedlings expressing the 4mt-YC3.6 probe (mitochondria).
(c) Statistical analysis of peak Ca^{2+} increases in the cytoplasm and mitochondria measured in response to various eATP concentrations. Values are means ± SE. Asterisks indicate statistically significant differences by Student's *t* test (**P* = 0.00873, ***P* = 0.00669).

tested stimuli. Indeed, differences in the kinetics of $[Ca^2]_m$ changes among cell types in response to eATP were clearly revealed by our analysis. These differences may depend on the fact that the Cameleon allowed monitoring of specific regions in the root, whereas the response monitored by aequorin reflected the cell population of the seedling.

Mitochondria Ca^{2+} analyses in single cells of plant roots

As mentioned above, use of Cameleons allows imaging of changes in Ca^{2+} of single cells, or even single organelles. In the case of guard cells, for example, this can easily be achieved using a wide-field fluorescence microscope, but a confocal microscope is necessary to study single cells in a more complex organ such as the root tip (Tanaka *et al.*, 2010b). We therefore used CLSM to monitor the Ca^{2+} responses in the root tip of 4mt-YC3.6-expressing plants, measuring single-cell responses to eATP administration (Figure 8a and Movie S8). As shown in Figure 8(a), the resolution of the CLSM was sufficient to allow monitoring of mitochondrial Ca^{2+} accumulation in single cells of the root transition zone (indicated by red and green arrows in Figure 8a). Figure 8(b) shows that the two cells analyzed, from two different root cell layers, responded with very similar Ca^{2+} kinetics. It is interesting to note that the single-cell mitochondrial Ca^{2+} accumulation kinetics are similar to those observed in the entire root tip (blue trace in Figure 8a,b) or using the wide-field fluorescence microscope (Figures 6e and 7b). These results demonstrate that use of the 4mt-YC3.6 Cameleon itself provides sufficient resolution to observe a single cell in a single focal plane even in a complex organ, such as the root tip. Interestingly, also with the CLSM, we observed what we call a 'mitochondrial Ca^{2+} wave' (Movie S8), but, compared with wide-field fluorescence microscopy analyses, the 'wave' was more uniform (Movie S8). The drawbacks of using CLSM for such analyses were the high laser power required for imaging cells in the deeper root tissues and the time required for each acquisition, which meant that, at this time, we are unable to obtain better resolution or perform very long experiments. The development of new high-resolution and less-invasive imaging systems will overcome these limitations (Fischer *et al.*, 2011), and potentially offer a means to monitor mitochondrial Ca^{2+} handling during long time-lapse experiments, such as during development.

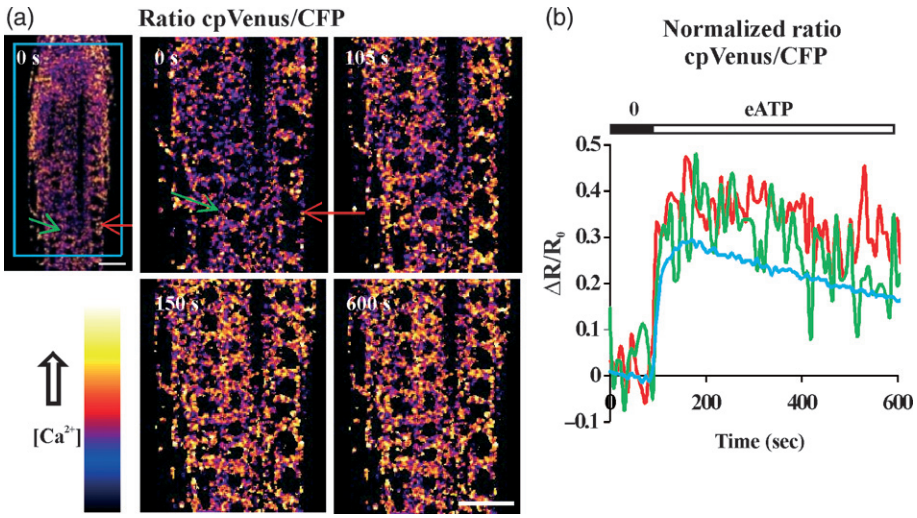

Figure 8. Single-cell mitochondrial Ca^{2+} monitoring in Arabidopsis seedling root.
Effects of 500 μM eATP on the $[Ca^{2+}]_m$ response in Arabidopsis root tip monitored by CLSM at 7.5 sec intervals. Scale bar = 25 μm.
(a) Ratio image of the entire root tip pre-stimulus, and higher magnifications of ratio images for selected frames. The area outlined in blue and the cells marked by green and red arrows were used for the ratio calculations in (b).
(b) ATP-induced changes in $[Ca^{2+}]_m$ in the areas indicated in (a).

Moreover, in the future, it will be interesting to compare the responses of plant expressing mitochondria targeted Cameleon or aequorin in the same organs/tissues. This will be feasible by using the new generation of ultrasensitive Electron Multiplying CCD (EMCCD) camera for aequorin–GFP detection.

CONCLUSIONS

We have generated Arabidopsis transgenic plants harboring a genetically encoded Ca^{2+} probe, Cameleon YC3.6, that is specifically targeted to the mitochondria. We monitored mitochondrial Ca^{2+} dynamics in various tissues and cell types in response to two stimuli (osmotic stress and eATP treatment). Generation of plant cells co-expressing nuclear and mitochondrial targeted Cameleons allowed comparison of mitochondrial $[Ca^{2+}]$ kinetics with cytosolic/nuclear signals. We demonstrated that mitochondrial Ca^{2+} accumulation in response to osmotic stress is strictly dependent on $[Ca^{2+}]_c$ increase, and that, even for the eATP response, mitochondrial Ca^{2+} accumulation strictly depends on the cytoplasmic Ca^{2+} increase. Finally, use of CLSM and the mitochondrial targeted Cameleon allowed monitoring of dynamic changes in Ca^{2+} within the organelles of single root cells. Plants expressing Cameleons in both the nucleus and the mitochondria represent a useful tool for better understanding of the *in vivo* impact of mitochondrial Ca^{2+} handling on the cytoplasmic Ca^{2+} signature and specific downstream cellular responses. Additionally, simultaneous analyses of Ca^{2+} in two compartments may shed light on the mechanism and role of mitochondria retrograde signaling.

EXPERIMENTAL PROCEDURES

Plant material and growth conditions

All *Arabidopsis thaliana* plants used in this study were of the Columbia ecotype. Plants for guard cell imaging were grown in Jiffy pots (http://www.jiffypot.com/) under 16 h light (70 μmol m^{-2} - sec^{-1})/8 h dark at 22°C and 75% relative humidity. Seeds of Arabidopsis were surface-sterilized by vapor-phase sterilization (Clough and Bent, 1998), and plated on half-strength MS medium (Murashige and Skoog, 1962) ((Duchefa, http://www.duchefa.com/) supplemented with 0.1% sucrose, 0.05% MES, pH 6.0, and solidified using 0.8% plant agar (Duchefa). After stratification at 4°C in the dark for 3 days, the seeds were transferred to the growth chamber under 16 h light (70 μmol m^{-2} sec^{-1})/8 h dark at 24°C. The plates were kept vertically. The seedlings used for the analyses were 11–12 days old, with a mean root length of 4.5 cm.

Transgenic NES-YC3.6 Arabidopsis plants, in which the Cameleon is targeted to the cytoplasm by a nuclear export signal (NES) and NLS-YC3.6 Arabidopsis plants, in which the Cameleon is targeted to the nucleus by a nuclear localization signal (NLS) were kindly provided by Dr Karin Schumacher (Department of Developmental Biology, University of Heidelberg, Germany) (Krebs *et al.*, 2012).

DNA constructs

The YC3.6 coding sequence was digested from the pcDNA3-YC3.6 vector (Nagai *et al.*, 2004) using *Hin*dIII and *Eco*RI restriction enzymes, and ligated into the p35S-2 vector (http://www.pgreen.ac.uk/JIT/JIT_fr.htm). In order to generate the 4mt-YC3.6 construct, the 4mt targeting peptide was isolated by digestion of pcDNA3-4mt-D1cpv (Zampese *et al.*, 2011) with *Hin*dIII, and ligated into the 35S-YC3.6. The clone obtained was sequenced to verify the correct orientation of the targeting peptide, and then the entire cassette (35S-4mt-YC3.6-Ter) was PCR-amplified using Phusion® DNA polymerase (Finnzymes, http://www.finnzymes.fi/). For 35S-4mt-YC3.6-Ter cassette amplification, we used the primers 5′-CATGGGTACCGATATCGTACCCCTACTCCAAAAAT-3′ (forward) and 5′-CATGGGTACC

GATATCGATCTGGATTTTAGTA-3′ (reverse), in which *Kpn*I restriction sites (underlined) are present at the 5′ and 3′ ends, respectively. The amplicon for the entire expression cassette was digested using *Kpn*I, and ligated into the pGreen 0179 binary vector (Hellens *et al.*, 2000). The binary vector was then introduced in the *Agrobacterium tumefaciens* GV3101 strain.

Transgenic plants

The *Agrobacterium* strains obtained were used to generate transgenic Arabidopsis plants by the floral-dip method (Clough and Bent, 1998). For each construct, independent transgenic lines were selected, and two lines were used for imaging experiments.

Confocal microscopy analyses

Confocal microscopy analyses were performed using a Leica SP5 laser scanning confocal imaging system (http://www.leica-microsystems.com). For cpVenus fluorescence, excitation was at 514 nm and emission was between 525/540 nm. For chlorophyll detection, excitation was at 514 nm and detection at >600 nm. For TMRM analysis, the seedlings were stained for 10 min in 5 mM KCl, 10 mM MES, 10 mM Ca^{2+}, pH 5.8, supplemented with 500 nM TMRM. Seedlings were washed for 5 minutes with the same solution and analyzed by means of a confocal microscope. Excitation was at 543 nm and emission was between 590–620 nm. For the co-localization analyses of cpVenus and TMRM, sequential excitation in the confocal microscope scanning configuration was used. Image analyses were performed using ImageJ software (http://rsb.info.nih.gov/ij/).

For Ca^{2+} imaging analyses, the roots were imaged using a 40× lens (HCX PL APO CS 40×/1.25–0.75 oil), and YC3.6 was excited using the 458 nm line of the argon laser with 15% total power. The CFP and cpVenus emissions were collected at 473–505 and 526–536 nm, respectively, and the pinhole diameter was 2 airy units. Images were collected every 7.5 sec. False-color ratio images were obtained using the ImageJ 'Ratio Plus Plugin' (Palmer and Tsien, 2006).

Guard cell and root tip imaging

The imaging techniques used are described in Data S1.

Measurement of the YC3.6 dynamic range in mitochondria and nuclei

In order to determine the *in vivo* dynamic range of the probe ($\Delta R_{max}/R_0$) within mitochondria and the nucleus, leaf epidermal cells were permeabilized by treating them for 4 min with 0.2 mM digitonin in an intracellular-like medium containing 100 mM potassium gluconate, 1 mM $MgCl_2$, 10 mM HEPES, pH 7.5, and 5 mM EGTA. The digitonin was then removed, and the cells were held for 5 min in the same medium containing 5 mM EGTA, and finally washed and maintained in 1 mM EGTA. In order to measure the $\Delta R_{max}/R_0$, 10 mM Ca^{2+} was added to the medium. The ratio measurements were performed by observing single non-moving mitochondria (n = 9) or nuclei (n = 13). The ratios reported are means ± SD.

Statistical analysis

All the data are representative of at least nine cells or roots. Reported traces correspond to the typical observed responses.

ACKNOWLEDGEMENTS

We thank Karin Schumacher (Department of Developmental Biology, University of Heidelberg, Germany) for providing the NES-YC3.6 and NLS-YC3.6 Arabidopsis plants. We tank Paulo Magalhães for help with ImageJ analyses. This work was supported by a grant from the Ministero dell'Istruzione, dell'Università e della Ricerca, fondi PRIN to F.L.S., and grants from the Ministero dell'Istruzione, dell'Universitá e della Ricerca (Futuro in Ricerca Bando 2010) to A.C., and from the Veneto Region (Biotech 2) to T.P.

SUPPORTING INFORMATION

Additional Supporting Information may be found in the online version of this article:

Figure S1. Schematic representation of the 4mt-YC3.6 Cameleon vector.

Figure S2. Schematic map of pGreen Binary vector backbones, modified from http://www.pgreen.ac.uk/JIT/JIT_fr.htm.

Figure S3. 4mt-YC3.6 and NLS-YC3.6 Cameleon probes are ubiquitously co-expressed in Arabidopsis seedlings.

Movie S1. CLSM image series of leaf epidermal cell mitochondria expressing the 4mt-YC3.6 Cameleon probe.

Movie S2. CLSM image series of leaf epidermal cell mitochondria stained with TMRM in wild-type plants.

Movie S3. Series of cytoplasmic Ca^{2+} ratio images of a representative leaf epidermal strip of NES-YC3.6 Arabidopsis plants challenged by hyper- and hypo-osmotic stresses.

Movie S4. Series of mitochondrial Ca^{2+} ratio images of a representative leaf epidermal strip of 4mt-YC3.6 Arabidopsis plants challenged by hyper- and hypo-osmotic stresses.

Movie S5. Series of cytoplasmic Ca^{2+} ratio images of an Arabidopsis seedling root tip expressing NES-YC3.6 and challenged with 2 mM eATP.

Movie S6. Series of nuclear Ca^{2+} ratio images of an Arabidopsis seedling root tip expressing NLS-YC3.6 and challenged with 2 mM eATP.

Movie S7. Series of mitochondrial Ca^{2+} ratio images of an Arabidopsis seedling root tip expressing 4mt-YC3.6 and challenged with 2 mM eATP.

Movie S8. Series of mitochondrial Ca^{2+} ratio images of an Arabidopsis seedling root tip expressing 4mt-YC3.6 and challenged with 500 μM eATP analyzed by CLSM.

Data S1. Guard cell and root tip imaging.

Please note: As a service to our authors and readers, this journal provides supporting information supplied by the authors. Such materials are peer-reviewed and may be re-organized for online delivery, but are not copy-edited or typeset. Technical support issues arising from supporting information (other than missingfiles) should be addressed to the authors.

REFERENCES

Allen, G.J., Kwak, J.M., Chu, S.P., Llopis, J., Tsien, R.Y., Harper, J.F. and Schroeder, J.I. (1999) Cameleon calcium indicator reports cytoplasmic calcium dynamics in Arabidopsis guard cells. *Plant J.* **19**, 735–747.

Baughman, J.M., Perocchi, F., Girgis, H.S. *et al.* (2011) Integrative genomics identifies MCU as an essential component of the mitochondrial calcium uniporter. *Nature*, **476**, 341–345.

Clough, S.J. and Bent, A.F. (1998) Floral dip: a simplified method for *Agrobacterium*-mediated transformation of *Arabidopsis thaliana*. *Plant J.* **16**, 735–743.

Contreras, L., Drago, I., Zampese, E. and Pozzan, T. (2010) Mitochondria: the calcium connection. *Biochim. Biophys. Acta*, **1797**, 607–618.

Costa, A., Drago, I., Behera, S., Zottini, M., Pizzo, P., Schroeder, J.I., Pozzan, T. and Lo Schiavo, F. (2010) H_2O_2 in plant peroxisomes: an *in vivo* analysis uncovers a Ca^{2+}-dependent scavenging system. *Plant J.* **62**, 760–772.

De Stefani, D., Raffaello, A., Teardo, E., Szabò, I. and Rizzuto, R. (2011) A forty-kilodalton protein of the inner membrane is the mitochondrial calcium uniporter. *Nature*, **476**, 336–340.

Demidchik, V., Shang, Z., Shin, R. *et al.* (2009) Plant extracellular ATP signalling by plasma membrane NADPH oxidase and Ca^{2+} channels. *Plant J.* **58**, 903–913.

van Der Luit, A.H., Olivari, C., Haley, A., Knight, M.R. and Trewavas, A.J. (1999) Distinct calcium signaling pathways regulate calmodulin gene expression in tobacco. *Plant Physiol.* **121**, 705–714.

Dodd, A.N., Kudla, J. and Sanders, D. (2010) The language of calcium signaling. *Annu. Rev. Plant Biol.* **61**, 593–620.

Fasano, J.M., Massa, G.D. and Gilroy, S. (2002) Ionic signaling in plant responses to gravity and touch. *J. Plant Growth Regul.* **21**, 71–88.

Filippin, L., Abad, M.C., Gastaldello, S., Magalhães, P.J., Sandonà, D. and Pozzan, T. (2005) Improved strategies for the delivery of GFP-based Ca^{2+} sensors into the mitochondrial matrix. *Cell Calcium*, **37**, 129–136.

Fischer, R.S., Wu, Y., Kanchanawong, P., Shroff, H. and Waterman, C.M. (2011) Microscopy in 3D: a biologist's toolbox. *Trends Cell Biol.* **12**, 682–691.

Giacomello, M., Drago, I., Bortolozzi, M., Scorzeto, M., Gianelle, A., Pizzo, P. and Pozzan, T. (2010) Ca^{2+} hot spots on the mitochondrial surface are generated by Ca^{2+} mobilization from stores, but not by activation of store-operated Ca^{2+} channels. *Mol. Cell*, **38**, 280–290.

Hellens, R.P., Edwards, E.A., Leyland, N.R., Bean, S. and Mullineaux, P.M. (2000) pGreen: a versatile and flexible binary Ti vector for *Agrobacterium*-mediated plant transformation. *Plant Mol. Biol.* **42**, 819–832.

Hetherington, A.M. and Brownlee, C. (2004) The generation of Ca^{2+} signals in plants. *Annu. Rev. Plant Biol.* **55**, 401–427.

Iwano, M., Entani, T., Shiba, H. *et al.* (2009) Fine-tuning of the cytoplasmic Ca^{2+} concentration is essential for pollen tube growth. *Plant Physiol.* **150**, 1322–1334.

Johnson, C.H., Knight, M.R., Kondo, T., Masson, P., Sedbrook, J., Haley, A. and Trewavas, A. (1995) Circadian oscillations of cytosolic and chloroplastic free calcium in plants. *Science*, **269**, 1863–1865.

Kim, T.H., Böhmer, M., Hu, H., Nishimura, N. and Schroeder, J.I. (2010) Guard cell signal transduction network: advances in understanding abscisic acid, CO_2, and Ca^{2+} signaling. *Annu. Rev. Plant Biol.* **61**, 561–591.

Knight, M.R., Campbell, A.K., Smith, S.M. and Trewavas, A.J. (1991) Transgenic plant aequorin reports the effects of touch and cold-shock and elicitors on cytoplasmic calcium. *Nature*, **352**, 524–526.

Knight, H., Trewavas, A.J. and Knight, M.R. (1996) Cold calcium signalling in Arabidopsis involves two cellular pools and a change in calcium signature after acclimation. *Plant Cell*, **8**, 489–503.

Knight, H., Brandt, S. and Knight, M.R. (1998) A history of stress alters drought calcium signalling pathways in Arabidopsis. *Plant J.* **16**, 681–687.

Krebs, M., Held, K., Binder, A., Hashimoto, K., Den Herder, G., Parniske, M., Kudla, J. and Schumacher, K. (2012) FRET-based genetically encoded sensors allow high-resolution live cell imaging of Ca^{2+} dynamics. *Plant J.* **69**, 181–192.

Kudla, J., Batistic, O. and Hashimoto, K. (2010) Calcium signals: the lead currency of plant information processing. *Plant Cell*, **22**, 541–563.

Logan, D.C. (2010) The dynamic plant chondriome. *Semin. Cell Dev. Biol.* **21**, 550–557.

Logan, D.C. and Knight, M.R. (2003) Mitochondrial and cytosolic calcium dynamics are differentially regulated in plants. *Plant Physiol.* **133**, 21–24.

Mazars, C., Brière, C., Bourque, S. and Thuleau, P. (2011) Nuclear calcium signaling: an emerging topic in plants. *Biochimie*, **93**, 2068–2074.

McAinsh, M.R. and Pittman, J.K. (2009) Shaping the calcium signature. *New Phytol.* **181**, 275–294.

Monshausen, G.B., Messerli, M.A. and Gilroy, S. (2008) Imaging of the Yellow Cameleon 3.6 indicator reveals that elevations in cytosolic Ca^{2+} follow oscillating increases in growth in root hairs of Arabidopsis. *Plant Physiol.* **147**, 1690–1698.

Murashige, T. and Skoog, F. (1962) A revised medium for rapid growth and bioassays with tobacco tissue cultures. *Physiol. Plant.* **15**, 473–497.

Nagai, T., Yamada, S., Tominaga, T., Ichikawa, M. and Miyawaki, A. (2004) Expanded dynamic range of fluorescent indicators for Ca^{2+} by circularly permuted yellow fluorescent proteins. *Proc. Natl Acad. Sci. USA*, **101**, 10554–10559.

Palmer, A.E. and Tsien, R.Y. (2006) Measuring calcium signaling using genetically targetable fluorescent indicators. *Nat. Protoc.* **1**, 1057–1065.

Palmer, A.E., Giacomello, M., Kortemme, T., Hires, S.A., Lev-Ram, V., Baker, D. and Tsien, R.Y. (2006) Ca^{2+} indicators based on computationally redesigned calmodulin-peptide pairs. *Chem. Biol.* **13**, 521–530.

Palmer, A.E., Qin, Y., Park, J.G. and McCombs, J.E. (2011) Design and application of genetically encoded biosensors. *Trends Biotechnol.* **29**, 144–152.

Rincón-Zachary, M., Teaster, N.D., Sparks, J.A., Valster, A.H., Motes, C.M. and Blancaflor, E.B. (2010) Fluorescence resonance energy transfer-sensitized emission of yellow cameleon 3.60 reveals root zone-specific calcium signatures in Arabidopsis in response to aluminum and other trivalent cations. *Plant Physiol.* **152**, 1442–1458.

Rizzuto, R. and Pozzan, T. (2006) Microdomains of intracellular Ca^{2+}: molecular determinants and functional consequences. *Physiol. Rev.* **86**, 369–408.

Roux, S.J. and Steinebrunner, I. (2007) Extracellular ATP: an unexpected role as a signaler in plants. *Trends Plant Sci.* **12**, 522–527.

Rudolf, R., Mongillo, M., Magalhães, P.J. and Pozzan, T. (2004) *In vivo* monitoring of Ca^{2+} uptake into mitochondria of mouse skeletal muscle during contraction. *J. Cell Biol.* **166**, 527–536.

Sieberer, B.J., Chabaud, M., Timmers, A.C., Monin, A., Fournier, J. and Barker, D.G. (2009) A nuclear-targeted cameleon demonstrates intranuclear Ca^{2+} spiking in *Medicago truncatula* root hairs in response to rhizobial nodulation factors. *Plant Physiol.* **151**, 1197–1206.

Stael, S., Wurzinger, B., Mair, A., Mehlmer, N., Vothknecht, U.C. and Teige, M. (2011) Plant organellar calcium signalling: an emerging field. *J. Exp. Bot.* **63**, 1525–1542.

Subbaiah, C.C., Bush, D.S. and Sachs, M.M. (1998) Mitochondrial contribution to the anoxic Ca^{2+} signal in maize suspension-cultured cells. *Plant Physiol.* **118**, 759–771.

Swanson, S.J., Choi, W.G., Chanoca, A. and Gilroy, S. (2011) *In vivo* imaging of Ca^{2+}, pH, and reactive oxygen species using fluorescent probes in plants. *Annu. Rev. Plant Biol.* **62**, 273–297.

Tanaka, K., Gilroy, S., Jones, A.M. and Stacey, G. (2010a) Extracellular ATP signaling in plants. *Trends Cell Biol.* **20**, 601–608.

Tanaka, K., Swanson, S.J., Gilroy, S. and Stacey, G. (2010b) Extracellular nucleotides elicit cytosolic free calcium oscillations in Arabidopsis. *Plant Physiol.* **154**, 705–719.

Tang, W., Brady, S.R., Sun, Y., Muday, G.K. and Roux, S.J. (2003) Extracellular ATP inhibits root gravitropism at concentrations that inhibit polar auxin transport. *Plant Physiol.* **131**, 147–154.

Yang, Y., Costa, A., Leonhardt, N., Siegel, R.S. and Schroeder, J.I. (2008) Isolation of a strong Arabidopsis guard cell promoter and its potential as a research tool. *Plant Methods*, **19**, 4–6.

Yoshida, K., Shibata, M., Terashima, I. and Noguchi, K. (2010) Simultaneous determination of *in vivo* plastoquinone and ubiquinone redox states by HPLC-based analysis. *Plant Cell Physiol.* **51**, 836–841.

Zampese, E., Fasolato, C., Kipanyula, M.J., Bortolozzi, M., Pozzan, T. and Pizzo, P. (2011) Presenilin 2 modulates endoplasmic reticulum (ER)-mitochondria interactions and Ca^{2+} cross-talk. *Proc. Natl Acad. Sci. USA*, **15**, 2777–2782.

Zhang, W., Fan, L.M. and Wu, W.H. (2007) Osmo-sensitive and stretch-activated calcium-permeable channels in *Vicia faba* guard cells are regulated by actin dynamics. *Plant Physiol.* **143**, 1140–1151.

Zottini, M. and Zannoni, D. (1993) The use of fura-2 fluorescence to monitor the movement of free calcium ions into the matrix of plant mitochondria (*Pisum sativum* and *Helianthus tuberosus*). *Plant Physiol.* **102**, 573–578.

Zottini, M., Barizza, E., Bastianelli, F., Carimi, F. and Lo Schiavo, F. (2006) Growth and senescence of *Medicago truncatula* cultured cells are associated with characteristic mitochondrial morphology. *New Phytol.* **172**, 239–247.

FIGURE S1

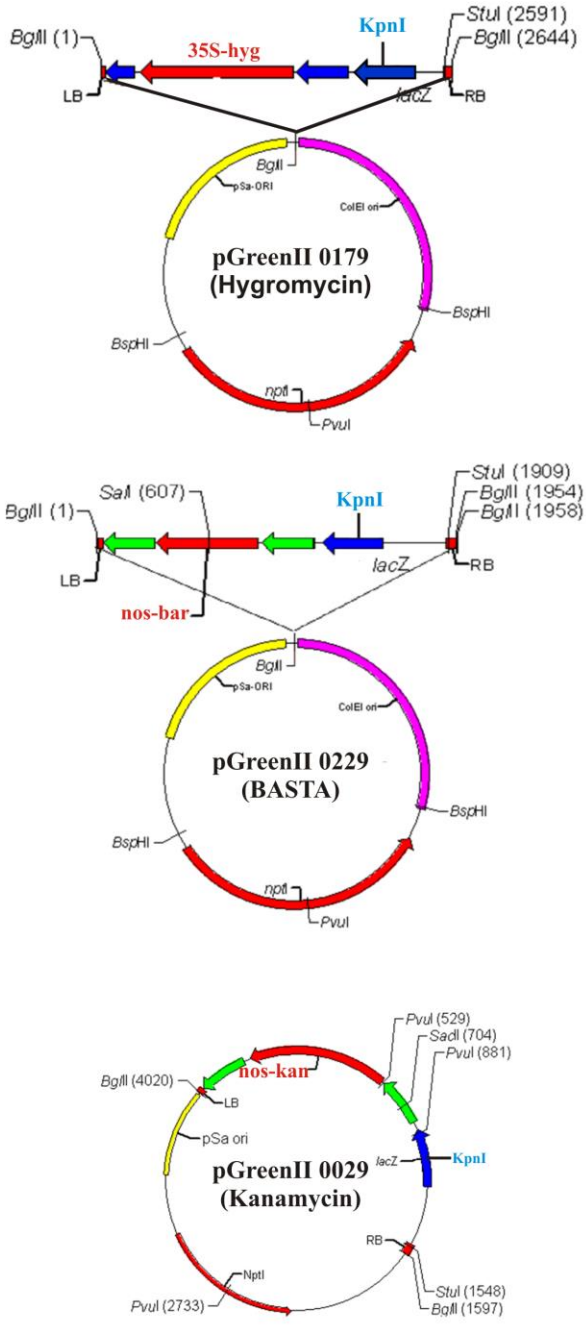
BglII (1)
35S-hyg
KpnI
StuI (2591)
BglII (2644)
LB
lacZ
RB
BglII
pSa-ORI
ColEI ori
pGreenII 0179
(Hygromycin)
BspHI
BspHI
nptI
PvuI
SalI (607)
StuI (1909)
BglII (1954)
BglII (1958)
nos-bar
pGreenII 0229
(BASTA)
PvuI (529)
SacII (704)
PvuI (881)
BglII (4020)
nos-kan
pSa ori
pGreenII 0029
(Kanamycin)
NptI
PvuI (2733)
StuI (1548)
BglII (1597)

FIGURE S2

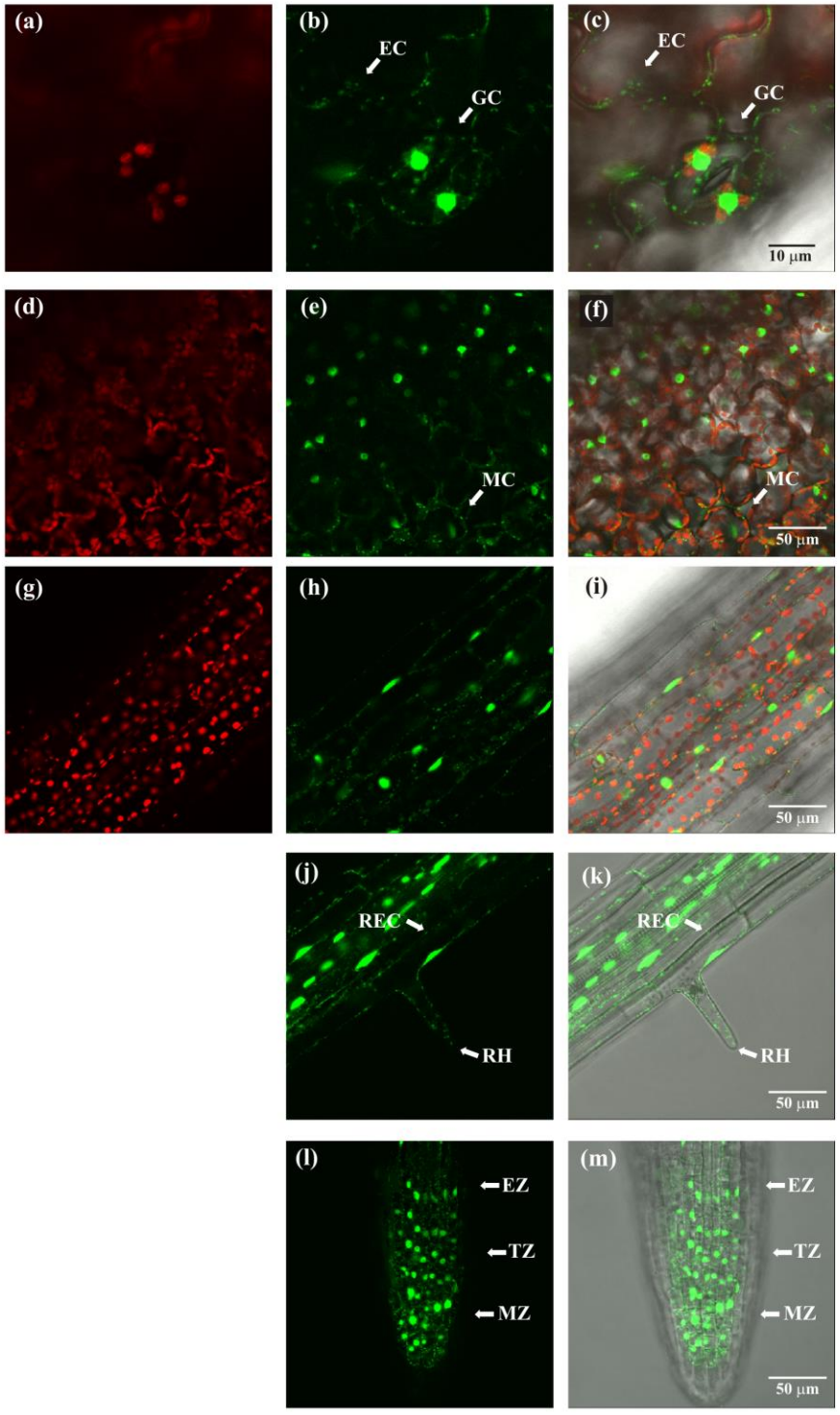
(a)
(b)
EC
GC
(c)
EC
GC
10 µm
(d)
(e)
MC
(f)
MC
50 µm
(g)
(h)
(i)
50 µm
(j)
REC
RH
(k)
REC
RH
50 µm
(l)
EZ
TZ
MZ
(m)
EZ
TZ
MZ
50 µm

FIGURE S3

Supplementary Information

Figure S1. Schematic representation of 4mt-YC3.6 Cameleon vector.

Cameleon YC3.6 was fused with the 4mt mitochondria targeting peptide and placed under control of a single CaMV35S promoter and CaMV35S terminator. The Cameleon cassette was inserted in the pGreen0179 polylinker that brings as plant selectable marker hygromycin. Left border (LB), Right border (RB).

Figure S2. Schematic map of pGreen Binary vector backbones. Modified from http://www.pgreen.ac.uk/JIT/JIT_fr.htm web site.

Figure S3. 4mt-YC3.6 and NLS-YC3.6 Cameleon probes are ubiquitously co-expressed in Arabidopsis seedlings.

(a-f) CLSM analyses of leaf cells expressing 4mt-YC3.6 and NLS-YC3.6 probes. The cpVenus signal was detected both in mitochondria structures and nuclei in epidermal (EC), stomata (GC) and mesophyll cells (MC).

(a and d) Chlorophyll fluorescence.

(b and e) cpVenus Cameleon fluorescence.

(c and f) Overlay images of chlorophyll, cpVenus and transmitted light.

(g-i) 4mt-YC3.6 cpVenus signal was detected in hypocotyl cells in all cell layers both in presence or absence of chloroplasts.

(g) Chlorophyll fluorescence.

(h) cpVenus Cameleon fluorescence and (i) overlay images of chlorophyll, cpVenus and transmitted

light.

(j-m) In root cells 4mt-YC3.6 and NLS-YC3.6 probes were present in all cell types of the root mature zone (j and k), including root epidermal cells (REC) and root hair cells (RH). In the tip region (l and m) the probe was present in the meristematic (MZ), transition (TZ) and elongation zones (EZ).

(j and l) cpVenus Cameleon fluorescence.

(k and m) Overlay images of cpVenus and transmitted light.

Movie S1. CLSM image series of leaf epidermal cell mitochondria expressing 4mt-YC3.6 Cameleon probe. The movie plays 5 times at real-time with 1.6 sec intervals.

Movie S2. CLSM image series of leaf epidermal cell mitochondria, stained with TMRM, in wild type plants. The movie plays 5 times at real-time with 1.6 sec intervals.

Movie S3. Series of cytoplasmic Ca^{2+} ratio images of a representative leaf epidermal strip of NES-YC3.6 Arabidopsis plants challenged with hyper- and hypoosmotic stresses. The movie plays 26 times at real-time with 5 sec intervals.

Movie S4. Series of mitochondrial Ca^{2+} ratio images of a representative leaf epidermal strip of 4mt-YC3.6 Arabidopsis plants challenged with hyper- and hypoosmotic stresses. No obvious changes in the motility of mitochondria were observed after addition of the stimuli. The movie plays 26 times at real-time with 5 sec intervals.

Movie S5. Series of cytoplasmic Ca^{2+} ratio images of an Arabidopsis seedling root tip expressing NES-YC3.6 challenged with 2 mM eATP. The movie plays 25 times at real-time with 5 sec intervals.

Movie S6. Series of nuclear Ca^{2+} ratio images of an Arabidopsis seedling root tip expressing NLS-YC3.6 challenged with 2 mM eATP. The movie plays 25 times at real-time with 5 sec intervals.

Movie S7. Series of mitochondrial Ca^{2+} ratio images of an Arabidopsis seedling root tip expressing 4mt-YC3.6 challenged with 2 mM eATP. The movie plays 25 times at real-time with 5 sec intervals.

Movie S8. Series of mitochondrial Ca^{2+} ratio images of an Arabidopsis seedling root tip expressing 4mt-YC3.6 challenged with 500 μM eATP analyzed by CLSM. No obvious changes in the motility of mitochondria were observed after addition of the stimulus. The movie plays 38 times at real-time with 7.5 sec intervals.

Experimental procedures S1.

Guard cell and root tip imaging

For guard cell imaging leaves of 5-week-old Arabidopsis plants were attached to microscope cover glasses using a medical adhesive (Hollister Inc., Libertyville, IL). A paintbrush was used to gently press the leaf to the coverslip and upper cell layers were carefully removed using a razor blade. Leaf epidermal strips were preincubated in a buffer solution (5 mM KCl, 10 mM Mes, 50 μM Ca^{2+} pH 6.15 adjusted whit Tris) for 2-4 h in white light (125 μmol $m^{-2} \cdot s^{-1}$) to induce stomata opening in order to get turgid guard cells. For root cell imaging the 12-day-old seedlings grown vertically were gently transferred to microscope cover glasses in a drop of solution. To keep fixed the root during the experiments, a 1% agar block was gently placed over the seedling. The shoot was not submerged in the

solution.

The microscope cover glasses were mounted into an open-top chamber. For the osmotic stress experiments with guard cells the solution was the same used for the stomata opening (5 mM KCl, 10 mM Mes, 50 μM Ca^{2+} pH 6.15 adjusted whit Tris) and the cells where perfused with the same solution or with the solution supplemented with 250 mM of sorbitol. For the experiment performed in root seedlings the solution used was 5 mM KCl, 10 mM Mes, 10 mM Ca^{2+} pH 5.8 adjusted with Tris. The ATP was added as disodium salt (Sigma-Aldrich) to the chamber by perfusion with the same solution supplemented with ATP and not removed from the medium throughout the entire experiment. The pH of the solution was re-adjusted to 5.8 after the addition of ATP.

Guard cells and seedling roots expressing the fluorescent probes were imaged *in vivo* by a an inverted fluorescence microscope (Leica DMI6000 B, Germany, http://www.leica-microsystems.com/) with dry and immersion oil objectives (X20, N.A. 0.5, X40, N.A. 1.3 and 63X, N.A. 1.40). Excitation light was produced by a fluorescent lamp at 440 nm (436/20 nm, dichroic 455DCXR). The emitted light was collected through a beam-splitter (OES s.r.l., Padua, Italy) (emission filters ET 480/40M for cyan fluorescent protein and ET 535/30M for yellow fluorescent protein) and a dichroic mirror (515 DCXR). Filters and dichroic mirrors were purchased from Omega Optical and Chroma. Images were acquired using a cooled CCD camera (OES s.r.l, Padova) attached to a 12-bit frame grabber. Exposure time and frequency of image capture varied from 100 to 500 ms and from 1 to 0.2 Hz, respectively. The acquired images were analyzed by ImageJ software. The false color ratio images were obtained by using the ImageJ "Ratio Plus Plugin" without background subtraction and represents the Ca^{2+} dynamics observed. For time course experiments, the fluorescence intensity was determined over Regions Of Interests (ROIs) corresponding to an entire guard cell or root regions or covering single or small groups of mitochondria and/or nucleus. Regions corresponding to background for each wavelength were analyzed and subtracted from values measured for the different ROIs of the two

channels (CFP and cpVenus). The background subtracted values for the selected ROIs were used for the Ratio (R) calculation and normalized to the initial Ratio (R_0) and plotted versus time ($\Delta R/R_0$).

To verify the YC3.6 ratio efficiency in the correction of eventual focal plane changes we changed the focus on purpose in non stimulated cells, and in all cases the ratio nicely corrected possible artifacts, since no changes of $\Delta R/R_0$ were observed even for quite substantial focus changes.

2.3 The D3cpv Cameleon reports Ca^{2+} dynamics in plant mitochondria with similar kinetics of the YC3.6 Cameleon, but with a lower sensitivity

Journal of Microscopy

Journal of Microscopy, 2012
Received 5 July 2012; accepted 10 October 2012
doi: 10.1111/j.1365-2818.2012.03683.x

The D3cpv Cameleon reports Ca^{2+} dynamics in plant mitochondria with similar kinetics of the YC3.6 Cameleon, but with a lower sensitivity

G. LORO*,†, C. RUBERTI*, M. ZOTTINI* & A. COSTA†
*Dipartimento di Biologia, Università degli Studi di Padova, Via U. Bassi, Padova, Italia
†Dipartimento di Bioscienze, Università degli Studi di Milano, Via G. Celoria, Milano, Italia

Key words. Cameleon, Ca^{2+} imaging, FRET, plant mitochondria.

Summary

Mitochondria are key organelles involved in many aspects of plant physiology and, their ability to generate specific Ca^{2+} signatures in response to abiotic and biotic stimuli has been reported as one of their roles. The recent identification of the mammalian mitochondrial Ca^{2+} uniporter opens a new research area in plant biology. To study the mitochondrial Ca^{2+} handling, it is essential to have a reliable probe. Here we have reported the generation of an Arabidopsis transgenic line expressing the genetically encoded probe Cameleon D3cpv targeted to mitochondria, and compared its properties with the already known Cameleon YC3.6.

Introduction

Mitochondria are key organelles involved in many aspects of the eukaryotic cell functions, ranging from cell metabolism to stress response and programmed cell death regulation (McAinsh & Pittman, 2009; Contreras *et al.*, 2010). Several studies carried out in mammalian cells, have revealed the ability of mitochondria to accumulate Ca^{2+} upon specific stimuli (Drago *et al.*, 2011 and reference therein). Moreover, the molecular identity of the so-called 'mitochondrial Ca^{2+} uniporter', the inner membrane channel responsible for the mitochondrial Ca^{2+} accumulation in mammalian cells, has been recently identified by two independent groups (Baughman *et al.*, 2011; De Stefani *et al.*, 2011). Interestingly, six predicted isoforms of this channel, with different tissue specificities, have been identified in Arabidopsis (Stael *et al.*, 2012).

To study the mitochondrial Ca^{2+} handling in plant cells *in vivo*, we recently generated transgenic Arabidopsis plants expressing the genetically encoded Ca^{2+} probe Cameleon YC3.6 targeted to the mitochondria (Loro *et al.*, 2012). The YC3.6 Cameleon probe efficiently reported mitochondrial Ca^{2+} dynamics in response to different stimuli in guard and root cells (Loro *et al.*, 2012), and it was chosen for its reported high dynamic range (changes in Ca^{2+} concentration are efficiently transduced) and Ca^{2+} affinity (K_D for Ca^{2+} is 0.25 μM *in vitro*; refs. Nagai *et al.*, 2004; Palmer & Tsien, 2006).

It was very recently reported that the Arabidopsis *AtCML30* gene codes for a calmodulin (CaM)-like protein localized in mitochondria (Chigri *et al.*, 2012) and that this gene is ubiquitously expressed throughout the entire plant life cycle, as indicated by published microarray data (Schmid *et al.*, 2005, http://jsp.weigelworld.org/expviz/expviz.jsp). The presence of this mitochondrial CaM-like protein might potentially affect the Cameleon response, as reported for some of the original YCs (Yellow Cameleon), which for example failed to report Ca^{2+} variations when targeted to plasma membrane (Heim & Griesbeck, 2004), where CaM can reach mM concentrations (Palmer *et al.*, 2006). Because of this, Palmer *et al.* (2006) developed a new family of Cameleons, called Dcpv. Briefly, the Dcpv family derived from the classical Cameleons in which the two green fluorescent protein (GFP) variants, cyan fluorescent protein (CFP) and cpVenus (cpv; a yellow fluorescent protein (YFP) circularly permuted variant), are linked together through a mutated CaM and M13 peptide to abolish or strongly reduce the interference from endogenous CaM (Palmer *et al.*, 2006). As in the classical Cameleon, in the Dcpv family, the Ca^{2+} binding induces the conformational change of CaM and its binding to M13. The consequently reduced distance between CFP and cpv results in an increase in the fluorescence resonance energy transfer (FRET). FRET (and thus the $[Ca^{2+}]$) increase can be conveniently measured by the increase of the ratio between the emission intensities of cpv and CFP, respectively, upon CFP excitation. Analyses of mitochondrial Ca^{2+} dynamics, carried out with the YC3.6

Correspondence to: Alex Costa, Dipartimento di Bioscienze, Università degli Studi di Milano, Via G. Celoria 26, 20133 Milano, Italy. Tel: +39-02-50314831; fax: +39-02-50314815; e-mail: alex.costa@unimi.it

(Loro *et al.*, 2012), could not provide clues about a possible attenuation, because of the presence of endogenous CaM, of the Cameleon-dependent response. Hence, to evaluate this possibility, in this work we have generated Arabidopsis plants expressing the D3cpv Cameleon probe targeted to mitochondria and compared its functional properties with the previously characterized YC3.6.

Materials and methods

Plant material

The *Arabidopsis thaliana* (Columbia ecotype) plants used in this study were grown as previously reported (Loro *et al.*, 2012).

Genetic materials

The D3cpv coding sequence was digested from the pcDNA3-D3cpv (Palmer *et al.*, 2006) vector with HindIII and EcoRI restriction enzymes and ligated into the 35S-CaMV cassette vector (http://www.pgreen.ac.uk/JIT/JIT_fr.htm). To generate the 4mt-D3cpv construct, the 4mt targeting peptide was isolated by digestion of pcDNA3–4mt-D1cpv (Zampese *et al.*, 2011) with HindIII and ligated into the 35S-D3cpv linearized vector. The obtained clone was sequenced to verify the right orientation of the targeting peptide and then the entire cassette '35S-4mt- D3cpv-Ter' was PCR amplified by using Phusion DNA Polymerase (Finnzymes, http://www.finnzymes.fi/). For the '35S-4mt-D3cpv-Ter' cassette amplification, we used the following forward and reverse primers: 5′-CATGGGTACCGATATCGTACCCCTACTCCAAAAAT-3′ and 5′-CATGGGTACCGATATCGATCTGGATTTTAGTA-3′, where KpnI restriction sites were introduced at the 5′ and 3′ end. The amplicon of the entire expression cassette was digested with KpnI and ligated in the pGreen0179 binary vector (Hellens *et al.*, 2000). The binary vectors were then introduced in the *Agrobacterium tumefaciens* GV3101 strain.

Transgenic plants

The obtained *Agrobacterium* strain was used to generate transgenic Arabidopsis plants by the floral-dip method (Clough & Bent, 1998). Five Arabidopsis-independent transgenic lines were selected and two independent lines were used for imaging experiments.

Confocal microscopy analyses

Confocal microscopy analyses were performed using a Leica SP5 (Leica, Germany, http://www.leica-microsystems.com) laser scanning confocal imaging system. For Cameleon-dependent-cpVenus, excitation was at 514 nm and emission between 525 and 540 nm. For tetramethylrhodamine methyl ester (TMRM) analysis, the seedlings were stained for 10 min in 5 mM KCl, 10 mM Mes, 10 mM Ca^{2+} pH 5.8 supplemented with 500 nM TMRM. Seedlings were washed with the same solution and analysed by means of confocal microscopy with excitation set at 543 nm and emission between 590 and 620 nm. For the colocalization analyses of cpVenus and TMRM, sequential excitation in the confocal microscope scanning configuration was adopted. Image analyses were performed by using the ImageJ bundle software (http://rsb.info.nih.gov/ij/).

Root tip Ca^{2+} imaging

For root cell imaging, the vertically grown 12-day-old seedlings were gently transferred to microscope cover glasses in a drop of the imaging solution. To keep the root in a fixed position during the experiments, a 1% agar block was gently placed over the seedling, and the shoot was not submerged by the solution. For the experiments performed in seedling roots, the solution was 5 mM KCl, 10 mM Mes, 10 mM Ca^{2+}, pH 5.8 adjusted with Tris. ATP was added as disodium salt (Sigma-Aldrich, St. Louis, MO, U.S.A.) to the chamber by perfusion with the same solution supplemented with ATP, which was not removed from the medium throughout the entire experiment. The pH of the solution was readjusted to 5.8 after Adenosine 5'-triphosphate (ATP) addition. Seedling roots expressing the fluorescent probes were imaged *in vivo* by an inverted fluorescence microscope (Leica DMI6000 B, Germany, http://www.leica-microsystems.com/) with 20x, numerical aperture (NA) 0.5, dry objective. Excitation light was produced by a fluorescent lamp at 440 nm (436/20 nm, dichroic 455DCXR). The light emitted was collected through a beam-splitter (OES s.r.l., Padua, Italy; emission filters ET 480/40 M for CFP and ET 535/30 M for cpVenus) and a dichroic mirror (515 DCXR). Filters and dichroic mirrors were purchased from Omega Optical and Chroma. Images were acquired using a cooled CCD camera (OES s.r.l, Padua, Italy) attached to a 12-bit frame grabber. Exposure time was 500 ms with a 4 × 4 charge-coupled device (CCD) binning. The acquired images were analysed by ImageJ software. As regards time course experiments, fluorescence intensity was determined over regions of interest (ROIs) which correspond to a root region or which cover single or small groups of mitochondria. Regions corresponding to the background for each wavelength were analysed and subtracted from values measured for the different ROIs of the two channels (CFP and cpVenus). The background-subtracted values for the selected ROIs were used for the ratio (R) calculation and normalized to the initial ratio (R_0) and plotted versus time ($\Delta R/R_0$).

Measurement of D3cpv and YC3.6 dynamic ranges in mitochondria

To determine the *in vivo* maximum response of the two probes ($\Delta R_{max}/R_0$) within mitochondria, leaf epidermal cells were

permeabilized with 0.2 mM digitonin in an intracellular-like medium containing 100 mM potassium-gluconate, 1 mM $MgCl_2$, 10 mM Hepes, pH 7.5 and 5 mM ethylene glycol tetraacetic acid (EGTA) for 4 min. At the end of this period the digitonin was removed and the cells were kept in the same medium with 5 mM EGTA for 5 min first, and then maintained in 1 mM EGTA. To measure the $\Delta R_{max}/R_0$, 10 mM Ca^{2+} was added to the medium. The ratio measurements were performed looking at single immobile mitochondria with the same microscope acquisition system and parameters used for root cell imaging, but with a 63x, N.A. 1.40 immersion oil objective. The ratios were then averaged and reported ±SE ($n = 15$ for 4mt-D3cpv and $n = 10$ for 4mt-YC3.6).

Statistical analysis

All data are representative of at least 9 analysed different cells or roots. Reported traces are the most representative.

Results and discussion

We have recently reported the use of Cameleon YC3.6 for monitoring of Ca^{2+} dynamics in plant mitochondria (Loro *et al.*, 2012). Because of the discovery of a mitochondrial localized CaM-like protein (AtCML30) (Chigri *et al.*, 2012), we wondered if its ubiquitous presence (Fig. S1) can affect the mitochondrial Ca^{2+} measurements in terms of kinetic and response resolution. Thus, we decided to perform a comparison between YC3.6 response properties and D3cpv, the CaM insensitive Cameleon probe (Palmer *et al.*, 2006).

To this aim, we first generated stable Arabidopsis plants expressing the D3cpv (Palmer *et al.*, 2006) targeted to mitochondria. The mitochondrial localization of D3cpv was achieved following the same strategy adopted for YC3.6. We fused to the N-terminal of the probe the mitochondrial targeting sequence from subunit VIII of human cytochrome c oxidase repeated four time (4mt; Palmer *et al.*, 2006; Fig. 1a) and, to ensure the ubiquitous expression in plant, the probe was placed under the control of a single 35S-CaMV promoter (Fig. 1a) in the backbone of pGreen0179 binary vector (Hellens *et al.*, 2000). The construct was then introduced in Arabidopsis by floral dip method (Clough & Bent, 1998), and several independent lines were selected. We confirmed the mitochondrial localization of 4mt-D3cpv probe using the TMRM dye, a cationic potentiometric probe that specifically accumulates in mitochondria with a hyperpolarized inner membrane potential (Figs. 1b–d; Schwarzländer *et al.*, 2012). The sequential confocal microscope acquisitions of cpv and TMRM fluorescences (Fig. 1b–c) showed a clear merge of the two fluorescences in mitochondria of the analysed root cells (Fig. 1d).

To compare the 4mt-D3cpv properties with the 4mt-YC3.6, we first treated Arabidopsis seedling root tips with 2 mM

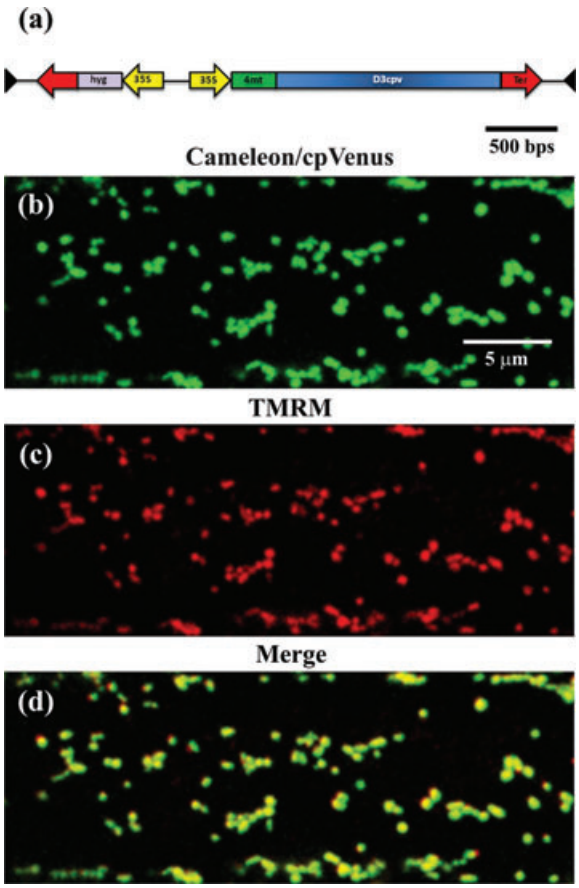

Fig. 1. 4mt-D3cpv probe localizes to mitochondria. (a) Schematic representation of 4mt-D3cpv Cameleon vector. (b–d) Sequential CLSM acquisitions indicate colocalization of the two fluorescences emitted in a representative root cell of seedling expressing the 4mt-D3cpv loaded with TMRM dye. The correspondence of the TMRM emitted signal with the Cameleon cpVenus demonstrates the mitochondrial localization of the probe. (b) cpVenus Cameleon fluorescence. (c) TMRM fluorescence. (d) Merged image of (b) and (c).

external ATP (eATP) and monitored the mitochondrial Ca^{2+} accumulation and response kinetics in both transgenic lines. From the traces shown in Figure 2(a), it was evident that both probes allowed the monitoring of $[Ca^{2+}]_m$ variations but they reported different maximum ratio changes and recovery times ($t/2$, 665 s ± 0.26 SE for YC3.6 and 455 s ± 0.52 SE for D3cpv) to the same stimulus, with the D3cpv showing the smaller amplitude and faster recovery compared with the YC3.6 (Fig. 2a). Hence, to better define *in vivo* the differences between the two probes, we availed ourselves of the observation that root tip cells treated with different eATP concentrations respond in a dose-dependent fashion both in cytoplasm and mitochondria (Loro *et al.*, 2012). We treated the Arabidopsis seedling expressing the 4mt-D3cpv Cameleon probe with 2, 0.5, and 0.01 mM eATP, and compared the results with those previously obtained with the 4mt-YC3.6 plants (Loro *et al.*, 2012). The data thus obtained demonstrate

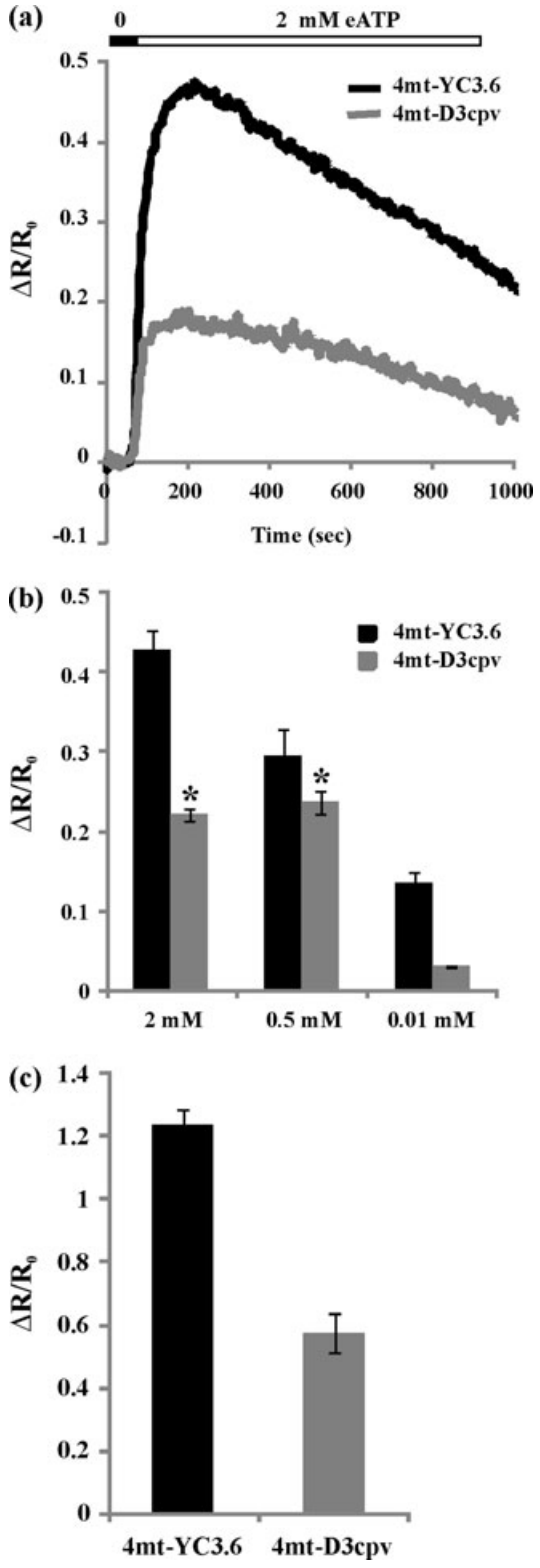

Fig. 2. 4mt-D3cpv reports mitochondrial Ca^{2+} accumulation with similar kinetics of 4mt-YC3.6 but with smaller dynamic range. (a) Root tips of 12-day-old seedlings of 4mt-D3cpv and 4mt-YC3.6 lines were bathed in 5 mM KCl, 10 mM Mes, 10 mM Ca^{2+} pH 5.8 and at the indicated time 2 mM eATP were added to the chamber. Ca^{2+} dynamics are reported as normalized cpVenus/CFP ratio variations ($\Delta R/R_0$). Representative traces show that both probes reported mitochondrial Ca^{2+} dynamics with apparently very similar kinetics, but with different $\Delta R/R_0$ peaks. (b) Root tips of 12-day-old seedlings of 4mtD3cpv and 4mt-YC3.6 lines were bathed in 5 mM KCl, 10 mM Mes, 10 mM Ca^{2+} pH 5.8 and at the indicated time 2, 0.5 or 0.01 mM eATP was added to the perfusion chamber. The analyses were performed considering the entire imaged root and the response, in terms of maximum Ca^{2+} rise after the stimulus, was clearly dose-dependent only in plants expressing the 4mt-YC3.6 probe. 4mt-D3cpv probe failed to report different Ca^{2+} accumulations in response to 2 and 0.5 mM eATP. Values are expressed as mean ± SE. Asterisks in the histogram indicate the different *p* values by Student's *t*-test (*p value 0.3581). (c) Mitochondria in permeabilized leaf epidermal cells were first bathed in a Ca^{2+} free solution (1 mM EGTA) and afterwards 5 mM Ca^{2+} was added. The maximum change in the measured ratio from 0 to 5 mM Ca^{2+} was reported as $\Delta R_{max}/R_0$ and compared between the two probes. The maximum response of the two mitochondrial Ca^{2+} probes revealed that 4mt-D3cpv shows a dynamic range that is only one half of the one measured for the 4mt-YC3.6. Values are expressed as mean ± SE ($n = 15$ and $n = 10$, respectively).

that the 4mt-D3cpv probe (Fig. 2b, grey bars) reports the mitochondrial Ca^{2+} accumulation in response to all tested concentrations, but with smaller peak amplitudes compared to 4mt-YC3.6 (Fig. 2b, black bars). In particular, the maximum ratio variation of 4mt-D3cpv in response to 0.01 mM eATP was four times smaller than that of 4mt-YC3.6 (Fig. 2b). Besides, the 4mt-D3cpv did not report differences in the $[Ca^{2+}]_m$ peak in response to 2 and 0.5 mM eATP (p value < 0.5). We then tested the 4mt-D3cpv response, in plant mitochondria, in permeabilized leaf epidermal cells (Costa *et al.*, 2010; Loro *et al.*, 2012). The mitochondria were first bathed in 1 mM EGTA buffer (to chelate free Ca^{2+}) and then perfused with 5 mM Ca^{2+}. We measured the Cameleon ratios before and after the addition of Ca^{2+} and calculated the maximum ratio variations in both transgenic lines (Fig. 2c). In this condition (from 0 to 5 mM Ca^{2+}), the maximum mitochondrial Ca^{2+} accumulation is supposed to occur (Palmer & Tsien, 2006), and therefore the maximum probe/s response/s observed. In the experiment shown in Figure 2(c), the maximum response ($\Delta R_{max}/R_0$) of the 4mt-YC3.6 (1.23 ± 0.051 SE) was double compared to the 4mt-D3cpv (0.575 ± 0.061 S.E.), demonstrating that in mitochondria the latter has a smaller dynamic range. Interestingly, the smaller dynamic range of D3cpv, compared with YC3.6, was previously reported by Hendel *et al.* (2008) in presynaptic boutons of Drosophila larvae neurons. In their experimental conditions, the *in vivo* maximum ratio change, in the cytoplasm, was 1.36 for YC3.6 and 0.9 for D3cpv, close to our observations in mitochondria. In the same work, Hendel *et al.* also reported the *in vivo* K_D for both probes, which was 0.36 μM for YC3.6 and 0.49 μM for D3cpv (Hendel *et al.*, 2008), values close to those measured *in vitro* (0.25 μM for YC3.6 and 0.6 μM for D3cpv) in the original papers (Nagai *et al.*, 2004; Palmer *et al.*, 2006), but

slightly different. The different K_D value of the two probes, both *in vivo* and *in vitro*, is probably the reason of the lower D3cpv responsiveness. Hence, the different responses we observed between the two analysed probes in mitochondria, seem mainly to depend on the intrinsic probe properties and not to other factor/s, such as endogenous mitochondrial CaM.

In conclusion, the comparison between the two different Cameleon probes here reported demonstrates that both 4mt-YC3.6 and 4mt-D3cpv allow monitoring of mitochondrial Ca^{2+} dynamics, but the former offers a better sensitivity, due mainly to its higher dynamic range and lower K_D. Last but not least, the comparison between these probes allows to assert that the endogenous mitochondrial CaM levels seem not to affect the Ca^{2+} measurements performed with 4mt-YC3.6 probe, making the latter the preferred one for monitoring Ca^{2+} dynamics in plant cells.

Acknowledgements

We thank Dr. Claudio Olivari for critical comments on the paper. Work partially supported by the Italian Ministero dell'Istruzione, dell'Università e della Ricerca (MIUR) through the grant FIRB 2010 (RBFR10S1LJ_001) to A.C.

References

Baughman, J.M., Perocchi, F., Girgis, H.S., *et al.* (2011) Integrative genomics identifies MCU as an essential component of the mitochondrial calcium uniporter. *Nature* **476**, 341–345.

Chigri, F., Flosdorff, S., Pilz, S., Kölle, E., Dolze, E., Gietl, C. & Vothknecht, U.C. (2012) The Arabidopsis calmodulin-like proteins AtCML30 and AtCML3 are targeted to mitochondria and peroxisomes, respectively. *Plant Mol. Biol.* **78**, 211–222.

Clough, S.J. & Bent, A.F. (1998) Floral dip: a simplified method for Agrobacterium-mediated transformation of Arabidopsis thaliana. *Plant J.* **16**, 735–743.

Contreras, L., Drago, I., Zampese, E. & Pozzan, T. (2010) Mitochondria: the calcium connection. *Biochim. Biophys. Acta.* 1797, 607–618.

Costa, A., Drago, I., Behera, S., Zottini, M., Pizzo, P., Schroeder, J.I., Pozzan, T. & Lo Schiavo, F. (2010) H_2O_2 in plant peroxisomes: an *in vivo* analysis uncovers a Ca^{2+}-dependent scavenging system. *Plant J.* **62**, 760–772.

De Stefani, D., Raffaello, A., Teardo, E., Szabò, I. & Rizzuto, R. (2011) A forty-kilodalton protein of the inner membrane is the mitochondrial calcium uniporter. *Nature* **476**, 336–340.

Drago, I., Pizzo, P. & Pozzan, T. (2011) After half a century mitochondrial calcium in- and efflux machineries reveal themselves. *EMBO J.* **30**, 4119–4125.

Hellens, R.P., Edwards, E.A., Leyland, N.R., Bean, S. & Mullineaux, P.M. (2000) pGreen: a versatile and flexible binary Ti vector for Agrobacterium-mediated plant transformation. *Plant Mol. Biol.* **42**, 819–832.

Heim, N. & Griesbeck, O. (2004) Genetically encoded indicators of cellular calcium dynamics based on troponin C and green fluorescent protein. *J. Biol. Chem.* **279**, 14280–14286.

Hendel, T., Mank, M., Schnell, B., Griesbeck, O., Borst, A. & Reiff, D.F. (2008) Fluorescence changes of genetic calcium indicators and OGB-1 correlated with neural activity and calcium *in vivo* and *in vitro*. *J. Neurosci.* **28**, 7399–7411.

Loro, G., Drago, I., Pozzan, T., Lo Schiavo, F., Zottini, M. & Costa, A. (2012) Targeting of Cameleon to different subcellular compartments reveals a strict cytoplasmic/mitochondrial Ca^{2+} handling relationship in plant cells. *Plant J.* **71**, 1–13.

McAinsh, M.R. & Pittman, J.K. (2009) Shaping the calcium signature. *New Phytol.* **181**, 275–294.

Nagai, T., Yamada, S., Tominaga, T., Ichikawa, M. & Miyawaki, A. (2004) Expanded dynamic range of fluorescent indicators for Ca^{2+} by circularly permuted yellow fluorescent proteins. *Proc. Natl. Acad. Sci. USA* **101**, 10554–10559.

Palmer, A.E., Giacomello, M., Kortemme, T., Hires, S.A., Lev-Ram, V., Baker, D. & Tsien, R.Y. (2006) Ca^{2+} indicators based on computationally redesigned calmodulin-peptide pairs. *Chem. Biol.* **13**, 521–530.

Palmer, A.E. & Tsien, R.Y. (2006) Measuring calcium signaling using genetically targetable fluorescent indicators. *Nat. Protoc.* **1**, 1057–1065.

Schmid, M., Davison, T.S., Henz, S.R., *et al.* (2005) A gene expression map of *Arabidopsis thaliana* development. *Nat. Genet.* **37**, 501–506.

Stael, S., Wurzinger, B., Mair, A., Mehlmer, N., Vothknecht, U.C. & Teige, M. (2012) Plant organellar calcium signalling: an emerging field. *J. Exp. Bot.* **63**, 1525–1542.

Schwarzländer, M., Logan, D.C., Johnston, I.G., Jones, N.S., Meyer, A.J., Fricker, M.D. & Sweetlove, L.J. (2012) Pulsing of membrane potential in individual mitochondria: a stress-induced mechanism to regulate respiratory bioenergetics in Arabidopsis. *Plant Cell.* **24**, 1188–1201.

Zampese, E., Fasolato, C., Kipanyula, M.J., Bortolozzi, M., Pozzan, T. & Pizzo, P. (2011) Presenilin 2 modulates endoplasmic reticulum (ER)-mitochondria interactions and Ca^{2+} cross-talk. *Proc. Natl Acad. Sci. USA* **15**, 2777–2782.

Supporting Information

Additional Supporting Information may be found in the online version of this paper at the publisher's web site:

Fig. S1. Expression of *Arabidopsis* calmodulin (CaM)-like (*AtCML30*) gene in different plant organs (root, stem, leaf, whole plant, rosette, apex, flower and pollen) during development. The *AtCML30* gene expression data were obtained and modified from the AtGeneExpress Visualization Tool (http://jsp.weigelworld.org/expviz/expviz.jsp).

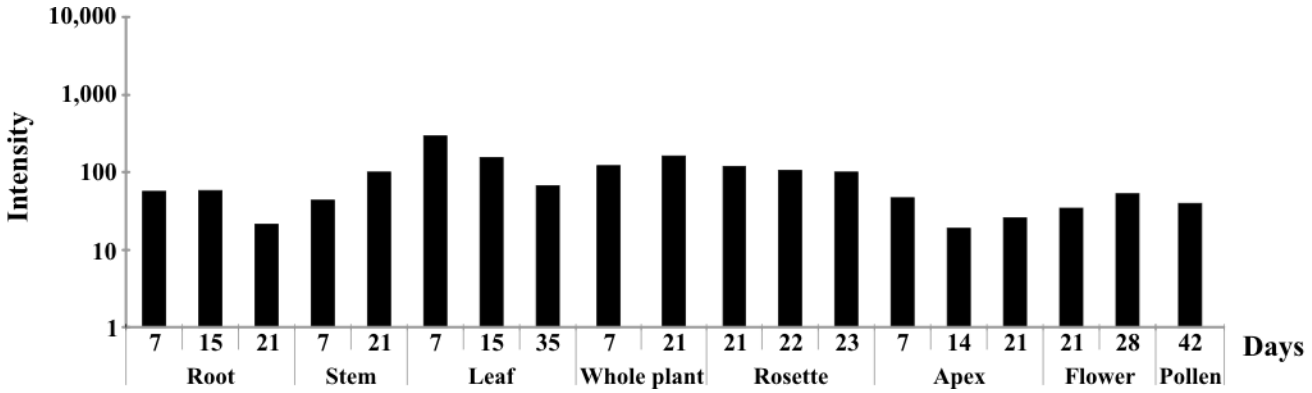

Fig. S1. Expression of *Arabidopsis* calmodulin (CaM)-like (*AtCML30*) gene in different plant organs (root, stem, leaf, whole plant, rosette, apex, flower and pollen) during development. The *AtCML30* gene expression data were obtained and modified from the AtGeneExpress Visualization Tool (http://jsp.weigelworld.org/expviz/expviz.jsp).

Chapter 3:

Endoplasmic reticulum Ca^{2+}-dynamics

3.1 Introduction on ER Ca^{2+}-dynamics

The endoplasmic reticulum (ER) is an interconnected network of stacked-membrane sheets and tubules that stretches throughout the cytoplasm. This compartment plays many essential roles in the cell, including synthesis, folding, modification and trafficking of both secreted and plasma membrane proteins (Chen et al. 2012). Furthermore, ER is the main Ca^{2+} store in animal cells; its role during the muscle contractions has been chiefly described, proper Ca^{2+} storage, release, and re-uptake are essential for normal skeletal muscle function (Rossi and Dirksen. 2006).

Although, Ca^{2+} dynamics across ER membrane are poorly characterized even if the activity of Ca^{2+}-permeable channels, Ca^{2+}-pumps and Ca^{2+}-binding proteins has been already identified (Sanders et al. 2002).

The molecular identity of the ER channels involved in Ca^{2+} release, in plants, is still unknown, in fact, two putative candidates were identified from *Bryonia dioica* and *Lepidium sativum* (Klusener et al. 1997, Klusener and Weiler. 1999) and biochemically characterized, but evidences on their *in vivo* roles are still lacking. In addition, studies performed with Ca^{2+} isotopes on microsomes isolated from cauliflower and red beet support the presence of outward channels in the ER membrane. In fact, although higher plants show no homologues of mammalian InsP3 and ryanodine receptors, IP3, nicotinic acid adenine dinucleotide phosphate (NAAD) and cyclic adenosine diphosphoribose (cADPR) can evoke a Ca^{2+} release (Navazio et al. 2000,Navazio et al. 2001). Interestingly several algae species have these receptors, suggesting that they were present in ancestral eukaryotes and lost by land plants during evolution (Wheeler and Brownlee. 2008).

Several Ca^{2+}-pumps ECAs (for ER-type Ca^{2+}-ATPase) and ACAs (for auto-inhibited Ca^{2+}-ATPase) are present, or predicted to be, at the plant ER membrane (Bonza and De Michelis. 2011,Pittman et al. 2011). In particular, ECA1 and ACA2 localization was defined (Liang et al. 1997,Hong et al. 1999), although their involvement in Ca^{2+} homeostasis is still under investigation.

In the presented paper, the development of a new molecular tool for the *in vivo* study of Ca^{2+} status and dynamics in the ER is reported. The performed analyses revealed differences between animal and plant ER Ca^{2+} dynamics, suggesting that in plant ER mainly functions as capacitor of cytosolic Ca^{2+} and not as a Ca^{2+} store, a function fulfilled by the vacuoles that are missing in mammalian cells.

3.2 Analyses of Ca^{2+} accumulation and dynamics in the endoplasmic reticulum of Arabidopsis root cells using a genetically encoded Cameleon sensor

Analyses of Ca^{2+} Accumulation and Dynamics in the Endoplasmic Reticulum of Arabidopsis Root Cells Using a Genetically Encoded Cameleon Sensor[1][C][W]

Maria Cristina Bonza[2], Giovanna Loro[2], Smrutisanjita Behera, Andrea Wong, Jörg Kudla, and Alex Costa*

Department of Biosciences, University of Milan, 20133 Milan, Italy (M.C.B., G.L., A.C.); Department of Biology (G.L.) and Department of Biomedical Sciences (A.W.), University of Padua, 35131 Padova, Italy; Institut für Biologie und Biotechnologie der Pflanzen, Universität Münster, 48149 Münster, Germany (S.B., J.K.); and Institute of Biophysics, Consiglio Nazionale delle Ricerche, 20133 Milan, Italy (A.C.)

In planta, very limited information is available about how the endoplasmic reticulum (ER) contributes to cellular Ca^{2+} dynamics and homeostasis. Here, we report the generation of an ER-targeted Cameleon reporter protein suitable for analysis of Ca^{2+} accumulation and dynamics in the lumen of the ER in plant cells. Using stably transformed Arabidopsis (*Arabidopsis thaliana*) plants expressing this reporter protein, we observed a transiently enhanced accumulation of Ca^{2+} in the ER in response to stimuli inducing cytosolic Ca^{2+} rises in root tip cells. In all experimental conditions, ER Ca^{2+} dynamics were substantially different from those monitored in the cytosol. A pharmacological approach enabled us to evaluate the contribution of the different ER-resident Ca^{2+}-ATPase classes in the regulation of the ER Ca^{2+} homeostasis. Taken together, our results do not provide evidence for a role of the ER as a major source that releases Ca^{2+} for stimulus-induced increases in cytosolic Ca^{2+} concentration. Instead, our results show that the luminal ER Ca^{2+} elevations typically follow cytosolic ones, but with distinct dynamics. These findings suggest fundamental differences for the function of the ER in cellular Ca^{2+} homeostasis in plants and animals.

In plants, rises in cytosolic Ca^{2+} concentration ($[Ca^{2+}]_{cyt}$) occur in response to both biotic and abiotic stimuli (Hetherington and Brownlee, 2004; McAinsh and Pittman, 2009; Kudla et al.., 2010; Bose et al., 2011). Depending on the stimulus, these rises can display the form of a single transient or repetitive Ca^{2+} oscillations and are commonly designated as "Ca^{2+} signatures" (Webb et al., 1996; Allen et al., 2000, 2001; Sanders et al., 2002; Young et al., 2006; Kudla et al., 2010).

The generation and shaping of $[Ca^{2+}]_{cyt}$ signatures depends on fine-tuning of Ca^{2+} influxes and effluxes occurring at both the plasma membrane (PM) and membranes of the different subcellular compartments (Pittman and Hirschi, 2003; Hetherington and Brownlee, 2004; Dodd et al., 2010; Spalding and Harper, 2011). The opening of Ca^{2+}-permeable influx channels in response to a stimulus will release Ca^{2+} into the cytosol and cause the generation of a Ca^{2+} spike, while the activity of Ca^{2+} efflux transporters (H^+-Ca^{2+} antiporters and Ca^{2+}-ATPases) will return the $[Ca^{2+}]_{cyt}$ to resting concentrations (McAinsh and Pittman, 2009; Bonza and De Michelis, 2011; Spalding and Harper, 2011).

Recently, the development and application of genetically encoded Ca^{2+} reporter proteins like Cameleons has allowed the study of Ca^{2+} dynamics in several compartments with organ, tissue, and single-cell resolution (Allen et al., 1999; Monshausen et al., 2008; Yang et al., 2008; Sieberer et al., 2009; Costa et al., 2010; Rincón-Zachary et al., 2010; Tanaka et al., 2010; Michard et al., 2011; Krebs et al., 2012; Loro et al., 2012; Behera et al., 2013). Cameleons are fluorescence resonance energy transfer (FRET)-based indicators in which two GFP variants, cyan fluorescent protein (CFP) and yellow fluorescent protein (YFP; or circularly permuted variants of YFP), are linked together by the Ca^{2+}-binding protein calmodulin (CaM) and a CaM-binding peptide (Miyawaki et al., 1997). Binding of Ca^{2+} to the Ca^{2+}-responsive elements alters the efficiency of FRET, allowing for quantitative measurements of Ca^{2+} dynamics. Different Cameleon variants have been developed since the first report about this reporter protein (Miyawaki et al., 1997). This involved, for example, advanced versions with improved fluorescence, larger changes in FRET upon Ca^{2+} binding, and a broad range of Ca^{2+} affinities (Palmer and Tsien, 2006). Moreover, mutational modification of the original Cameleon in the case of the

[1] This work was supported by Ministero dell'Istruzione, dell'Università e della Ricerca Fondo per gli Investimenti della Ricerca di Base (grant no. 2010 RBFR10S1LJ_001 to A.C.), by the German Research Foundation (grant nos. FOR 964 and SFB 629 to J.K.), by the International Max Planck Research School-Cell Dynamics and Disease (Ph.D. fellowship to S.B.), and by a binational Deutscher Akademischer Austausch Dienst/VIGONI grant.

[2] These authors contributed equally to the article.

* Address correspondence to alex.costa@unimi.it.

The author responsible for distribution of materials integral to the findings presented in this article in accordance with the policy described in the Instructions for Authors (www.plantphysiol.org) is: Alex Costa (alex.costa@unimi.it).

[C] Some figures in this article are displayed in color online but in black and white in the print edition.

[W] The online version of this article contains Web-only data.

www.plantphysiol.org/cgi/doi/10.1104/pp.113.226050

D family of indicators ensured that their function is no longer perturbed by large excesses of native CaM (Palmer et al., 2006). The use of Cameleons in plants has allowed the study of cytosolic (Krebs et al., 2012), nuclear (Sieberer et al., 2009; Krebs et al., 2012), peroxisomal (Costa et al., 2010, 2013), and mitochondrial (Loro et al., 2012, 2013) Ca^{2+} dynamics in specific plant organs and single cells. However, despite all these advances, very limited data have been reported regarding in vivo analyses of endoplasmic reticulum (ER) Ca^{2+} dynamics in plants (Iwano et al., 2009).

In animal cells, the ER represents an important Ca^{2+} storage organelle in which the free Ca^{2+} concentration varies between 50 and 500 μM (Coe and Michalak, 2009). Ca^{2+} release from the ER is involved in many different processes, including exocytosis, contraction, metabolism, regulation of transcription, fertilization, and apoptosis. The major Ca^{2+} entry pathway in electrically nonexcitable cells is represented by the "store-operated Ca^{2+} entry" (SOCE; Feske et al., 2012). Here, PM-localized calcium release-activated channels are activated in response to the emptying of intracellular ER Ca^{2+} stores (Parekh and Putney, 2005; Carrasco and Meyer, 2010). Moreover, in several mammalian cell types upon stimulation, Ca^{2+} is released from the ER into the cytosol through the activity of different classes of ER-resident Ca^{2+}-permeable channels activated by second messengers such as inositol 1,4,5-trisphosphate (IP3) and cyclic adenosine diphosphoribose (Parekh and Putney, 2005; Berridge, 2009; Galione and Chuang, 2012). In sharp contrast, for plant cells, no precise data on ER Ca^{2+} concentration ($[Ca^{2+}]_{ER}$) are available (Stael et al., 2012), and in vivo investigations about the Ca^{2+} storage properties of the ER have remained very limited (Iwano et al., 2009).

Moreover, SOCE has not been reported in plants, and stromal interaction molecule (STIM) proteins, which are central components of SOCE, are not encoded in the genomes of higher plants (Collins and Meyer, 2011). Despite some biochemical evidence for Ca^{2+} release in response to IP3, nicotinic acid adenine dinucleotide phosphate, and cyclic adenosine diphosphoribose (Muir and Sanders, 1997; Navazio et al., 2000, 2001), electrophysiological analyses supporting the existence of voltage-gated ER-localized Ca^{2+} channels (Klüsener et al., 1995, 1997), homologous for the respective IP3 and ryanodine receptors, are missing in higher plants (Wheeler and Brownlee, 2008; Kudla et al., 2010). All considered, this situation suggests that the role of the ER for cellular Ca^{2+} dynamics may be fundamentally different in plants as compared with animal cells.

Plants contain two major types of Ca^{2+} pumps named ECA (for ER-type Ca^{2+}-ATPase) and ACA (for autoinhibited Ca^{2+}-ATPase; Geisler et al., 2000; Sze et al., 2000; Bonza and De Michelis, 2011). Plant genomes encode different isoforms of both ECAs and ACAs. These are often coexpressed in certain cell types, and consequently, different cellular membranes in the same cell contain multiple Ca^{2+}-ATPase isoforms (Bonza and De Michelis, 2011). In Arabidopsis (*Arabidopsis thaliana*), immunological and membrane fractionation studies provided evidence for an ER localization of at least two distinct Ca^{2+} pumps, ECA1 and ACA2 (Liang et al., 1997; Harper et al., 1998; Liang and Sze, 1998; Hong et al., 1999; Hwang et al., 2000). Moreover, additional ECA and ACA isoforms are predicted to be ER localized (Geisler et al., 2000; Sze et al., 2000, Baxter et al., 2003; Bonza and De Michelis, 2011). Biochemical characterization revealed that ECA1 and ACA2, besides different regulatory properties, also have different affinities for Ca^{2+}, with one-half saturation concentration for free Ca^{2+} in the submicromolar and micromolar range, respectively (Liang and Sze, 1998; Hwang et al., 2000; Sze et al., 2000; Wu et al., 2002; Bonza and De Michelis, 2011), suggesting their participation in different aspects of ER Ca^{2+} regulation. The main predicted function for the ER Ca^{2+}-ATPases is Ca^{2+} loading into the ER lumen (Corbett and Michalak, 2000; Persson and Harper, 2006). However, how exactly these ER Ca^{2+}-ATPases contribute to ER and cytosolic Ca^{2+} dynamics awaits further investigation.

Here, we report the successful development and application of a genetically encoded Cameleon Ca^{2+} reporter protein for the in vivo analyses of Ca^{2+} dynamics in the ER lumen of Arabidopsis by the combination of mammalian and plant targeting signals. Using this tool, we were able to monitor ER Ca^{2+} dynamics in root cells with organ, tissue, and cell resolution. This approach allowed us to evaluate in vivo the contribution of the different Ca^{2+}-ATPase classes in $[Ca^{2+}]_{ER}$ homeostasis. Taken together, our data do not support a role of the ER as a major Ca^{2+}-releasing source for stimulus-induced increases in cytosolic Ca^{2+} concentration. Instead, our results show that the luminal ER Ca^{2+} transients typically follow cytosolic increases, but with distinct dynamics. These findings suggest fundamental differences for the function of the ER in cellular Ca^{2+} homeostasis in plants and animals.

RESULTS AND DISCUSSION

Generation of a Cameleon-Based Reporter Protein for Monitoring Ca^{2+} Dynamics in the ER of Plants

In order to enable analyses of Ca^{2+} dynamics in the ER of plant cells, we first took advantage of the available D1ER Cameleon Ca^{2+} reporter protein that had already been successfully used to study Ca^{2+} dynamics in the ER of mammalian cells (Palmer et al., 2004; Luciani et al., 2009; Jiménez-Moreno et al., 2010). In this reporter construct, fusion of the D1 reporter protein with a mammalian calreticulin signal sequence and a KDEL ER-retention signal results in specific localization of the Ca^{2+} reporter protein to the mammalian ER (Palmer et al., 2004). Although a modified version of D1ER (CRT-D1ER) was correctly localized at the ER in plant cells, we could detect neither an increase nor a decrease of $[Ca^{2+}]_{ER}$ in response to specific stimuli (for details concerning construct production and localization analysis, see Supplemental Text S1 and Supplemental Fig. S1, respectively).

Since D1 Cameleon has a biphasic Ca^{2+} dependency in vitro (dissociation constant = 0.8 and 60 μM; Palmer and Tsien, 2006), we supposed that the resting $[Ca^{2+}]_{ER}$ in the analyzed cells was above these values. Therefore, we decided to evaluate an alternative probe with a different affinity for Ca^{2+}. The Cameleon D4 variant has an in vitro dissociation constant for Ca^{2+} of 195 μM (Palmer et al., 2006) and was very recently used by two groups to monitor free Ca^{2+} levels in the ER lumen of mammalian cells (Ravier et al., 2011; Kipanyula et al., 2012). To efficiently target the D4 probe to the lumen of plant cell ER, we followed the same cloning strategy adopted for the production of the CRT-D1ER construct. The Arabidopsis CALRETICULIN1A (Christensen et al., 2010) signal peptide was fused upstream of the D4ER Cameleon reporter (Kipanyula et al., 2012), and the entire coding sequence was placed under the control of a single cauliflower mosaic virus (CaMV) 35S promoter. The resulting construct, CRT-D4ER (Fig. 1), was transiently expressed in tobacco (*Nicotiana benthamiana*) leaf epidermal cells (Fig. 1, A–C). Comparison with the localization of nWAK2-mCherry-HDEL (for a full description of the construct, see Nelson et al., 2007) as an ER marker that was coexpressed in these cells revealed that nWAK2-mCherry-HDEL and CRT-D4ER fluorescences fully merged in the nuclear envelope of tobacco epidermal cells (Fig. 1, C and D). The CRT-D4ER reporter construct was subsequently transformed into Arabidopsis plants, and 15 independent stable transgenic lines were selected. Figure 1, E to H, provides representative images of CRT-D4ER Arabidopsis transgenic plants, demonstrating that the probe was expressed in root (Fig. 1E), hypocotyl (Fig. 1F), and mature leaf cells (Fig. 1G). In these different tissues/organs, the typical ER morphology was clearly recognized (Boevink et al., 1999; Brandizzi et al., 2002), with 1- to 5-μm ER fusiform bodies (Hawes et al., 2001; Matsushima et al., 2002, 2003; Nelson et al., 2007) detected in the hypocotyl cells (Fig. 1G). The CRT-D4ER probe was also abundantly expressed in guard cells (Fig. 1, G and H). In order to investigate the Ca^{2+} reporter protein conformation status in resting conditions, we imaged the root tip of transgenic CRT-D4ER seedlings by means of a wide-field fluorescence microscope (excited with a 436/20-nm light wavelength) for the simultaneous acquisition of the CFP and YFP emission wavelengths. In root tip cells expressing CRT-D4ER, the fluorescences of both CFP and the FRET acceptor (YFP in the D4) were detected and were clearly above the level of organ autofluorescence (Fig. 1, I and J). Similar results were obtained by confocal microscopic analysis performed both in leaves and root cells (data not shown).

CRT-D4ER Allows the Visualization of ER Ca^{2+} Dynamics in Root Cells

Subsequently, we sought to use CRT-D4ER to visualize potential variations in $[Ca^{2+}]_{ER}$ in response to defined stimuli. To this end, we challenged 7-d-old Arabidopsis seedlings with different stimuli reported to induce cytosolic Ca^{2+} rises in root cells, such as external ATP (Tanaka et al., 2010; Loro et al., 2012, 2013), L-Glu (Qi et al., 2006), and NaCl (Kiegle et al., 2000). To allow for comparison with cytosolic Ca^{2+} dynamics and as a control for the efficiency of stimulus applications, we performed a series of parallel experiments using either seedlings expressing the cytosol-localized Cameleon YC3.6 (NES-YC3.6; Nagai et al., 2004; Krebs et al., 2012) or expressing CRT-D4ER (Fig. 2).

One millimolar L-Glu was able to stimulate a fast and transient $[Ca^{2+}]_{cyt}$ increase in root tip cells (Fig. 2, A and G). In particular, L-Glu triggered a response in the cells of the root tip region, and then Ca^{2+} elevations spread out quickly to the upper root tip cells (Fig. 2A; Supplemental Movies S1 and S2). The L-Glu-Ca^{2+}-induced elevation is probably dependent on the activity of members of the ionotropic Glu receptors, channels that have been demonstrated to facilitate Ca^{2+} influx across the PM (Michard et al., 2011; Vincill et al., 2012, 2013). Several members of this large family (20 members in Arabidopsis; Lacombe et al., 2001) are in fact expressed in the different tissues of root tip, as reported by published microarray and experimental data (Winter et al., 2007; Vincill et al., 2013).

The same stimulus also triggered a concomitant increase of $[Ca^{2+}]_{ER}$ (Fig. 2, B and G), which was more sustained compared with the rise observed in the cytosol (Fig. 2, B and H). Importantly, separate analyses of the two CFP and FRET fluorescences revealed an evident FRET response, manifested by a decrease of CFP and an increase of YFP emissions (Supplemental Fig. S2A).

A similar series of experiments was then performed with the addition of 0.5 mM ATP (Fig. 2, C and D). In agreement with previous reports, high extracellular ATP concentration resulted in a strong and sustained $[Ca^{2+}]_{cyt}$ increase, with a typical dynamics consisting of different sequential Ca^{2+} peaks due to the influx of external Ca^{2+} and the release of Ca^{2+} from nonidentified internal stores (Fig. 2C; Supplemental Movie S3; Tanaka et al., 2010; Loro et al., 2012). This stimulus also induced an ER Ca^{2+} accumulation (Fig. 2D) in which the maximum level of $[Ca^{2+}]_{ER}$ was reached later as compared with the cytosol (Fig. 2G) but was stronger and even more sustained as compared with the one induced by L-Glu (Fig. 2, D, H, and I). In none of these experiments did we observe a measurable reduction in $[Ca^{2+}]_{ER}$ before the occurrence of the $[Ca^{2+}]_{cyt}$ increase. To further address this aspect, a series of experiments was performed with 0.01 mM ATP, a concentration reported to stimulate ER Ca^{2+} release in HeLa cells (Palmer et al., 2004). As reported previously, root tip cells stimulated with 0.01 mM ATP displayed $[Ca^{2+}]_{cyt}$ dynamics, albeit of lower magnitude (Supplemental Fig. S3, A and C–E; Loro et al., 2012). However, again, only an increase in $[Ca^{2+}]_{ER}$ was observed (Supplemental Fig. S3, B–E). These results strongly support the conclusion that the ER does not represent the internal Ca^{2+}-releasing store involved in the generation of the ATP-induced cytosolic

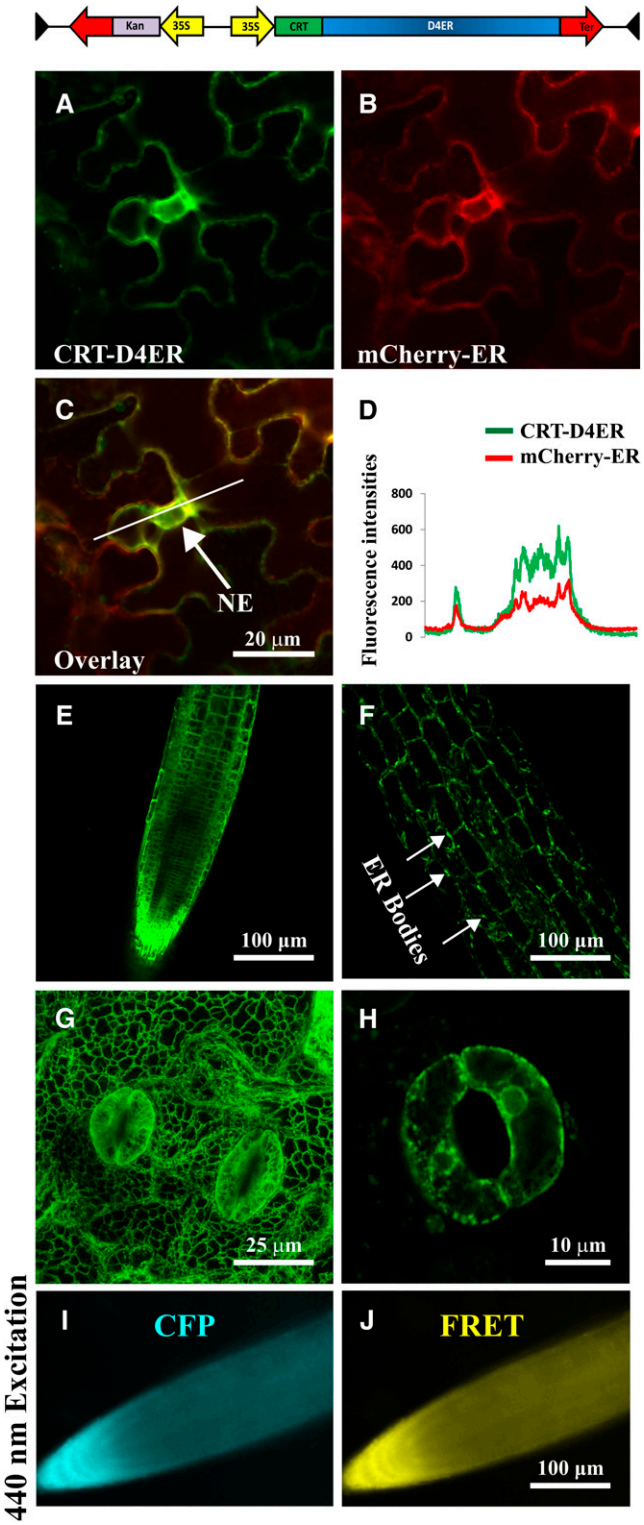

Figure 1. Subcellular distribution of CRT-D4ER in plant cells and simultaneous detection of CFP and FRET emissions. The top panel shows a schematic structure of the CRT-D4ER Cameleon probe. A to C, Confocal images of tobacco agroinfiltrated epidermal cells cotransformed with CRT-D4ER and the ER marker nWAK2-mCherry-HDEL (Nelson et al., 2007). A, Cameleon YFP fluorescence in tobacco epidermal cells. B, mCherry fluorescence in the same cells shown in A. C, The YFP signal of CRT-D4ER colocalizes with mCherry, as revealed by colocalization of the two fluorescence signals at the level of the nuclear envelope (NE). D, Plot profile of YFP and mCherry fluorescences corresponding to the marked white line shown in C. E to H, Confocal microscopy analyses revealed efficient CRT-D4ER YFP expression in different organs of Arabidopsis stable transgenic plants with a subcellular distribution showing typical ER features. E, Root tip cells. F, Hypocotyl cells, showing the presence of fusiform bodies. G, Three-dimensional maximum projection of a mature leaf region. H, Stomata guard cells. I and J, Representative root tip of a CRT-D4ER seedling excited with 440-nm light for FRET detection. I, CFP emission. J, FRET emission. The simultaneous detection of the two emissions demonstrates that CFP was not quenched and YFP was properly excited trough FRET.

Ca^{2+} dynamics. Finally, salt stress was analyzed as a third stimulus that is known to elicit an increase in cytosolic Ca^{2+} in root cells. The effect of NaCl was analyzed in the root mature zone, since these cells respond in a more pronounced manner than root tip cells to salt stress (data not shown). The addition of 100 mM NaCl induced a fast cytosolic Ca^{2+} increase (Fig. 2, E and G), which was accompanied by a Ca^{2+} accumulation in the ER (Fig. 2, F, H, and I). In the latter case, the source of cytosolic Ca^{2+} has been demonstrated to be both from extracellular and intracellular calcium stores, mainly from vacuole (Knight et al., 1997). Our results indeed demonstrate that the ER is not part of such intracellular stores. Moreover, it is worth noting that, compared with the response to L-Glu (Fig. 2, G–I), the increases in $[Ca^{2+}]_{cyt}$ were similar in terms of peak intensities and duration, while the ER Ca^{2+} accumulation induced by NaCl treatment was smaller. This observation could be related to the fact that cells of the root mature zone have extensive vacuoles compared with the meristematic cells of the root tip, hence probably also contributing to Ca^{2+} sequestration (Peiter, 2011).

Altogether, these results indicate that plant cells transiently accumulate Ca^{2+} in the ER in response to different stimuli, similar to what was observed in the apoplast and mitochondria (Gao et al., 2004; Loro et al., 2012). The subsequent decrease in $[Ca^{2+}]_{ER}$, which is especially evident with L-Glu, low ATP concentration, and NaCl treatments, occurs only after the initial accumulation and is likely to be dependent on the activity of ER membrane-resident Ca^{2+}-permeable channels (Klüsener et al., 1995, 1997; Muir and Sanders, 1997; Navazio et al., 2000, 2001). Importantly, these results suggest that, at least in the cases investigated here, the ER does not contribute to the generation of the observed cytosolic Ca^{2+} increases by releasing Ca^{2+}. Instead, it appears that the ER represents a system that mimics $[Ca^{2+}]_{cyt}$ increases, but with distinct dynamics, as marked by the different times at which the peaks of $[Ca^{2+}]_{cyt}$ and $[Ca^{2+}]_{ER}$ are reached after the stimuli perception (Fig. 2G). The delayed ER Ca^{2+} accumulation was particularly evident in ATP-stimulated cells (Fig. 2H; Supplemental Fig. S3E). These dynamics of ER Ca^{2+} accumulation may reflect the intrinsic properties

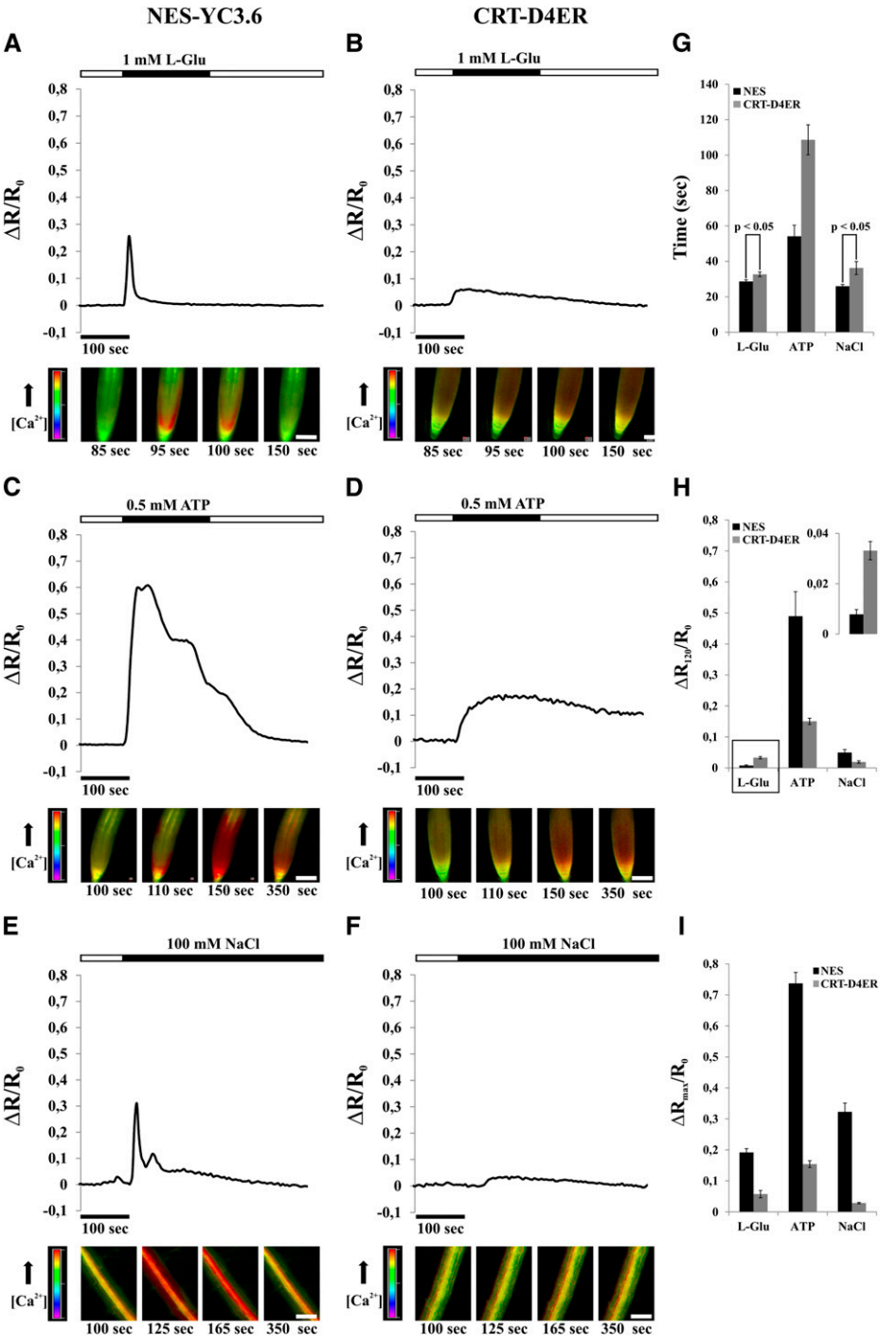

Figure 2. $[Ca^{2+}]_{cyt}$ and $[Ca^{2+}]_{ER}$ monitoring in roots of Arabidopsis seedlings expressing the NES-YC3.6 (cytosolic Cameleon) and CRT-D4ER (ER Cameleon) probes, challenged with different stimuli (L-Glu, ATP, and NaCl) for the indicated times (black rectangles above traces) and analyzed with a wide-field fluorescence microscope. Traces represent the normalized ratio (FRET/CFP) variations observed during the entire experiment. Images at bottom are representative ratio images of the experiment shown in the corresponding trace above. A, L-Glu (1 mM) induced a single steep and fast Ca^{2+} transient in the cytosol of root tip cells. B, The same stimulus of A induced an ER Ca^{2+} accumulation showing a slow kinetic and a sustained Ca^{2+} recovery phase. C, ATP (0.5 mM) induced a strong cytosolic Ca^{2+} transient in the cytosol of root tip cells, where different peaks were recognizable. The recovery phase was more sustained compared with 1 mM L-Glu. D, The same stimulus of C induced an ER Ca^{2+} accumulation showing a slow kinetic, but with values about four times higher than those observed with 1 mM L-Glu and, afterward, with a small $[Ca^{2+}]_{ER}$ decrease. E, NaCl (100 mM) induced a biphasic cytosolic Ca^{2+} response with two peaks of different intensities in cells of the root mature zone. F, The same salt concentration of E led to a small ER Ca^{2+} accumulation followed by a slow $[Ca^{2+}]_{ER}$ decrease. G, Statistical analysis of times at which the maximum $\Delta R/R_0$ variations were measured in both compartments in response to different applied stimuli. H, Statistical analysis of $\Delta R/R_0$ variations measured in both compartments 120 s after sensing of the different applied stimuli. The inset shows a magnification of L-Glu Ca^{2+} peak averages. I, Statistical analysis of maximum $\Delta R/R_0$ variations measured in both compartments in response to different applied stimuli. *P* values were calculated using Student's *t* test. Bars = 100 μm. [See online article for color version of this figure.]

of the ER-resident active Ca^{2+} transport systems (Bonza and De Michelis, 2011; Bose et al., 2011). Instead, the $[Ca^{2+}]_{cyt}$ increase is mainly dependent on the activity of channels occurring at very much faster rate than transporters.

To corroborate that Ca^{2+} accumulation in the ER mimics cytosolic Ca^{2+} rises, we performed a series of experiments in which two different ATP concentrations were applied successively (0.01 mM followed by 0.5 mM) to root tip cells (Fig. 3). In particular, the second administration was applied before both $[Ca^{2+}]_{cyt}$ and $[Ca^{2+}]_{ER}$ were completely recovered to resting values. Figure 3A reports the superimposition of representative normalized ratio variations measured in the cytosol and ER, clearly showing that, in correspondence with each $[Ca^{2+}]_{cyt}$ rise, a $[Ca^{2+}]_{ER}$ rise occurs. Hence, the ER is able to accumulate Ca^{2+} at different levels in response to $[Ca^{2+}]_{cyt}$ increases (Fig. 3B), supporting a role in

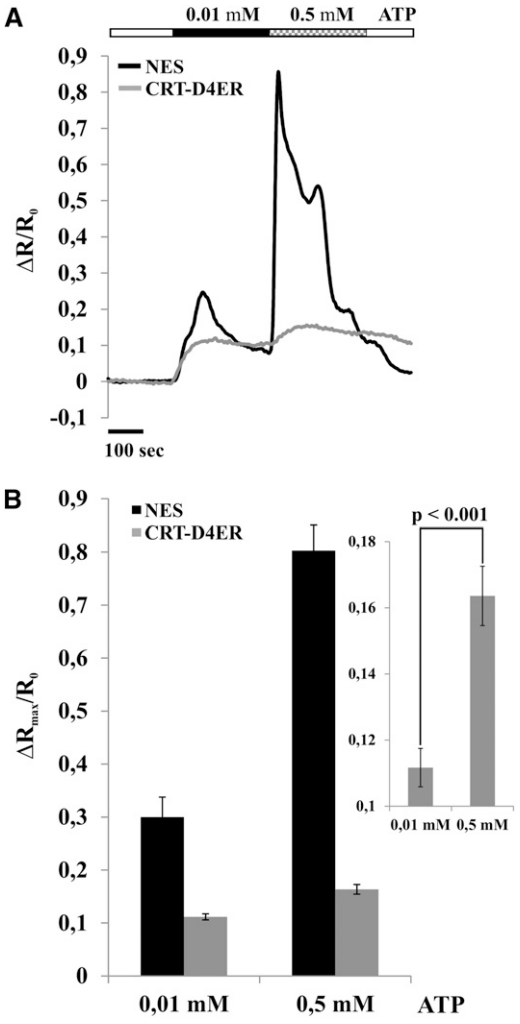

Figure 3. $[Ca^{2+}]_{cyt}$ and $[Ca^{2+}]_{ER}$ monitoring in root tips of Arabidopsis seedlings expressing the NES-YC3.6 (cytosolic Cameleon) and CRT-D4ER (ER Cameleon) probes challenged with 0.01 and 0.5 mM ATP for the indicated times (black and checkered rectangles above traces) and analyzed with a wide-field fluorescence microscope. A, Superimposition of representative normalized ratio variations for each transgenic line. B, Statistical analysis of maximum $\Delta R/R_0$ variations measured in both compartments. The inset shows a magnification of Ca^{2+} peak averages measured in the ER in response to 0.01 and 0.5 mM ATP. *P* values were calculated using Student's *t* test.

buffering the cytosolic Ca^{2+} rises. Together, these results indicate that Ca^{2+} accumulation in the ER is strictly dependent on the $[Ca^{2+}]_{cyt}$.

Finally, when root cells were challenged with a series of hyperpolarizing-depolarizing buffers, known to induce repetitive cytosolic Ca^{2+} transients in guard and root cells (Allen et al., 2000, 2001; Weinl et al., 2008; Krebs et al., 2012), repetitive ER Ca^{2+} accumulations were also observed (Supplemental Fig. S4, A and B). Chelating extracellular Ca^{2+} with EGTA prevented both cytosolic and ER Ca^{2+} transients (Supplemental Fig. S4, C and D), confirming that the ER does not contribute as an intracellular Ca^{2+} store to the generation of stimulus-induced cytosolic Ca^{2+} rises observed. However, we can currently not fully exclude that localized Ca^{2+} releases from ER occur in specific microdomains of cells (Rizzuto and Pozzan, 2006). Based on our microscope resolution, the predominant response of a defined population of root tip cells was measurable that consequently represents the predominant component of ER Ca^{2+} dynamics in these cells.

Comparison of ER Ca^{2+} dynamics induced in root tip cells by L-Glu and ATP revealed that Ca^{2+} accumulation in the ER was directly dependent on the magnitude of cytosolic Ca^{2+} elevation, with ATP inducing the strongest increase (compare the $\Delta R/R_0$ in Fig. 2, B, D, and I). In particular, the observed differences between the responses of root tip cells to L-Glu and ATP may result from a different number of cells responding primarily or secondarily to the stimulus (see the image sequences below the graphs in Fig. 2). In each single cell, the two stimuli may produce an increase in $[Ca^{2+}]_{ER}$ of different amplitude. In order to appreciate Ca^{2+} dynamics in single cells, we performed an analysis of CRT-D4ER-expressing seedlings by means of confocal microscopy. The results, depicted in Figure 4 and Supplemental Movies S4 and S5, demonstrated that amplitudes and dynamics of ER Ca^{2+} transients induced by L-Glu and ATP in single cells essentially reflected the general root tip response. Importantly, these results confirm that our wide-field analyses faithfully reflect the cellular responsiveness of root tip cells to the stimuli investigated.

Altogether, these experiments demonstrate that the CRT-D4ER represents a reliable probe to monitor ER Ca^{2+} dynamics in vivo at both the organ and single-cell levels. Moreover, our results suggest that, in the cells investigated under the conditions examined here, the ER does not represent a major store for releasing Ca^{2+} into the cytosol.

ER-Localized Ca^{2+}-ATPases Modulate ER Ca^{2+} Homeostasis

Having established that dynamic changes in Ca^{2+} accumulation occur in the ER in response to defined stimuli, we next aimed at elucidating the contribution of ER-resident Ca^{2+}-ATPases to $[Ca^{2+}]_{ER}$ homeostasis. In Arabidopsis, members of both classes of Ca^{2+} pumps are resident in the ER membrane (Sze et al., 2000; Bonza and De Michelis, 2011). ECAs are specifically inhibited by cyclopiazonic acid (CPA; Liang and Sze, 1998), while ACAs are particularly sensitive to inhibition by fluorescein derivatives such as erythrosin B or eosin Y (Eos; De Michelis et al., 1993; Geisler et al., 2000; Sze et al., 2000; Bonza et al., 2004; Bonza and De Michelis, 2011). Therefore, in order to evaluate the contribution of the different types of Ca^{2+}-ATPases to ER Ca^{2+} homeostasis, a pharmacological approach was pursued. Published microarray data (Winter et al., 2007) confirmed that root tips of young Arabidopsis seedlings express Ca^{2+} pumps

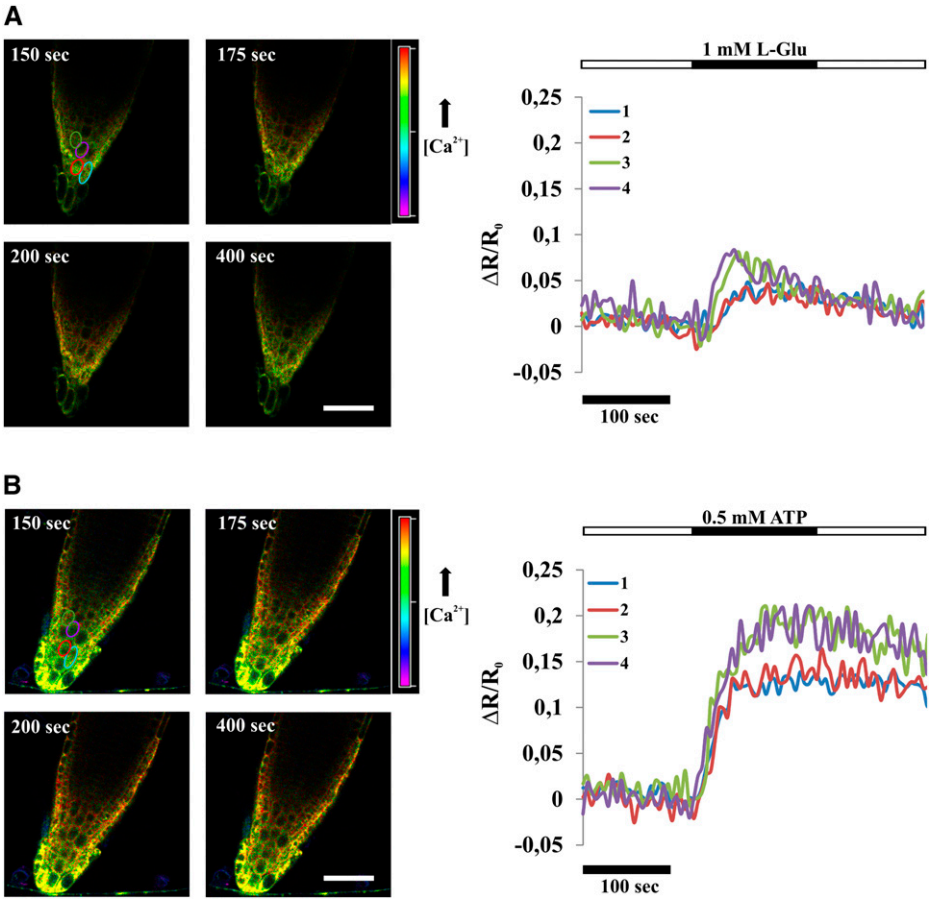

Figure 4. Single-cell $[Ca^{2+}]_{ER}$ monitoring in Arabidopsis CRT-D4ER seedling root tips subjected to L-Glu and ATP for the indicated times (black rectangles above traces). A, Effects of 1 mM L-Glu on the $[Ca^{2+}]_{ER}$ response in Arabidopsis root tip cells. Ratio images for selected frames are shown. B, Effects of 0.5 mM ATP on the $[Ca^{2+}]_{ER}$ response in Arabidopsis root tip cells. Ratio images for selected frames are shown. In both panels, elliptic areas, marked with different colors corresponding to different cells, were used for the ratio calculations (reported as normalized ratio variations $[\Delta R/R_0]$) plotted in the graphs. The two different stimuli triggered responses of different amplitudes, with ATP able to induce higher ER Ca^{2+} accumulations in all analyzed cells compared with L-Glu. Bars = 50 μm.

of both types at various cellular membranes, including the ER-localized Ca^{2+}-ATPase isoforms ACA2 and ECA1 (data not shown).

Arabidopsis seedlings expressing the CRT-D4ER or NES-YC3.6 Cameleon reporter protein were incubated for 10 or 60 min with or without 25 μM CPA, 0.5 μM Eos, and 25 μM CPA plus 0.5 μM Eos. In order to evaluate the $[Ca^{2+}]_{ER}$ and $[Ca^{2+}]_{cyt}$ levels in the different tested conditions, root tips were then analyzed by measuring the ratio values for both CRT-D4ER and NES-YC3.6 probes (Fig. 5). Root tip cells were chosen for the analysis because they harbor smaller vacuoles compared with cells of the mature zone. In this way, we probably reduced the relative contribution of the vacuolar Ca^{2+} transport systems to the regulation of cytosolic Ca^{2+} homeostasis (Cheng et al., 2005; Conn et al., 2011; Peiter, 2011).

The ECA inhibitor CPA affected the CRT-D4ER ratio already after 10 min of treatment, resulting in a significant decrease in the $[Ca^{2+}]_{ER}$ compared with the control condition (Fig. 5A, gray bar). Surprisingly, treatment with the ACA inhibitor Eos did not lead to a $[Ca^{2+}]_{ER}$ decrease but to a $[Ca^{2+}]_{ER}$ increase (Fig. 5A, white bar). Interestingly, when treatments were performed with both inhibitors simultaneously (Fig. 5A, striped bar), the $[Ca^{2+}]_{ER}$ was lower than in the Eos treatment alone but higher than with CPA alone. This suggests that the CPA-sensitive component is just partially responsible for the observed Eos-induced ER Ca^{2+} accumulation. After 60 min of incubation, the results were quite similar with CPA (Fig. 5B, gray bar), while the Eos effect on $[Ca^{2+}]_{ER}$ increases was dramatically enhanced (Fig. 5B, white bar). In the latter condition, the presence of CPA was still able to reduce the $[Ca^{2+}]_{ER}$ (Fig. 5B, striped bar). When the effect of inhibitors was tested on NES-YC3.6 seedlings, we observed that treatment with CPA for 10 min barely affected the $[Ca^{2+}]_{cyt}$ (Fig. 5C, gray bar), while treatment with Eos led to an increase of $[Ca^{2+}]_{cyt}$ (Fig. 5C, gray bar) that was further slightly increased by the simultaneous addition of CPA (Fig. 5C, striped bar). Extension of the treatment to 60 min caused similar, but more pronounced, results.

In summary, the combined analyses of Ca^{2+} dynamics in ER and cytosol with Ca^{2+}-ATPase inhibitors revealed that, under basal conditions, CPA-sensitive ECAs substantially contribute to ER Ca^{2+} accumulation but have a minor role in the control of $[Ca^{2+}]_{cyt}$ levels. Application of Eos compromised the activity of the ACA pumps that are fundamental for the maintenance of basal $[Ca^{2+}]_{cyt}$ in resting conditions but did not prevent the accumulation of Ca^{2+} in the ER, which

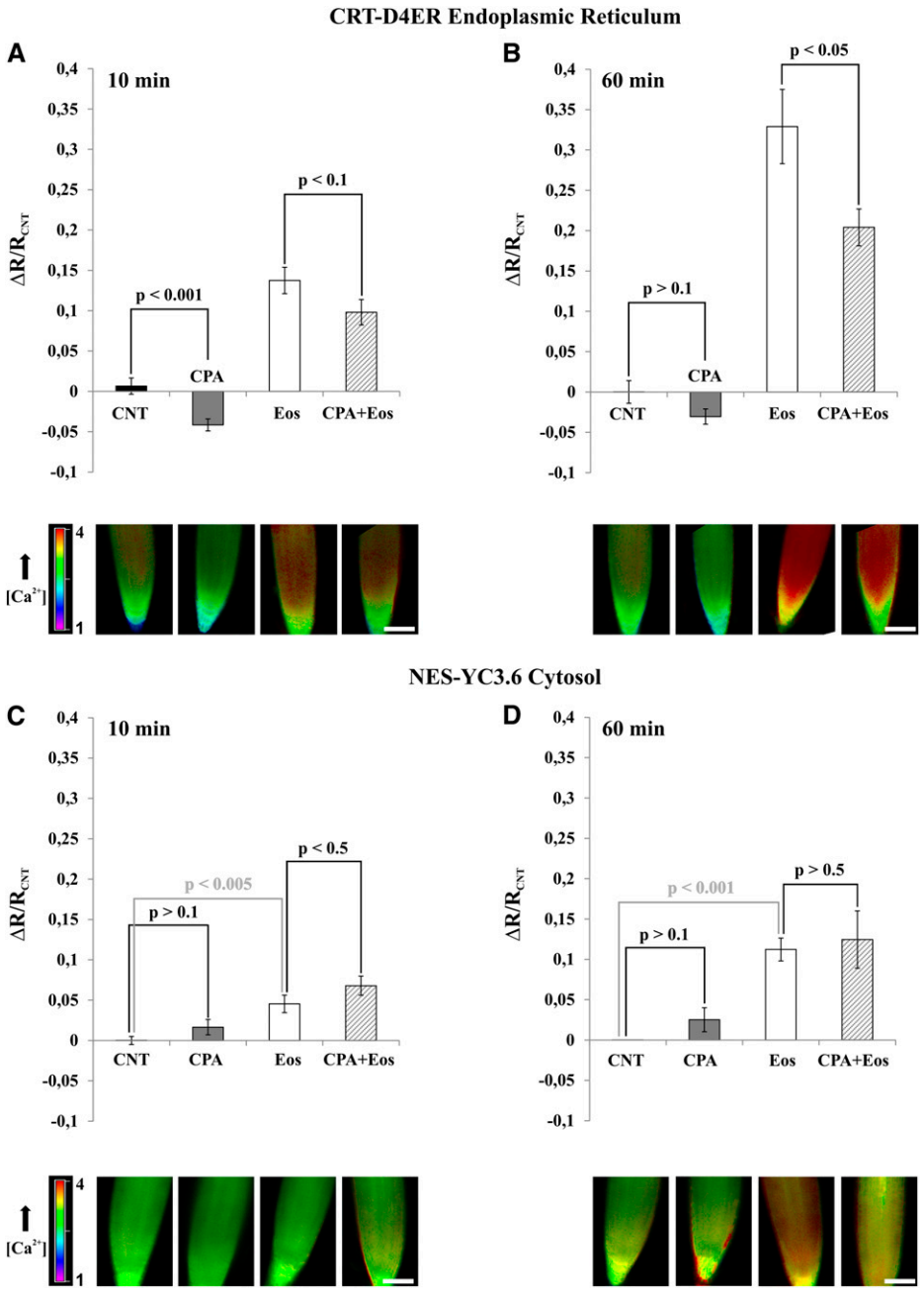

Figure 5. Effects of Ca^{2+}-ATPase inhibitors on $[Ca^{2+}]_{cyt}$ and $[Ca^{2+}]_{ER}$ in root tip cells of Arabidopsis. Seedlings expressing NES-YC3.6 and CRT-D4ER were incubated for 10 and 60 min in control buffer (see "Materials and Methods") or in the presence of 25 μM CPA, 0.5 μM Eos, and 25 μM CPA + 0.5 μM Eos. Root tips were analyzed with a wide-field fluorescence microscope. Bars represent the averaged normalized ratios ($\Delta R/R_{CNT}$) ± SE. The ratios were normalized to the average ratio (R_{CNT}) of each control experiment. The images at bottom are representative ratio images of each tested condition. A and B, $[Ca^{2+}]_{ER}$ Cameleon ratio variations measured in root tip of CRT-D4ER seedlings treated for 10 and 60 min, respectively, with the different inhibitors. C and D, $[Ca^{2+}]_{cyt}$ Cameleon ratio variations measured in root tip of NES-YC3.6 seedlings treated for 10 and 60 min, respectively, with the different inhibitors. *P* values were calculated using Student's *t* test. Bars = 100 μm. [See online article for color version of this figure.]

actually increased. This increase was reduced, but not fully suppressed, by CPA. Considering that under the applied conditions CPA suppressed ECA activity, these results indicate that, under elevated $[Ca^{2+}]_{cyt}$, ECAs contribute to $[Ca^{2+}]_{ER}$ accumulation, but other transport systems are also involved. We cannot exclude that the Eos concentration used in this study was sufficient to inhibit ACA localized at cellular membranes such as PM and tonoplast (Bonza and De Michelis, 2011; Bose et al., 2011) but not fully effective in completely blocking the activity of the ER-resident ACAs (e.g. ACA2; Harper et al., 1998). Hence, it is plausible that the observed elevation of cytosolic Ca^{2+}, due to the inhibition of cytosolic Ca^{2+} removal, leads to higher ER Ca^{2+} accumulation.

CONCLUSION

In this work, we report (1) the generation of the CRT-D4ER Cameleon reporter protein as a suitable tool for the analysis of Ca^{2+} status and dynamics in the ER of plant cells; (2) the analysis of ER Ca^{2+} dynamics in root tip cells in response to defined stimuli; and (3) the evaluation of the contribution of ECA and ACA Ca^{2+}-ATPases to the control of ER Ca^{2+} homeostasis.

The application of CRT-D4ER enables the study of the dynamics of $[Ca^{2+}]_{ER}$ and its interconnection with cytosolic Ca^{2+} signatures in different cell types, genetic backgrounds, and developmental and stress-response processes.

Using this tool, we comparatively analyzed the dynamics of $[Ca^{2+}]_{ER}$ and $[Ca^{2+}]_{cyt}$ in response to different stimuli like ATP, L-Glu, NaCl, and alternate applications of depolarizing and hyperpolarizing buffer. In conclusion, all our data do not support a significant role of $[Ca^{2+}]_{ER}$ as a source of Ca^{2+} release that contributes to the formation of cytosolic Ca^{2+} signatures, at least in the cell types and during the responses investigated in this study. Instead, our data support the hypothesis that, in plant cells, the ER functions primarily as a mimicking system for cytosolic Ca^{2+} signaling. These findings point to fundamental differences in the role of the ER for cellular Ca^{2+} dynamics in plants and animals.

MATERIALS AND METHODS

Plant Material and Growth Conditions

All Arabidopsis (*Arabidopsis thaliana*) plants used in this study were of the Columbia ecotype. Plants were grown on 16/8-h cycles of light (70 μmol m^{-2} s^{-1}) at 22°C and 75% relative humidity. Seeds of Arabidopsis were surface sterilized by vapor-phase sterilization (Clough and Bent, 1998) and plated on one-half Murashige and Skoog medium (Murashige and Skoog medium plus M0222 elements including vitamins; Duchefa [http://www.duchefa-biochemie.nl/]; Murashige and Skoog, 1962) supplemented with 0.1% (w/v) Suc and 0.05% (w/v) MES, pH 6.0, and solidified with 0.8% (w/v) plant agar (Duchefa). After stratification at 4°C in the dark for 3 d, seeds were transferred to the growth chamber with 16/8-h cycles of light (70 μmol m^{-2} s^{-1}) at 24°C. The plates were kept vertically. Seedlings used for the analyses were 7 to 8 d old, which corresponds to an average root length of 3 cm.

DNA Constructs

In order to generate the binary vectors for the expression of the Cameleon ER probes in plants, we inserted the single CaMV 35S promoter and the CaMV poly(A) terminator in the polylinker of the pGreen0029 binary vector (Hellens et al., 2000) by using the *Kpn*I and *Sac*I restriction sites, respectively. The CaMV 35S and CaMV poly(A) were PCR amplified using the 35S-CaMV cassette vector as a template (http://www.pgreen.ac.uk/JIT/JIT_fr.htm) and the following primer pairs: 35S-For, 5′-CATGggtaccGATATCGTACCCCTACTCCA-3′; 35S-Rev, 5′-CATGggtaccGGGCTGTCCTCTCCAAATGAA-3′; Ter-For, 5′-CATGgagctcGGTACGCTGAAATCACCAGT-3′; and Ter-Rev, 5′-CATGgagctcATCGATCTGGATTTTAGTACTGGA-3′ (the sequences of the restriction sites are shown in lower-case letters). D1ER (AY796115.1) and D4ER (Plasmid 37473: pBAD-D4; http://www.addgene.org/37473/) coding sequences were digested from the pcDNA3-D1ER and pcDNA3-D4ER vectors with *Hin*dIII and *Eco*RI restriction enzymes and ligated into the modified pGreen0029-35S-Ter binary vector. In order to generate the CRT-D1ER and CRT-D4ER constructs, the first 66 nucleotides (CRT) of the Arabidopsis CALRETICULIN1A gene (At1g56340) were PCR amplified and fused upstream the D1ER and D4ER coding sequences by using the *Hin*dIII restriction site. The primers used were as follows: CRT-For, 5′-CATGaagcttATGGCGAAACTAAACCCTAAATT-3′; and CRT-Rev, 5′-CATGaagcttgAGCAGAGACGATCACCACGA-3′. The amplicon was isolated by digestion and ligated into the 35S-D1ER and 35S-D4ER linearized vectors. The obtained clones were sequenced to verify the right orientation of the CRT sequence.

The binary vectors were then introduced into the *Agrobacterium tumefaciens* GV3101 strain.

Transgenic Plants and Tobacco Transient Transformation

The *A. tumefaciens* strains obtained as reported above were used to generate transgenic Arabidopsis plants by the floral dip method (Clough and Bent, 1998). For each construct, 15 Arabidopsis independent transgenic lines were selected, and four independent lines were employed for imaging experiments. Experiments were carried out in seedlings of the T1 and T2 generations for CRT-D4ER transgenic lines. Mature T2 plants were affected by silencing. To minimize this problem, work is in progress to test different vector backbones and promoters.

Transient expression of CRT-D4ER in tobacco (*Nicotiana benthamiana*) epidermal leaf cells was performed as described by Waadt and Kudla (2008).

Seedling Preparation for Ca^{2+} Imaging

For root cell imaging, 7-d-old seedlings grown vertically were prepared accordingly to Behera and Kudla (2013) in dedicated chambers and overlaid with wet cotton in order to continuously perfuse the root with the imaging solution (5 mM KCl, 10 mM MES, 10 mM Ca^{2+}, pH 5.8, adjusted with Tris for ATP and L-Glu, or 0.1 mM KCl, 10 mM MES, 1 mM Ca^{2+}, pH 5.8, adjusted with Tris for NaCl). The shoot was not submerged in the solution. L-Glu and ATP were added as disodium or magnesium salt, respectively, to the chamber by perfusion with the same solution. For chemical treatments, seedlings were preincubated for 10 or 60 min in 5-cm petri dishes in the imaging solution supplemented with 25 μM CPA, 0.5 μM Eos, or a combination of both. Control seedlings were kept for the same times in the imaging solution supplemented with 0.25% (v/v) dimethyl sulfoxide. Seedlings were then transferred to the imaging chamber and allowed to recover for approximately 7 min prior to measurement.

Time-Lapse Ca^{2+} Imaging and Confocal Microscopy Analyses

Cameleon seedling roots and leaves were imaged in vivo by an inverted fluorescence Nikon microscope (Ti-E; http://www.nikon.com/) with a CFI planfluor 4× numerical aperture 0.13 dry objective and a CFI PLAN APO 20× VC dry objective. Excitation light was produced by a fluorescent lamp (Prior Lumen 200 PRO; Prior Scientific; http://www.prior.com) at 440 nm (436/20 nm) set to 20%. Images were collected with a Hamamatsu Dual CCD camera (ORCA-D2; http://www.hamamatsu.com/). For Cameleon analysis, the FRET CFP/YFP optical block A11400-03 (emission 1, 483/32 nm for CFP; emission 2, 542/27 nm for FRET) with a dichroic 510-nm mirror (Hamamatsu) was used for the simultaneous CFP and FRET acquisitions (citrine for D1, YFP for D4, and cpVenus for YC3.6). Exposure time was from 100 to 400 ms with a 2 × 2 CCD binning for cytosolic Cameleon (NES-YC3.6) and a 4 × 4 CCD binning for ER Cameleons (CRT-D1ER and CRT-D4ER). Images where acquired every 5 s. Filters and the dichroic mirror were purchased from Chroma Technology (http://www.chroma.com/). NIS-Elements (Nikon; http://www.nis-elements.com/) was used as a platform to control microscope, illuminator, camera, and post-acquisition analyses.

With regard to time-course experiments, fluorescence intensity was determined over regions of interest that correspond to the root tip zone. FRET and CFP emissions of the analyzed regions of interest were used for the ratio (R) calculation (FRET/CFP) and normalized to the initial ratio (R_0) and plotted versus time ($\Delta R/R_0$). The background was independently subtracted for both channels before calculating the ratio.

Confocal microscopy analyses were performed using Nikon C2 (http://www.nikoninstruments.com) and Leica SP5 (http://www.leica-microsystems.com) laser scanning confocal imaging systems. For Cameleon-dependent citrine (D1), YFP (D4), and cpVenus (YC3.6), excitation was at 488 nm and emission was between 525 and 540 nm. For mCherry detection, excitation was at 561 nm and emission was between 590 and 620 nm. Image analyses were done with the ImageJ bundle software (http://rsb.info.nih.gov/ij/).

For Ca^{2+} imaging analyses, roots were imaged with a 63× lens (H 63X PL APO numerical aperture 1.20 water immersion), and the Cameleons were excited with the 458-nm line of the argon laser with 15% of total power. The CFP and FRET emissions were collected at 473 to 505 nm and 526 to 536 nm, respectively, and the pinhole diameter was 2 to 4 airy units depending on the line used. Images were collected every 5 s. The false color ratio images were obtained by using the NIS-Elements (Nikon; http://www.nis-elements.com/). For time-course experiments, fluorescence intensity was determined over regions of interest that correspond to single cells in the root tip zone. FRET and CFP emissions of the analyzed regions of interest were used for the ratio (R) calculation (FRET/CFP) and normalized to the initial ratio (R_0) and plotted versus time ($\Delta R/R_0$).

All the data are representative of at least six independent cells or roots analyzed unless otherwise stated. Reported traces are representative ones

chosen from a set of six or more identical experiments, and the data shown as bar diagrams are averages from corresponding data sets. Data are reported as averages ± SE, and statistical significance was calculated by Student's *t* test.

In Vivo Dynamic Range of CRT-D4ER

In order to determine the in vivo dynamic range of the CRT-D4ER probe ($\Delta R_{max}/R_0$), we considered the R_{min} and R_{max} measured in the experiments performed in root tip seedlings incubated with Ca^{2+}-ATPase inhibitors. The measured R_{min} was 2.71 ± 0.021 in the presence of 25 μM CPA after 10 min of incubation, whereas the R_{max} was 3.78 ± 0.18 in the presence of 0.5 μM Eos for 60 min. Hence, the calculated $\Delta R_{max}/R = 0.395$ shows that the responses to the different observed stimuli did not lead to a probe saturation.

Supplemental Data

The following materials are available in the online version of this article.

Supplemental Figure S1. Subcellular distribution of CRT-D1ER in transgenic Arabidopsis plants and simultaneous detection of CFP and FRET emissions.

Supplemental Figure S2. FRET detection in Arabidopsis seedlings expressing the CRT-D4ER (ER Cameleon) probe challenged with 1 mM L-Glu, 0.1 mM ATP, and 100 mM NaCl.

Supplemental Figure S3. $[Ca^{2+}]_{cyt}$ and $[Ca^{2+}]_{ER}$ dynamics in root cells of Arabidopsis seedlings expressing the NES-YC3.6 (cytosolic Cameleon) and CRT-D4ER (ER Cameleon) probes challenged with 0.01 mM ATP.

Supplemental Figure S4. $[Ca^{2+}]_{cyt}$ and $[Ca^{2+}]_{ER}$ dynamics in root cells of Arabidopsis seedlings expressing the NES-YC3.6 (cytosolic Cameleon) and CRT-D4ER (ER Cameleon) probes challenged with repetitive depolarizing-hyperpolarizing buffer changes in the presence or absence of EGTA.

Supplemental Text S1. Generation and analysis of Arabidopsis plants expressing the CRT-D1ER Cameleon probe.

Supplemental Movie S1. Series of cytosolic Ca^{2+} ratio images (low magnification, 4×) of an Arabidopsis seedling root tip expressing NES-YC3.6 challenged with 1 mM L-Glu.

Supplemental Movie S2. Series of cytosolic Ca^{2+} ratio images of an Arabidopsis seedling root tip expressing NES-YC3.6 challenged with 1 mM L-Glu analyzed by confocal laser scanning microscopy.

Supplemental Movie S3. Series of cytosolic Ca^{2+} ratio images of an Arabidopsis seedling root tip expressing NES-YC3.6 challenged with 0.5 mM ATP analyzed by confocal laser scanning microscopy.

Supplemental Movie S4. Series of ER Ca^{2+} ratio images of an Arabidopsis seedling root tip expressing CRT-D4ER challenged with 1 mM L-Glu analyzed by confocal laser scanning microscopy.

Supplemental Movie S5. Series of ER Ca^{2+} ratio images of an Arabidopsis seedling root tip expressing CRT-D4ER challenged with 0.5 mM ATP analyzed by confocal laser scanning microscopy.

ACKNOWLEDGMENTS

We thank Maria Ida De Michelis (University of Milan) for critical reading of the manuscript; Prof. Anna Moroni (University of Milan) for helpful discussions; Karin Schumacher (University of Heidelberg) for providing us the UBQ10-NES-YC3.6 Arabidopsis plants; Roger Tsien (University of California, San Diego) for providing us the pCDNA3-D1ER vector; and Tullio Pozzan (University of Padova) for the pCDNA3-D1ER vector.

Received August 1, 2013; accepted September 30, 2013; published September 30, 2013.

LITERATURE CITED

Allen GJ, Kwak JM, Chu SP, Llopis J, Tsien RY, Harper JF, Schroeder JI (1999) Cameleon calcium indicator reports cytoplasmic calcium dynamics in Arabidopsis guard cells. Plant J **19:** 735–747

Allen GJ, Chu SP, Schumacher K, Shimazaki CT, Vafeados D, Kemper A, Hawke SD, Tallman G, Tsien RY, Harper JF, et al (2000) Alteration of stimulus-specific guard cell calcium oscillations and stomatal closing in Arabidopsis det3 mutant. Science **289:** 2338–2342

Allen GJ, Chu SP, Harrington CL, Schumacher K, Hoffmann T, Tang YY, Grill E, Schroeder JI (2001) A defined range of guard cell calcium oscillation parameters encodes stomatal movements. Nature **411:** 1053–1057

Baxter I, Tchieu J, Sussman MR, Boutry M, Palmgren MG, Gribskov M, Harper JF, Axelsen KB (2003) Genomic comparison of P-type ATPase ion pumps in Arabidopsis and rice. Plant Physiol **132:** 618–628

Behera S, Krebs M, Loro G, Schumacher K, Costa A, Kudla J (2013) Ca^{2+} imaging in plants using genetically encoded Yellow Cameleon Ca^{2+} indicators. Cold Spring Harb Protoc **2013:** 700–703

Behera S, Kudla J (2013) High-resolution imaging of cytoplasmic Ca^{2+} dynamics in Arabidopsis roots. Cold Spring Harb Protoc **2013:** 665–669

Berridge MJ (2009) Inositol trisphosphate and calcium signalling mechanisms. Biochim Biophys Acta **1793:** 933–940

Boevink P, Martin B, Oparka K, Santa Cruz S, Hawes C (1999) Transport of virally expressed green fluorescent protein through the secretory pathway in tobacco leaves is inhibited by cold shock and brefeldin A. Planta **208:** 392–400

Bonza MC, De Michelis MI (2011) The plant Ca^{2+}-ATPase repertoire: biochemical features and physiological functions. Plant Biol (Stuttg) **13:** 421–430

Bonza MC, Luoni L, De Michelis MI (2004) Functional expression in yeast of an N-deleted form of At-ACA8, a plasma membrane Ca^{2+}-ATPase of *Arabidopsis thaliana*, and characterization of a hyperactive mutant. Planta **218:** 814–823

Bose J, Pottosin II, Shabala SS, Palmgren MG, Shabala S (2011) Calcium efflux systems in stress signaling and adaptation in plants. Front Plant Sci **2:** 85

Brandizzi F, Fricker M, Hawes C (2002) A greener world: the revolution in plant bioimaging. Nat Rev Mol Cell Biol **3:** 520–530

Carrasco S, Meyer T (2010) Cracking CRAC. Nat Cell Biol **12:** 416–418

Cheng NH, Pittman JK, Shigaki T, Lachmansingh J, LeClere S, Lahner B, Salt DE, Hirschi KD (2005) Functional association of Arabidopsis CAX1 and CAX3 is required for normal growth and ion homeostasis. Plant Physiol **138:** 2048–2060

Christensen A, Svensson K, Thelin L, Zhang W, Tintor N, Prins D, Funke N, Michalak M, Schulze-Lefert P, Saijo Y, et al (2010) Higher plant calreticulins have acquired specialized functions in Arabidopsis. PLoS ONE **5:** e11342

Clough SJ, Bent AF (1998) Floral dip: a simplified method for Agrobacterium-mediated transformation of *Arabidopsis thaliana.* Plant J **16:** 735–743

Coe H, Michalak M (2009) Calcium binding chaperones of the endoplasmic reticulum. General Physiology and Biophysics **28:** F96–F103

Collins SR, Meyer T (2011) Evolutionary origins of STIM1 and STIM2 within ancient Ca^{2+} signaling systems. Trends Cell Biol **21:** 202–211

Conn SJ, Gilliham M, Athman A, Schreiber AW, Baumann U, Moller I, Cheng NH, Stancombe MA, Hirschi KD, Webb AA, et al (2011) Cell-specific vacuolar calcium storage mediated by CAX1 regulates apoplastic calcium concentration, gas exchange, and plant productivity in *Arabidopsis*. Plant Cell **23:** 240–257

Corbett EF, Michalak M (2000) Calcium, a signaling molecule in the endoplasmic reticulum? Trends Biochem Sci **25:** 307–311

Costa A, Drago I, Behera S, Zottini M, Pizzo P, Schroeder JI, Pozzan T, Lo Schiavo F (2010) H_2O_2 in plant peroxisomes: an *in vivo* analysis uncovers a Ca^{2+}-dependent scavenging system. Plant J **62:** 760–772

Costa A, Drago I, Zottini M, Pizzo P, Pozzan T (2013) Peroxisome Ca^{2+} homeostasis in animal and plant cells. Subcell Biochem **69:** 111–133

De Michelis MI, Carnelli A, Rasi-Caldogno F (1993) The Ca^{2+} pump of the plasma membrane of *Arabidopsis thaliana*: characteristics and sensitivity to fluorescein derivatives. Bot Acta **106:** 20–25

Dodd AN, Kudla J, Sanders D (2010) The language of calcium signaling. Annu Rev Plant Biol **61:** 593–620

Feske S, Skolnik EY, Prakriya M (2012) Ion channels and transporters in lymphocyte function and immunity. Nat Rev Immunol **12:** 532–547

Geisler M, Axelsen KB, Harper JF, Palmgren MG (2000) Molecular aspects of higher plant P-type Ca^{2+}-ATPases. Biochim Biophys Acta **1465:** 52–78

Galione A, Chuang KT (2012) Pyridine nucleotide metabolites and calcium release from intracellular stores. Adv Exp Med Biol **740:** 305–323

Gao D, Knight MR, Trewavas AJ, Sattelmacher B, Plieth C (2004) Self-reporting Arabidopsis expressing pH and [Ca^{2+}] indicators unveil ion dynamics in the cytoplasm and in the apoplast under abiotic stress. Plant Physiol **134:** 898–908

Harper JF, Hong B, Hwang I, Guo HQ, Stoddard R, Huang JF, Palmgren MG, Sze H (1998) A novel calmodulin-regulated Ca^{2+}-ATPase (ACA2) from Arabidopsis with an N-terminal autoinhibitory domain. J Biol Chem **273:** 1099–1106

Hawes C, Saint-Jore C, Martin B, Zheng HQ (2001) ER confirmed as the location of mystery organelles in Arabidopsis plants expressing GFP! Trends Plant Sci **6:** 245–246

Hellens RP, Edwards EA, Leyland NR, Bean S, Mullineaux PM (2000) pGreen: a versatile and flexible binary Ti vector for Agrobacterium-mediated plant transformation. Plant Mol Biol **42:** 819–832

Hetherington AM, Brownlee C (2004) The generation of Ca^{2+} signals in plants. Annu Rev Plant Biol **55:** 401–427

Hong B, Ichida A, Wang Y, Gens JS, Pickard BG, Harper JF (1999) Identification of a calmodulin-regulated Ca^{2+}-ATPase in the endoplasmic reticulum. Plant Physiol **119:** 1165–1176

Hwang I, Sze H, Harper JF (2000) A calcium-dependent protein kinase can inhibit a calmodulin-stimulated Ca^{2+} pump (ACA2) located in the endoplasmic reticulum of Arabidopsis. Proc Natl Acad Sci USA **97:** 6224–6229

Iwano M, Entani T, Shiba H, Kakita M, Nagai T, Mizuno H, Miyawaki A, Shoji T, Kubo K, Isogai A, et al (2009) Fine-tuning of the cytoplasmic Ca^{2+} concentration is essential for pollen tube growth. Plant Physiol **150:** 1322–1334

Jiménez-Moreno R, Wang ZM, Messi ML, Delbono O (2010) Sarcoplasmic reticulum Ca^{2+} depletion in adult skeletal muscle fibres measured with the biosensor D1ER. Pflugers Arch **459:** 725–735

Kiegle E, Moore CA, Haseloff J, Tester MA, Knight MR (2000) Cell-type-specific calcium responses to drought, salt and cold in the Arabidopsis root. Plant J **23:** 267–278

Kipanyula MJ, Contreras L, Zampese E, Lazzari C, Wong AK, Pizzo P, Fasolato C, Pozzan T (2012) Ca^{2+} dysregulation in neurons from transgenic mice expressing mutant presenilin 2. Aging Cell **11:** 885–893

Klüsener B, Boheim G, Liss H, Engelberth J, Weiler EW (1995) Gadolinium-sensitive, voltage-dependent calcium release channels in the endoplasmic reticulum of a higher plant mechanoreceptor organ. EMBO J **14:** 2708–2714

Klüsener B, Boheim G, Weiler EW (1997) Modulation of the ER Ca^{2+} channel BCC1 from tendrils of *Bryonia dioica* by divalent cations, protons and H_2O_2. FEBS Lett **407:** 230–234

Knight H, Trewavas AJ, Knight MR (1997) Calcium signalling in *Arabidopsis thaliana* responding to drought and salinity. Plant J **12:** 1067–1078

Krebs M, Held K, Binder A, Hashimoto K, Den Herder G, Parniske M, Kudla J, Schumacher K (2012) FRET-based genetically encoded sensors allow high-resolution live cell imaging of Ca^{2+} dynamics. Plant J **69:** 181–192

Kudla J, Batistic O, Hashimoto K (2010) Calcium signals: the lead currency of plant information processing. Plant Cell **22:** 541–563

Lacombe B, Becker D, Hedrich R, DeSalle R, Hollmann M, Kwak JM, Schroeder JI, Le Novère N, Nam HG, Spalding EP, et al (2001) The identity of plant glutamate receptors. Science **292:** 1486–1487

Liang F, Cunningham KW, Harper JF, Sze H (1997) ECA1 complements yeast mutants defective in Ca^{2+} pumps and encodes an endoplasmic reticulum-type Ca^{2+}-ATPase in *Arabidopsis thaliana.* Proc Natl Acad Sci USA **94:** 8579–8584

Liang F, Sze H (1998) A high-affinity Ca^{2+} pump, ECA1, from the endoplasmic reticulum is inhibited by cyclopiazonic acid but not by thapsigargin. Plant Physiol **118:** 817–825

Loro G, Drago I, Pozzan T, Schiavo FL, Zottini M, Costa A (2012) Targeting of Cameleons to various subcellular compartments reveals a strict cytoplasmic/mitochondrial Ca^{2+} handling relationship in plant cells. Plant J **71:** 1–13

Loro G, Ruberti C, Zottini M, Costa A (2013) The D3cpv Cameleon reports Ca^{2+} dynamics in plant mitochondria with similar kinetics of the YC3.6 Cameleon, but with a lower sensitivity. J Microsc **249:** 8–12

Luciani DS, Gwiazda KS, Yang TL, Kalynyak TB, Bychkivska Y, Frey MH, Jeffrey KD, Sampaio AV, Underhill TM, Johnson JD (2009) Roles of IP3R and RyR Ca^{2+} channels in endoplasmic reticulum stress and beta-cell death. Diabetes **58:** 422–432

Matsushima R, Hayashi Y, Kondo M, Shimada T, Nishimura M, Hara-Nishimura I (2002) An endoplasmic reticulum-derived structure that is induced under stress conditions in Arabidopsis. Plant Physiol **130:** 1807–1814

Matsushima R, Kondo M, Nishimura M, Hara-Nishimura I (2003) A novel ER-derived compartment, the ER body, selectively accumulates a beta-glucosidase with an ER-retention signal in Arabidopsis. Plant J **33:** 493–502

McAinsh MR, Pittman JK (2009) Shaping the calcium signature. New Phytol **181:** 275–294

Michard E, Lima PT, Borges F, Silva AC, Portes MT, Carvalho JE, Gilliham M, Liu LH, Obermeyer G, Feijó JA (2011) Glutamate receptor-like genes form Ca^{2+} channels in pollen tubes and are regulated by pistil D-serine. Science **332:** 434–437

Miyawaki A, Llopis J, Heim R, McCaffery JM, Adams JA, Ikura M, Tsien RY (1997) Fluorescent indicators for Ca^{2+} based on green fluorescent proteins and calmodulin. Nature **388:** 882–887

Monshausen GB, Messerli MA, Gilroy S (2008) Imaging of the Yellow Cameleon 3.6 indicator reveals that elevations in cytosolic Ca^{2+} follow oscillating increases in growth in root hairs of Arabidopsis. Plant Physiol **147:** 1690–1698

Muir SR, Sanders D (1997) Inositol 1,4,5-trisphosphate-sensitive Ca^{2+} release across nonvacuolar membranes in cauliflower. Plant Physiol **114:** 1511–1521

Murashige T, Skoog F (1962) A revised medium for rapid growth and bioassays with tobacco tissue cultures. Physiol Plant **15:** 473–497

Nagai T, Yamada S, Tominaga T, Ichikawa M, Miyawaki A (2004) Expanded dynamic range of fluorescent indicators for Ca^{2+} by circularly permuted yellow fluorescent proteins. Proc Natl Acad Sci USA **101:** 10554–10559

Navazio L, Bewell MA, Siddiqua A, Dickinson GD, Galione A, Sanders D (2000) Calcium release from the endoplasmic reticulum of higher plants elicited by the NADP metabolite nicotinic acid adenine dinucleotide phosphate. Proc Natl Acad Sci USA **97:** 8693–8698

Navazio L, Mariani P, Sanders D (2001) Mobilization of Ca^{2+} by cyclic ADP-ribose from the endoplasmic reticulum of cauliflower florets. Plant Physiol **125:** 2129–2138

Nelson BK, Cai X, Nebenführ A (2007) A multicolored set of *in vivo* organelle markers for co-localization studies in Arabidopsis and other plants. Plant J **51:** 1126–1136

Palmer AE, Jin C, Reed JC, Tsien RY (2004) Bcl-2-mediated alterations in endoplasmic reticulum Ca^{2+} analyzed with an improved genetically encoded fluorescent sensor. Proc Natl Acad Sci USA **101:** 17404–17409

Palmer AE, Giacomello M, Kortemme T, Hires SA, Lev-Ram V, Baker D, Tsien RY (2006) Ca^{2+} indicators based on computationally redesigned calmodulin-peptide pairs. Chem Biol **13:** 521–530

Palmer AE, Tsien RY (2006) Measuring calcium signaling using genetically targetable fluorescent indicators. Nat Protoc **1:** 1057–1065

Parekh AB, Putney JW Jr (2005) Store-operated calcium channels. Physiol Rev **85:** 757–810

Peiter E (2011) The plant vacuole: emitter and receiver of calcium signals. Cell Calcium **50:** 120–128

Persson S, Harper J (2006) The ER and cell calcium. *In* DG Robinson, ed, The Plant Endoplasmic Reticulum: Plant Cell Monographs. Springer-Verlag, Heidelberg, pp 251–278

Pittman JK, Hirschi KD (2003) Don't shoot the (second) messenger: endomembrane transporters and binding proteins modulate cytosolic Ca^{2+} levels. Curr Opin Plant Biol **6:** 257–262

Qi Z, Stephens NR, Spalding EP (2006) Calcium entry mediated by GLR3.3, an Arabidopsis glutamate receptor with a broad agonist profile. Plant Physiol **142:** 963–971

Ravier MA, Daro D, Roma LP, Jonas JC, Cheng-Xue R, Schuit FC, Gilon P (2011) Mechanisms of control of the free Ca^{2+} concentration in the endoplasmic reticulum of mouse pancreatic β-cells: interplay with cell metabolism and $[Ca^{2+}]_c$ and role of SERCA2b and SERCA3. Diabetes **60:** 2533–2545

Rincón-Zachary M, Teaster ND, Sparks JA, Valster AH, Motes CM, Blancaflor EB (2010) Fluorescence resonance energy transfer-sensitized emission of yellow cameleon 3.60 reveals root zone-specific calcium signatures in Arabidopsis in response to aluminum and other trivalent cations. Plant Physiol **152:** 1442–1458

Rizzuto R, Pozzan T (2006) Microdomains of intracellular Ca^{2+}: molecular determinants and functional consequences. Physiol Rev **86:** 369–408

Sanders D, Pelloux J, Brownlee C, Harper JF (2002) Calcium at the crossroads of signaling. Plant Cell (Suppl) **14:** S401–S417

Sieberer BJ, Chabaud M, Timmers AC, Monin A, Fournier J, Barker DG (2009) A nuclear-targeted cameleon demonstrates intranuclear Ca^{2+}

spiking in *Medicago truncatula* root hairs in response to rhizobial nodulation factors. Plant Physiol **151:** 1197–1206

Spalding EP, Harper JF (2011) The ins and outs of cellular Ca^{2+} transport. Curr Opin Plant Biol **14:** 715–720

Stael S, Wurzinger B, Mair A, Mehlmer N, Vothknecht UC, Teige M (2012) Plant organellar calcium signalling: an emerging field. J Exp Bot **63:** 1525–1542

Sze H, Liang F, Hwang I, Curran AC, Harper JF (2000) Diversity and regulation of plant Ca^{2+} pumps: insights from expression in yeast. Annu Rev Plant Physiol Plant Mol Biol **51:** 433–462

Tanaka K, Swanson SJ, Gilroy S, Stacey G (2010) Extracellular nucleotides elicit cytosolic free calcium oscillations in Arabidopsis. Plant Physiol **154:** 705–719

Vincill ED, Bieck AM, Spalding EP (2012) Ca^{2+} conduction by an amino acid-gated ion channel related to glutamate receptors. Plant Physiol **159:** 40–46

Vincill ED, Clarin AE, Molenda JN, Spalding EP (2013) Interacting glutamate receptor-like proteins in Phloem regulate lateral root initiation in *Arabidopsis*. Plant Cell **25:** 1304–1313

Waadt R, Kudla J (2008) In planta visualization of protein interactions using bimolecular fluorescence complementation (BiFC). Cold Spring Harb Protoc **2008:** pdb.prot4995,

Webb AAR, McAinsh MR, Taylor JE, Hetherington AM (1996) Calcium ions as intracellular second messengers in higher plants. Adv Bot Res **22:** 45–96

Weinl S, Held K, Schlücking K, Steinhorst L, Kuhlgert S, Hippler M, Kudla J (2008) A plastid protein crucial for Ca^{2+}-regulated stomatal responses. New Phytol **179:** 675–686

Wheeler GL, Brownlee C (2008) Ca^{2+} signalling in plants and green algae: changing channels. Trends Plant Sci **13:** 506–514

Winter D, Vinegar B, Nahal H, Ammar R, Wilson GV, Provart NJ (2007) An "Electronic Fluorescent Pictograph" browser for exploring and analyzing large-scale biological data sets. PLoS ONE **2:** e718

Wu Z, Liang F, Hong B, Young JC, Sussman MR, Harper JF, Sze H (2002) An endoplasmic reticulum-bound Ca^{2+}/Mn^{2+} pump, ECA1, supports plant growth and confers tolerance to Mn^{2+} stress. Plant Physiol **130:** 128–137

Yang Y, Costa A, Leonhardt N, Siegel RS, Schroeder JI (2008) Isolation of a strong Arabidopsis guard cell promoter and its potential as a research tool. Plant Methods **4:** 6

Young JJ, Mehta S, Israelsson M, Godoski J, Grill E, Schroeder JI (2006) CO_2 signaling in guard cells: calcium sensitivity response modulation, a Ca^{2+}-independent phase, and CO_2 insensitivity of the *gca2* mutant. Proc Natl Acad Sci USA **103:** 7506–7511

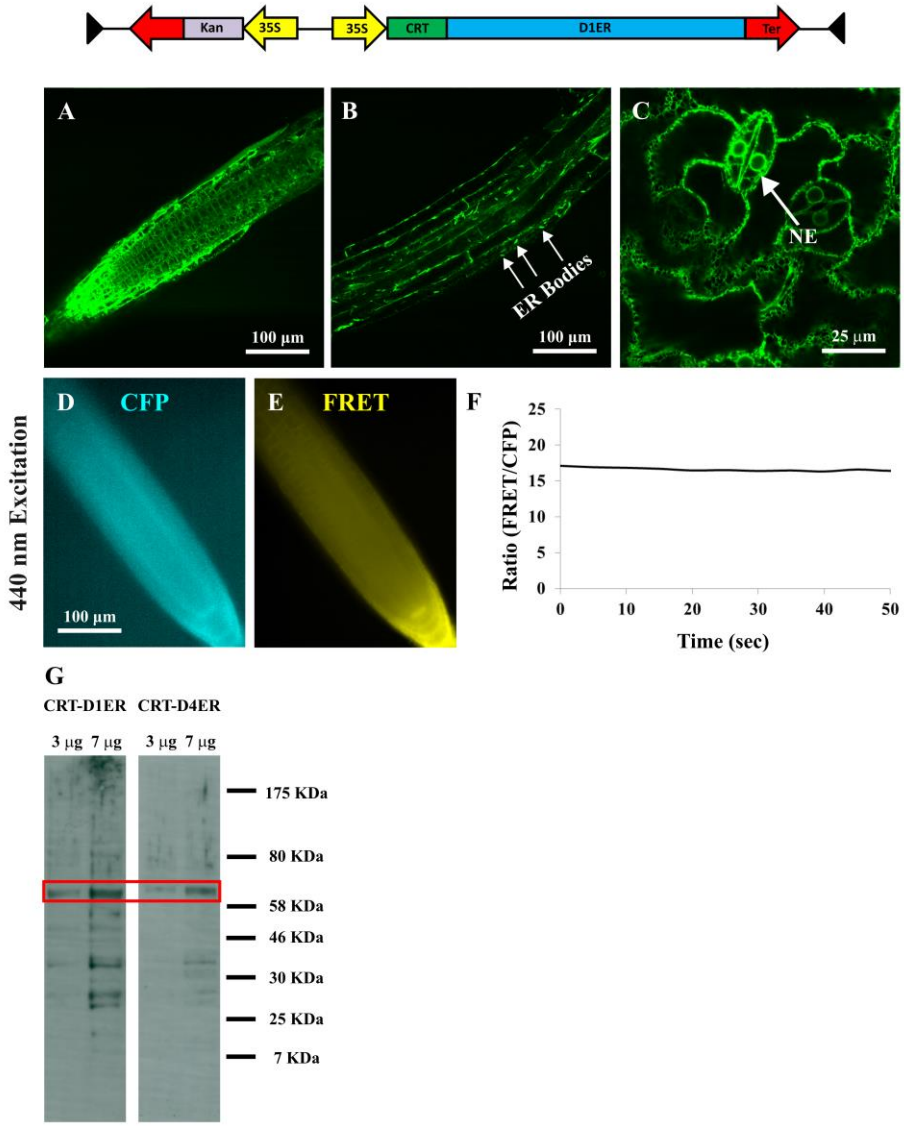

Figure S1. Subcellular distribution of CRT-D1ER in transgenic Arabidopsis plants and simultaneous detection of CFP and FRET emissions. Top panel. Schematic structure of the CRT-D1ER Cameleon probe. A-C, Confocal microscopy analyses revealed that CRT-D1ER YFP signal was detected in different organs of Arabidopsis stable transgenic plants with a subcellular distribution showing typical ER features. A, Root tip cells. B, Hypocotyl cells showing the presence of fusiform bodies (Hawes et al., 2001; Matsushima et al., 2002; Matsushima et al., 2003). C, Mature leaf cells with stomata guard cells where it can be appreciated the clear staining of the Nuclear Envelope (NE). D and E, Representative root tip of a CRT-D1ER seedling excited with the 440 nm light for FRET detection. D, CFP emission. In this case the signal to noise ratio was very low, hence, in order to present a non-dark image the grey scale was modified. E, FRET emission. The simultaneous detection of the two emissions demonstrate that CFP was almost completely quenched, but YFP was properly excited trough FRET. F, FRET/CFP ratio plot from the selected root tip shown in D and E. G, Western Blot analysis with an anti-GFP antiserum performed with 3 and 7 µg of total protein extracts from 7-day-old Arabidopsis transgenic seedlings expressing the CRT-D1ER and the functional CRT-D4ER as control. The red rectangle marks the first bands appearing during the film development. Bands correspond to the expected probes size.

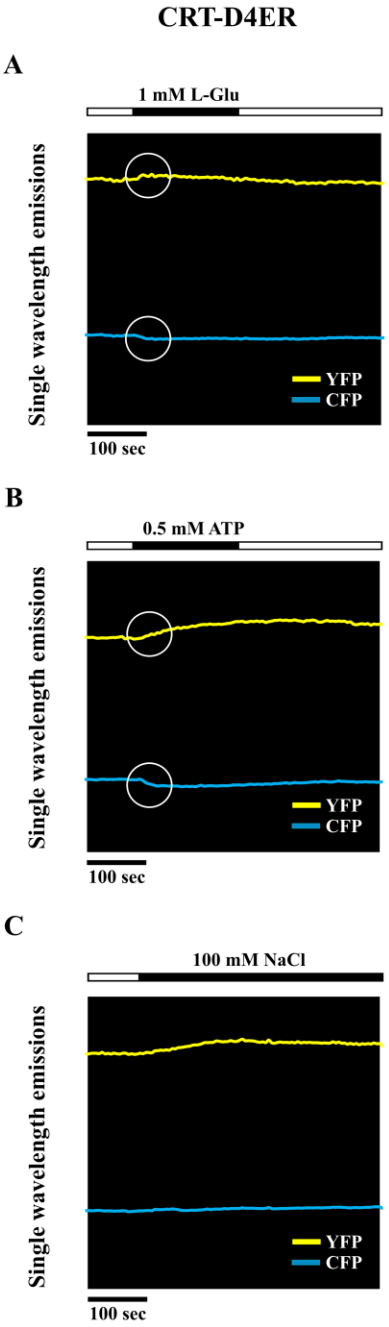

Figure S2. FRET detection in Arabidopsis seedlings expressing the CRT-D4ER probe (ER Cameleon) challenged with 1 mM L-Glu, 0.5 mM ATP and 100 mM NaCl. A, Single wavelength emissions of CFP (540 nm) and YFP (480 nm) used for the ratio measurement shown in Figure 2B in the course of L-Glu stimulation. B, Single wavelength emissions of CFP and YFP used for the ratio measurement shown in Figure 2D in the course of ATP stimulation. C, Single wavelength emissions of CFP and YFP used for the ratio measurement shown in Figure 2F in the course of NaCl treament. Note that after the application of the stimuli the two fluorescence emissions, YFP and CFP, have a clear antiparallel behaviour (A and B). In some cases (C) the change of the solution from 0 to 100 mM NaCl determines a sample movement affecting both fluorescence emissions. Potential artifacts, however, were nicely corrected by the ratiometric values (Figure 2F) that allows to appreciate even small FRET changes.

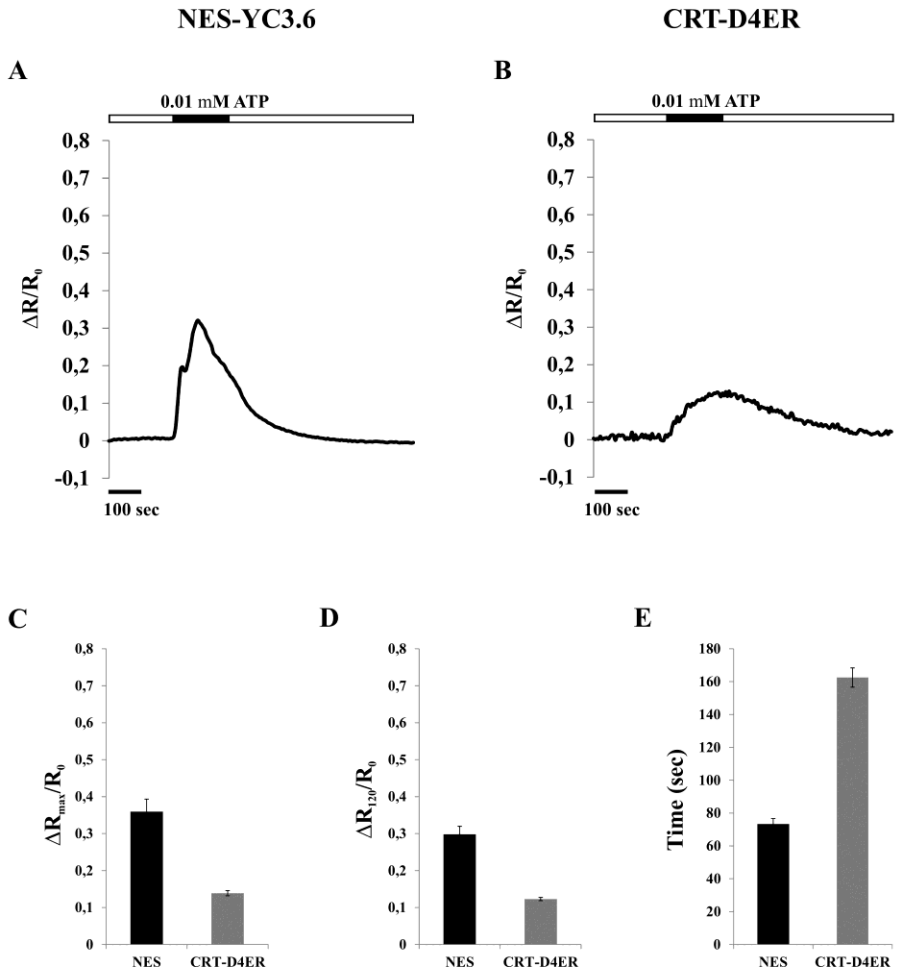

Figure S3. $[Ca^{2+}]_{cyt}$ and $[Ca^{2+}]_{ER}$ dynamics in root cells of Arabidopsis seedlings expressing the NES-YC3.6 (cytosolic Cameleon) and CRT-D4ER (ER Cameleon) probes, challenged with 0.01 mM of ATP. Root tip cells of seedlings were challenged with 0.01 mM of ATP for the indicated time (black rectangles above traces) and analyzed with a widefield fluorescence microscope. Traces are representative experiments reporting the normalized ratio (FRET/CFP) variations observed during the entire experiment. A, 0.01 mM of ATP induced a cytosolic Ca^{2+} transient in root tip cells. B, The same stimulus of A induced a slow ER Ca^{2+} accumulation followed by a $[Ca^{2+}]_{ER}$ decrease. C, Statistical analysis of maximum $\Delta R/R_0$ variations measured in both compartments in response to different applied stimuli. D, Statistical analysis of $\Delta R/R_0$ variations measured in both compartments 120 sec after the sensing of the different applied stimuli. E, Statistical analysis of times at which the maximum $\Delta R/R_0$ variations are measured in both compartments in response to different applied stimuli.

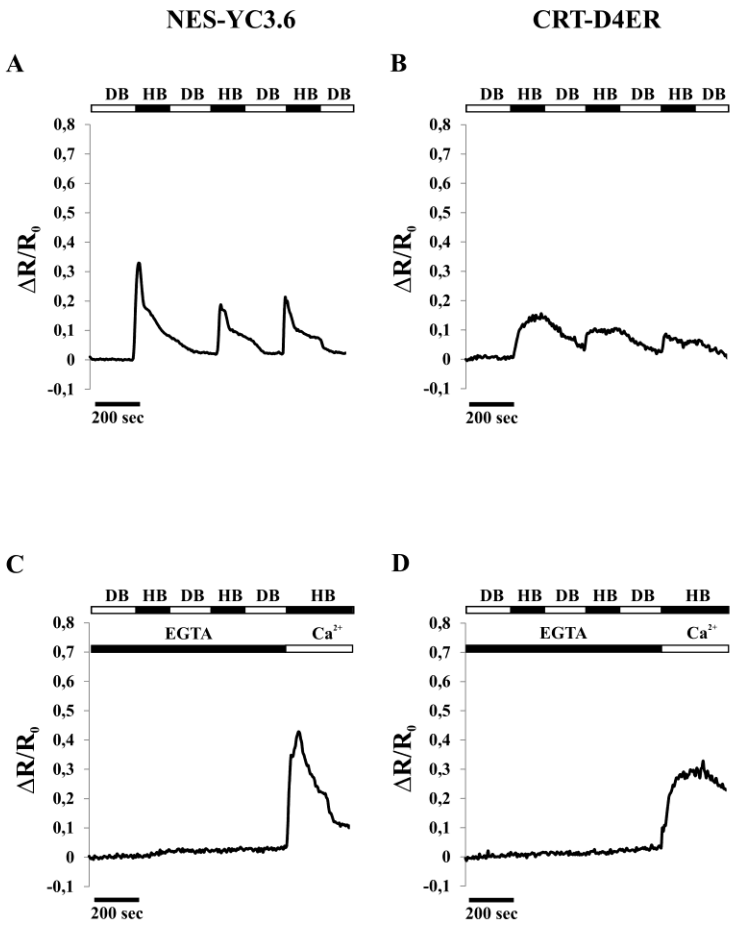

Figure S4. $[Ca^{2+}]_{cyt}$ and $[Ca^{2+}]_{ER}$ dynamics in root cells of Arabidopsis seedlings expressing the NES-YC3.6 (cytosolic Cameleon) and CRT-D4ER (ER Cameleon) challenged with repetitive depolarizing-hyperpolarizing buffer changes in presence or absence of EGTA. Cytosolic and ER Ca^{2+} transients were induced by alternate application of depolarizing (50 mM KCl, 10 mM MES, pH 5.6 with Tris) and hyperpolarizing buffer (1 mM KCl, 1 mM $CaCl_2$, 10 mM MES, pH 5.6 with Tris) as described in Krebs et al. (2012). A, Repetitive $[Ca^{2+}]_{cyt,}$ transients. B, Repetitive $[Ca^{2+}]_{ER}$ transients. C, Chelation of extracellular Ca^{2+} with 5 mM EGTA prevented the $[Ca^{2+}]_{cyt}$ transients. D, Chelation of extracellular Ca^{2+} with 5 mM EGTA prevented the $[Ca^{2+}]_{ER}$ transients. Note that in the experiments of figure C and D, the depolarizing and hyperpolarizing buffers containing 5 mM EGTA were also devoided of any added source of Ca^{2+}. The final application of hyperpolarizing buffer in presence of 1 mM $CaCl_2$ was sufficient to induce both $[Ca^{2+}]_{cyt,}$ and $[Ca^{2+}]_{ER}$ elevations demonstrating the requirement of extracellular Ca^{2+} in the generation of observed responses. Traces are representative of n=5 independent experiments.

Chapter 4:

Chloroplast Ca^{2+}-dynamics

4.1 Introduction on chloroplast Ca^{2+}-dynamics

Chloroplasts are characteristic organelles of photosynthetic eukaryotes, in which many pivotal metabolic pathways, other than photosynthesis, occur, thus providing essential functions for the plant, even in non-photosynthetic tissues.

The first evidences of the presence of Ca^{2+} into chloroplasts were produced more than 70 years ago (Neish. 1939), showing a very high total amount of Ca^{2+} (15-25mM) (Yamagishi et al. 1981) and a free-Ca^{2+} concentration in the stroma ($[Ca^{2+}]_{chl}$) in the range of hundreds of nano-molar (approximately 150nM) (Nomura et al. 2012). The majority of Ca^{2+} resides in the thylakoid lumen and it is associated with macromolecules, among which several Ca^{2+}-binding proteins (Brand and Becker. 1984).

Moreover, Calmodulins (CaMs) have several regulatory roles in the chloroplast, suggesting that many physiological processes localized in these organelles are directly or indirectly regulated by Ca^{2+}. The Ca^{2+}/CaM complex promotes the import of chloroplastic proteins, interacting with the TOC/TIC system (Translocon at the Outer envelope of Chloroplast and Translocon at the Inner envelope of Chloroplast respectively) and regulating the TIC1 subunit Tic1-10 (Balsera et al. 2009). In addition, CaMs modulate NAD kinase activity. This enzyme catalyzes the phosphorylation of NAD into NADP, the final acceptor of electrons in the photosynthetic electron transport chain. AtNADK2, one of the three NAD kinase isoforms present in *A. thaliana*, has a long CaM-binding extension at the N-terminus (Turner et al. 2004). Moreover, psaN, the only subunit of photosystem I located entirely in the thylakoid lumen, is a CaM binding protein, thus linking the photosynthetic activity to the presence of Ca^{2+}/CaM (Reddy et al. 2002). Despite all these functional data, chloroplastic CaMs have not been identify so far.

Furthermore, Ca^{2+} affects chloroplast division, in fact, the ATPase activity of AtMinD1 (ACCUMULATION AND REPLICATION OF CHLOROPLASTS 11), which is a component of the chloroplast fission machinery, depends on Ca^{2+} (Aldridge and Moller. 2005).

Studies based on the use of the genetically encoded probe aequorin, targeted to the chloroplast stroma, identified a Ca^{2+}-rise during the transition from light to dark. Few minutes after the light was switched off, a Ca^{2+} transient was detected in the stroma, and remained sustained for tens of minutes (Nomura et al. 2012,Johnson et al. 1995,Sai and Johnson. 2002). The magnitude of the Ca^{2+}-transient was proportional to the duration of light exposure before the dark, and it occurred every day at the end of the light period. The authors proposed that chloroplasts sequester Ca^{2+} into the thylakoids during the day, and release it back to the stroma during the night (Sai and Johnson. 2002).

Moreover, stromal Ca^{2+} responses are associated with biotic elicitors like bacterial flagellin (fgl22) and pathogen-associated molecular pattern (PAMP) signals that cause a Ca^{2+} transient in the cytoplasm, followed by an increase in stromal Ca^{2+} (Nomura et al. 2012).

Ca^{2+}-transporters in the chloroplast

Although functional evidences of the presence of a voltage-dependent Ca^{2+} uptake on the inner envelope of spinach chloroplasts are very dated (Kreimer et al. 1985), the molecular identity of chloroplast Ca^{2+}-transporters is still unknown and how $[Ca^{2+}]_{chl}$ is maintained remains an open question.

An auto-inhibited Ca^{2+}-ATPase (ACA1) was initially identified on the chloroplast inner membrane (Huang et al. 1993), but further studies detected no Ca^{2+}-ATPase activity on these membranes (Roh et al. 1998) and proteomic analyses relocated the ACA1 pump to the ER membrane (Dunkley et al. 2006). Then, HEAVY METAL ATPASE 1 (HMA1) was characterized as a Cu^{+}-ATPase resident on chloroplast membranes (Ferro et al. 2003), but showing high-affinity for Ca^{2+}, it could play a role in chloroplast Ca^{2+} influx (Moreno et al. 2008).

Several putative channels have been reported to localize to the chloroplast. In fact, two members of the plant-homolog animal-glutamate-receptor family (AtGLR3.4 and AtGLR3.5) were described in the chloroplast. Interestingly, both proteins show a dual-localization pattern: AtGLR3.4 localizes both to

the plasma membrane and chloroplasts/plastids while AtGLR3.5 localizes to mitochondria and chloroplasts (Teardo et al. 2011,Teardo et al. 2015).
MSL2 and MSL3, are two putative chloroplastic mechanosensitive ion channels, involved in chloroplasts division, whose permeability to Ca^{2+} has not been described so far (Haswell and Meyerowitz. 2006,Wilson et al. 2011,Jensen and Haswell. 2012).
Ca^{2+} concentration into the thylakoid lumen is higher than in the stroma, thus the existence of a Ca^{2+} transporter on thylakoid membranes is expected. Biochemical evidences indeed support the existence of a Ca^{2+}/H^{+} exchanger (CAX) activity in the thylakoid membranes (Ettinger et al. 1999), but its molecular identity is still unknown. Nonetheless, PPF1 (post-floral-specific gene1) represents a good candidate as thylakoid CAX, in fact, this Pea protein led to a significant inward Ca^{2+} ion currents when expressed in human hepatoma cells (Wang et al. 2003). Moreover, the over expression of PPF1 in *A. thaliana* determined an higher amount of Ca^{2+} in the chloroplast, while the knockout mutant showed a strong decrease (Wang et al. 2003). Although these findings, a direct *in vivo* evidence of its role in sequestering Ca^{2+} into the thylakoids is still lacking.

The Ca^{2+}-Sensing receptor CAS

The Ca^{2+}-sensing receptor (CAS) has a crucial role in the generation of cytosolic Ca^{2+}-oscillations (Nomura et al. 2008). This protein shows low affinity and high capacity for Ca^{2+} binding and localizes to thylakoid membranes (Weinl et al. 2008). Guard cells of the *A. thaliana cas* mutant are impaired in cytosolic Ca^{2+} rises in response to external Ca^{2+} treatment, thus in the consequent stomatal closure. In this mutant, the imposition of an artificial Ca^{2+} signature in the cytosol leads to a complete recovery of stomatal closure (Weinl et al. 2008,Han et al. 2003). Furthermore, this protein is involved in the plant immune response and in the light to dark transition (Nomura et al. 2012). Both these stimuli cause a Ca^{2+} transient in the stroma that is reduced in the *cas* mutant. Since CAS localizes to thylakoids membranes, it may be involved in the generation of the stromal

Ca^{2+} signal by the release of Ca^{2+} from thylakoids (Nomura et al. 2012). Furthermore, in the plant immune response, CAS acts upstream of salicylic acid in PAMP-induced gene expression, likely through $^1O_2^-$ mediated retrograde signalling (Nomura et al. 2012).

Studies in *Chlamydomonas reinhardtii* revealed that CAS is involved in the response to high light. In fact, *cas* knockdown mutant shows severe light sensitivity, a down regulation of the light-harvesting protein LHCSR3, which is fundamental for the nonphotochemical quenching, and an impairment in the activity and recovery of photosystem II (PSII) (Petroutsos et al. 2011). Interestingly, increasing Ca^{2+} concentration in the growth medium rescued normal levels of LHCSR3 and the functionality of the PSII (Petroutsos et al. 2011).

These latter results assigned to chloroplasts a key role in plant-cell Ca^{2+} homeostasis, and points out the importance of chloroplastic Ca^{2+} in regulating photosynthesis.

Aim of the work

In vivo chloroplast Ca^{2+}-dynamics have only been investigated using aequorin, a low-resolution reporter system that has not allowed to distinguish responses of chloroplasts from those of other plastids (e.g root leucoplast). In fact, the analyses were carried out at entire seedling or entire leaf levels, in which the discrimination of organelle types was not achievable (e.g chloroplasts in mesophyll and guard cells and proplastids in meristematic cells coexists in the leaf). Chloroplasts and plastids could theoretically show differences in Ca^{2+} regulation as chloroplasts present the fully developed thylakoid system, which is missing in proplastids and leucoplasts. Ca^{2+} concentrations in the stroma and in the thylakoid lumen substantially differ, making this organelle able to generate its own Ca^{2+} signaling, through the activity of channels/transporter present in the different membranes.

In conclusion, based on these observations, our aim was to generate a molecular tool that will enable to perform and to distinguish Ca^{2+} analyses in chloroplast and other plastid types and to evaluate individual chloroplast responses at single cell level.

4.2 Results and Discussion

Development of tools for Ca^{2+}-analysis in chloroplasts and plastids

Chloroplasts are potential intracellular Ca^{2+}-stores in plant cells, in fact, the total amount of chloroplast Ca^{2+} is in the range of tens of millimolar, although the majority resides into thylakoid lumen, bound to Ca^{2+}-binding proteins (Neish. 1939,Johnson et al. 1995,Sai and Johnson. 2002). The resting concentration of free Ca^{2+} in the stroma ($[Ca^{2+}]_{str}$), is far from the milli-molar concentration, being in the range of hundreds of nano-molar (Sai and Johnson. 2002,Nomura et al. 2008).

Targeting of Cameleon probes to the chloroplast stroma

In order to investigate chloroplast Ca^{2+}-dynamics *in vivo* at high-resolution, we chose the genetically encoded probe Cameleon (Miyawaki et al. 1997). Since the expected $[Ca^{2+}]_{str}$ is in the same range of cytosolic values, we decided to use the YC3.6 Cameleon probe (K_d 250nM) (Nagai et al. 2004), that has been successfully used to monitor cytosolic, nuclear and mitochondrial Ca^{2+}-dynamics in plant cells (Krebs et al. 2012,Loro et al. 2012).

Beyond the choice of an appropriate probe, its correct localization is mandatory for the analyses of organellar Ca^{2+}. In order to target the YC3.6 probe to the stroma we chose the targeting peptide of the *A. thaliana* chloroplast-localized β-amylase 4 (Bam4) (At5g55700). We amplified the DNA region encoding the first 62 aminoacids of the protein (Fulton et al. 2008), and fused the sequence to the N-terminus end of the probe, then the entire construct was placed under the control of the CaMV35S promoter, within the 0029 pGreen backbone.

In order to verify the proper localization of the probe, we transiently transformed *N. tabacum* leaves with the 35S:Bam4-YC3.6 construct and analyzed the fluorescence, yielded from the cpVenus, by laser scanning confocal microscopy (LSCM). The analysis revealed a multiple localization of

the probe into the chloroplasts, but also in the cytosol, and into the nucleus (Fig 4.1 A). As the single Bam4 targeting sequence was not sufficient for the unique targeting of the probe to the stroma, we tried to force the stromal localization by doubling the Bam4 peptide leading to the generation of the pGreen 0029 35S:2Bam4-YC3.6 construct. When the construct was expressed in tobacco leaves, the YC3.6 probe correctly localized only into chloroplasts (Fig 4.1B: note the yellow signal in the overlay channel derived from the co-localization between the cpVenus and chlorophyll fluorescences), with no signal detected either in the cytosol or in the nucleus (Fig 4.1 B). Hence, the proper localization of the YC3.6 demonstrated the efficacy of doubling the Bam4 targeting sequence as targeting approach.

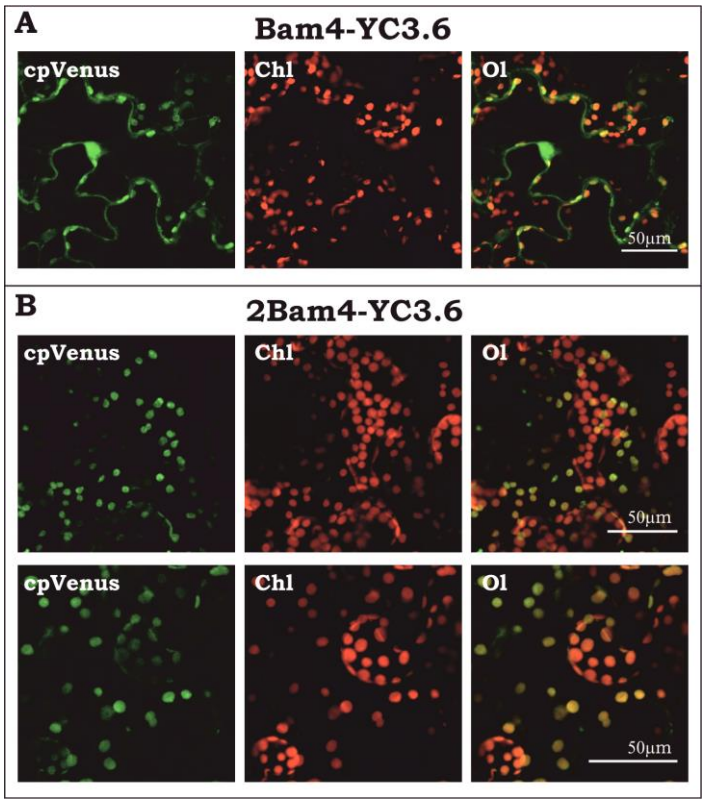

Figure 4.1 Subcellular distribution of Bam4-YC3.6 and 2Bam4-YC3.6 probes.
Confocal images of *N. tabacum* epidermal cells transformed by agrobacterium harboring (A) Bam4-YC3.6 or (B) 2Bam4-YC3.6. cpVenus: Cameleon cpVenus fluorescence, Ex: 488 nm line of the Argon laser, Em: 510-540 nm. Chl: Chlorophyll autofluorescence, Ex: 488 nm, Em: 650-750 nm. Ol: merge of the two channels.

Generation of stable transformed *A. thaliana* lines harboring chloroplastic Cameleon probe

Having demonstrated the localization of the 2Bam4-YC3.6 in transiently transformed tobacco cells the 35S:2Bam4-YC3.6 construct was inserted in the genome of *A. thaliana* plants (ecotype Columbia 0) through floral dip (Clough and Bent. 1998). Four independent transgenic lines were selected on kanamycin-enriched growth medium and seeds harvested separately.
Although these lines resulted positive to the antibiotic selection, no fluorescence was yielded in leaves of young seedlings (4 and 12 Days After Germination, DAG) (Fig 4.2 first and second rows). Fluorescence of the probe was only detected in the columella and in some epidermal cells of 4-day-old seedling roots (Fig 4.2 third row) while no fluorescence was detected in the root of older seedlings (12 DAG) (Fig 4.2 second and fourth row). In addition, the presence of the transgene in the genome of the selected lines was confirmed by PCR (data not shown) suggesting that the lack of fluorescence could be associate to a gene-silencing phenomenon (Hamilton and Baulcombe. 1999).

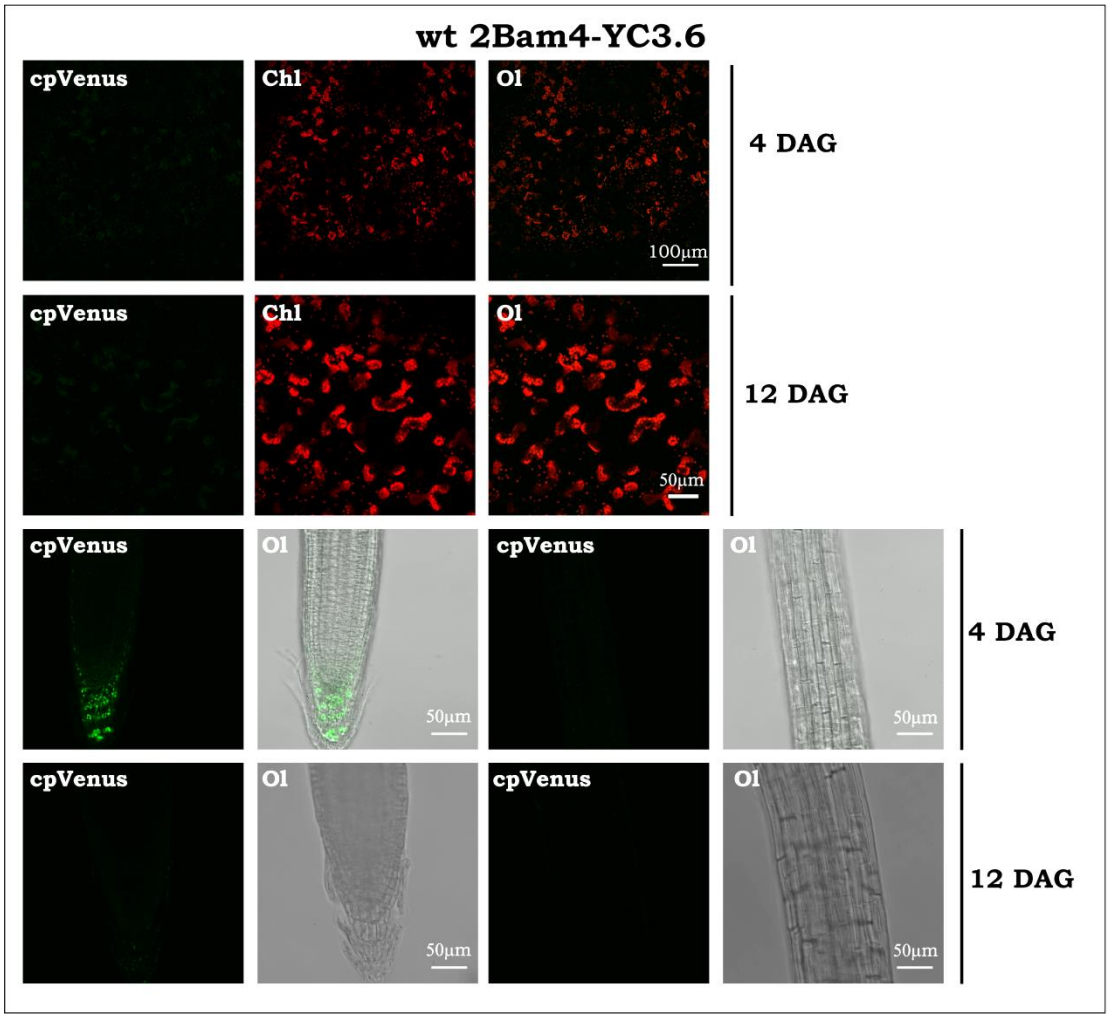

Figure 4.2: No signal of 2Bam4-YC3.6 probe was detected in stable transformed lines of *A. thaliana*.

The expression of the probe in leaves (first and second row) and roots (third and fourth row) of seedlings at 4 and 12 Days After Germination (DAG) was analyzed detecting the cpVenus fluorescence of the Cameleon (cpVenus: Ex: 488 nm, Em: 510-540 nm). No fluorescence coming from the Cameleon probe was collected in leaves, in the root only the very tip region of seedlings at 4DAG showed signal. In leaves, chlorophyll was used as marker for chloroplasts (Chl: Ex: 488 nm, Em: 650-750 nm). The Overlay channel (Ol) is the merge between the cpVenus and Chl in the leaves, and cpVenus and the bright field in the root.

To verify and, if possible, overcome the silencing effect, we decided to introduce the 35S:2Bam4-YC3.6 construct in the *A. thaliana rdr6* genetic background. The *rdr6* mutant has a point mutation in the At3g49500 gene, which encodes for an RNA-dependent RNA polymerase, and it is impaired in gene silencing (Peragine et al. 2004). This mutant was successfully employed to overcome silencing issues in *A. thaliana* plants harboring a FRET-based glucose nanosensor (Deuschle et al. 2006). We transformed *rdr6* plants with the 35S:2Bam4-YC3.6 construct and 12 transgenic independent lines were isolated by antibiotic selection. Confocal microscope analyses of cotyledon cells showed a detectable cpVenus fluorescence (Fig. 4.3 first row)(absent in the wild type background) that clearly co-localized with chlorophyll autofluorescence, confirming the localization of the 2Bam-YC3.6 probe in stable-transformed lines (Fig 4.3 second row). Furthermore, these lines showed the cpVenus fluorescence in leaves and roots of both young and old seedlings (4 and 12 DAG) (Fig 4.3 first three rows and fifth and sixth row) and in leaves of mature plants (Fig 4.3 fourth row). This result confirms that a silencing phenomenon indeed occurred in wild type lines, and that we were able to efficiently express the probe in the *rdr6* genetic background.

As reported above, our choice to use the YC3.6 Cameleon was based on the reported stromal Ca^{2+} concentration ($[Ca^{2+}]_{str}$) that is in the same range of cytosolic one (Nomura et al. 2012). Nonetheless, in order to extend the range of measurable $[Ca^{2+}]_{str}$, we decided to test the functionality of a second Cameleon probe, the YC4.6 (Nagai et al. 2004), which has an *in vitro* biphasic Ca^{2+}-dependency (K_d 56nM and 14μM). The generation of different transgenic lines expressing probes with different Ca^{2+}-affinities would allow to perform analyses of Ca^{2+}-dynamics in a larger range of Ca^{2+}-concentrations. In particular, the lower K_d of YC4.6 (56 nM) would allow to report subtle $[Ca^{2+}]_{str}$ transients, as reported in the cytosol using Nano-Cameleon (K_d of 65nM) (Choi et al. 2014b), whereas strong $[Ca^{2+}]_{str}$ increase can be monitored using the second K_d (14 μM). We followed the same targeting strategy used for the YC3.6 probe and we obtained four independent transgenic lines of *rdr6* 2Bam4-YC4.6. The LSCM analysis

revealed that the 2Bam4-YC4.6 probe was expressed and correctly localized only into chloroplasts (Fig 4.4 second row), moreover as the YC3.6, the YC4.6 probe showed a constitutive expression throughout the plant development, since cpVenus fluorescence was observed in leaves and in roots of seedlings at different developmental stages (4 and 12 DAG) (Fig 4.4 first four rows and sixth and seventh rows) and in the leaves of mature plants (Fig. 4.4 fifth row). Furthermore, as shown in Figures 4.3 and 4.4, a strong signal was observed in amyloplasts of the columella cells, which are involved in gravity perception and gravitropic responses (Evans and Ishikawa. 1997,Toyota et al. 2013). In conclusion, the use of the *rdr6* genetic background enabled the expression of both 2Bam4-YC3.6 and 2Bam4-YC4.6 in all the analyzed tissues of seedlings and mature plants, thus potentially allowing analyses of Ca^{2+}-dynamics both in chloroplasts (in leaf tissues) and in plastids (in root tissues).

In addition, since for the expression of the chloroplast localized Cameleons we need to use the *rdr6* mutant background, we also transformed *rdr6* plants with the cytosolic Cameleon probe using the Nuclear Export Signal-YC3.6 (NES-YC3.6) construct (Krebs et al. 2012). We selected six independent transgenic lines and LSCM analyses showed that the probe correctly localized to the cytosol in all the observed tissues (Fig 4.4). The comparison between the wt and the *rdr6* lines harboring the NES-YC3.6 probe allows to verify whether cytosolic Ca^{2+}-dynamics in the mutant background are the same of those observed in the wild type.

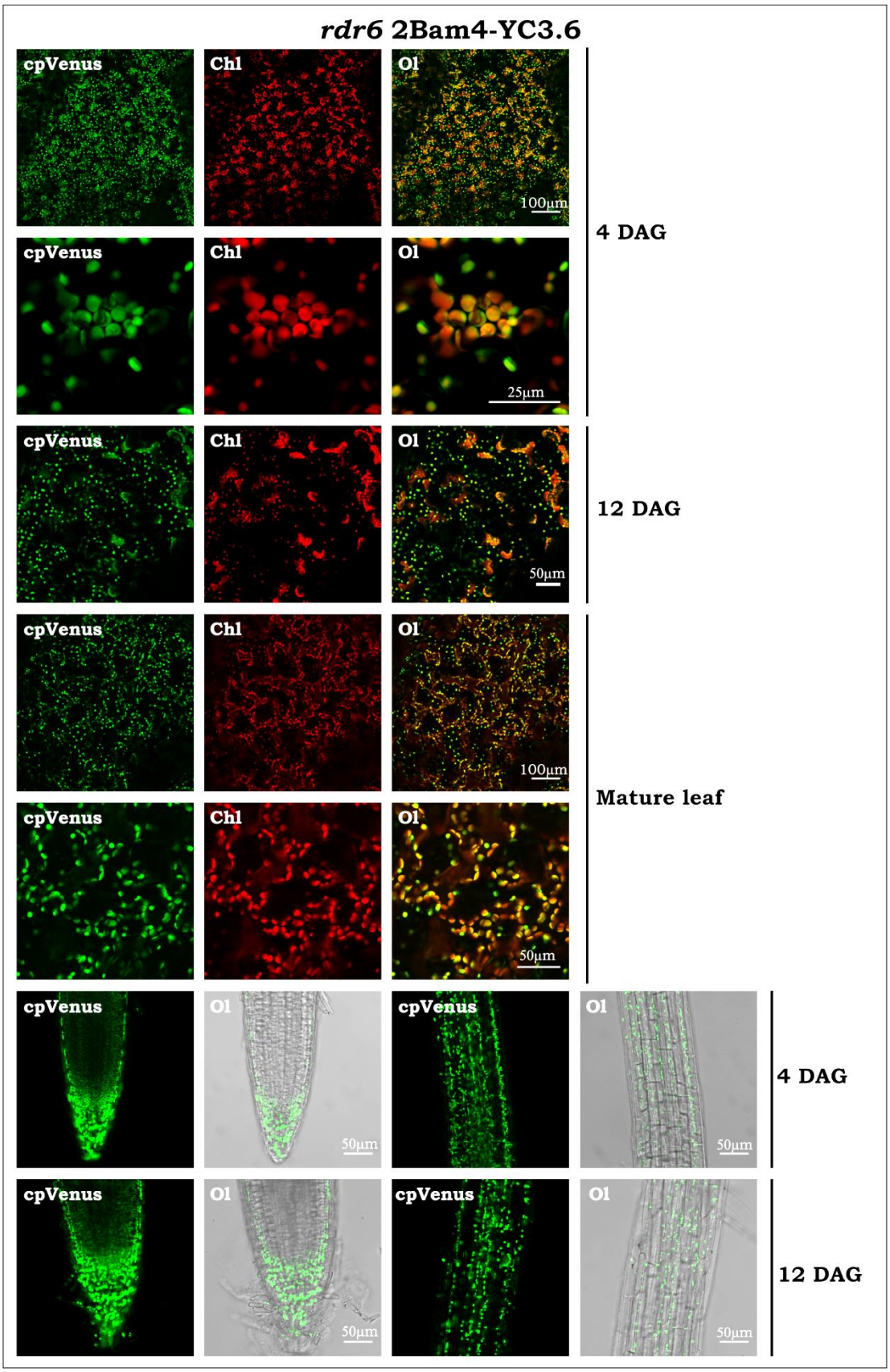
rdr6 2Bam4-YC3.6
cpVenus
Chl
Ol
100µm
4 DAG
cpVenus
Chl
Ol
25µm
cpVenus
Chl
Ol
50µm
12 DAG
cpVenus
Chl
Ol
100µm
cpVenus
Chl
Ol
50µm
Mature leaf
cpVenus
Ol
cpVenus
Ol
50µm
4 DAG
cpVenus
Ol
cpVenus
Ol
50µm
12 DAG

Figure 4.3: Expression of 2Bam4-YC3.6 probe in stable transformed *rdr6* mutant lines. The expression of the probe was analyzed detecting the cpVenus fluorescence of the Cameleon (cpVenus: Ex: 488 nm, Em: 510-540 nm) in leaves of seedlings at 4 and 12 Days After Germination (DAG) (first to fourth row), in leaves of mature plants (fourth and fifth row) and in the root at 4 and 12 DAG (sixth and seventh row). In leaves, chlorophyll was used as maker for chloroplasts (Chl: Ex: 488 nm, Em: 650-750 nm). The Overlay channel (Ol) is the merge between the cpVenus and Chl in leaves, and cpVenus and the bright field in roots.

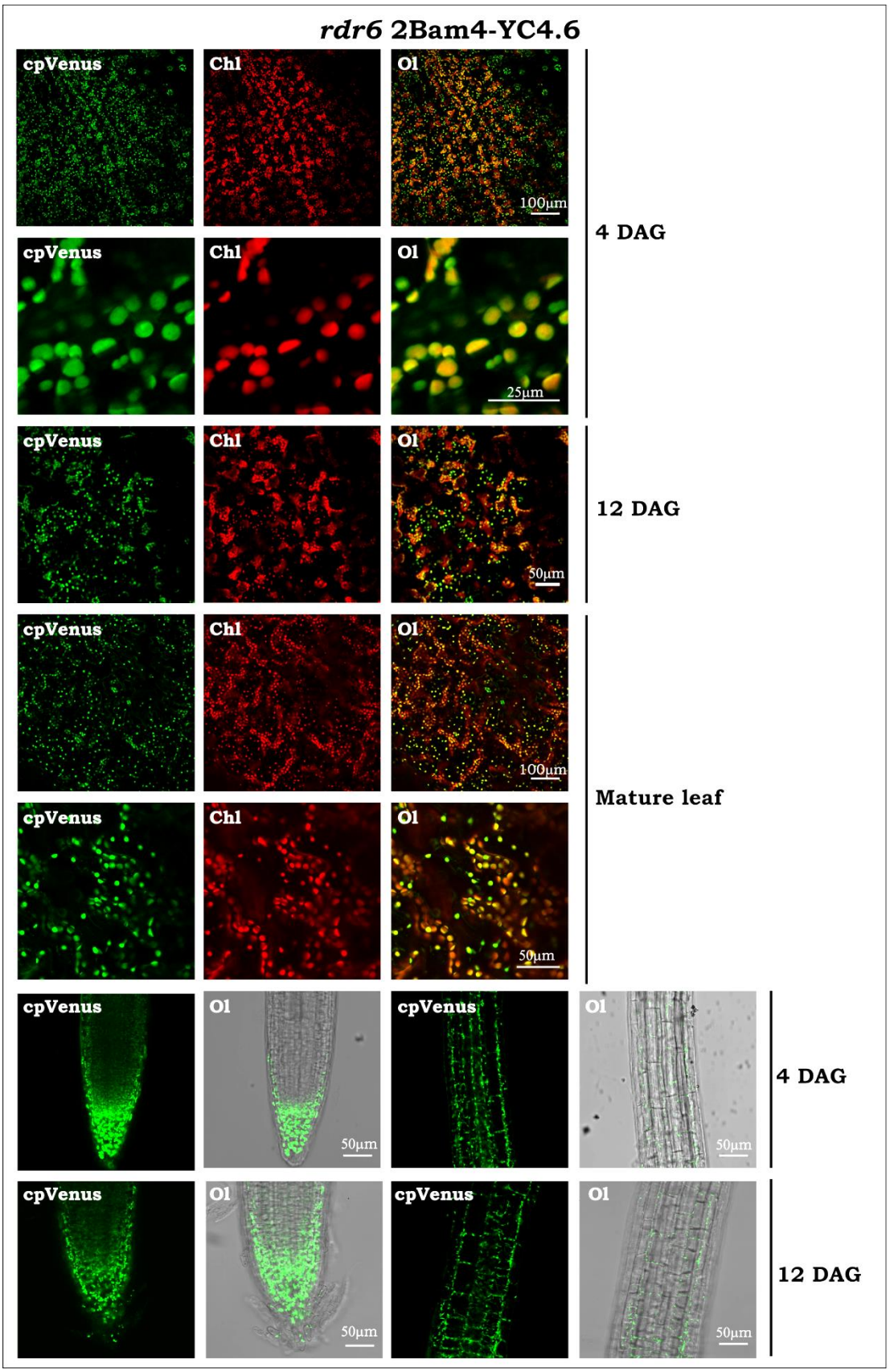
rdr6 2Bam4-YC4.6
cpVenus
Chl
Ol
100µm
4 DAG
25µm
12 DAG
50µm
Mature leaf
4 DAG
12 DAG

Figure 4.4: Expression of 2Bam4-YC4.6 probe in stable transformed *rdr6* mutant lines. The expression of the probe was analyzed detecting the cpVenus fluorescence of the Cameleon (cpVenus: Ex: 488 nm, Em: 510-540 nm) in leaves of seedlings at 4 and 12 Days After Germination (DAG) (first to fourth row), in leaves of mature plants (fourth and fifth row) and in the root at 4 and 12 DAG (sixth and seventh row). In leaves, chlorophyll was used as maker for chloroplasts (Chl: Ex: 488 nm, Em: 650-750 nm). The Overlay channel (Ol) is the merge between the cpVenus and Chl in leaves, and cpVenus and the bright field in roots.

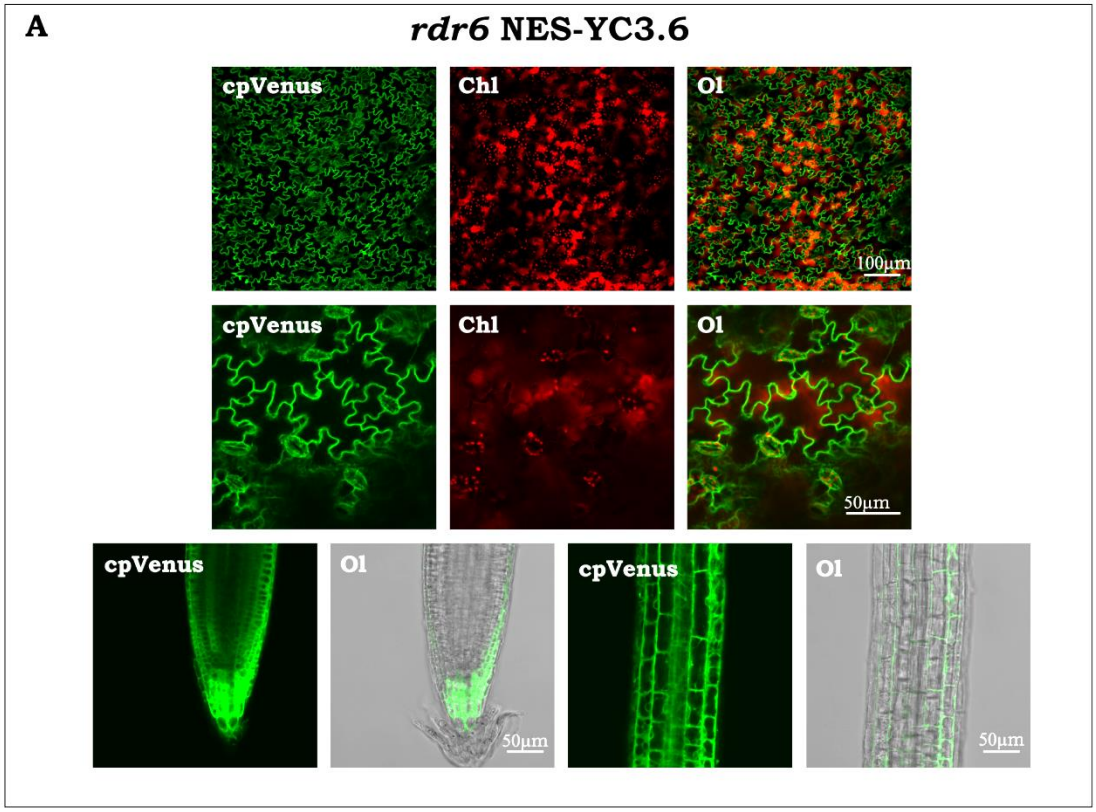

Figure 4.5: Expression of NES-YC3.6 probe in stable transformed *rdr6* mutant lines.
The expression of the probe was analyzed detecting the cpVenus fluorescence of the Cameleon (cpVenus: Ex: 488 nm, Em: 510-540 nm) in the leaves (first and second row) and in roots (third row) of seedlings. Chl: Chlorophyll autofluorescence Ex: 488 nm, Em: 650-750 nm. Ol: merge of the two channels cpVenus and Chl in leafs and cpVenus and bright field in the root.

Analysis of plastidial Ca^{2+}-dynamics in response to extracellular ATP in root

Extracellular adenosine 5'-triphosphate (eATP) is a signaling molecule involved in several processes such as plant growth, development and stress response. Among stress responses, eATP mediates the damage-associated molecular pattern (DAMP) (Tanaka et al. 2014), in which the cell recognizes several intracellular compounds such as nucleotides, saccharides, peptides and volatile molecules, as danger signals (Tanaka et al. 2014). Only for few of these molecules a receptor was described, in particular, DORN1 (defective in lectin receptor kinase I.9) was identified as a plasma membrane receptor of extracellular ATP (Choi et al. 2014a). eATP-activated DAMP causes a Ca^{2+}-transient in the cytosol and a consequent Ca^{2+}-accumulation in mitochondria and in the ER (Loro et al. 2012,Tanaka et al. 2010,Bonza et al. 2013). In root, eATP is initially perceived by the cells of the meristematic zone, then a Ca^{2+}-wave travels from this region to the elongation zone (Loro et al. 2012,Tanaka et al. 2010).

Plastids of the root meristem show a Ca^{2+}-transient in response to extracellular ATP

We analyzed plastidial Ca^{2+}-dynamics in response to 500μM eATP in the root meristem cells of seedlings and, in parallel, we monitored Ca^{2+} dynamics in the cytosol using both wild type and *rdr6* NES-YC3.6 lines (Krebs et al. 2012).

As reported in figure 4.1 A and B, a Ca^{2+}-transient was appreciable in plastids in response to eATP, demonstrating that these organelles accumulate and release Ca^{2+}. The accumulation of Ca^{2+} in the plastids was slower than in the cytosol, in fact, both plastidial probes reached the maximum fluorescence upon the stimulus in 150 seconds (155 ± 7 sec and 150 ± 9 sec for 2Bam-YC3.6 and 2Bam4-YC4.6 lines respectively) while it required about 30 seconds in the cytosol (28,8 ± 7,5 sec). Moreover, the

recovery of the resting Ca^{2+} level in the cytosol was more rapid than in plastids. In fact pre-stimulus $[Ca^{2+}]_{cyt}$ was completely recovered in less than 6 minutes, while, after the same period of time, the $[Ca^{2+}]_{str}$ remained above its pre-stimulus value (the $\Delta R/R_0$ measured at 360seconds are 0,29±0,2 and 0,16±0,04 for 2Bam4-YC3.6 and 2Bam4-YC4.6 line respectively) (Fig 4.6B). These experiments demonstrated that both probes are able to report Ca^{2+}-dynamics in plastids. Furthermore, although both probes outlined a similar shape of the transient, the 2Bam4-YC3.6 line showed a significantly higher FRET response, since the maximum $\Delta R/R_0$ was significantly higher compared to the one observed with 2Bam4-YC4.6 line (Fig 4.1 C). Considering the *in vitro* Ca^{2+} titration curves of the two probes, the increase of Ca^{2+} from 50nM to 1μM, causes a wider cpVenus/CFP ratio change in the YC3.6 probe compared to the YC4.6 (Nagai et al. 2004,Iwano et al. 2009). This observation was confirmed by our *in vivo* recordings of the single cpVenus and CFP emissions (Fig 4.1 D and E) that showed different FRET efficiencies for YC3.6 and YC4.6 (note the smaller cpVenus increase in the case of YC4.6 compared to YC3.6). Altogether, these results demonstrate that both probes are able to report Ca^{2+}-changes in plastids, but despite of similar kinetics, YC3.6 shows a higher dynamic range than YC4.6.

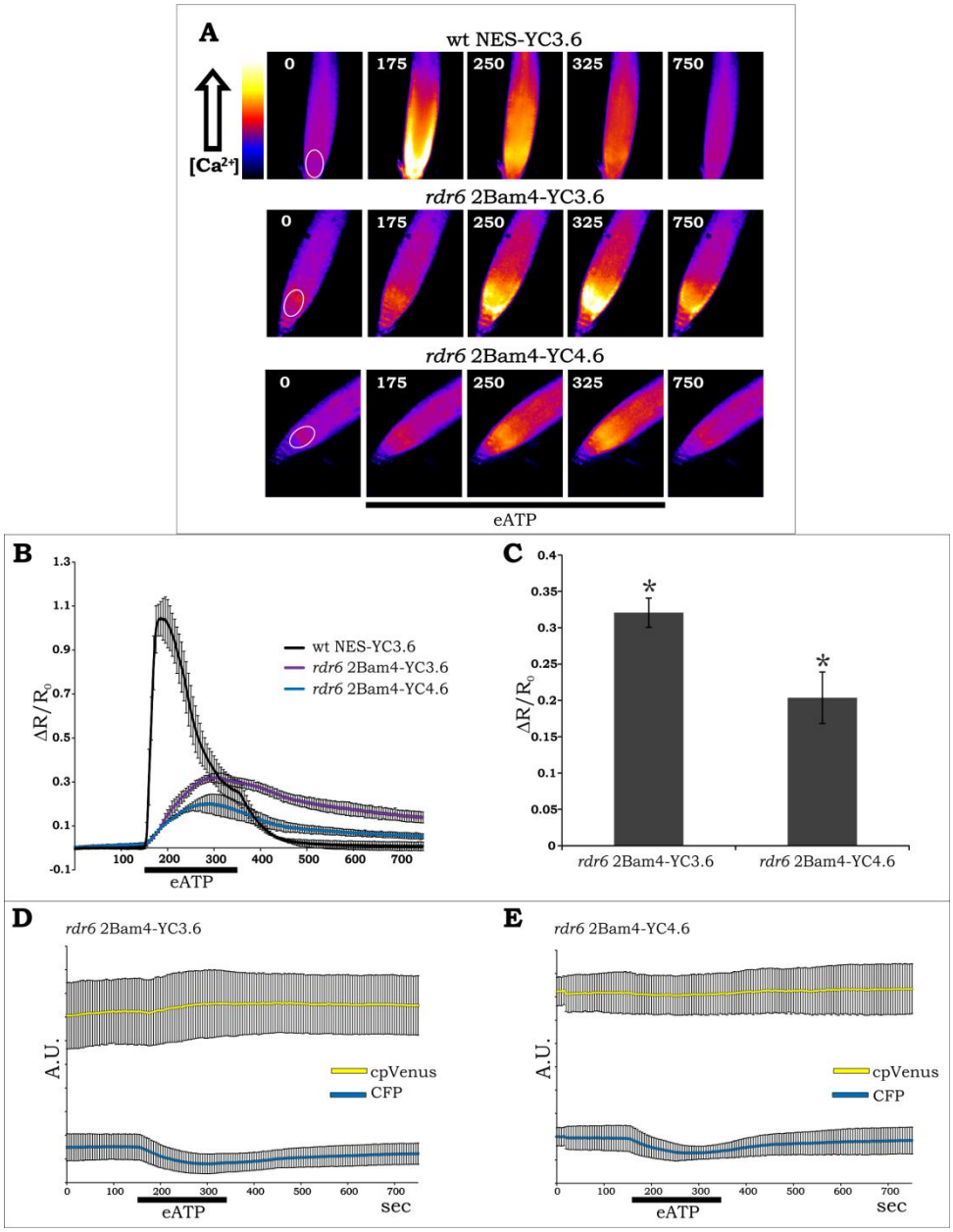

Figure 4.6: Plastidial and cytosolic Ca^{2+} response in the root tip of seedlings treated with extracellular ATP (eATP).

(A): times series of ratiometric images of root tip treated with 500µM of eATP. Cytosolic Ca^{2+}-response measured by the wt NES-YC3.6 line (first row) and Ca^{2+} dynamics in plastids monitored by rdr6 2Bam4-YC3.6 (second row) and rdr6 2Bam4-YC4.6 (third row). The white circle on the first image indicates the region analyzed, the number indicates the time (seconds after the beginning of acquisition). The black line under images indicate the treatment with eATP.

(B) Normalized ratio, reported as $\Delta R/R_0$ ± S.D, measured in response to eATP in root tip. Cytosolic response measured by wt NES-YC3.6 line (black trace) and plastidial response measured by *rdr6* 2Bam4-YC3.6 (the purple trace) and *rdr6* 2Bam4-YC4.6 (light blue trace) respectively. Traces are the average of at least three experiments. The black line under the axis of abscissae indicates the treatment with eATP.
(C) Statistical analysis of maximum plastidial variations reported as $\Delta R/R_0$ ± S.D., measured in the response to 500μM eATP (*= student's t test $p<0.01$).
(D) and (E) Single wavelength emissions of cpVenus (yellow trace) and CFP (light blue trace), of the 2Bam4-YC3.6 (D) and of 2Bam4-YC4.6 (E) probes. Intensity is expressed in arbitrary units (A.U.). The black line under the axis of abscissae indicate the treatment with eATP. Black bar= st. dev.

In order to link the observed plastidial Ca^{2+} accumulation to the cytosolic Ca^{2+} rise triggered by eATP, we investigated the plastidial response to eATP in details, by carrying out a dose-dependent-response analysis. We treated the roots of seedlings of the three different transgenic lines (*rdr6* 2Bam4-YC3.6, *rdr6* 2Bam4-YC4.6 and NES-YC3.6) with 10, 100 and 500 μM of eATP. Moreover, in order to verify that the *rdr6* background has no effects on cytosolic Ca^{2+} responses to eATP, we tested the *rdr6* NES-YC3.6 line in parallel.

The three eATP concentrations triggered Ca^{2+}-transients of different intensities in plastids (Fig 4.7 A and B) as well as in the cytosol (Fig 4.7 D). In both compartments, a clear dose-dependent response to eATP was observed, thus supporting the link between plastidial Ca^{2+}-accumulations and cytosolic Ca^{2+}-transients. Furthermore, the 2Bam4-YC3.6 was again the best performing probe, since it efficiently reported differences in the maximum Ca^{2+}-accumulation in response to 100 and 500 μM, whereas the 2Bam4-YC4.6 did not (Fig 4.7 C). Moreover, we compared the response to the three-eATP concentrations in wild type and *rdr6* NES-YC3.6 lines (Fig 4.7 E) and no significant differences in cytosolic Ca^{2+}-dynamics were observed, suggesting that the *rdr6* mutation does not alter the Ca^{2+} response induced by eATP (Fig 4.7 F).

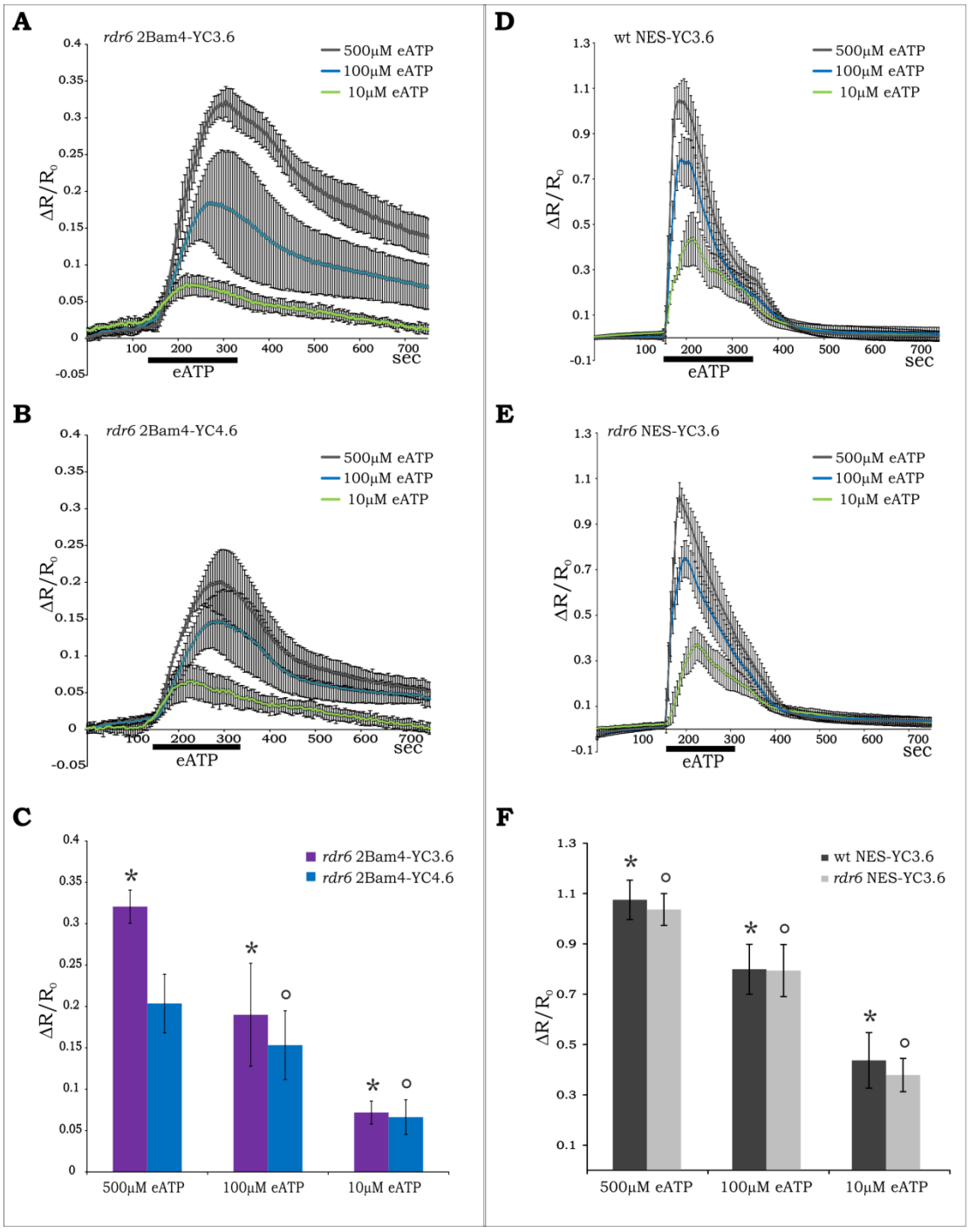

Figure 4.7: Plastidial and cytosolic Ca^{2+} response in the root tip of seedlings treated with different extracellular ATP concentrations.

(A) and (B): normalized ratio (cpVenus/CFP signal), reported as $\Delta R/R_0$ ± S.D., measured in plastids of root tip of (A) *rdr6* 2Bam4-YC3.6 and (B) *rdr6* 2Bam4-YC4.6 lines, in response to 500 (grey line), 100 (light blue line) and 10µM (green line) of eATP respectively. The black line

under the axis of abscissae indicates the treatment with eATP. Traces are the average of at least three experiments.
(C) Statistical analysis of maximum plastidial variations reported as $\Delta R/R_0$ ± S.D., measured in response to 10, 100 and 500 μM eATP by *rdr6* 2Bam4-YC3.6 (purple histogram) or *rdr6* 2Bam4-YC4.6 (light blue histogram), (* and °= student's t test $p<0.01$).
(D) and (E): normalized ratio (cpVenus/CFP signal), reported as $\Delta R/R_0$ ± S.D., measured in the cytosol of root tip of (D) wt NES-YC3.6 and (E) *rdr6* NES-YC3.6 lines, in response to 500 (grey line), 100 (light blue line) and 10μM (green line) of eATP respectively. The black line under the axis of abscissae indicate the treatment with eATP. The traces are the average of at least three experiments.
(F) Statistical analysis of maximum cytosolic variations reported as $\Delta R/R_0$ ± S.D., measured in response to 10, 100 and 500 μM eATP in wt (dark histogram) and rdr6 NES-YC3.6 (grey histogram) lines (* and °= student's t test $p<0.01$).

Analysis of stromal Ca^{2+}-dynamics in the light to dark transition in guard cells

Differently to plastids, chloroplasts develop the thylakoid-membrane system, a sub-compartment in these organelles. Ca^{2+} plays pivotal roles in chloroplasts (e.g. Ca^{2+} is required within the thylakoid lumen for proper functioning of PSII during the day) (Sai and Johnson. 2002) and the Ca^{2+} concentration among the two chloroplastic spaces substantially differs (Yamagishi et al. 1981). Hence, the stroma and the thylakoid lumen can potentially communicate by Ca^{2+} fluxes, giving the bases for a specific signaling in chloroplasts, not being investigated so far.
Studies performed with chloroplast targeted aequorin revealed that the light to dark transition triggers a stromal Ca^{2+}-increase (Sai and Johnson. 2002), and we demonstrated that this stimulus is not perceived in non-photosynthetic tissues, like the root. During our experiment, in fact, we did not detect any Ca^{2+}-increase into the plastids of the root due to the transition from light to dark. Thus, we decided to analyze this stimulus in chloroplasts of guard cells in epidermal strips of *rdr6* 2Bam4-YC3.6 and of *rdr6* 2Bam4-YC4.6 lines

Analysis of chloroplast Ca^{2+}-dynamics in single chloroplasts of guard cell

The high-resolution achievable by Cameleon probes, allowed us to monitor Ca^{2+}-dynamics at the level of single chloroplast within guard cells. In parallel, we monitored cytosolic Ca^{2+}-dynamics in both wt and *rdr6* NES-YC3.6 lines. Few minutes after that the specimens were moved from light to dark, we detected an increase in the $[Ca^{2+}]_{str}$ that reached the maximum level within approximately 6 minutes and remained sustained for the following 15 minutes. This sustained Ca^{2+} transient was detected in 92% of analyzed chloroplasts of both *rdr6* 2Bam4-YC3.6 (Fig 4.8 A) and *rdr6* 2Bam4-YC4.6 (Fig 4.8 B) lines. Furthermore, the transients measured in the *rdr6* 2Bam4-YC3.6 line reached a maximum $\Delta R/R_0$ significantly higher than the ones detected in the *rdr6* 2Bam4- YC4.6 line (Fig 4.9 C), confirming that the YC3.6 is the most suitable probe to measure $[Ca^{2+}]_{str}$-dynamics. Interestingly, single chloroplast analyses allowed us to evidence an oscillatory component in the slow Ca^{2+} rise observed during light to dark transition. We observed that these oscillations were a quite common event, being detected in 86% of analyzed chloroplasts. Moreover, those oscillations appear to rise in an asynchronous way among chloroplasts, even in the same guard cell. In Fig 4.8 A, the ratiometric images and the chart show an example of asynchronous oscillations between chloroplasts belonging to the same cell. The chloroplast marked in light blue shows two strong oscillations (at about 200 seconds) whereas, several seconds after, less-marked Ca^{2+}-oscillations were detected in the chloroplast marked in green. Altogether, these observations suggest that chloroplasts are able to regulate these Ca^{2+}-oscillations independently.

When we repeated the light to dark transition experiments with the plants expressing the cytosolic localized YC3.6, we observed the typical spontaneous Ca^{2+}-oscillations (Schroeder et al. 2001), in both wt (Fig 4.8 D grey trace) and *rdr6* NES-YC3.6 backgrounds (Fig 4.9 A grey trace). These oscillations are strictly dependent by the presence of free apoplastic Ca^{2+} since the treatment with EGTA, a Ca^{2+}-chelating agent, completely abolished

them (Fig 4.8 D black trace and 4.9 A black trace). Of note, EGTA treatment did not affect the basal levels of $[Ca^{2+}]_{cyt}$ in the two genetic backgrounds (Fig 4.9 B).

In order to understand whether the stromal Ca^{2+}-oscillations are correlated to cytosolic ones, we analyzed chloroplast dynamics in epidermal strip treated with EGTA. The chelation of apoplastic Ca^{2+} did not affect Ca^{2+} dynamics in chloroplast during light to dark transition, being both Ca^{2+}-oscillations and the sustained transient still present (Fig 4.10 B), in fact the percentage of chloroplasts showing Ca^{2+}-oscillations was unaffected (Fig 4.10 E). This latter result suggests that chloroplast Ca^{2+} transients are not dependent on cytosolic Ca^{2+}-oscillations, but the cytosol could still represent a Ca^{2+} source, since EGTA treatment did not affect the cytosolic resting Ca^{2+} level. In order to shed light on chloroplast Ca^{2+}-sources, we permeabilized the guard cell with 200nM Digitonin and, in order to chelate the Ca^{2+} outside chloroplasts, we treated the permeabilized cells with EGTA. The chelation of extra-chloroplast Ca^{2+} neither affect the basal level of $[Ca^{2+}]_{str}$ (Fig 4.10 D) nor the sustained Ca^{2+} transients, but clearly affected the asynchronous Ca^{2+} oscillations (Fig 4.10 C). In fact, the number of chloroplasts that presented Ca^{2+}-oscillations dropped down from 86% to 15% (Fig 4.10 C and table 4.10 E). This result suggests that Ca^{2+} oscillations and the sustained transient may have different sources of Ca^{2+}: the oscillations mainly depend on an extra-chloroplast Ca^{2+} source whereas the sustained Ca^{2+} transient depends on intra-chloroplast Ca^{2+} sources.

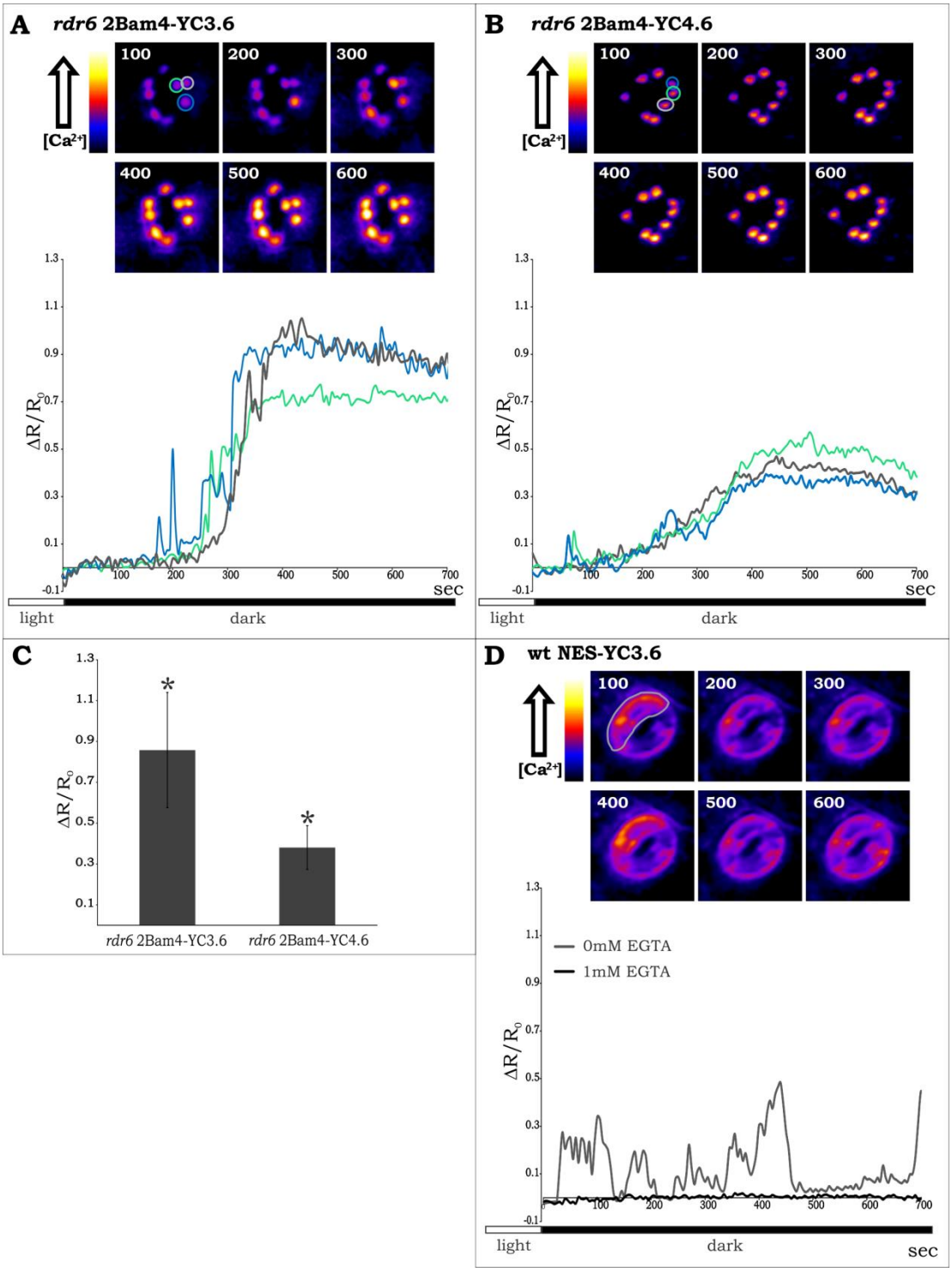
A
rdr6 2Bam4-YC3.6
[Ca2+]
100
200
300
400
500
600
ΔR/R0
sec
light
dark
B
rdr6 2Bam4-YC4.6
C
rdr6 2Bam4-YC3.6
rdr6 2Bam4-YC4.6
D
wt NES-YC3.6
0mM EGTA
1mM EGTA

Figure 4.8: Chloroplastic and cytosolic Ca^{2+} response in guard cells in response to light to dark transition.

(A) Chloroplasts Ca^{2+}-dynamics measured in *rdr6* 2Bam4-YC3.6 lines. Times series of ratiometric images of chloroplasts in response to light to dark transition (upper part of the panel), the number on the images indicates the time (seconds after the beginning of acquisition). Normalized ratio (lower part of the panel), reported as $\Delta R/R_0$, measured in the chloroplast indicated with colored circles in the first image of the times series. The white and the black rectangles under the axis of abscissae indicate the switch between light to dark.

(B) Chloroplasts Ca^{2+}-dynamics measured in *rdr6* 2Bam4-YC4.6 line. Times series of ratiometric images of chloroplasts in response to light to dark transition (upper part of the panel), the number on the images indicates the time (seconds after the beginning of acquisition). Normalized ratio (lower part of the panel), reported as $\Delta R/R_0$, measured in the chloroplast indicated with colored circles in the first image of the times series. The white and the black rectangles under the axis of abscissae indicate the switch between light to dark.

(C) Statistical analysis of Maximum chloroplastic variations measured as $\Delta R/R_0 \pm$ S.D. in *rdr6* 2Bam4-YC3.6 and *rdr6* 2Bam4-YC4.6 lines in response to light to dark transition (* and °= student's t test $p<0.01$).

(D) Cytosolic Ca^{2+}-dynamics measured by wt NES-YC3.6 line. Times series of ratiometric images of cytosol in light to dark transition (upper part of the panel), the number on the images indicate the time (seconds after the beginning of acquisition). Normalized ratio (lower part of the panel), reported as $\Delta R/R_0$, measured in the cytosol the guard cell indicated in the first image of the times series (grey). The black trace is representative of cytosolic Ca^{2+}-dynamics in guard cells treated with 1mM EGTA. The white and the black rectangle under the axis of abscissae indicate the switch between light to dark.

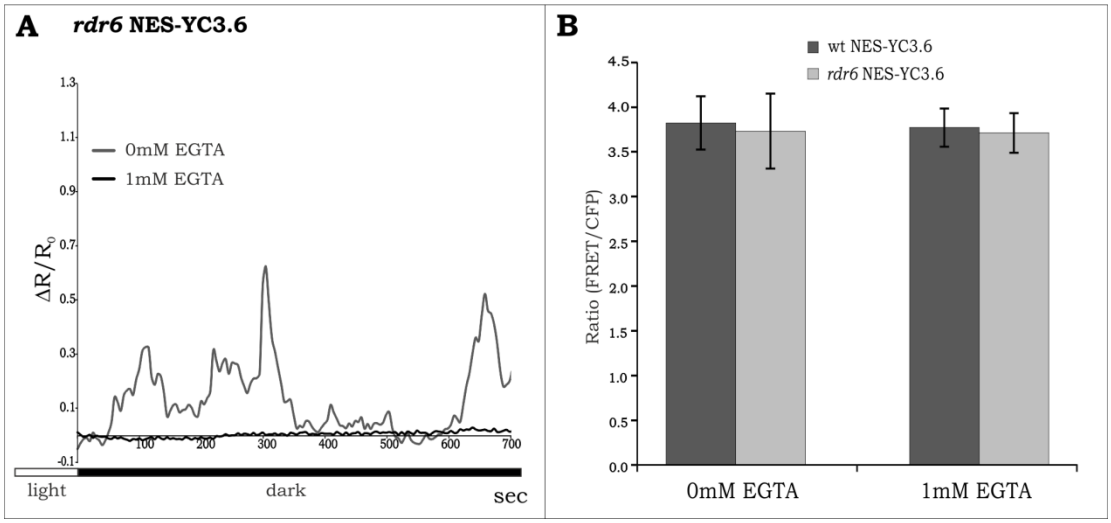

Figure 4.9: Analysis of cytosolic Ca^{2+}-dynamics in guard cell in *rdr6* NES-YC3.6 line.

(A) Normalized (cpVenus/CFP signal) ratio, reported as $\Delta R/R_0$ ± S.D., measured in the cytosol of *rdr6* NES-YC3.6 guard cells during light to dark transition, in control condition (gray line) or treated with 1mM of EGTA (black line). The white and the black rectangle under the axis of abscissae indicate the switch between light to dark.

(B) Comparison of the cytosolic basal [Ca^{2+}] in guard cells of the wt and *rdr6* NES-YC3.6 lines in control condition or treated with EGTA. The data are reported as cpVenus/CFP ratio ± S.D. in the wt NES-YC3.6 line (dark gray histogram) and in *rdr6* NES-YC3.6 line (light grey histogram) in presence of 0 or 1mM EGTA.

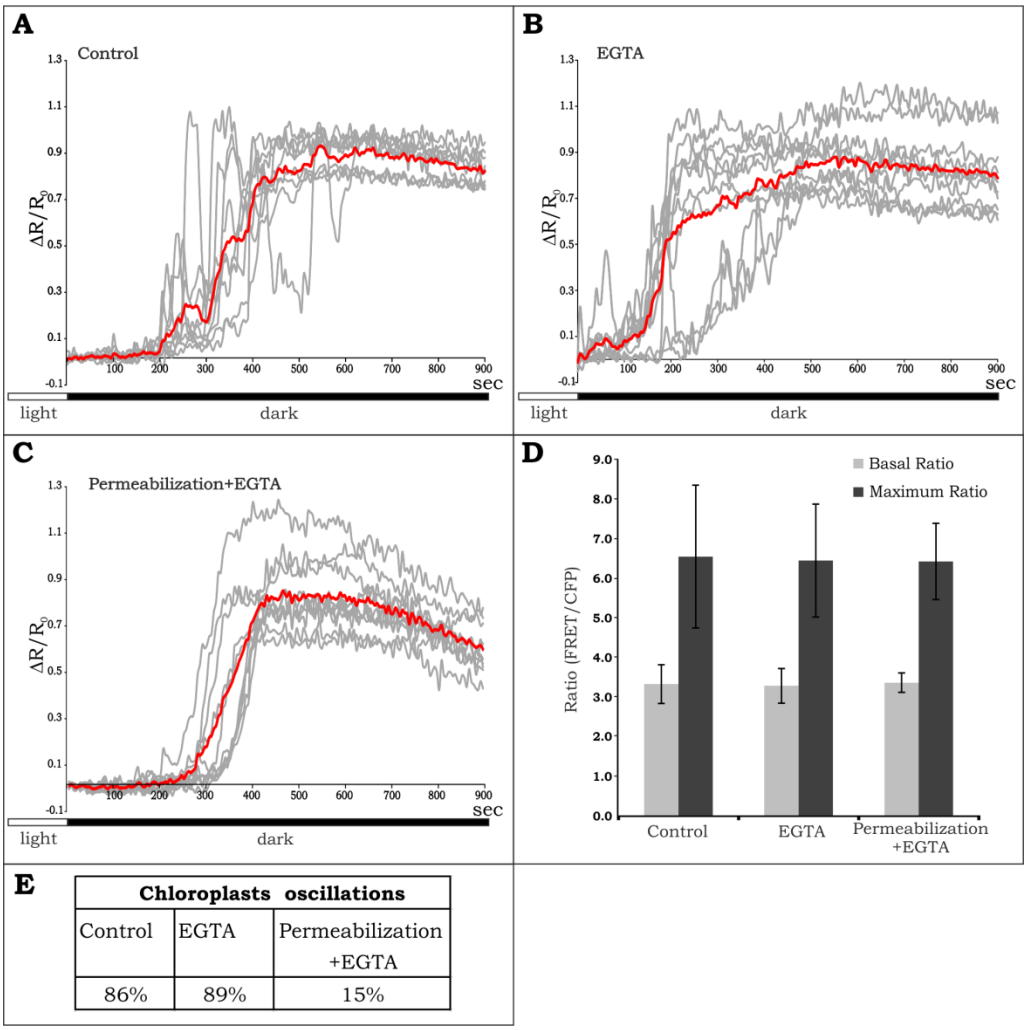

E

Chloroplasts oscillations		
Control	EGTA	Permeabilization +EGTA
86%	89%	15%

Figure 4.10: Components of chloroplastic Ca^{2+}-dynamics measured in *rdr6* 2Bam4-YC3.6 line

(A), (B) and (C): Normalized cpVenus/CFP ratio, reported as $\Delta R/R_0$. Response of ten different single chloroplasts (grey lines) in guard cells during light to dark transition in (A) control condition (Control), (B) treated with 1mM of EGTA (EGTA) or (C) permeabilized with 200nM digitonin and treated with 1mM EGTA (Permeabilization + EGTA). Red trace: average of the ten greys traces. The white and the black rectangle under the axis of abscissae indicate the switching between light to dark.(D) Comparison of the chloroplastic basal [Ca^{2+}] (light grey histogram) and the maximum [Ca^{2+}] (dark grey histogram) reached in the organelles in response to light to dark transition reported as cpVenus/CFP ratio ± S.D: in control conditions (Control), treated with 1mM EGTA (EGTA) or permeabilized with 200nM digitonin and treated with EGTA (Permeabilization + EGTA). (E) Table of the percentage of chloroplasts that show Ca^{2+}-oscillations in different conditions: control condition (Control), treated with 1mM EGTA (EGTA) or permeabilized with 200nM digitonin and treated with EGTA (Permeabilization + EGTA).

Chloroplast Ca^{2+}-dynamics in entire leaves: response to wounding

We analyzed chloroplasts Ca^{2+}-dynamics in entire leaves in response to wounding, which, in accord to previous data, triggers a rapid $[Ca^{2+}]_{cyt}$ transient in the region surrounding the damaged area. This response is characterized by a first rapid Ca^{2+} transient followed by a second smaller and slower transient (Fig 4.11 A)(Benikhlef et al. 2013,Beneloujaephajri et al. 2013). We repeated the experiment in the *rdr6*-NES-YC3.6 line and verified that wounding, also in this genetic background, induced the typical $[Ca^{2+}]_{cyt}$ response (Fig. 4.11 B).

Then, we analyzed the response of *A. thaliana* leaves of the *rdr6* 2Bam4-YC3.6 line to the wounding stimulus. Wounding induced a single short chloroplastic Ca^{2+}-transient immediately after the stimulus, lasting for about 30 seconds (Fig 4.11 B). We speculate that this rapid chloroplastic response could depend on the cytosolic Ca^{2+} increase similarly to what we have observed in root plastids in response to eATP.

We found that chloroplasts can both mimic cytosolic transients and act autonomously, but further experiments are needed to characterize the former response.

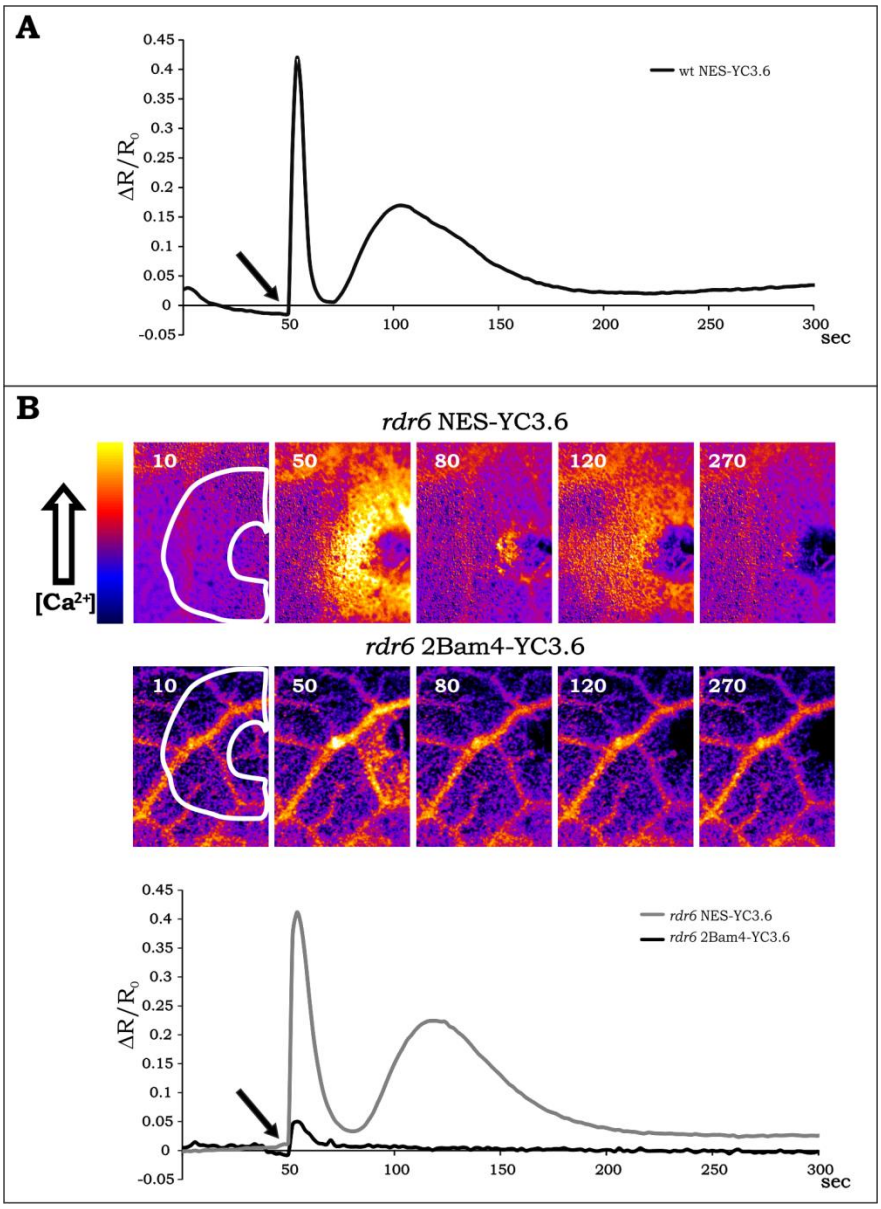

Figure 4.11: cytosolic and chloroplastic Ca^{2+}-dynamics after wounding

(A) Normalized ratio, reported as $\Delta R/R_0$, measured in leaf of wt NES-YC3.6 line (black trace) after wounding. The experiment were repeated four times giving comparable results, one representative trace is presented. The black arrow indicates the moment at which wounding was performed. (B) Top: time series of ratiometric images of leaf during the wounding treatment in *rdr6* NES-YC3.6 (first row) and *rdr6* 2Bam4-YC3.6 (second row) lines. The numbers on the images indicates the time (seconds after the beginning of acquisition). Bottom: normalized ratio, reported as $\Delta R/R_0$, measured in the selected ROIs (region of interest) indicated by the white line reported in the first ratio images of the series. The black arrow indicates the moment at which wounding was performed.

4.3 Conclusions

It has been known from more than 70 years that chloroplasts are able to accumulate Ca^{2+}, and this ion is involved in the regulation of several plastidial/chloroplastic processes (Nomura et al. 2012,Balsera et al. 2009,Turner et al. 2004,Aldridge and Moller. 2005,Nomura et al. 2008). Although different roles for Ca^{2+} in these organelles have been described, the $[Ca^{2+}]$-regulation mechanisms and the identity of Ca^{2+}-transporters are unclear. The possibility to image *in vivo* chloroplastic and plastidial Ca^{2+}-dynamics at high resolution will help to shed light on these unsolved questions.

In this study, we generated, in the silencing suppressed *rdr6 A. thaliana* genetic background (Peragine et al. 2004), transgenic lines expressing two different chloroplasts/plastids localized Cameleon probes, (*rdr6* 2Bam4-YC3.6 and *rdr6* 2Bam4-YC4.6), and the cytosolic localized YC3.6 probe (*rdr6* NES-YC3.6). In this way, we developed a complete toolkit by which we can monitor the cytosolic and the chloroplastic/plastidial response, in parallel. By comparing the *rdr6* NES-YC3.6 and the wt NES-YC3.6 (Krebs et al. 2012) lines, we could verify that the *rdr6* mutation does not interfere with Ca^{2+}-responses evaluated in this work.

First, we demonstrated that the 2Bam4-YC3.6 and the 2Bam4-YC4.6 probes are suitable for the analyses of Ca^{2+}-dynamics in chloroplasts and plastids, acting in a range of $[Ca^{2+}]$ compatible to the intra-organellar environment. These probes allowed to measure the *in vivo* Ca^{2+}-dynamics in entire organs, like roots and leaves, at single cell level analyzing guard cells where we were even able to push out our observations to single chloroplast.

In the experiments reported in this study, the 2Bam4-YC3.6 Cameleon probe proved to be the most appropriate to measure Ca^{2+}-dynamics in root plastids and in the stroma of chloroplasts, as it showed higher response in term of $\Delta R/R_0$ compared to the 2Bam4-YC4.6. This is in accordance to the *in vitro* affinity curve for Ca^{2+}, in which the YC3.6 probe has higher FRET variations than the YC4.6 between 50nM and 1μM $[Ca^{2+}]$ range (Nagai et al. 2004). Unfortunately, attempts for an *in vivo* calibration of the Cameleon

probes were unsuccessful (data not shown), indeed the peculiar intra-organelle environment could affects the Ca^{2+} affinity of the probes, but despite that, we can speculate that chloroplastic and plastidial Ca^{2+}-responses are in the nano molar range of $[Ca^{2+}]$. In support to this hypothesis, previous studies performed with the aequorin probe reported that the basal $[Ca^{2+}]_{str}$ is in the range of 100-150 nM while it reaches 200 nM upon several stimuli (Nomura et al. 2012).

One of the first result of this study was the demonstration that plastids respond in terms of Ca^{2+}-transient to the extracellular ATP stimulus. Interestingly, the plastidial Ca^{2+}-response was correlated to the magnitude of cytosolic Ca^{2+}-transients, in fact, both compartments showed a dose dependent response. Therefore, our data suggest that plastids could have a role in restoring cytosolic Ca^{2+} basal level, contributing to the shape of an appropriate Ca^{2+}-signature acting as cytosolic Ca^{2+}-capacitors.

We deepened this study analyzing chloroplastic Ca^{2+}-dynamics at single cell level, in guard cells, and thanks to the high resolution offered by the Cameleon probes, we were able to observe Ca^{2+}-transients in single chloroplasts. Studies based on the aequorin probe targeted to the stroma reported that the light to dark transition induces an increase in the $[Ca^{2+}]_{str}$ (Nomura et al. 2012,Sai and Johnson. 2002). We tested this response in our system and we were able, not only to confirm the stromal Ca^{2+}-accumulation in guard cell chloroplasts, but we also detected asynchronous Ca^{2+}-transients that occur in the stroma immediately before and during the sustained transient. These oscillations were present in the majority of chloroplasts (86%) and they were asynchronous even among chloroplasts belonging to the same guard cell. This kind of event can be detectable only by single chloroplast analyses; in fact, the integration of the asynchronous signals of several chloroplasts resulted in a slow single sustained transient (red trace in Figure 4.10 A). This result highlights that this organelles act as independent organelles that are able to modulate specific Ca^{2+}-dynamics.

Ca^{2+}-oscillations in the cytosol of guard cells is a well described event (Schroeder et al. 2001), but we here demonstrated that chloroplasts are also able to generate rapid Ca^{2+}-transients in the stroma which are independent

from the cytosolic ones. Chloroplasts showed an autonomous regulation of stromal Ca^{2+} level, hence, we investigated on the Ca^{2+}-sources of the observed oscillations. Our experiments revealed that chloroplast Ca^{2+}-dynamics that followed the light to dark transition did not require apoplastic Ca^{2+}, whereas cytosolic oscillation did. Furthermore, we can hypothesize that at least two Ca^{2+}-sources participate in the generation of chloroplast Ca^{2+}-transients. In fact, while asynchronous oscillations are strongly reduced by the chelation of cytosolic Ca^{2+}, the sustained transient was unaffected. This result indicates that the cytosolic Ca^{2+} is probably the Ca^{2+} source for the asynchronous oscillations, while the long sustained transient is dependent on an intra-chloroplast Ca^{2+}-store. Thylakoid lumen shows very high Ca^{2+} concentrations and indeed it likely represents the intra-chloroplast Ca^{2+} source.

The two different kinetics identified in the stromal Ca^{2+}-uptake suggest that they might be involved different Ca^{2+}-transporters/channels. The Ca^{2+}-oscillation show a rapid increase in the $[Ca^{2+}]_{str}$ and could be associated to an activity of a Ca^{2+}-transporter located on the inner membrane, to support this hypothesis several studies suggest the presence of a chloroplastic uniport at this membrane (Kreimer et al. 1985,Roh et al. 1998), but the molecular identity of this transporter is still unknown.

The sustained Ca^{2+}-transient, probably associated to a Ca^{2+}-release from thylakoids, could be due to the activity of the putative Ca^{2+}/H^{+} (CAX) present on thylakoids membrane (Ettinger et al. 1999). Further experiments are needed to proof these hypotheses and, the identification of chloroplast Ca^{2+}-transporters will be pivotal for an exhaustive comprehension of chloroplast Ca^{2+}-regulation.

Eventually, we also analyzed the chloroplast Ca^{2+} response to wounding, in entire leaves. Preliminary experiments revealed that chloroplasts sense the strong and rapid wounding-induced cytosolic Ca^{2+} increase. In fact, in our experiments, chloroplasts of the cells surrounding the damaged area responded with a small and fast Ca^{2+}-transient. To some extent the dynamic of this transient resembles the asynchronous oscillations observed at single chloroplast level. In fact, the Ca^{2+}-source for this events it is probably the

cytosol, moreover both show a rapid Ca^{2+}-increase followed by a quick recovery of the resting $[Ca^{2+}]_{str}$, suggesting they might be dependent on the regulation of the same Ca^{2+}-transporters/channels present on the inner envelope. Of note we can also consider that during the experiments performed with entire intact leaf, we did not observe in the chloroplasts, the sustained Ca^{2+}-transient associated to the light to dark transition So far we do not have a definitive explanation for this result, but we can hypothesize that it could be due to the low magnification, hence, low resolution, used in this experiment. Nevertheless, altogether these data suggest that chloroplasts are able to generate proper intra-organellar Ca^{2+}-transient but also to sense strong cytosolic Ca^{2+}increases.

In conclusion, we developed a series of tools that allowed to perform analyses of Ca^{2+}-dynamics in single chloroplasts, and thank to this high resolution we identified unprecedented observed stromal Ca^{2+}-oscillations. The future direction of this work will be the use of our transgenic lines for the identification of the transporters/channels involved in stromal Ca^{2+} regulation. In fact, the possibility to cross *A. thaliana* mutants defective for putative chloroplastic Ca^{2+} transporters/channels with our *rdr6* cytosolic and chloroplastic/plastidial Cameleon lines will allow to shed light on important physiological aspects.

4.4 Materials and Methods

Plant material and growth conditions

All *A. thaliana* lines used in this thesis belongs to the Columbia (Col 0) ecotype. Plants were grown in Jiffy soil under short day light period (8 h light /16 h dark, 150 μmol m^{-2} s^{-1}) at 22 °C and 75% relative humidity.

Seeds of *A. thaliana* transgenic lines were surface-sterilized by vapor-phase sterilization (Clough and Bent, 1998) and plated on half-strength MS medium (Murashige and Skoog, 1962) (Duchefa) supplemented with 0.1% sucrose, 0.05% MES, pH 6.0, and 0.8% plant agar (Duchefa). After stratification at 4 °C in the dark for 2 days, plates were transferred to the growth chamber under long day light period (16h light/8h dark, 150 μmol m^{-2} s^{-1}) at 22°C. The plates were kept vertically and seedlings were analyzed at 7 DAG.

The *rdr6-11* mutant line was kindly provided by Prof Wolf Frommer (Dept of Plant Biology, Stanford). Transgenic NES-YC3.6 *A. thaliana* plants, in which the Cameleon is targeted to the cytosol by a Nuclear Export Signal (NES), were kindly provided by Dr Karin Schumacher (Department of Developmental Biology, University of Heidelberg, Germany) (Krebs et al., 2012).

DNA constructs

pGreen 0029 35S:Bam4-YC3.6

The construct pGreen 0029 35S:Bam4-YC3.6 was obtained from the pGreen 0029 35S:4mt-YC3.6 (Loro et al. 2012), in which the mitochondrial target sequence 4mt was excised and replaced with the chloroplast target sequence Bam4 (Fulton et al. 2008).

The sequence encoding Bam4 was amplified directly from genomic DNA of *A. thaliana* using following primers:

forward 5'-CATGaagcttATGACGGAGACTGGAGTAAT-3'

reverse: 5'-CATGaagcttACGCAACTTAGTGATGAAA-3'

in which the HindIII restriction sites (underlined) were inserted at the 5' and 3' ends. The sequence was fused at the N-terminus of the YC3.6 probe by HindIII restriction. To double the Bam4 target sequence, the signaling peptide was amplified using the following primers:

forward 5'-CATGgggcccATGACGGAGACTGGAGTAAT-3'
reverse 5'-CATGgggcccACGCAACTTAGTGATGAAA-3'

in which the ApaI restriction sites (underlined) were inserted at the 5' and 3' ends. The sequence was fused at the N-terminus of the Bam4-YC3.6 construct by ApaI restriction. In both the cloning steps, the direction of the insertion was verified through Sanger sequencing. DNA amplification by PCR were carried out using Phusion DNA polymerase (Finnzymes).

pGreen 0029 35S:2Bam4-YC4.6

The YC4.6 Cameleon probe was excised from pcCDNA3 vector, through digestion with BamHI and EcoRI, and placed in the p35S2 vector (http://www.pgreen.ac.uk/JIT/JIT_fr.htm).
The sequence encoding Bam4 was amplified directly from genomic DNA of *A. thaliana* using the following primers:

Bam4 forward 5'-CATGaagcttATGACGGAGACTGGAGTAAT-3'
Bam4 reverse: 5'-CATGaagcttACGCAACTTAGTGATGAAA-3'

in which the HindIII restriction sites (underlined) were inserted at the 5' and 3' ends. The sequence was placed at the N-terminal of the YC4.6 probe in the p35S2 vector using HindIII restriction site. The direction of the insertion was verified by Sanger sequencing. The second Bam4 sequence was amplified using the following primers:

forward 5'-CATGaagcttATGACGGAGACTGGAGTAAT-3'
reverse 5'- CATGggatccCCACGCAACTTAGTGATGAAA-3'

in which a HindIII restriction site (underlined) is present at the 5' of the forward primer and a BamHI restriction site (underlined) is present at the 5' of the reverse primer. The sequence was placed between the first Bam4

sequence and the YC4.6 probe by HindIII and BamHI restriction. The entire cassette (35S:2Bam4-YC3.6-term) was amplified using the following primers, in which KpnI restriction sites (underlined) are present at the 5' and 3' ends.

forward 5'-CATGggtaccGATATCGTACCCCTACTCCAAAAAT-3'
reverse 5'-CATGggtaccGATATCGATCTGGATTTTAGTA-3'

The entire cassette was transferred in the pGreen 0029 vector by KpnI restriction. DNA amplification by PCR were carried out using Phusion DNA polymerase (Finnzymes).

Bacterial strains

Plasmid amplification was performed in the *DH5α Escherichia coli*. The *Agrobacterium tumefaciens* strain used for plant transformation was *GV3101*

Transgenic plants

The *GV3101 A. tumefaciens* strains, transformed with the construct of interest, was used to generate transgenic plants by the floral-dip method (Clough and Bent,1998). Several independent transgenic lines were isolated by antibiotic selection, for each construct.

The pGreen 0029 35S:2Bam4-YC3.6 construct was introduced both in wild type *A. thaliana* plants and in the *rdr6-11 A. thaliana* mutant line.

The pGreen 0029 35S:2Bam4-YC4.6 construct was introduced in the *rdr6-11 A. thaliana* mutant line.

The pGPTVII Ubq10:NES-YC3.6 construct (Krebs et al. 2012) that was insert in the *rdr6-11 A thaliana* mutant line and seeds of wt plants expressing NES-YC3.6 construct were kindly provided by Dr Karin Schumacher (Department of Developmental Biology, University of Heidelberg, Germany) (Krebs et al. 2012) .

At least two independent lines of each reporter were used for imaging experiments.

Laser scanning confocal microscopy analyses

Laser scanning confocal microscopy (LSCM) analyses were performed using a Leica SP5 imaging system. cpVenus was excited by the 514 nm line of the Argon laser and the emission was collected between 525/540 nm. Chlorophyll was excited at 514 nm and the emission was collected between 650 and 750 nm. Images were acquired by a 25X water immersion objective with different digital zoom, and analyzed using IMAGEJ software (http://rsb.info.nih.gov/ij/).

Imaging microscopy analyses

Roots and guard cells of the Cameleon reporter lines were analyzed *in vivo* using an inverted fluorescence microscope (Nikon Ti-E). The objectives used were: a dry 20X for roots and for the analysis of guard cells reported in figure 4.10; a 40X objective for the analysis of guard cells reported in fig 4.9. 440 nm (436/20 nm) excitation light was produced by a fluorescent lamp. Images were collected by ORCA-D2 Hamamatsu Dual CCD camera.

For Cameleon analysis, the FRET CFP/YFP optical block A11400-03 (CFP emission 1, 483/32 nm; emission 2, 542/27 nm for FRET) with a dichroic 510-nm mirror was used for the simultaneous acquisitions of CFP and FRET (cpVenus) fluorescence. Exposure time was between 100 and 300 milli-seconds with a 2X2 CCD binning for cytosolic Cameleon (wt NES-YC3.6 and *rdr6* NES-YC3.6) and a 4X4 CCD binning for chloroplastic/plastidial Cameleon (*rdr6* 2Bam4-YC3.6 and *rdr6* 2Bam4-YC4.6). Images were acquired every 5 seconds. Post-acquisition analyses were performed using the IMAGEJ software.

Guard cells imaging

For guard cell imaging, leaves of 4-week old *Arabidopsis* transgenic plants were used. A small piece of the leaf (approximately 10 mm^2) was glued to the cover slide using medical adhesive (Hollister Inc., Libertyville, IL). Upper cell layers were gently removed with a razor blade. The obtained epidermal strips were incubated in the guard cell solution (5 mM KCl, 10 mM MES, 50 µM $CaCl_2$ pH 6.15 adjusted with Tris-base) and placed under light in the growth

chamber for 5 to 10 minutes, before starting the measurements or treatments.

Ethylene Glycol Tetra-acetic Acid (EGTA) treatment

Samples prepared as described were placed in the EGTA solution (guard cell solution added of 1mM of EGTA) and left under light in the growth chamber for 5 minutes before starting the measurement.

Permeabilization and treatment with EGTA

Samples prepared as describe above were placed in the permeabilization solution (100mM K-Gluconate, 1mM $MgCl_2$, 10mM Hepes, 5mM EGTA, 200nM Digitonin, pH 7.5 adjusted with Tris-base) for 4 minutes. Then the sample was placed in the maintaining solution (100mM K-Gluconate, 1mM $MgCl_2$, 10mM Hepes, 1mM EGTA, pH 7.5 adjusted with Tris-base) and left under light in the growth chamber for 5 minutes, before starting the measurement.

Root seedlings imaging

7-day-old seedlings were used for root imaging. Seedlings were gently removed from the plate, accordingly to Behera and Kudla (2013)(Behera and Kudla. 2013), placed in the dedicated chambers and overlaid with wet cotton. The seedling root was continuously perfused with the imaging solution (5mM KCl, 10mM Mes 10mM $CaCl_2$ pH 5.8 adjusted with Tris-base) while the shoot was not submerged. The eATP treatment was administered during the imaging experiment perfusing for 3 minutes the imaging solution added with different concentration of eATP (10, 100 or 500µM).

Wounding

Leaves of 4-week old *A. thaliana* transgenic plants were used in wounding analyses. An entire leaf was placed under the cover slide. 30 seconds after the beginning of the experiment, leaves were stimulated with tweezer

Chapter 5:

Main conclusions

Plants are sessile organisms, which have to cope with environmental challenges. Complex biological responses trigger signal cascades and guarantee the appropriate transcriptional and metabolic responses. The modulation of second messengers is a key step in these pathways regulating several downstream events by activating or inhibiting biochemical reactions. Despite the large number of stimuli, plants uses only few second messengers, and, among these, Ca^{2+} has a prominent role, being involved in the response to several biotic and abiotic stresses and developmental stimuli.

How the cell can maintained and activate the correct response to this omnipresent second messenger remains an open question. Several hypothesis were proposed, one of them is that the cell can codify specific Ca^{2+}-signature (the shape of the transient in terms of spatial-temporal oscillations) (McAinsh and Pittman. 2009,Scrase-Field and Knight. 2003). The possibility to analyze the Ca^{2+}-dynamics at high resolution will help for shed light on this unresolved question. Furthermore, several studies indicate that Ca^{2+} modulates processes in subcellular compartments as chloroplasts, mitochondria, peroxisomes and the ER (Stael et al. 2012,Nomura and Shiina. 2014).

The aim of this PhD project was to achieve a deeper comprehension of Ca^{2+}-dynamics in the organelles and to discern the role of subcellular compartments in shaping the Ca^{2+}-signature. In this view, we developed new tools that allow *in vivo* high resolution Ca^{2+}-imaging in mitochondria, ER and plastids. We chose the genetically encoded probe Cameleon, which was previously used to analyze Ca^{2+}-dynamics in the cytosol, in the nucleus, in the peroxisome lumen and at the level of plasma membrane (Krebs et al. 2012,Costa et al. 2010).

We generated stable transformed *A. thaliana* lines harboring the mitochondrial, the ER or the chloroplastic/plastidial probes. The constitutive expression of the chloroplastic/plastidial probe was affected by post transcriptional gene silencing, that we bypassed transforming the *A. thaliana rdr6* mutant (Peragine et al. 2004) that allowed the constitutive expression of the probe and the successive Ca^{2+}-dynamic analyses. By the

mean of these lines, we monitored organellar Ca^{2+} dynamics in different tissues with an unprecedented resolution.

We tested several stimuli for the different compartments, and in particular, we characterized Ca^{2+}-dynamics in response to extracellular ATP (eATP) in the root tip cells (Fig. 5.1) and during the light to dark transition in the guard cell (Fig. 5.2).

eATP is involved in the immune response to damage-associated molecular pattern (DAMP) (Tanaka et al. 2014) and recently the eATP receptor DORN1 has been identified on the plasma membrane (Choi et al. 2014). The Ca^{2+}-response transient due to the treatment with eATP mainly depends on the entry of extracellular Ca^{2+}, but the release of Ca^{2+} from intracellular store was also predicted as source of Ca^{2+} (Tanaka et al. 2010). In this study, we analyzed the Ca^{2+}-dynamics in the ER, in mitochondria and in plastids. As reported in Fig 5.1, all the analyzed compartments showed a Ca^{2+}-transient in response to this treatment, but we did not detect any Ca^{2+}-release. In addition, other studies performed on peroxisomes showed that in response to eATP not even this organelle releases Ca^{2+}, but it just mimics the cytosolic Ca^{2+}-transient (Costa et al. 2013). These data strongly suggest that the vacuole could be the main component of the intracellular Ca^{2+}-store involved in the generation of the cytosolic Ca^{2+} transient. Moreover, despite Ca^{2+}-kinetics in response to eATP are similar between plastids and mitochondria, the former seems to recover the basal Ca^{2+} level faster than mitochondria, suggesting that this organelles might have a more efficient system for the Ca^{2+} extrusion.

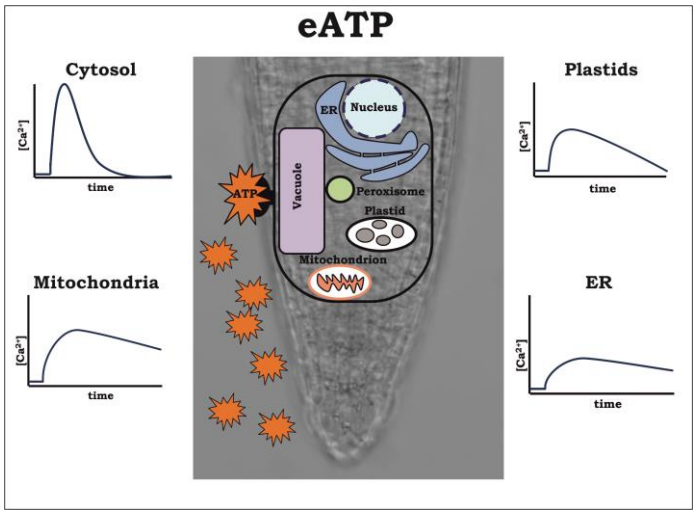

Figure 5.1: Schematic representation of Ca^{2+}-dynamics in intracellular compartments during eATP response, in the root tip. Representative traces of Ca^{2+}-transient in the cytosol, in mitochondria, in plastids and in the ER are reported.

The experiments carried out in stomata have the advantage to allow to perform experiments in single isolated cells, in fact, the guard cell lacks of plasmodesmata. In these cells we analyzed the *in vivo* Ca^{2+}-dynamics during the dark to light transition in the cytosol, in mitochondria and at the level of single chloroplast. In the cytosol we observed the typical spontaneous Ca^{2+}-oscillations already reported in other studies (Schroeder et al. 2001). The analysis of mitochondrial Ca^{2+}-dynamics revealed that this organelle did not response to light/dark transition, showing no Ca^{2+}-transients during this stimulus (Fig 5.2) that, on the contrary, were clearly observed in chloroplasts. The presence of the photosynthetic apparatus in chloroplasts, strictly links this organelle to light reactions and the circadian cycle, which are Ca^{2+}-regulated processes (Sai and Johnson. 2002). Interestingly, thanks to the single chloroplast resolutions we observed asynchronous Ca^{2+}-oscillations in the stroma superimposed to the sustained Ca^{2+}-transient, which was previously described with aequorin (Sai and Johnson. 2002,Nomura et al. 2012). This unique behavior among organelles demonstrates that chloroplast are able to regulate Ca^{2+}-dynamics autonomously.

Moreover, our experiments demonstrated that stromal Ca^{2+}-dynamics neither are generated by extracellular Ca^{2+} nor are linked to spontaneous cytosolic Ca^{2+}-oscillations (Schroeder et al. 2001), but they depends on intra-cellular and intra-chloroplast Ca^{2+}-stores.

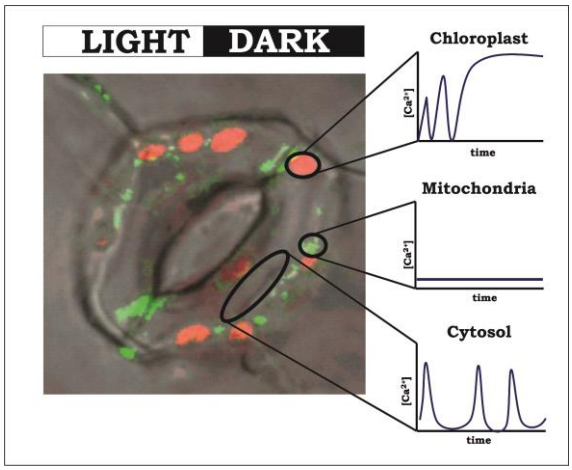

Figure 5.2: Schematic representation of Ca^{2+}-dynamics in intracellular compartments during light to dark transition, in guard cell. Representative traces of Ca^{2+}-transient in chloroplasts, in mitochondria and in the cytosol are reported.

In conclusion, the transgenic lines we generated allowed to study Ca^{2+}-dynamics in intracellular compartments and will help to shed light on their role in Ca^{2+}-signalling. Moreover, these tools will permit to identify Ca^{2+}-transporters involved in the Ca^{2+}-dynamics of these organelles and to achieve a wider knowledge of Ca^{2+}-kinetics in plant cells.

Chapter 6:

Appendix

Ca^{2+} Imaging in Plants Using Genetically Encoded Yellow Cameleon Ca^{2+} Indicators

Smrutisanjita Behera, Melanie Krebs, Giovanna Loro, Karin Schumacher, Alex Costa and Jörg Kudla

Cold Spring Harb Protoc; doi: 10.1101/pdb.top066183

Topic Introduction

Ca^{2+} Imaging in Plants Using Genetically Encoded Yellow Cameleon Ca^{2+} Indicators

Smrutisanjita Behera,[1] Melanie Krebs,[2] Giovanna Loro,[3,4] Karin Schumacher,[2] Alex Costa,[4] and Jörg Kudla[1,5]

[1]*Institute of Plant Biology and Biotechnology, University of Münster, 48149 Münster, Germany;* [2]*Department of Developmental Biology, Centre for Organismal Studies (COS), University of Heidelberg, 69120 Heidelberg, Germany;* [3]*Department of Biology, University of Padova, 35131 Padova, Italy;* [4]*Department of Biosciences, University of Milan, 20133 Milan, Italy*

Temporally and spatially defined changes in cellular calcium (Ca^{2+}) concentration represent stimulus-specific signals and regulate a myriad of biological processes. The development of ratiometric Ca^{2+} reporter proteins like Yellow Cameleons (YCs) has greatly advanced our ability to analyze Ca^{2+} dynamics in vivo with unprecedented spatial and temporal resolution. In plants, the application of these Ca^{2+} reporter proteins has been pioneered for the investigation of Ca^{2+} dynamics in guard cells, and recently their use has been extended to other single-cell models like growing pollen tubes and root hairs. However, in plants, the use of YC reporter proteins has largely remained restricted to the investigation of cytoplasmic alterations of Ca^{2+} concentrations. Here, we provide an introduction to current methods for imaging Ca^{2+} dynamics with increasing sophistication.

INTRODUCTION

Calcium (Ca^{2+}) represents one of the most versatile second messengers in all eukaryotic organisms. In plants, Ca^{2+} is involved in nearly all aspects of development and participates in many regulatory processes (Dodd et al. 2010; Kudla et al. 2010). Ca^{2+} signals are perceived as transient increases in cytosolic free Ca^{2+} concentration ($[Ca^{2+}]_c$) arising through fluxes from external sources and internal subcellular compartments (Hetherington and Brownlee 2004; Dodd et al. 2010). Specificity in Ca^{2+} signaling is achieved (at least in part) by stimulus-specific, spatially and temporally distinct changes in cellular Ca^{2+} concentrations, designated as "Ca^{2+} signatures" (Webb et al. 1996). Specific Ca^{2+} signatures that are formed in response to different stimuli—including drought, salt, or osmotic stresses, temperature, light, and plant hormones—occur as a result of the tightly regulated activities of channels and transporters in different membranes (Dodd et al. 2010; Kudla et al. 2010).

The visualization and analysis of intracellular Ca^{2+} dynamics in living plants was revolutionized through the introduction of genetically encoded Ca^{2+} indicators (GECIs): aequorin, GFP-based Ca^{2+} probes, and, very recently, BRET-based indicators (Saito et al. 2012), detected either by photon emission measurements or fluorescence microscopy. These developments were facilitated by the relative ease of obtaining stably transformed transgenic plants, especially tobacco and *Arabidopsis*, and by the simplicity of storing and propagating the transgenic lines as seeds. (For further details on

[5]Correspondence: jkudla@uni-muenster.de

Cite this article as *Cold Spring Harb Protoc;* 2013; doi:10.1101/pdb.top066183

plant transformation and propagation, refer to Arabidopsis *Protocols* [Salinas and Sanchez-Serrano 2006]). The first tools developed for in vivo intracellular analyses of Ca^{2+} dynamics in plants were based on aequorin targeted to the cytoplasm (Knight et al. 1991), nucleus (van Der Luit et al. 1999), chloroplasts (Johnson et al. 1995), tonoplast (Knight et al. 1996), and mitochondria (Logan and Knight 2003). Recently, aequorin has been targeted to the stroma as well as the inner and outer chloroplast envelope membranes (Mehlmer et al. 2012). These experiments produced very reliable data, but merely reflected the response of a population of cells or plants; hence, intercellular heterogeneity could not be investigated. The limited resolution and rather low emission intensity of aequorin measurements underscored the need for an advanced Ca^{2+} detection system with the combined ability to record Ca^{2+} transients at high resolution and express the Ca^{2+} indicator in the desired tissues or intracellular locations.

YELLOW CAMELEON Ca^{2+} INDICATORS

In recent years, the development and application of ratiometric Ca^{2+} reporter proteins (YCs or Cameleons) has greatly advanced the spatial and temporal resolution of Ca^{2+} signaling studies. Consequently, these Ca^{2+} sensors have been increasingly used among the GECIs that are available for such studies in plants. YCs are fluorescence resonance energy transfer (FRET)-based indicator proteins (Fig. 1). They harbor two GFP variants, CFP and YFP (or circularly permuted variants of YFP) linked together by the Ca^{2+}-binding protein calmodulin and the calmodulin-binding peptide M13. Binding of Ca^{2+} to the calmodulin of YC leads to a conformational change in the indicator,

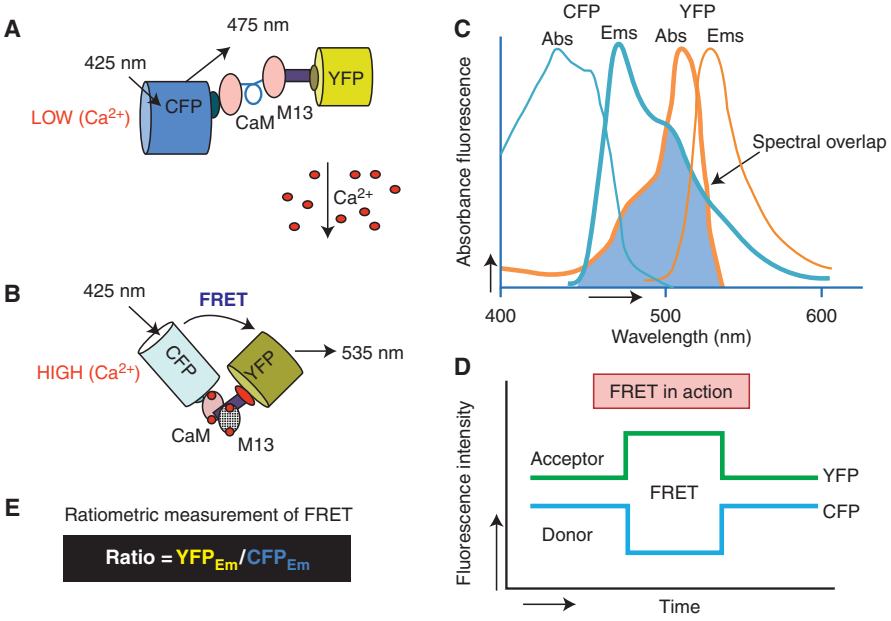

FIGURE 1. The functional principle of the genetically encoded Ca^{2+} indicator Yellow Cameleon (YC). (*A*) Functional components of the Cameleon probe: the two fluorophores CFP and YFP, the calcium binding element CaM, and the M13 connector. (*B*) Demonstration of FRET between CFP and YFP as the fluorophores move into close proximity due to a conformational change after the binding of Ca^{2+} to CaM. (*C*) Absorption and emission spectra of CFP and YFP, showing spectral overlap between CFP emission and YFP excitation. This spectral overlap allows excitation of YFP by CFP emission. (*D*) Read-out of a typical Cameleon measurement showing the emission intensity of CFP (donor) and YFP (acceptor) after CFP excitation. (E) FRET efficiency measured as the ratio between acceptor (YFP) emission and donor (CFP) emission.

bringing CFP and YFP into close proximity and allowing enhanced FRET between CFP and YFP. The efficiency of FRET allows quantitative measurements of Ca^{2+} dynamics to be made by recording the ratio shifts along a time-course.

Allen et al. (1999) reported the first successful application of YC in plants, using the YC2.1 version to monitor Ca^{2+} dynamics in guard cells. During the last few years, new YC variants with improved fluorescence, larger changes in FRET on Ca^{2+} binding, and broader ranges of Ca^{2+} affinities have been developed (Palmer and Tsien 2006; Palmer et al. 2011). With these YC variants, it has now become possible to monitor Ca^{2+} in different organs and tissues and subcellular compartments. Plants expressing the improved YC3.6 version of Cameleon (Nagai et al. 2004) were used to record cell type-specific Ca^{2+} oscillations evoked by extracellular nucleoside-triphosphates (Tanaka et al. 2010) and toxic metals (Rincón-Zachary et al. 2010), and have been used to study events in growing root hair tips (Monshausen et al. 2008), mechanically stimulated roots (Monshausen et al. 2009), and pollen tubes (Iwano et al. 2009). Nuclear- and plasma membrane-targeted YC3.6 allow the visualization of dynamic changes in Ca^{2+} concentration within the nucleus and in the subplasma membrane compartment (Sieberer et al. 2009; Krebs et al. 2012).

A further advantage of YC is that it can be easily adapted for different Ca^{2+} binding affinities. This feature enabled the recent investigation of Ca^{2+} dynamics in the endoplasmic reticulum (which contains high concentrations of Ca^{2+}) using version YC4.6 (Iwano et al. 2009). Moreover, in the D family of Cameleon indicators (Palmer et al. 2006), the basic structure of the probe remains unchanged, but both calmodulin (CaM) and the calmodulin-binding peptide have been mutated to abolish or strongly reduce the interference of the reporter protein with endogenous calmodulin. The first use of the D3cpv version of Cameleon in plants enabled the monitoring of Ca^{2+} dynamics in plant peroxisomes (Costa et al. 2010), where CaM is indeed present (Chigri et al. 2012). The most recent, successful implementation of mitochondria-targeted YC3.6 enhanced the understanding of Ca^{2+} dynamics in the mitochondria of both guard and root cells in plants (Loro et al. 2012). Additionally, concurrent expression of differentially targeted YC3.6 reporters in the same cell facilitated simultaneous recordings of mitochondrial and nuclear Ca^{2+} dynamics in *Arabidopsis* (Loro et al. 2012).

ANALYZING Ca^{2+} DYNAMICS IN PLANT CELLS

We have provided a set of detailed protocols describing current, well-established techniques and methodologies for using YC indicators. This compilation should provide the interested user with a broad tool kit to study Ca^{2+} dynamics in various contexts. We begin with a basic protocol for analyses of cytoplasmic Ca^{2+} dynamics in guard cells in **Live Cell Imaging of Cytoplasmic Ca^{2+} Dynamics in *Arabidopsis* Guard Cells** (Behera and Kudla 2013a). In **High-Resolution Imaging of Cytoplasmic Ca^{2+} Dynamics in *Arabidopsis* Roots** (Behera and Kudla 2013b), we extend this repertoire to include analyses of cytoplasmic Ca^{2+} in complex tissues. A third protocol, **Live Cell Imaging of Cytoplasmic and Nuclear Ca^{2+} Dynamics in *Arabidopsis* Roots** (Krebs and Schumacher 2013), advances the use of spatial resolution to achieve the combined imaging of cytoplasmic and nuclear Ca^{2+}. The final protocol, **Imaging of Mitochondrial and Nuclear Ca^{2+} Dynamics in *Arabidopsis* Roots** (Loro and Costa 2013), further describes development of this technique for simultaneous recording of mitochondrial and nuclear Ca^{2+} dynamics.

These readily implementable methods will allow users to pursue Ca^{2+} imaging and analyses in guard and root cells. Our descriptions are focused on the most versatile YC3.6 version of Cameleon probe and its analysis using both wide-field fluorescence and laser scanning confocal microscopy. We have paid particular attention to describing the preparation and manipulation of transgenic plants, and provided in-depth instructions for performing imaging analyses in cells from different organs and tissues and in different subcellular compartments. Thus, these protocols will enable the reader to successfully perform Cameleon-based Ca^{2+} imaging recordings in different plant cell types, using various transgenic plants available to the broader scientific community (Yang et al. 2008; Krebs et al.

Cite this article as *Cold Spring Harb Protoc*; 2013; doi:10.1101/pdb.top066183

2012; Loro et al. 2012). Moreover, we hope that this compendium of methods for the study of Ca^{2+} dynamics will aid the development of additional, novel approaches that further advance our understanding of this important phenomenon in plant biology.

ACKNOWLEDGMENTS

This work was supported by grants from the Deutsche Forschungsgemeinschaft and the Human Frontier Science Program to J.K. and a PhD fellowship from the International Max Planck Research School-Cell Dynamics and Disease to S.B. We thank Dr. Katrin Held and Jan N. Offenborn for their contribution to the figures.

REFERENCES

Allen GJ, Kwak JM, Chu SP, Llopis J, Tsien RY, Harper JF, Schroeder JI. 1999. Cameleon calcium indicator reports cytoplasmic calcium dynamics in *Arabidopsis* guard cells. *Plant J* **19:** 735–747.

Behera S, Kudla J. 2013a. Live cell imaging of cytoplasmic Ca^{2+} dynamics in *Arabidopsis* guard cells. *Cold Spring Harb Protoc* doi: 10.1101/pdb.prot72983.

Behera S, Kudla J. 2013b. High-resolution imaging of cytoplasmic Ca^{2+} dynamics in *Arabidopsis* roots. *Cold Spring Harb Protoc* doi: 10.1101/pdb.prot073023.

Chigri F, Flosdorff S, Pilz S, Kölle E, Dolze E, Gietl C, Vothknecht UC. 2012. The *Arabidopsis* calmodulin-like proteins AtCML30 and AtCML3 are targeted to mitochondria and peroxisomes, respectively. *Plant Mol Biol* **78:** 211–222.

Costa A, Drago I, Behera S, Zottini M, Pizzo P, Schroeder JI, Pozzan T, Lo Schiavo F. 2010. H_2O_2 in plant peroxisomes: An in vivo analysis uncovers a Ca^{2+} dependent scavenging system. *Plant J* **62:** 760–772.

Dodd AN, Kudla J, Sanders D. 2010. The language of calcium signaling. *Annu Rev Plant Biol* **61:** 593–620.

Hetherington A, Brownlee C. 2004. The generation of Ca^{2+} signals in plants. *Annu Rev Plant Biol* **55:** 401–427.

Iwano M, Entani T, Shiba H, Kakita M, Nagai T, Mizuno H, Miyawaki A, Shoji T, Kubo K, Isogai A, et al. 2009. Fine-tuning of the cytoplasmic Ca^{2+} concentration is essential for pollen tube growth. *Plant Physiol* **150:** 1322–1334.

Johnson CH, Knight MR, Kondo T, Masson P, Sedbrook J, Haley A, Trewavas A. 1995. Circadian oscillations of cytosolic and chloroplastic free calcium in plants. *Science* **269:** 1863–1865.

Krebs M, Schumacher K. 2013. Live cell imaging of cytoplasmic and nuclear Ca^{2+} dynamics in *Arabidopsis* roots. *Cold Spring Harb Protoc* doi: 10.1101/pdb.prot073031.

Krebs M, Held K, Binder A, Hashimoto K, Den Herder G, Parniske M, Kudla J, Schumacher K. 2012. FRET-based genetically encoded sensors allow high-resolution live cell imaging of Ca^{2+} dynamics. *Plant J* **69:** 181–192.

Knight H, Trewaves AJ, Knight MR. 1996. Cold calcium signaling in *Arabidopsis* involves two cellular pools and a change in calcium signature after acclimation. *Plant cell* **8:** 489–503.

Knight MR, Campbell AK, Smith SM, Trewavas AJ. 1991. Transgenic plant aequorin reports the effect of touch and cold-shock and elicitors on cytoplasmic calcium. *Nature* **352:** 524–526.

Kudla J, Batistic O, Hashimoto K. 2010. Calcium signals: The lead currency of plant information processing. *Plant Cell* **22:** 541–563.

Logan DC, Knight MR. 2003. Mitochondrial and cytosolic calcium dynamics are differentially regulated in plants. *Plant Physiol* **133:** 21–24.

Loro G, Costa A. 2013. Imaging of mitochondrial and nuclear Ca^{2+} dynamics in *Arabidopsis* roots. *Cold Spring Harb Protoc* doi: 10.1101/pdb.prot073049.

Loro G, Drago I, Pozzan T, Lo Schiavo F, Zottini M, Costa A. 2012. Targeting of Cameleon to different subcellular compartments reveals a strict cytoplasmic/mitochondrial Ca^{2+} handling relationship in plant cells. *Plant J* **71:** 1–13.

Mehlmer N, Parvin N, Hurst CH, Knight MR, Teige M, Vothknecht U. 2012. A toolset of aequorin expression vectors for *in planta* studies of subcellular calcium concentrations in *Arabidopsis thaliana*. *J Exp Bot* **63:** 1751–1761.

Monshausen GB, Messerli MA, Gilroy S. 2008. Imaging of the Yellow Cameleon 3.6 indicator reveals that elevations in cytosolic Ca^{2+} follow oscillating increases in growth in root hairs of *Arabidopsis*. *Plant Physiol* **147:** 1690–1698.

Monshausen G, Bibikova T, Weisenseel M, Gilroy S. 2009. Ca^{2+} regulates reactive oxygen species production and pH during mechanosensing in *Arabidopsis* roots. *Plant Cell* **21:** 2341–2356.

Nagai T, Yamada S, Tominaga T, Ichikawa M, Miyawaki A. 2004. Expanded dynamic range of fluorescent indicators for Ca^{2+} by circularly permuted yellow fluorescent proteins. *Proc Natl Acad Sci* **101:** 10554–10559.

Palmer AE, Tsien RY. 2006. Measuring calcium signaling using genetically targetable fluorescent indicators. *Nat Protoc* **1:** 1057–1065.

Palmer AE, Giacomello M, Kortemme T, Hires S, Lev-Ram V, Baker D, Tsien RY. 2006. Ca^{2+} indicators based on computationally redesigned calmodulin–peptide pairs. *Chem Biol* **13:** 521–530.

Palmer AE, Qin Y, Park JG, McCombs JE. 2011. Design and application of genetically encoded biosensors. *Trends Biotechnol* **29:** 144–152.

Rincón-Zachary M, Teaster ND, Sparks JA, Valster AH, Motes CM, Blancaflor EB. 2010. Fluorescence resonance energy transfer-sensitized emission of Yellow Cameleon 3.60 reveals root zone-specific calcium signatures in *Arabidopsis* in response to aluminum and other trivalent cations. *Plant Physiol* **152:** 1442–1458.

Saito K, Hatsugai N, Horikawa K, Kobayashi K, Matsu-Ura T, Mikoshiba K, Nagai T. 2012. Auto-luminescent genetically-encoded ratiometric indicator for real-time Ca^{2+} imaging at the single cell level. *PLoS One* **5.**

Salinas J, Sanchez-Serrano JJ. 2006. Methods in molecular biology. Arabidopsis *protocols*, 2nd ed. Humana Press, New York, NY.

Sieberer B, Chabaud M, Timmers A, Monin A, Fournier J, Barker D. 2009. A nuclear-targeted Cameleon demonstrates intranuclear Ca^{2+} spiking in *Medicago truncatula* root hairs in response to rhizobial nodulation factors. *Plant Physiol* **151:** 1197–1206.

Tanaka K, Swanson S, Gilroy S, Stacey G. 2010. Extracellular nucleotides elicit cytosolic free calcium oscillations in *Arabidopsis*. *Plant Physiol* **154:** 705–719.

van Der Luit A, Olivari C, Haley A. 1999. Distinct calcium signaling pathways regulate calmodulin gene expression in tobacco. *Plant Physiol* **121:** 705–714.

Webb AR, McAinsh MR, Taylor JE, Hetherington AM. 1996. Calcium ions as intracellular second messengers in higher plants. *Adv Bot Res* **22:** 45–96.

Yang Y, Costa A, Leonhardt N, Siegel RS, Schroeder JI. 2008. Isolation of a strong *Arabidopsis* guard cell promoter and its potential as a research tool. *Plant Methods* **4:** 6.

Imaging of Mitochondrial and Nuclear Ca^{2+} Dynamics in *Arabidopsis* Roots

Giovanna Loro and Alex Costa

Cold Spring Harb Protoc; doi: 10.1101/pdb.prot073049

Protocol

Imaging of Mitochondrial and Nuclear Ca^{2+} Dynamics in *Arabidopsis* Roots

Giovanna Loro[1,2] and Alex Costa[2,3]

[1]*Department of Biology, University of Padova, 35131 Padova, Italy;* [2]*Department of Biosciences, University of Milan, 20133 Milan, Italy*

Here we report a method for analyzing mitochondrial Ca^{2+} dynamics in plant root cells by means of the newly generated cameleon probe 4mt-YC3.6. The use of plants expressing both nuclear- and mitochondrial-targeted cameleon, along with the resolution of confocal laser scanning microscopy (CLSM), allow simultaneous recordings of mitochondrial and nuclear Ca^{2+} dynamics within the same cell.

MATERIALS

It is essential that you consult the appropriate Material Safety Data Sheets and your institution's Environmental Health and Safety Office for proper handling of equipment and hazardous material used in this protocol.

RECIPES: Please see the end of this article for recipes indicated by <R>. Additional recipes can be found online at http://cshprotocols.cshlp.org/site/recipes.

Reagents

Agar

Arabidopsis seedlings expressing mitochondrial-targeted cameleon (4mt-YC3.6) or coexpressing mitochondrial- and nuclear-targeted YC3.6 cameleon (4mt-YC3.6 and NLS-YC3.6; Loro et al. 2012) (7- to 14-d-old; see Steps 1–3)

Ca^{2+} elicitor for treatment (e.g., 500 μM Na_2ATP in imaging solution [pH 5.8])

Growth medium (*Arabidopsis*) <R>

Hydrochloric acid (37%)

Imaging solution (*Arabidopsis*) <R>

Sodium hypochlorite (15%)

Equipment

Closed bath chamber for round coverslips (Fig. 1A-1)

Coverslips (round; 24-mm diameter)

Greenhouse or plant growth device to maintain stable growth conditions

ImageJ with Ratio Plus plugin (National Institutes of Health)

[3]Correspondence: alex.costa@unimi.it

Cite this article as *Cold Spring Harb Protoc*; 2013; doi:10.1101/pdb.prot073049

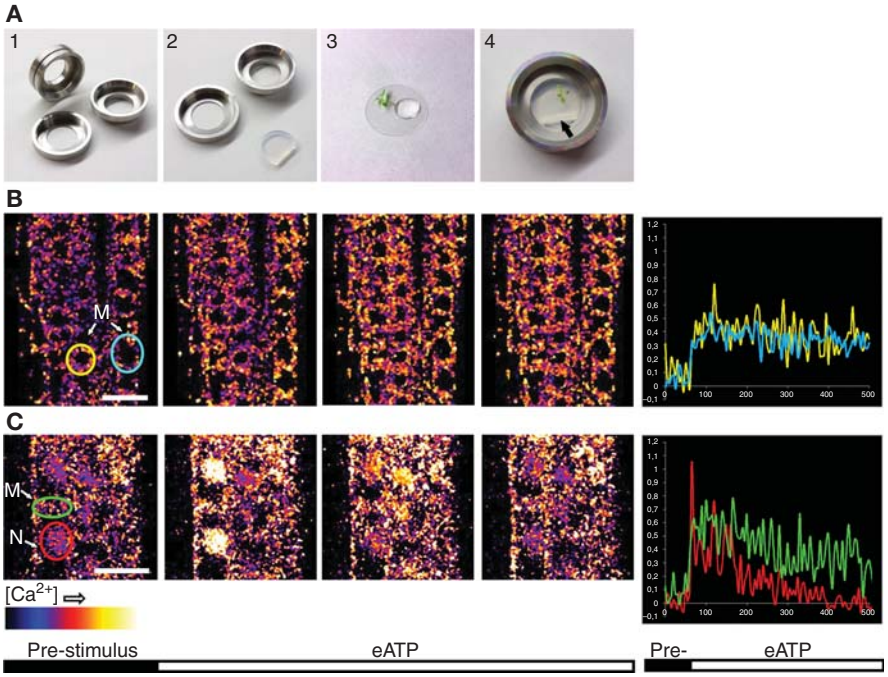

FIGURE 1. Example of a typical recording of Ca^{2+} transients in *Arabidopsis* seedling roots expressing the mitochondrial-targeted or dual-localized Cameleon, in response to 500 µM external ATP. (*A*) Specimen preparation with the microscope open-top chamber. (*B*) Ratio images of selected frames of cells expressing the 4mt-YC3.6 probe and normalized ratio traces for the indicated ROIs (yellow and bright blue). (*C*) Ratio images of selected frames of cells co-expressing the 4mt-YC3.6 and NLS-YC3.6 probes and normalized ratio traces for the indicated ROIs (green and red). The outlined colored areas are examples of possible selected ROIs chosen for mitochondria and nuclei line traces. M = mitochondria, N = nuclei. Scale bar, 25 µm.

Inverted confocal laser scanning microscope with 458-nm line argon laser, dual emission photomultipliers (473–505 nm for cyan fluorescent protein [CFP] and 526–536 nm for circularly permuted Venus [cpVenus]) and 40× or 63× objective

Laminar flow cabinet

Medical tape (3M Micropore)

Microcentrifuge tubes (2-mL)

Perfusion system

Scalpel

Square plates (sterile)

Syringe with tubing

Toothpicks (sterile)

Tweezers

Vacuum desiccator

METHOD

Seed Sterilization and Growth of Plantlets

1. Place a small amount of *Arabidopsis* seeds (approximately 100) in a 2-mL microcentrifuge tube and place it open into a vacuum desiccator. Sterilize the seeds by vapor-phase chloride (100 mL of 15% sodium hypochlorite with 3 mL 37% hydrochloric acid) for 5 h (Clough and Bent 1998).

Cite this article as *Cold Spring Harb Protoc*; 2013; doi:10.1101/pdb.prot073049

2. Working in sterile conditions, use a sterile toothpick to plate the seeds individually on the growth medium in square dishes, and seal them with medical tape. Perform stratification at 4°C in the dark for 3 d.
3. Transfer the plates (keeping them vertical) to the growth chamber with 16/8 h cycles of light (100 $\mu mol/m^{-2}/sec^{-1}$) at 24°C.

Sample Preparation

4. To make a round agar block for root tip cell imaging, prepare 1% agar in 1× imaging solution. Pour 1 mL into the microscope bath chamber. Once solidified, cut an edge with a scalpel (Fig. 1A-2).
5. Place 80 µL of imaging solution on a round microscope coverslip. Gently transfer one seedling into the solution, taking care to submerge the root tip to avoid sample desiccation (Fig. 1A-3).
6. Carefully place the agar block over the root without covering the shoot. With a pair of tweezers, pull the seedling very lightly to move the root tip under the agar block, as close as possible to the agar edge (Fig. 1A-4).

CLSM Analysis

7. Place the specimen on the microscope stage and use the 40× or 63× objective to focus on the root tip using bright field illumination.
8. Prepare for the addition of elicitor solution in Step 10 by setting up the perfusion system (syringe and tube) on the top of the chamber.

   See Troubleshooting.
9. Excite the cameleon probe with the 458-nm line of the argon laser (for CFP excitation), using as little laser power as possible. Set the CFP and cpVenus emissions for the two photomultipliers. If a spectral confocal is available, narrow down the emission wavelength windows to 473–505 nm (for CFP) and 526–536 nm (for cpVenus). Set the pinhole diameter to a maximum of 2 Airy Units and collect the images every 3–5 sec.

   See Troubleshooting.
10. Once the imaging experiment has started, wait about ten frames and add the solution containing the selected elicitor (e.g., 500 µM Na_2ATP in imaging solution) to the chamber. For online analysis of the Ca^{2+} dynamics, define "regions of interest" (ROIs) and determine the fluorescence intensity for both wavelengths (CFP and cpVenus) (Fig. 1B,C).

Imaging Analyses

11. Perform post-acquisition analyses with the provided confocal software or an open-source software such as ImageJ. Export averaged fluorescence intensity values into a data processing software and calculate the ratio between cpVenus and CFP according to

$$\text{Ratio}_{\text{cpVenus/CFP}} = \frac{\text{cpVenus}_{\text{Mean intensity}} - \text{Background cpVenus}_{\text{Mean intensity}}}{\text{CFP}_{\text{Mean intensity}} - \text{Background CFP}_{\text{Mean intensity}}}.$$

12. Calculate the ratio normalization according to

$$\Delta R/R_0 = (\text{ratio at time "}t_n\text{"} - \text{ratio at time "}t_0\text{"})/\text{ratio at time "}t_0\text{"}.$$

13. Obtain the false color ratio images (Fig. 1B,C) using the ImageJ Ratio Plus plugin for a representation of the Ca^{2+} dynamics.

TROUBLESHOOTING

Problem (Step 8): The root drifts during imaging.

Solution: The CLSM Ca^{2+} imaging analysis requires an almost null sample drift or focus change. A good fixation of the sample and gentle addition of the stimulus are the key steps.

Problem (Step 9): Wavelengths overlap and there is low spatial resolution.

Solution: To avoid fluorescence bleed-through between CFP and cpVenus, the emission filters should be adjusted as specified in Step 9. Also, mitochondria and nuclei show different intensities of fluorescence, with the latter showing the brightest signal. To achieve a good mitochondrial signal, the CLSM "gain" and "offset" must be set properly. These settings must be determined empirically to avoid signal saturation in the nucleus that would limit the dynamic range of Cameleon.

Problem (Step 9): There is low spatial resolution.

Solution: The cells of the differentiation/elongation zones are the best choice for achieving good signal separation between mitochondria and nuclei. To get into the deeper layers of the root, the confocal pinhole should be open; note that the higher the pinhole aperture, the lower the resolution. This setting could affect the capability to distinguish signals originating from mitochondria versus nuclei.

Problem (Step 9): Mitochondrial movement affects imaging.

Solution: Due to the high motility of mitochondria, when performing high magnification analyses, high acquisition speed is favorable. A compromise between speed (image acquisition) and resolution (i.e., pinhole aperture) must be determined empirically.

DISCUSSION

The simultaneous analysis of Ca^{2+} dynamics in two different compartments allows comparison of mitochondrial and cytosolic/nuclear Ca^{2+} kinetics in the same cell. The use of NLS-YC3.6 and 4mt-YC3.6 can help the investigator to better understand the reciprocal interactions between these two compartments in terms of Ca^{2+} handling.

RECIPES

Growth Medium (Arabidopsis)

0.5× Murashige and Skoog (MS) medium (Duchefa M0222)
0.1% sucrose (Duchefa)
0.05% MES buffer (pH 6.0)
0.8% plant agar (Duchefa)

Autoclave at 1 atm for 20 min.

Imaging Solution (Arabidopsis)

10 mM MES–Tris base (pH 5.8)
10 mM $CaCl_2$
5 mM KCl

ACKNOWLEDGMENTS

This work was supported by the Ministero dell'Istruzione, dell'Università e della Ricerca through the grant FIRB 2010 (RBFR10S1LJ_001) to A.C.

REFERENCES

Clough SJ, Bent AF. 1998. Floral dip: A simplified method for *Agrobacterium*-mediated transformation of *Arabidopsis thaliana*. *Plant J* **16:** 735–743.

Loro G, Drago I, Pozzan T, Lo Schiavo F, Zottini M, Costa A. 2012. Targeting of cameleon to different subcellular compartments reveals a strict cytoplasmic/mitochondrial Ca^{2+} handling relationship in plant cells. *Plant J* **71:** 1–13.

Acknowledgments

I would like to thank Professor Tullio Pozzan's laboratory of the Bioscience Department at the Padova University and the group of Professor Alex Costa at the Department of Bioscience at the University of Milano for their collaboration, help and essential scientific support. In particular I am grateful to Dott. Smrutisanjita Behera for her valuable technical assistance. I am glad to thank Professor Jörg Kudla and his laboratory of Plant Biology and Biotechnology Department at the University of Münster for the hospitality and exciting critical discussion on the research.

References

Aldridge, C. and S.G. Moller. 2005. The plastid division protein AtMinD1 is a Ca2+-ATPase stimulated by AtMinE1. J. Biol. Chem. **280**, 31673-31678.

Allen, G.J., et al. 2001. A defined range of guard cell calcium oscillation parameters encodes stomatal movements. Nature. **411**, 1053-1057.

Allen, G.J., et al. 2000. Alteration of stimulus-specific guard cell calcium oscillations and stomatal closing in Arabidopsis det3 mutant. Science. **289**, 2338-2342.

Arpagaus, S., A. Rawyler, and R. Braendle. 2002. Occurrence and characteristics of the mitochondrial permeability transition in plants. J. Biol. Chem. **277**, 1780-1787.

Balsera, M., et al. 2009. Characterization of Tic110, a channel-forming protein at the inner envelope membrane of chloroplasts, unveils a response to Ca(2+) and a stromal regulatory disulfide bridge. J. Biol. Chem. **284**, 2603-2616.

Batistic, O. and J. Kudla. 2012. Analysis of calcium signaling pathways in plants. Biochim. Biophys. Acta. **1820**, 1283-1293.

Baxter, I., et al. 2003. Genomic comparison of P-type ATPase ion pumps in Arabidopsis and rice. Plant Physiol. **132**, 618-628.

Behera, S. and J. Kudla. 2013. High-resolution imaging of cytoplasmic Ca2+ dynamics in Arabidopsis roots. Cold Spring Harb Protoc. **2013**, 10.1101/pdb.prot073023.

Beneloujaephajri, E., et al. 2013. Production of reactive oxygen species and wound-induced resistance in Arabidopsis thaliana against Botrytis cinerea are preceded and depend on a burst of calcium. BMC Plant. Biol. **13**, 160-2229-13-160.

Benikhlef, L., et al. 2013. Perception of soft mechanical stress in Arabidopsis leaves activates disease resistance. BMC Plant. Biol. **13**, 133-2229-13-133.

Blatt, M.R. 2000. Cellular signaling and volume control in stomatal movements in plants. Annu. Rev. Cell Dev. Biol. **16**, 221-241.

Bonora, M., et al. 2013. Subcellular calcium measurements in mammalian cells using jellyfish photoprotein aequorin-based probes. Nat. Protoc. **8**, 2105-2118.

Bonza, M.C. and M.I. De Michelis. 2011. The plant Ca2+ -ATPase repertoire: biochemical features and physiological functions. Plant. Biol. (Stuttg). **13**, 421-430.

Bonza, M.C., et al. 2013. Analyses of Ca2+ accumulation and dynamics in the endoplasmic reticulum of Arabidopsis root cells using a genetically encoded Cameleon sensor. Plant Physiol. **163**, 1230-1241.

Bonza, M.C., et al. 2000. At-ACA8 encodes a plasma membrane-localized calcium-ATPase of Arabidopsis with a calmodulin-binding domain at the N terminus. Plant Physiol. **123**, 1495-1506.

Bose, J., et al. 2011. Calcium efflux systems in stress signaling and adaptation in plants. Front. Plant. Sci. **2**, 85.

Brand, J.J. and D.W. Becker. 1984. Evidence for direct roles of calcium in photosynthesis. J. Bioenerg. Biomembr. **16**, 239-249.

Brini, M. and E. Carafoli. 2009. Calcium pumps in health and disease. Physiol. Rev. **89**, 1341-1378.

Carrie, C., et al. 2008. Type II NAD(P)H dehydrogenases are targeted to mitochondria and chloroplasts or peroxisomes in Arabidopsis thaliana. FEBS Lett. **582**, 3073-3079.

Catala, R., et al. 2003. Mutations in the Ca2+/H+ transporter CAX1 increase CBF/DREB1 expression and the cold-acclimation response in Arabidopsis. Plant Cell. **15**, 2940-2951.

Chen, C., et al. 2009. Antiquity and function of CASTOR and POLLUX, the twin ion channel-encoding genes key to the evolution of root symbioses in plants. Plant Physiol. **149**, 306-317.

Chen, J., et al. 2012. The endoplasmic reticulum: a social network in plant cells. J. Integr. Plant. Biol. **54**, 840-850.

Cheng, N.H., et al. 2004. Characterization of CXIP4, a novel Arabidopsis protein that activates the H+/Ca2+ antiporter, CAX1. FEBS Lett. **559**, 99-106.

Chigri, F., et al. 2012. The Arabidopsis calmodulin-like proteins AtCML30 and AtCML3 are targeted to mitochondria and peroxisomes, respectively. Plant Mol. Biol. **78**, 211-222.

Chiu, J.C., et al. 2002. Phylogenetic and expression analysis of the glutamate-receptor-like gene family in Arabidopsis thaliana. Mol. Biol. Evol. **19**, 1066-1082.

Choi, J., et al. 2014a. Identification of a plant receptor for extracellular ATP. Science. **343**, 290-294.

Choi, W.G., et al. 2014b. Salt stress-induced Ca2+ waves are associated with rapid, long-distance root-to-shoot signaling in plants. Proc. Natl. Acad. Sci. U. S. A. **111**, 6497-6502.

Clifton, R., et al. 2005. Stress-induced co-expression of alternative respiratory chain components in Arabidopsis thaliana. Plant Mol. Biol. **58**, 193-212.

Clough, S.J. and A.F. Bent. 1998. Floral dip: a simplified method for Agrobacterium-mediated transformation of Arabidopsis thaliana. Plant J. **16**, 735-743.

Conn, S. and M. Gilliham. 2010. Comparative physiology of elemental distributions in plants. Ann. Bot. **105**, 1081-1102.

Costa, A., et al. 2010. H2O2 in plant peroxisomes: an in vivo analysis uncovers a Ca(2+)-dependent scavenging system. Plant J. **62**, 760-772.

Costa, A., et al. 2013. Peroxisome Ca(2+) homeostasis in animal and plant cells. Subcell. Biochem. **69**, 111-133.

Dadacz-Narloch, B., et al. 2011. A novel calcium binding site in the slow vacuolar cation channel TPC1 senses luminal calcium levels. Plant Cell. **23**, 2696-2707.

De Stefani, D., et al. 2011. A forty-kilodalton protein of the inner membrane is the mitochondrial calcium uniporter. Nature. **476**, 336-340.

Demidchik, V. and F.J. Maathuis. 2007. Physiological roles of nonselective cation channels in plants: from salt stress to signalling and development. New Phytol. **175**, 387-404.

Deuschle, K., et al. 2006. Rapid metabolism of glucose detected with FRET glucose nanosensors in epidermal cells and intact roots of Arabidopsis RNA-silencing mutants. Plant Cell. **18**, 2314-2325.

Dietrich, P., et al. 2010. Physiology and biophysics of plant ligand-gated ion channels. Plant. Biol. (Stuttg). **12 Suppl 1**, 80-93.

Dodd, A.N., J. Kudla, and D. Sanders. 2010. The language of calcium signaling. Annu. Rev. Plant. Biol. **61**, 593-620.

Dunkley, T.P., et al. 2006. Mapping the Arabidopsis organelle proteome. Proc. Natl. Acad. Sci. U. S. A. **103**, 6518-6523.

Elhafez, D., et al. 2006. Characterization of mitochondrial alternative NAD(P)H dehydrogenases in Arabidopsis: intraorganelle location and expression. Plant Cell Physiol. **47**, 43-54.

Ettinger, W.F., et al. 1999. Identification of a Ca2+/H+ antiport in the plant chloroplast thylakoid membrane. Plant Physiol. **119**, 1379-1386.

Evans, M.L. and H. Ishikawa. 1997. Cellular specificity of the gravitropic motor response in roots. Planta. **203**, S115-22.

Evans, N.H., M.R. McAinsh, and A.M. Hetherington. 2001. Calcium oscillations in higher plants. Curr. Opin. Plant Biol. **4**, 415-420.

Ferro, M., et al. 2003. Proteomics of the chloroplast envelope membranes from Arabidopsis thaliana. Mol. Cell. Proteomics. **2**, 325-345.

Fulton, D.C., et al. 2008. Beta-AMYLASE4, a noncatalytic protein required for starch breakdown, acts upstream of three active beta-amylases in Arabidopsis chloroplasts. Plant Cell. **20**, 1040-1058.

Geisler, D.A., et al. 2007. Ca2+-binding and Ca2+-independent respiratory NADH and NADPH dehydrogenases of Arabidopsis thaliana. J. Biol. Chem. **282**, 28455-28464.

Gerace, L. and B. Burke. 1988. Functional organization of the nuclear envelope. Annu. Rev. Cell Biol. **4**, 335-374.

Hamilton, A.J. and D.C. Baulcombe. 1999. A species of small antisense RNA in posttranscriptional gene silencing in plants. Science. **286**, 950-952.

Han, S., et al. 2003. A cell surface receptor mediates extracellular Ca(2+) sensing in guard cells. Nature. **425**, 196-200.

Haswell, E.S. and E.M. Meyerowitz. 2006. MscS-like proteins control plastid size and shape in Arabidopsis thaliana. Curr. Biol. **16**, 1-11.

Hong, B., et al. 1999. Identification of a calmodulin-regulated Ca2+-ATPase in the endoplasmic reticulum. Plant Physiol. **119**, 1165-1176.

Hua, B., et al. 2003. Functional interaction of calmodulin with a plant cyclic nucleotide gated cation channel. Plant Physiology and Biochemistry. **41**, 945-954.

Huang, L., et al. 1993. Characterization of a gene encoding a Ca(2+)-ATPase-like protein in the plastid envelope. Proc. Natl. Acad. Sci. U. S. A. **90**, 10066-10070.

Iwano, M., et al. 2009. Fine-tuning of the cytoplasmic Ca2+ concentration is essential for pollen tube growth. Plant Physiol. **150**, 1322-1334.

Jensen, G.S. and E.S. Haswell. 2012. Functional analysis of conserved motifs in the mechanosensitive channel homolog MscS-Like2 from Arabidopsis thaliana. PLoS One. **7**, e40336.

Jiang, D., L. Zhao, and D.E. Clapham. 2009. Genome-wide RNAi screen identifies Letm1 as a mitochondrial Ca2+/H+ antiporter. Science. **326**, 144-147.

Johnson, C.H., et al. 1995. Circadian oscillations of cytosolic and chloroplastic free calcium in plants. Science. **269**, 1863-1865.

Kang, S., et al. 2006. Overexpression in Arabidopsis of a plasma membrane-targeting glutamate receptor from small radish increases glutamate-mediated Ca2+ influx and delays fungal infection. Mol. Cells. **21**, 418-427.

Kao, J.P.Y. 1994. Chapter 7 Practical Aspects of Measuring [Ca2+] with Fluorescent Indicators. Methods Cell Biol. **40**, 155-181.

Kaplan, B., T. Sherman, and H. Fromm. 2007. Cyclic nucleotide-gated channels in plants. FEBS Lett. **581**, 2237-2246.

Kasai, M. and S. Muto. 1990. Ca2+ pump and Ca2+/H+ antiporter in plasma membrane vesicles isolated by aqueous two-phase partitioning from corn leaves. J. Membr. Biol. **114**, 133-142.

Kerscher, S.J. 2000. Diversity and origin of alternative NADH:ubiquinone oxidoreductases. Biochim. Biophys. Acta. **1459**, 274-283.

Klusener, B., G. Boheim, and E.W. Weiler. 1997. Modulation of the ER Ca2+ channel BCC1 from tendrils of Bryonia dioica by divalent cations, protons and H2O2. FEBS Lett. **407**, 230-234.

Klusener, B. and E.W. Weiler. 1999. A Calcium-Selective Channel from Root-Tip Endomembranes of Garden Cress. Plant Physiol. **119**, 1399-1406.

Kosuta, S., et al. 2008. Differential and chaotic calcium signatures in the symbiosis signaling pathway of legumes. Proc. Natl. Acad. Sci. U. S. A. **105**, 9823-9828.

Krebs, M., et al. 2012. FRET-based genetically encoded sensors allow high-resolution live cell imaging of Ca(2)(+) dynamics. Plant J. **69**, 181-192.

Kreimer, G., M. Melkonian, and E. Latzko. 1985. An electrogenic uniport mediates light-dependent Ca2+ influx into intact spinach chloroplasts. FEBS Lett. **180**, 253-258.

Kudla, J., O. Batistic, and K. Hashimoto. 2010. Calcium signals: the lead currency of plant information processing. Plant Cell. **22**, 541-563.

Kurosaki, F., H. Kaburaki, and A. Nishi. 1994. Involvement of plasma membrane-located calmodulin in the response decay of cyclic nucleotide-gated cation channel of cultured carrot cells. FEBS Lett. **340**, 193-196.

Kwak, J.M., et al. 2003. NADPH oxidase AtrbohD and AtrbohF genes function in ROS-dependent ABA signaling in Arabidopsis. EMBO J. **22**, 2623-2633.

Lacombe, B., et al. 2001. The identity of plant glutamate receptors. Science. **292**, 1486-1487.

Lee, S.M., et al. 2007. Identification of a calmodulin-regulated autoinhibited Ca2+-ATPase (ACA11) that is localized to vacuole membranes in Arabidopsis. FEBS Lett. **581**, 3943-3949.

Li, J., et al. 2006. A rice glutamate receptor-like gene is critical for the division and survival of individual cells in the root apical meristem. Plant Cell. **18**, 340-349.

Li, X., et al. 2005. - Arabidopsis AtCNGC10 rescues potassium channel mutants of E. coli, yeast and Arabidopsis and is regulated by calcium / calmodulin and cyclic GMP in E. coli. - Funct. Plant Biol., - 643.

Liang, F., et al. 1997. ECA1 complements yeast mutants defective in Ca2+ pumps and encodes an endoplasmic reticulum-type Ca2+-ATPase in Arabidopsis thaliana. Proc. Natl. Acad. Sci. U. S. A. **94**, 8579-8584.

Logan, D.C. and M.R. Knight. 2003. Mitochondrial and cytosolic calcium dynamics are differentially regulated in plants. Plant Physiol. **133**, 21-24.

Loro, G., et al. 2012. Targeting of Cameleons to various subcellular compartments reveals a strict cytoplasmic/mitochondrial Ca(2)(+) handling relationship in plant cells. Plant J. **71**, 1-13.

Maser, P., et al. 2001. Phylogenetic relationships within cation transporter families of Arabidopsis. Plant Physiol. **126**, 1646-1667.

Mattson, M.P. and S.L. Chan. 2003. Calcium orchestrates apoptosis. Nat. Cell Biol. **5**, 1041-1043.

Mazars, C., et al. 2011. Nuclear calcium signaling: An emerging topic in plants. Biochimie. **93**, 2068-2074.

McAinsh, M.R. and J.K. Pittman. 2009. Shaping the calcium signature. New Phytol. **181**, 275-294.

McAinsh, M.R., et al. 1995. Stimulus-Induced Oscillations in Guard Cell Cytosolic Free Calcium. Plant Cell. **7**, 1207-1219.

McAinsh, M.R. and A.M. Hetherington. 1998. Encoding specificity in Ca2+ signalling systems. Trends Plant Sci. **3**, 32-36.

McCombs, J.E. and A.E. Palmer. 2008. Measuring calcium dynamics in living cells with genetically encodable calcium indicators. Methods. **46**, 152-159.

McPhalen, C.A., N.C. Strynadka, and M.N. James. 1991. Calcium-binding sites in proteins: a structural perspective. Adv. Protein Chem. **42**, 77-144.

Mehlmer, N., et al. 2012. A toolset of aequorin expression vectors for in planta studies of subcellular calcium concentrations in Arabidopsis thaliana. J. Exp. Bot. **63**, 1751-1761.

Michalecka, A.M., et al. 2003. Arabidopsis genes encoding mitochondrial type II NAD(P)H dehydrogenases have different evolutionary origin and show distinct responses to light. Plant Physiol. **133**, 642-652.

Miernyk, J.A., T.K. Fang, and D.D. Randall. 1987. Calmodulin antagonists inhibit the mitochondrial pyruvate dehydrogenase complex. J. Biol. Chem. **262**, 15338-15340.

Mills, R.F., et al. 2008. ECA3, a Golgi-localized P2A-type ATPase, plays a crucial role in manganese nutrition in Arabidopsis. Plant Physiol. **146**, 116-128.

Miyawaki, A., et al. 1999. Dynamic and quantitative Ca2+ measurements using improved cameleons. Proc. Natl. Acad. Sci. U. S. A. **96**, 2135-2140.

Miyawaki, A., et al. 1997. Fluorescent indicators for Ca2+ based on green fluorescent proteins and calmodulin. Nature. **388**, 882-887.

Moller, J.V., et al. 2010. The sarcoplasmic Ca2+-ATPase: design of a perfect chemi-osmotic pump. Q. Rev. Biophys. **43**, 501-566.

Moreno, I., et al. 2008. AtHMA1 is a thapsigargin-sensitive Ca2+/heavy metal pump. J. Biol. Chem. **283**, 9633-9641.

Nagai, T., et al. 2004. Expanded dynamic range of fluorescent indicators for Ca(2+) by circularly permuted yellow fluorescent proteins. Proc. Natl. Acad. Sci. U. S. A. **101**, 10554-10559.

Navazio, L., et al. 2000. Calcium release from the endoplasmic reticulum of higher plants elicited by the NADP metabolite nicotinic acid adenine dinucleotide phosphate. Proc. Natl. Acad. Sci. U. S. A. **97**, 8693-8698.

Navazio, L., P. Mariani, and D. Sanders. 2001. Mobilization of Ca2+ by cyclic ADP-ribose from the endoplasmic reticulum of cauliflower florets. Plant Physiol. **125**, 2129-2138.

Neish, A.C. 1939. Studies on chloroplasts: Their chemical composition and the distribution of certain metabolites between the chloroplasts and the remainder of the leaf. Biochem. J. **33**, 300-308.

Nomura, H., et al. 2008. Evidence for chloroplast control of external Ca2+-induced cytosolic Ca2+ transients and stomatal closure. Plant J. **53**, 988-998.

Nomura, H., et al. 2012. Chloroplast-mediated activation of plant immune signalling in Arabidopsis. Nat. Commun. **3**, 926.

Nomura, H. and T. Shiina. 2014. Calcium Signaling in Plant Endosymbiotic Organelles: Mechanism and Role in Physiology. Mol. Plant.

Oldroyd, G.E. and J.A. Downie. 2006. Nuclear calcium changes at the core of symbiosis signalling. Curr. Opin. Plant Biol. **9**, 351-357.

Palmer, A.E., et al. 2004. Bcl-2-mediated alterations in endoplasmic reticulum Ca2+ analyzed with an improved genetically encoded fluorescent sensor. Proc. Natl. Acad. Sci. U. S. A. **101**, 17404-17409.

Palmer, A.E. and R.Y. Tsien. 2006. Measuring calcium signaling using genetically targetable fluorescent indicators. Nat. Protoc. **1**, 1057-1065.

Palmgren, M.G. and P. Nissen. 2011. P-type ATPases. Annu. Rev. Biophys. **40**, 243-266.

Pauly, N., et al. 2001. The nucleus together with the cytosol generates patterns of specific cellular calcium signatures in tobacco suspension culture cells. Cell Calcium. **30**, 413-421.

Pei, Z.M., et al. 2000. Calcium channels activated by hydrogen peroxide mediate abscisic acid signalling in guard cells. Nature. **406**, 731-734.

Peragine, A., et al. 2004. SGS3 and SGS2/SDE1/RDR6 are required for juvenile development and the production of trans-acting siRNAs in Arabidopsis. Genes Dev. **18**, 2368-2379.

Perocchi, F., et al. 2010. MICU1 encodes a mitochondrial EF hand protein required for Ca(2+) uptake. Nature. **467**, 291-296.

Petroutsos, D., et al. 2011. The chloroplast calcium sensor CAS is required for photoacclimation in Chlamydomonas reinhardtii. Plant Cell. **23**, 2950-2963.

Pittman, J.K., M.C. Bonza, and M.I. De Michelis. 2011. Ca^{2+} Pumps and Ca^{2+} Antiporters in Plant Development, pp. 133. *In* M. Geisler and K. Venema (eds.). **Transporters and Pumps in Plant Signaling**, Springer.

Pittman, J.K., et al. 2002. Mechanism of N-terminal autoinhibition in the Arabidopsis Ca(2+)/H(+) antiporter CAX1. J. Biol. Chem. **277**, 26452-26459.

Qi, Z., N.R. Stephens, and E.P. Spalding. 2006. Calcium entry mediated by GLR3.3, an Arabidopsis glutamate receptor with a broad agonist profile. Plant Physiol. **142**, 963-971.

Rasmusson, A.G., K.L. Soole, and T.E. Elthon. 2004. Alternative NAD(P)H dehydrogenases of plant mitochondria. Annu. Rev. Plant. Biol. **55**, 23-39.

Reddy, V.S., G.S. Ali, and A.S. Reddy. 2002. Genes encoding calmodulin-binding proteins in the Arabidopsis genome. J. Biol. Chem. **277**, 9840-9852.

Roh, M.H., et al. 1998. Direct measurement of calcium transport across chloroplast inner-envelope vesicles. Plant Physiol. **118**, 1447-1454.

Rossi, A.E. and R.T. Dirksen. 2006. Sarcoplasmic reticulum: the dynamic calcium governor of muscle. Muscle Nerve. **33**, 715-731.

Sai, J. and C.H. Johnson. 2002. Dark-stimulated calcium ion fluxes in the chloroplast stroma and cytosol. Plant Cell. **14**, 1279-1291.

Sanders, D., C. Brownlee, and J. Harper. 1999. Communicating with calcium. The Plant Cell. **11**, 691-706.

Sanders, D., et al. 2002. Calcium at the crossroads of signaling. Plant Cell. **14 Suppl**, S401-17.

Sato, Y., M. Wada, and A. Kadota. 2001. External Ca(2+) is essential for chloroplast movement induced by mechanical stimulation but not by light stimulation. Plant Physiol. **127**, 497-504.

Schiott, M., et al. 2004. A plant plasma membrane Ca2+ pump is required for normal pollen tube growth and fertilization. Proc. Natl. Acad. Sci. U. S. A. **101**, 9502-9507.

Schönknecht, G. 2013. Calcium Signals from the Vacuole. Plants. **2**, 589-614.

Schroeder, J.I., et al. 2001. Guard Cell Signal Transduction. Annu. Rev. Plant Physiol. Plant Mol. Biol. **52**, 627-658.

Schuurink, R.C., et al. 1998. Characterization of a calmodulin-binding transporter from the plasma membrane of barley aleurone. Proc. Natl. Acad. Sci. U. S. A. **95**, 1944-1949.

Scrase-Field, S.A. and M.R. Knight. 2003. Calcium: just a chemical switch?. Curr. Opin. Plant Biol. **6**, 500-506.

Shigaki, T. and K.D. Hirschi. 2006. Diverse functions and molecular properties emerging for CAX cation/H+ exchangers in plants. Plant. Biol. (Stuttg). **8**, 419-429.

Sivaguru, M., et al. 2003. Aluminum rapidly depolymerizes cortical microtubules and depolarizes the plasma membrane: evidence that these responses are mediated by a glutamate receptor. Plant Cell Physiol. **44**, 667-675.

Smith, C., et al. 2011. Alterations in the mitochondrial alternative NAD(P)H Dehydrogenase NDB4 lead to changes in mitochondrial electron transport chain composition, plant growth and response to oxidative stress. Plant Cell Physiol. **52**, 1222-1237.

Stael, S., et al. 2011. Arabidopsis calcium-binding mitochondrial carrier proteins as potential facilitators of mitochondrial ATP-import and plastid SAM-import. FEBS Lett. **585**, 3935-3940.

Stael, S., et al. 2012. Plant organellar calcium signalling: an emerging field. J. Exp. Bot. **63**, 1525-1542.

Subbaiah, C.C., D.S. Bush, and M.M. Sachs. 1998. Mitochondrial Contribution to the Anoxic Ca2+ Signal in Maize Suspension-Cultured Cells. Plant Physiology. **118**, 759-771.

Sun, J., et al. 2007. Mastoparan activates calcium spiking analogous to Nod factor-induced responses in Medicago truncatula root hair cells. Plant Physiol. **144**, 695-702.

Swarbreck, S.M., R. Colaco, and J.M. Davies. 2013. Plant calcium-permeable channels. Plant Physiol. **163**, 514-522.

Szabadkai, G. and M.R. Duchen. 2008. Mitochondria: the hub of cellular Ca2+ signaling. Physiology (Bethesda). **23**, 84-94.

Tanaka, K., et al. 2014. Extracellular ATP acts as a damage-associated molecular pattern (DAMP) signal in plants. Front. Plant. Sci. **5**, 446.

Tanaka, K., et al. 2010. Extracellular nucleotides elicit cytosolic free calcium oscillations in Arabidopsis. Plant Physiol. **154**, 705-719.

Teardo, E., et al. 2015. Alternative splicing-mediated targeting of the plant glutamate receptor AtGLR3.5 to mitochondria affects organelle morphology. Plant Physiol.

Teardo, E., et al. 2011. Dual localization of plant glutamate receptor AtGLR3.4 to plastids and plasmamembrane. Biochim. Biophys. Acta. **1807**, 359-367.

Tiwari, B.S., B. Belenghi, and A. Levine. 2002. Oxidative stress increased respiration and generation of reactive oxygen species, resulting in ATP depletion, opening of mitochondrial permeability transition, and programmed cell death. Plant Physiol. **128**, 1271-1281.

Toyota, M., et al. 2013. Amyloplast displacement is necessary for gravisensing in Arabidopsis shoots as revealed by a centrifuge microscope. Plant J. **76**, 648-660.

Turner, W.L., et al. 2004. Cloning and characterization of two NAD kinases from Arabidopsis. identification of a calmodulin binding isoform. Plant Physiol. **135**, 1243-1255.

Walter, A., et al. 2007. Structural requirements of jasmonates and synthetic analogues as inducers of Ca2+ signals in the nucleus and the cytosol of plant cells. Angew. Chem. Int. Ed Engl. **46**, 4783-4785.

Wang, D., et al. 2003. Transgenic expression of a putative calcium transporter affects the time of Arabidopsis flowering. Plant J. **33**, 285-292.

Weinl, S., et al. 2008. A plastid protein crucial for Ca2+-regulated stomatal responses. New Phytol. **179**, 675-686.

Whalley, H.J. and M.R. Knight. 2013. Calcium signatures are decoded by plants to give specific gene responses. New Phytol. **197**, 690-693.

Wheeler, G.L. and C. Brownlee. 2008. Ca2+ signalling in plants and green algae--changing channels. Trends Plant Sci. **13**, 506-514.

White, P.J. and M.R. Broadley. 2003. Calcium in plants. Ann. Bot. **92**, 487-511.

Wilson, M.E., G.S. Jensen, and E.S. Haswell. 2011. Two mechanosensitive channel homologs influence division ring placement in Arabidopsis chloroplasts. Plant Cell. **23**, 2939-2949.

Xiao, Y., J. Wang, and K. Dehesh. 2013. Review of stress specific organelles-to-nucleus metabolic signal molecules in plants. Plant Sci. **212**, 102-107.

Xiong, T.C., et al. 2008. Sphingolipid metabolites selectively elicit increases in nuclear calcium concentration in cell suspension cultures and in isolated nuclei of tobacco. Cell Calcium. **43**, 29-37.

Xiong, T.C., et al. 2004. Isolated plant nuclei as mechanical and thermal sensors involved in calcium signalling. Plant J. **40**, 12-21.

Yamagishi, A., K. Satoh, and S. Katoh. 1981. The concentrations and thermodynamic activities of cations in intact Bryopsis chloroplasts. Biochimica et Biophysica Acta (BBA) - Bioenergetics. **637**, 252-263.

Yang, T. and B.W. Poovaiah. 2002. Hydrogen peroxide homeostasis: activation of plant catalase by calcium/calmodulin. Proc. Natl. Acad. Sci. U. S. A. **99**, 4097-4102.

Zhang, B., et al. 2012. LETM proteins play a role in the accumulation of mitochondrially encoded proteins in Arabidopsis thaliana and AtLETM2 displays parent of origin effects. J. Biol. Chem. **287**, 41757-41773.

Zhao, J., et al. 2009a. Functional studies of split Arabidopsis Ca2+/H+ exchangers. J. Biol. Chem. **284**, 34075-34083.

Zhao, J., et al. 2009b. Interaction between Arabidopsis Ca2+/H+ exchangers CAX1 and CAX3. J. Biol. Chem. **284**, 4605-4615.